Identification des moteurs de l'activité de l'anhydrase carbonique dans les sols et son impact sur les échanges sol-atmosphère de CO18O et OCS, deux traceurs complémentaires du cycle du carbone

Joana Sauze

ÉCOLE DOCTORALE
SCIENCES ET ENVIRONNEMENT
SPÉCIALITÉ BIOGÉOCHIMIE ET ECOSYSTÈME

THÈSE présentée par : Joana Sauze

Soutenance prévue le : **06 Avril 2017**
pour obtenir le grade de : **Docteur de l'université de Bordeaux**

Identification des moteurs de l'activité de l'anhydrase carbonique dans les sols et son impact sur les échanges sol-atmosphère de $CO^{18}O$ et OCS, deux traceurs complémentaires du cycle du carbone

Thèse dirigée par :
Jérôme OGÉE

Co-encadrée par :
Pierre-Alain MARON
Lisa WINGATE

Jury :

Matthias CUNTZ,	DR, INRA Nancy,	Président
Nick OSTLE	PR, Université de Lancaster	Rapporteur
Claire ROLLION-BARD,	HDR CNRS, IPGP	Rapporteur
Hans SCHNYDER,	PR, Université de Munich	Rapporteur
Olivier CROUZET,	CR, INRA Versailles	Invité
Pierre-Alain MARON,	DR, INRA Dijon	Co encadrant
Lisa WINGATE,	CR, INRA Bordeaux	Co encadrant
Jérôme OGÉE,	CR, INRA Bordeaux	Directeur de thèse

Identification des moteurs de l'activité de l'anhydrase carbonique dans les sols et son impact sur les échanges sol-atmosphère de $CO^{18}O$ et OCS, deux traceurs complémentaires du cycle du carbone

Résumé : Les anhydrases carboniques (AC) sont des enzymes qui catalysent les réactions d'hydratation du CO_2 et d'hydrolyse de l'OCS. L'AC présente dans les plantes et les microorganismes du sol influence le bilan atmosphérique d'OCS ainsi que celui du $CO^{18}O$ car les isotopes de l'oxygène sont échangés avec ceux des pools d'eau pendant l'hydratation du CO_2. L'utilisation de l'OCS et du $CO^{18}O$ comme traceurs du cycle du C global ouvre une nouvelle voie pour estimer les contributions de la photosynthèse et de la respiration à grande échelle. Ceci requiert néanmoins une meilleure compréhension des facteurs contrôlant l'activité de l'AC des sols. Nous avons étudié le rôle du pH du sol et des communautés microbiennes sur l'activité de l'AC. Nous avons testé l'hypothèse que l'activité de l'AC serait (H1) inhibée dans les sols acides, et que (H2) les échanges isotopiques CO_2-H_2O seraient réduits dans les sols alcalins. Nous avons également présumé que l'activité de l'AC serait (H3) positivement corrélée à l'abondance des microorganismes phototrophes, et que (H4) la structure des communautés affecterait différemment les flux de $CO^{18}O$ et d'OCS. Nos résultats valident H1 et H2. Ils montrent aussi que les flux de CO_2 dans le sol et l'activité d'AC associée sont positivement corrélés à l'abondance des microorganismes phototrophes (H3), tandis que le dépôt d'OCS dans les sols dépend de l'abondance des champignons (H4). Ces résultats sont en cours d'intégration dans un modèle de l'activité de l'AC des sols mondiaux, ce qui permettra une estimation robuste des flux globaux de photosynthèse et de respiration à partir de bilans atmosphériques de COS et $CO^{18}O$.

Mots clés : anhydrase carbonique, CO_2, $CO^{18}O$, OCS, microorganismes du sol, pH

[INRA, UMR 1391 ISPA, 71 avenue Édouard Bourlaux 33882 Villenave d'Ornon cedex]

Identifying the drivers of carbonic anhydrase activity in soils and its impact on soil-atmosphere exchanges of $CO^{18}O$ and OCS, two complementary tracers of the global carbon cycle

Abstract : Carbonic anhydrases (CA) are a group of enzymes that catalyse CO_2 hydration and OCS hydrolysis. The presence of CA in plants and soil microorganisms is responsible for the largest atmosphere-biosphere exchange of OCS but also $CO^{18}O$, because oxygen isotopes are exchanged with soil and plant water pools during CO_2 hydration. Consequently, $CO^{18}O$ and OCS atmospheric mixing ratios have been proposed as complementary tracers of the global C cycle that could open avenues to estimate the contribution of photosynthesis and respiration at global scales. However, a mechanistic understanding of the drivers of CA activity is required. We investigated the role of soil pH and microbial community on soil CA activity. We hypothesised that CA activity should be (**H1**) inhibited in acidic soils but that (**H2**) the associated CO_2-H_2O exchange would also be reduced in alkaline soils. We further assumed that (**H3**) soil CA activity would be enhanced by an increase in soil phototrophs abundance, but that (**H4**) soil community structure would affect differently $CO^{18}O$ and OCS fluxes. Our results confirmed **H1** and **H2**. We also confirmed that soil CO_2 fluxes and the associated CA activity were positively correlated with phototrophic communities abundance (**H3**), while soil OCS uptake and the associated CA activity seemed driven by fungal abundance (**H4**). These findings are now being incorporated into a model of soil CA activity worldwide that will allow robust estimates of photosynthesis and respiration at large scales from the atmospheric budgets of OCS and $CO^{18}O$.

Keywords : carbonic anhydrase, CO_2, $CO^{18}O$, OCS, soil microorganisms, pH

[INRA, UMR 1391 ISPA, 71 avenue Édouard Bourlaux 33882 Villenave d'Ornon cedex]

Remerciements

Ce travail de thèse, fruit de plus de trois ans d'investissement, n'aurait pu aboutir sans les précieuses collaborations professionnelles et personnelles de nombreuses personnes que je tiens aujourd'hui à remercier. La liste est longue de toutes celles et ceux qui ont partagé cette partie de ma vie et j'espère n'oublier personne.

Avec un profond respect je remercie les rapporteurs et examinateurs, Claire Rollion-Bard, Nick Ostle, Hans Schnyder et Matthias Cuntz de m'avoir fait l'honneur d'évaluer ce travail.

Mes remerciements s'adressent également tout particulièrement à Jérôme Ogée et Lisa Wingate qui m'ont donné la chance de vivre cette aventure et sereinement guidée au travers des méandres de la thèse. Merci à vous deux d'avoir toujours su être présents, jusque dans les toutes dernières secondes, et d'avoir gardé un œil bienveillant sur moi.

Je remercie également Pierre-Alain Maron pour ses qualités humaines et scientifiques qui, malgré les presque 700 kilomètres de distance, a su m'accompagner et répondre présent au moment où j'en ai eu besoin.

Merci à ceux qui ont accepté de participer à mes comités de thèse, qui m'ont ainsi suivi, régulièrement aidé, et qui ont toujours répondu présent lorsque je les ai sollicités. Merci donc à Jürgen Kesselmeier, Bernard Genty et Olivier Crouzet. Dans cette lignée je tiens aussi à remercier Laura Meredith pour ces conseils, les discussions et les échanges enrichissants que nous avons eu.

Je tiens à dire merci aussi à ceux que j'ai sollicités, même ponctuellement, que ce soit pour un coup de main sur mes manips (et par la même occasion jeter un œil à mon vélo) ou bien au détour de questions venues d'ailleurs mais qui nécessitaient une réponse imminente. Merci à ces personnes, qui pour certaines ne m'avaient jamais vue jusqu'à l'instant T et qui ont répondu présentes avec le sourire. Merci à Anne-Marie Bouchon, Anne Budynek, Bernard Genty, Didier Garrigou, Jérôme Jolivet, Kiki Kruszewski, Cathy Lambrot, Alain Mollier et Virginie Nowak.

Je remercie également chaleureusement tous les membres de l'équipe EcoFun, permanents ou de passage, qui ont de près ou de loin contribué à mon travail, toujours dans la bonne humeur et sans qui le bâtiment C1 serait d'une tristesse absolue. Un merci un peu particulier à Valérie qui a toujours gérée de mains de maitre, et avec le sourrire, les tourments de la paperasserie. Je n'oublie pas non plus celles qui sont déjà parties vers d'autres horizons, mais qui ont fait pour moi un travail titanesque. Noelia « 1 » (S.B.), Noelia « 2 » (F.P. ; les filles vous m'obligez à donner vos initiales avec vos prénoms identiques…) et Ana, a día de hoy hablo español igual de mal, pero vosotras os asegurasteis de que un montón de mis experimentos en el laboratorio salieran redondos.

Je tiens à adresser un immense et tout particulier merci aux membres du bureau n°149. Aurore, Sam, Thomas, soyons bien d'accord : je ne vous ai jamais choisis ! Mais avec du recul je peux vous l'avouer j'ai été plutôt chanceuse sur le tirage. Merci à tous les trois à la fois pour la multitude de discussions (plus ou moins enrichissantes) que nous avons eues, les moments de folie et l'abondance de nourriture ! Dans cette lignée je tiens également à adresser un immense merci à mes voisins de bureau. Merci à Teresa pour ton sourire quotidien, les pasteis de nata et tes conseils de statisticienne professionnelle. Merci à Steve pour ton aide sur plus ou moins toutes mes manips mais aussi pour tes bonnes astuces en terme d'utilisation de la carboglace. Je me demande toujours néanmoins comment une si petite personne peut avoir autant la voix qui porte ☺ Je suis heureuse d'avoir partagé tant de moments avec vous tous, au labo comme en dehors.

Une pensée et un grand merci aux membres de l'équipe de volley, ET PAN (dans le mur…), avec qui j'ai pu me défouler, parfois m'énerver mais surtout beaucoup rire et partager. Un merci particulier à Tovo, Delphine, David, Duff, Chipaux. Sans vous, c'est vrai, ça n'aurait quand même pas été pareil.

Mon foie et moi-même souhaitons également remercier tous les toquards de l'INRA. Zaza, Emma, Captain Yoyo, Jube, Grem's, Mathy, Arthur et le Minimoy, merci pour tous ces moments de partage, de rires, pour les parties de carte et de pétanques (il va falloir s'y remettre un peu d'ailleurs..), les dérapages (et pas uniquement à vélo) et les ratés que nous avons vécus.

Merci également au clan des casseurs de cailloux, avec qui toute cette histoire a commencé, et qui sont présents dans ma vie depuis quelques années déjà. Merci à mes amis de longue date, Valou, le Petit Homme et Grosboul, les derniers mohicans de la tribu grenobloise, mais aussi aux nouvelles pièces du puzzle, La Praline, Maxou, Nolwenn et toutes ces belles personnes que j'ai pu rencontrer, Mamel, Sarah, Thomas,...

Je ne sais comment dire merci à mes amis de toujours, inlassablement présents, qui m'obligent aujourd'hui, une fois n'est pas coutume, à placer Ardèche et Drôme sur un pied d'égalité. Cycy, Suzette, Cassoulet vous aurez toujours une place unique dans mon cœur. Je n'oublie pas non plus tous ceux, qui au fil des années, se sont greffés et qui comptent tout autant, Chach, Fabiche, Alex, Raph, Mom's.

Ce travail n'aurait pu arriver à son terme sans le soutien sans faille de ma famille. Merci Maman, Papa, Lélé, Papinou, Maminou et Mamie pour l'amour et la fierté que je peux lire dans vos yeux (attention point trop n'en faut !). Une note toute particulière pour toi Maman, pour tes coups de fils hebdomadaires qui sont pour moi d'une saveur unique, ton soutien inconditionnel de chaque minute et surtout pour tes œufs à la neige du tonnerre.

Enfin, merci à toi Thouin Thouin, pour toutes ces années passées à tes côtés (ou presque), pour m'avoir fait voyager et découvrir, toujours avec curiosité et malice, quelques richesses de ce monde…. et moult jeu de sociétés ! Merci aussi pour ton soutien de tous les jours qu'il n'est pas si facile de manifester mais qu'à ta manière tu sais parfaitement exprimer.

Table des matières

Table des matières

Chapitre 1 : Étude bibliographique

Introduction au chapitre 1

Cette étude bibliographique a pour but de faire un état des connaissances sur le cycle du carbone planétaire, ses incertitudes et les outils et méthodes actuelles pour nous aider à mieux le caractériser et le modéliser. Au regard des connaissances présentées, cette section débouche sur les grandes questions scientifiques qui ont animé cette thèse.

La première section de ce chapitre est naturellement consacrée à des rappels autour du cycle du carbone et spécifiquement à la perturbation apportée depuis plusieurs décennies par les activités humaines conduisant à la grande problématique actuelle du changement climatique. La deuxième section présente les différents outils développés pour suivre et modéliser ce cycle au niveau des écosystèmes terrestres, et notamment comment les bilans atmosphériques de $CO^{18}O$ et d'OCS permettent de contraindre le cycle du carbone et les échanges de CO_2 qui ont lieu entre le sol et l'atmosphère. Dans la troisième section, au regard du rôle central joué par l'anhydrase carbonique dans la compréhension des deux traceurs du cycle du carbone précités, les connaissances sur cette enzyme sont développées, notamment concernant son activité dans les sols. Enfin dans une dernière section les différents objectifs de ma thèse sont présentés.

1.1.Le cycle du carbone

1.1.1. Les grands réservoirs du cycle du carbone

Il y a sur Terre une quantité extrêmement importante de carbone qui est présent dans les océans, les sols, les réserves de carbone fossile, la roche mère, l'atmosphère et la biomasse végétale. On appelle cycle du carbone le déplacement du carbone, sous ses diverses formes, entre quatre grands réservoirs naturels que sont l'atmosphère, l'hydrosphère (mers, océans ou eaux continentales), la lithosphère et la biosphère (**Fig. 1.1**). Ces réservoirs stockent environ 800, 40 000, et 2300 GtC respectivement pour l'atmosphère, l'hydrosphère et la biosphère et sont caractérisés par des temps de résidence radicalement différents. Ces quatre réservoirs sont toutefois interconnectés et les principaux mécanismes d'échange de carbone sont la photosynthèse, la respiration et l'oxydation (réaction chimique et biologique).

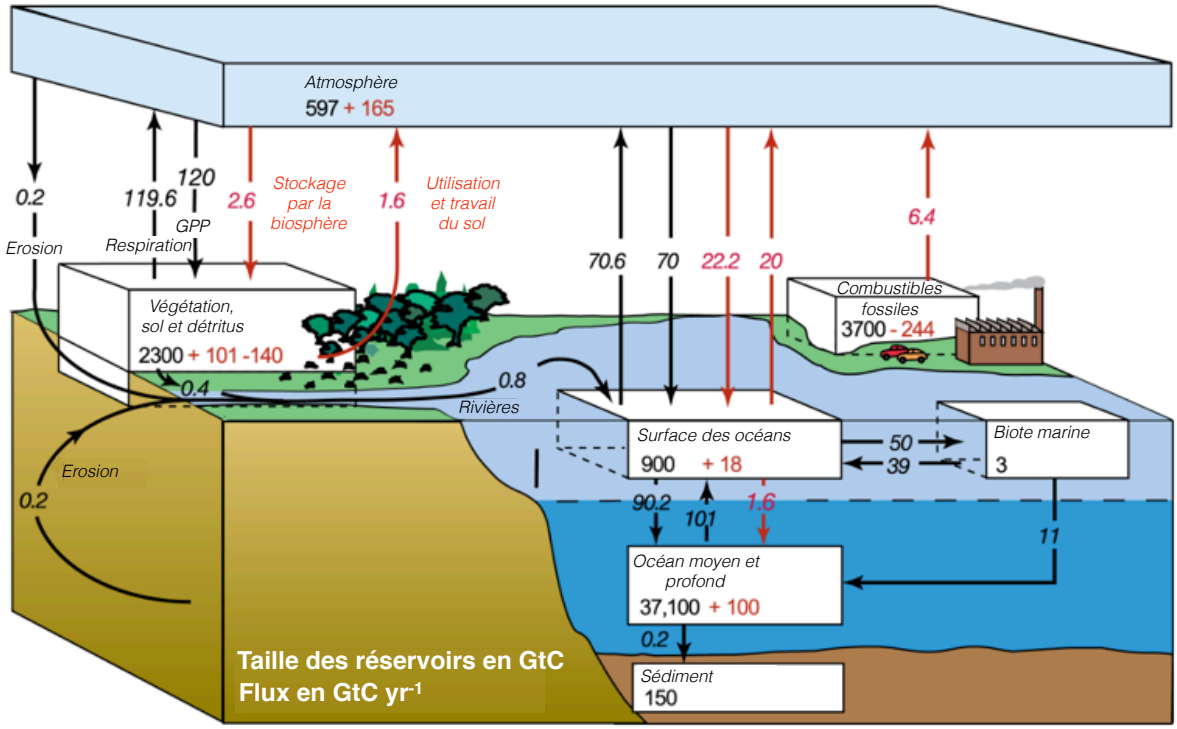

Figure 1.1 : Représentation simplifiée du cycle global du carbone (1990-2000) montrant les principaux flux annuels en GtC an^{-1} : les flux pré-industriels «naturels» en noir et flux «anthropiques» en rouge (modifiée d'après Denman et al., 2007, p. 515).

1.1.2. Approches top-down et bottom-up pour quantifier les flux nets de CO_2

Aux échelles de temps courtes qui nous intéressent ici (typiquement inférieures à la décennie), les échanges de carbone se font principalement entre l'atmosphère et l'hydrosphère ou l'atmosphère et la biosphère essentiellement sous la forme de CO_2 et de méthane (CH_4). Les flux nets de CO_2 entre l'atmosphère et les océans peuvent être estimés localement à l'aide de mesures directes de la pression partielle du CO_2 dans les eaux de surface (pCO_2) et d'un coefficient d'échange qui dépend de la vitesse du vent. Cependant, les fortes variations de la vitesse du vent ou des courants de surface limitent fortement la représentativité de ces mesures de pCO_2 pour estimer les flux de CO_2 océan-atmosphère à large échelle (Metzl et al., 1999). De même, la grande hétérogénéité spatiale de la biosphère continentale rend très locale les mesures d'échanges nets de CO_2 au-dessus des surfaces terrestres (Schmid, 1994). L'extrapolation des données mesurées *in situ* est une voie possible pour étendre la portée des données locales à des échelles régionales voire mondiales. Cette extrapolation de données s'appuie essentiellement sur des données satellitaires ou sur des proxys comme la température. La compilation de données de pCO_2 et leur extrapolation à l'aide d'un modèle océanique simple a par exemple permis de constituer une base de données climatologique de flux air-mer de CO_2 (Takahashi et al., 2002; Wanninkhof, 1992). Par ailleurs, l'utilisation de mesures directes de flux nets sur les continents pour valider des modèles de végétation comme ORCHIDEE (Krinner et al., 2005) a beaucoup aidé à apprécier les incertitudes liées à l'utilisation de ces modèles pour estimer des flux de CO_2 à large échelle. L'utilisation d'un modèle biogéochimique validé sur des observations directes et parfois aussi sur des reconstructions satellites est appelée l'approche montante (*bottom-up*). Les flux nets de CO_2 (océanique, biosphérique *etc.*) peuvent aussi être estimés par inversion de modèles de transport atmosphérique contraints par des mesures de concentrations de CO_2 dans l'atmosphère en différents points du globe (approches descendantes ; *top-down*). Les échelles spatiales représentées dépendent de la densité du réseau de mesures et vont généralement de l'échelle régionale à l'échelle mondiale.

Ciais et al. (2010) ont montré que dans l'hémisphère Nord l'estimation du puits terrestre de carbone était cohérente entre les approches dites « *top-down* » et « *bottom up* ». Toutefois ces auteurs ont souligné que (1) les résultats obtenus par inversion atmosphérique à l'hétérogénéité du réseau des stations atmosphériques ainsi qu'aux erreurs au sein des modèles de transport (*i.e.* forte variabilité quand au mélange vertical du CO_2) et que (2)

l'extrapolation des données mesurées *in situ* est biaisée par le manque de données concernant notamment les flux de carbone lié au transport latéral (flux aquatiques essentiellement).

Les transferts nets de CO_2 entre l'océan et l'atmosphère sont estimés pour la période 1990-2000 à 2.2 ±0.4 GtC an^{-1} et ceux entre la biosphère continentale et l'atmosphère à 2.6 ±0.7GtC an^{-1} (LeQuéré et al., 2010 ; voir aussi **Fig. 1.1**). Si ces deux compartiments présentent des capacités à stocker le CO_2 atmosphérique comparables en moyenne, le stockage du carbone par la biosphère continentale présente une bien plus forte variabilité interannuelle (**Fig. 1.2**). Cette forte variabilité interannuelle est due au fait que ce flux net de CO_2 biosphérique est le résultat d'un faible déséquilibre entre deux flux bruts de sens opposés (**Fig. 1.1**), qui eux-mêmes fluctuent avec le climat.

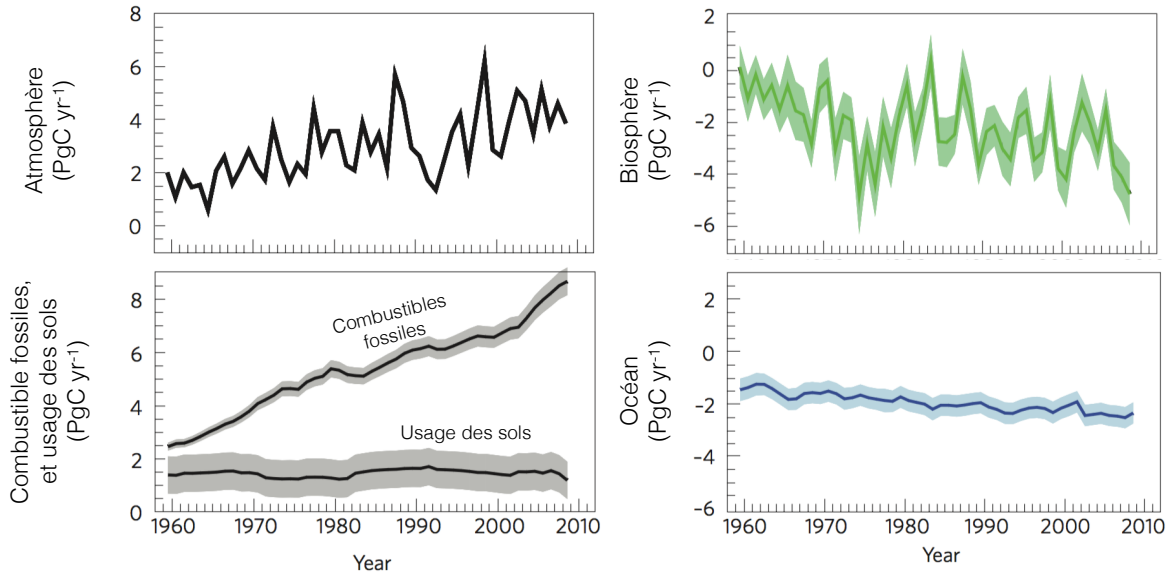

Figure 1.2 : Contributions respectives de l'océan (en bleu), de la biosphère (en vert ; sol et végétation), de l'atmosphère (en noir) et des combustibles fossiles / usage du sol (en gris) aux flux de CO_2 de 1960 à 2010 (modifiée d'après Le Quéré et al., 2009 et mise en évidence de la variabilité du stockage de carbone par la biosphère qui explique en grande partie les variabilités interannuelles du réservoir atmosphérique.

La biosphère continentale stocke néanmoins en moyenne près d'un quart des émissions anthropiques annuelles responsables du réchauffement climatique (**Fig. 1.1**). Ce stockage par la biosphère ralentit considérablement l'augmentation de la concentration du CO_2 atmosphérique. Si l'on souhaite appréhender et modéliser le devenir de ce puits de CO_2

biosphérique, il est donc important de bien comprendre les mécanismes qui gouvernent chacun des flux bruts sous-jacents.

1.1.3. Les échanges de CO_2 entre la biosphère continentale et l'atmosphère

Le terme de biosphère continentale en tant que réservoir de carbone englobe à la fois la végétation terrestre et les sols. Aux échelles de temps courtes qui nous intéressent (< 10 ans), les échanges de CO_2 les plus importants sont d'origine biochimique et émanent à la fois des végétaux et des sols. Au sein de la biosphère les végétaux se comportent le plus souvent comme un puits de CO_2. Les plantes absorbent le CO_2 *via* les stomates de leurs feuilles, le fixent puis le transforment en glucides grâce au processus de photosynthèse. Le flux brut de photosynthèse, au cours duquel est incorporé et hydraté le CO_2, est appelé productivité primaire brute (*Gross Primary Production* ou GPP). Détail qui aura son importance plus tard, la première étape de l'assimilation du CO_2 lors de la photosynthèse est une réaction d'hydratation réversible (Eq. 1), qui est catalysée par la présence d'une classe d'enzyme, les anhydrases carboniques :

$$H_2O + CO_2 \Leftrightarrow HCO_3^- + H^+ \quad (1)$$

L'enzyme principale de la photosynthèse reste néanmoins la RuBISCO, et celle-ci n'a pas que le CO_2 comme substrat mais peut aussi réagir avec le dioxygène (O_2) conduisant, par une suite de réactions en cascades, à une émission de CO_2 dénommée photo-respiration car n'ayant lieu qu'à la lumière. Une partie du CO_2 assimilé lors de la photosynthèse retourne aussi rapidement vers l'atmosphère lors de la consommation de glucides par la plante pour l'entretien et la croissance de ses tissus végétaux. Au final, seule une fraction des glucides formés est utilisée pour former de nouveaux tissus, séquestrant ainsi le carbone. La production primaire nette (*Net Primary Production* ou NPP) est la différence entre la productivité primaire brute et la respiration par les végétaux, aussi appelée respiration autotrophe (R_a) et incluant photo-respiration et respiration de croissance et d'entretien.

Les plantes peuvent aussi exsuder par leur racines une partie des sucres produits pendant la photosynthèse. Les racines fines, les feuilles et moins souvent les organes ligneux sont aussi régulièrement incorporés au sol sous forme de litière et sont ensuite dégradés par la microfaune du sol et des litières, constituant ce que l'on appelle la respiration hétérotrophe (R_h). Si l'on néglige les perturbations brutales (incendie, récolte, déforestation…) le flux net

de CO_2 entre un écosystème terrestre et l'atmosphère (*Net Ecosystem Exchange* ou *NEE*) est donc la résultante du flux de photosynthèse brute et des flux de respiration autotrophe et hétérotrophe :

$$NEE = R_a + R_h - GPP \quad (2)$$

Afin d'améliorer les projections à long terme des flux nets de CO_2, plusieurs méthodes ont été développées pour estimer chacun de ces flux bruts à grande échelle. La méthode dite des corrélations turbulentes (ou *Eddy Covariance*) permet de mesurer la *NEE* en mesurant la covariance temporelle entre les fluctuations turbulentes de la vitesse verticale du vent et celles de la concentration en CO_2 (Anav et al., 2015; Beer et al., 2010). Depuis presque 20 ans maintenant, la méthode des corrélations turbulentes a été utilisée sur plusieurs centaines d'écosystèmes de par le monde, pour caractériser les variations saisonnières et interannuelles de la NEE en relation avec le climat ou des perturbations anthropiques (récolte, éclaircies,…) ou suite à des évènements climatiques extrêmes (sécheresses, canicules, tempêtes, feux) (Baldocchi et al., 2001). Ce réseau d'observation a permis d'évaluer nos capacités à simuler la *NEE* à l'aide de modèles de surface continentale décrivant les transferts sol-végétation-atmosphère et le cycle du carbone associé (*e.g.* Krinner et al. 2005).

Au regard de l'Eq. 2, il est clair qu'une telle évaluation des modèles souffre d'un problème d'équi-finalité, car deux modèles peuvent prédire des flux bruts très différents mais des *NEE* similaires. Malheureusement l'estimation des flux bruts (R_a, R_h ou *GPP*) est encore plus difficile à mener à l'échelle de l'écosystème car les mesures directes de ces flux s'effectuent à l'échelle de la placette (R_h) ou de l'organe végétal (R_a, *GPP*). Face à la perturbation anthropique que nous connaissons et en vue d'une augmentation de la fréquence des évènements climatiques extrêmes, comprendre les mécanismes régulant le stockage du carbone par la biosphère (*i.e.* photosynthèse *versus* respiration) est indispensable pour connaitre, et prédire, la dynamique du carbone global.

1.1.4. La perturbation du cycle du carbone par les activités anthropiques et les conséquences sur le changement climatique

Depuis plusieurs millénaires, la concentration atmosphérique du CO_2 était stable, autour de 280 ppm. Les résultats des sondages glaciaires ont montré que depuis le début du second millénaire et jusqu'en 1800 la concentration en CO_2 atmosphérique fluctuait de plus ou moins 10 ppm. Ces variations sont 10 fois plus faibles que la perturbation de plus de 120 ppm apparue depuis seulement un siècle. La concentration en CO_2 atmosphérique est passée d'environ 280 ppm en 1750 (Joos and Spahni, 2008) à presque 400 ppm en 2014 (Dlugokencky and Tans., 2015; Le Quéré et al., 2015). Avec la vapeur d'eau et le méthane, le CO_2 est l'un des plus importants gaz à effet de serre. Bien qu'il soit responsable de moins d'un quart de l'effet de serre (Schmidt et al., 2010), son temps de résidence dans l'atmosphère est bien plus grand que celui de la vapeur d'eau (responsable à elle seule de près de 60 % de l'effet de serre ; Jacobson, 2005). Ainsi, la perturbation de la teneur en CO_2 dans l'atmosphère, même ponctuelle, peut avoir des conséquences à long terme sur le climat.

L'essentiel du réchauffement climatique observé aujourd'hui est dû aux concentrations croissantes des gaz à effet de serre dans l'atmosphère en lien avec l'activité anthropique (IPCC, 2013). L'occupation de la Terre par l'Homme est de plus en plus dense et les révolutions industrielles ont modifié la composition de notre air. La combustion de ressources fossiles entraîne la libération d'une grande quantité de carbone (9 GtC an^{-1}, IPCC, 2013) tout comme la déforestation notamment accrue dans les zones tropicales.

L'augmentation de la concentration en CO_2 atmosphérique engendre une hausse de la température de surface sur Terre qui risque également d'amplifier les contrastes climatiques déjà existants (IPCC, 2013). D'après ce rapport d'expertise et les simulations du climat futur existantes, les régions humides seront davantage soumises aux pluies et les régions les plus sèches le seront encore plus. Ce réchauffement climatique risque également de jouer sur les évènements météorologiques extrêmes. Ainsi sécheresses et moussons seraient à la fois plus intenses et plus fréquentes.

1.1.5. Problématiques actuelles

Les modèles de biosphère continentale (*e.g.* Cramer et al., 2001; Krinner et al., 2005; Sellers et al., 1996) permettent de représenter et de prédire les flux nets de CO_2 dans le continuum sol-végétation-atmosphère. Ils intègrent à la fois des processus biogéochimiques, biophysiques et biogéographiques. Bien que les flux nets de CO_2 actuels soient souvent bien prédits par ces différents modèles, leurs projections futures sont par contre extrêmement variables d'un modèle à l'autre (**Fig. 1.3**, Friedlingstein et al., 2006). Cette incertitude est essentiellement due aux différentes paramétrisations des flux de photosynthèse et de respiration utilisées dans les modèles et de leurs réponses à la hausse de la concentration du CO_2 et de la température. Pour trouver un accord à ces projections il est essentiel de séparer les flux nets de CO_2 en flux de photosynthèse et de respiration afin d'évaluer la capacité des modèles à représenter ces deux flux bruts de sens opposés. Mes travaux de thèse, bien que très en amont, s'inscrivent pleinement dans cette démarche.

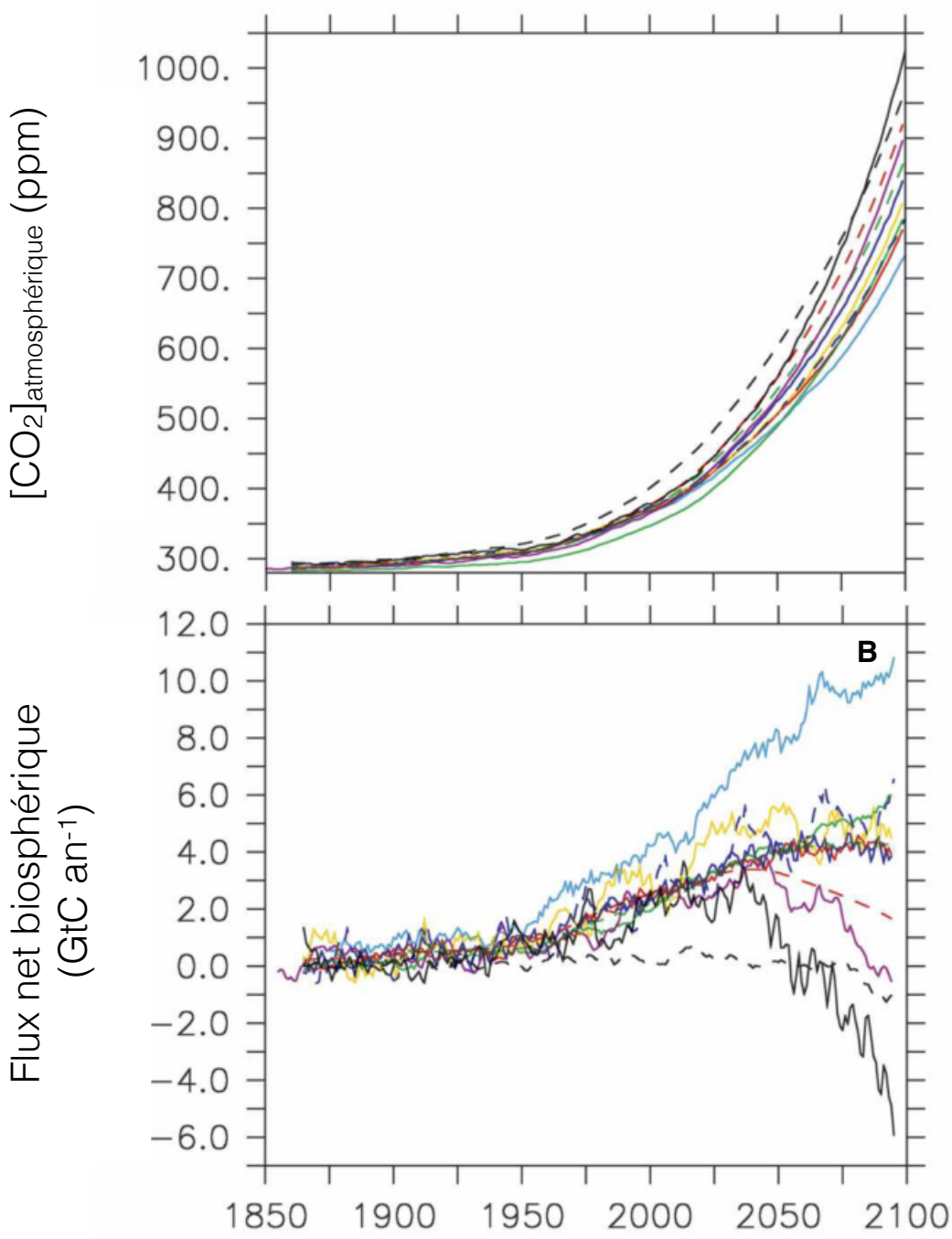

Figure 1.3 : Prédiction de l'évolution A) de la concentration atmosphérique du CO_2 et B) du flux net biosphérique de CO_2 issu de la surface continentale, incluant les signaux du sol et de la végétation, en GtC.an-1 selon 11 modèles globaux différents (modifiée d'après Friedlingstein et al., 2006).

La variabilité observée dans les prédictions de la GPP est essentiellement due à notre incapacité à intégrer et interpréter séparément les flux de photosynthèse et de respiration. Améliorer notre compréhension du comportement des puits et des sources de carbone dans la biosphère, fortement affectés par les changements climatiques (Pan et al., 2011; Piao et al., 2008) représente donc un enjeu actuel majeur pour la communauté scientifique (Friedlingstein et al., 2006; Piao et al., 2013) et est nécessaire, plus largement, pour conseiller et informer la société civile et les pouvoir publiques qui doivent prendre des mesures pour faire face à ces changements. Pour répondre à ces questions et utiliser correctement les outils de modélisation, de nouvelles informations sont nécessaires afin de déterminer le comportement de la biosphère vis-à-vis du réchauffement climatique. Pour cela une solution présentant un fort potentiel est d'observer des gaz qui partagent des mécanismes communs avec les flux de CO_2 mais qui permettent de mieux distinguer les flux de photosynthèse et de respiration pour perfectionner nos estimations de la GPP. Par exemple les isotopes stables de l'oxygène ($CO^{18}O$) portent des signatures isotopiques qui permettent de différencier les flux de GPP des flux de respiration, et l'oxysulfure de carbone (OCS) est considéré comme un analogue du CO_2 et partage à l'échelle de la feuille, des mécanismes communs lors de la photosynthèse à la différence qu'il n'est pas réémis dans l'atmosphère.

1.2. Le $CO^{18}O$ et l'OCS, deux traceurs complémentaires des flux de CO_2 biosphériques

1.2.1. La signature isotopique en oxygène, définitions et notations

L'élément oxygène possède trois isotopes stables (^{16}O, ^{17}O et ^{18}O), la forme ^{16}O étant de loin la plus abondante. Les molécules d'eau ou de CO_2 sont ainsi composées en majorité d'atomes d'oxygène ^{16}O, mais contiennent aussi quelques atomes plus lourds donnant des molécules du type $H^{17}O^{16}O$ ou $C^{17}O^{16}O$ (typiquement 0.004% en abondance naturelle) ou $H^{18}O^{16}O$ ou $C^{18}O^{16}O$ (autour de 0.2% en abondance naturelle). Ces différentes molécules sont appelées isotopologues. Pour la suite nous nous concentrerons uniquement sur les molécules d'eau et de CO_2 contenant des molécules d'oxygène de type ^{16}O et ^{18}O, les molécules de type ^{17}O étant actuellement mesurées avec encore beaucoup d'incertitudes.

On appelle « composition isotopique » le rapport (R) entre isotope lourd et isotope léger. Parce que les variations de composition isotopique dans l'environnement sont

généralement faibles, on les exprime comme un écart à la composition isotopique d'un standard international (R_s) : c'est la notation δ (Eq. 3) souvent exprimée en pour mille (‰).

Pour les isotopes de l'eau, le standard international est le Vienna Standard Mean Ocean Water (VSMOW), un mélange d'eaux océaniques distillées provenant de plusieurs points à la surface du globe, stocké à l'IAEA à Vienne. Son rapport isotopique $^{18}O/^{16}O$ est de 0.2005%. Par définition, la valeur de $\delta^{18}O$ de ce réservoir est donc de 0‰ VSMOW et celle de tout autre réservoir est calculé suivant :

$$\delta = \frac{R}{R_s} - 1 \quad (3)$$

Dire qu'un réservoir A est enrichi par rapport à un réservoir B, signifie que A possède une plus grande concentration en isotopes lourds que B : $\delta_A > \delta_B$.

1.2.1.1. Le fractionnement isotopique

Les différents isotopologues de l'eau et du CO_2 ont des masses et des symétries différentes. En conséquence, au cours de la plupart des processus physico-chimiques, apparait un fractionnement isotopique, *i.e.* une modification de la composition isotopique. Par exemple, lors de l'évaporation d'un réservoir d'eau, les molécules les plus lourdes se concentrent dans la phase la plus condensée (liquide), en raison d'une pression de vapeur saturante plus faible pour les isotopes lourds. A l'équilibre thermodynamique, ce fractionnement dépend uniquement de la température et diminue pour des températures élevées. Un autre exemple de fractionnement est celui qui s'opère lors de la diffusion des gaz. Du fait de la différence de masse et des sections de collision des différents isotopologues, la diffusivité moléculaire induit un fractionnement isotopique par lequel les molécules lourdes diffusent moins vite que les molécules légères.

1.2.1.2. Distribution spatiale du $\delta^{18}O$ des précipitations

La composition isotopique des eaux météorites (précipitations) à l'échelle planétaire s'explique par ces fractionnements isotopiques liés au changement de phase (évaporation, condensation), combinés aux gradients de température subis par une masse d'air (**Fig. 1.4**). Ceci aboutit à la distribution zonale du $\delta^{18}O$ avec une composition de plus en plus pauvre vers les hautes latitudes (**Fig. 1.4B**). Lorsqu'une masse d'air se dirige des basses latitudes vers les

pôles la température diminue, l'humidité spécifique à saturation aussi donc une partie de la vapeur condense et précipite. Les isotopes lourds se concentrent dans la phase la plus condensée et quittent la masse d'air par précipitation. Les évènements successifs de condensation et de précipitation résultent en un appauvrissement progressif de la masse d'air au cours de son transport vers les pôles (**Figs. 1.4A et 1.4B**). En conséquence, et sous l'action aussi du refroidissement de la masse d'air, l'appauvrissement des précipitations en provenance de cette masse d'air s'accélère au fur et à mesure de son transport vers les pôles (**Fig. 1.4B**). Ceci explique la distribution zonale de la composition isotopique, mais aussi l'appauvrissement des précipitations avec l'altitude ou la continentalité comme par exemple sur le continent eurasiatique (**Fig. 1.4B**). Les masses d'air peuvent aussi se recharger en vapeur d'eau et s'enrichir de nouveau du fait de l'évaporation (sur les océans) ou l'évapotranspiration sur les continents (**Fig. 1.4B**). Au dessus des continents, une partie des précipitations est définitivement perdue sous forme de ruissellement.

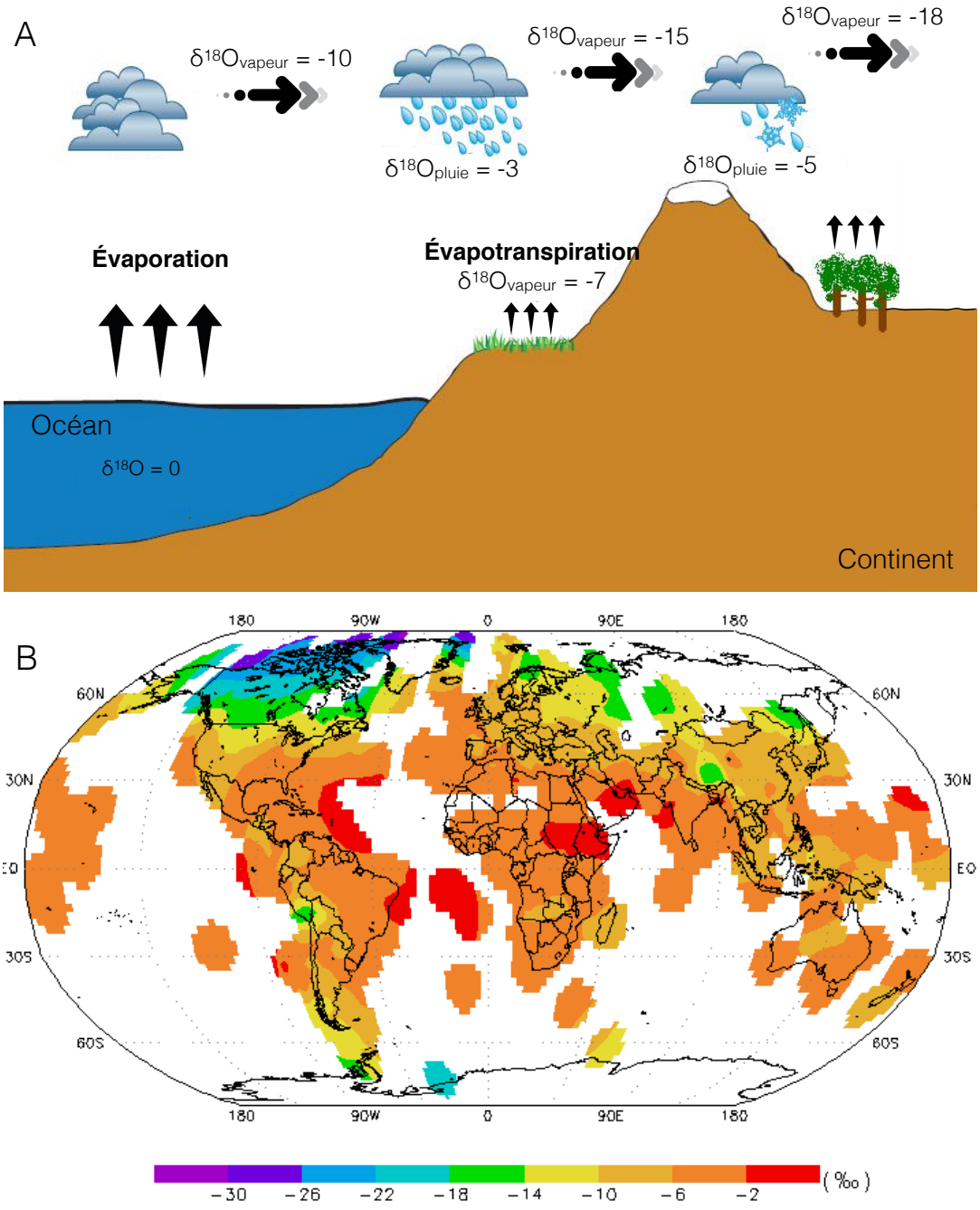

Figure 1.4 : A) Schéma illustrant les processus de fractionnement isotopique par évaporation, condensation et évapotranspiration (modifiée d'après http://serc.carleton.edu), B) Distribution spatiale de la composition isotopique des précipitations, collectée sur les stations du réseau international GNIP (modifiée d'après http://www-naweb.iaea.org/napc/ih/documents/userupdate/Waterloo).

1.2.1.3. Le $CO^{18}O$: un traceur des changements environnementaux

La distribution spatiale de la composition isotopique des précipitations se retrouve en grande partie dans les pools d'eau des plantes et des sols, et interagit avec le CO_2 durant son hydratation (Eq. 4) :

$$CO_2 + H_2{}^{18}O \leftrightarrow CO^{18}O + H_2O \quad (4)$$

De manière simplifiée, et du fait de la forte abondance des molécules d'eau par rapport aux molécules de CO_2, on peut dire que la composition isotopique du CO_2 qui a interagit avec le sol ou les feuilles porte les signatures des ces pools d'eau. Les feuilles et le sol portent des signatures isotopiques très différentes (**Fig. 1.5**). Les pools d'eau contenus dans les feuilles étant généralement plus petits que ceux du sol et l'évaporation proportionnellement plus grande, l'accumulation des molécules de $H_2{}^{18}O$ y est plus rapide (Dongmann et al., 1974; Farquhar and Cernusak, 2005). La signature isotopique de l'oxygène des feuilles est alors enrichie en ^{18}O par rapport à celle du sol. Le flux de CO_2 entre les feuilles et l'atmosphère sera donc généralement enrichi par rapport au flux de CO_2 en provenance du sol.

La variabilité du signal porté par les isotopes stables de l'oxygène du CO_2 constitue un outil très intéressant pour évaluer les contributions respectives de la photosynthèse et de la respiration à l'échange net de CO_2 entre un écosystème et l'atmosphère, que ce soit à l'échelle de l'écosystème (Bowling et al., 2003; Ogée et al., 2004; Yakir and Wang, 1996), ou jusqu'à l'échelle globale (Cuntz, 2003; Farquhar et al., 1993; Peylin et al., 1999; Yakir and Wang, 1996). Les travaux de la bibliographie dans ce domaine montrent bien l'intérêt de ces outils isotopiques pour améliorer notre compréhension du cycle du carbone en partitionnant les flux de photosynthèse et de respiration.

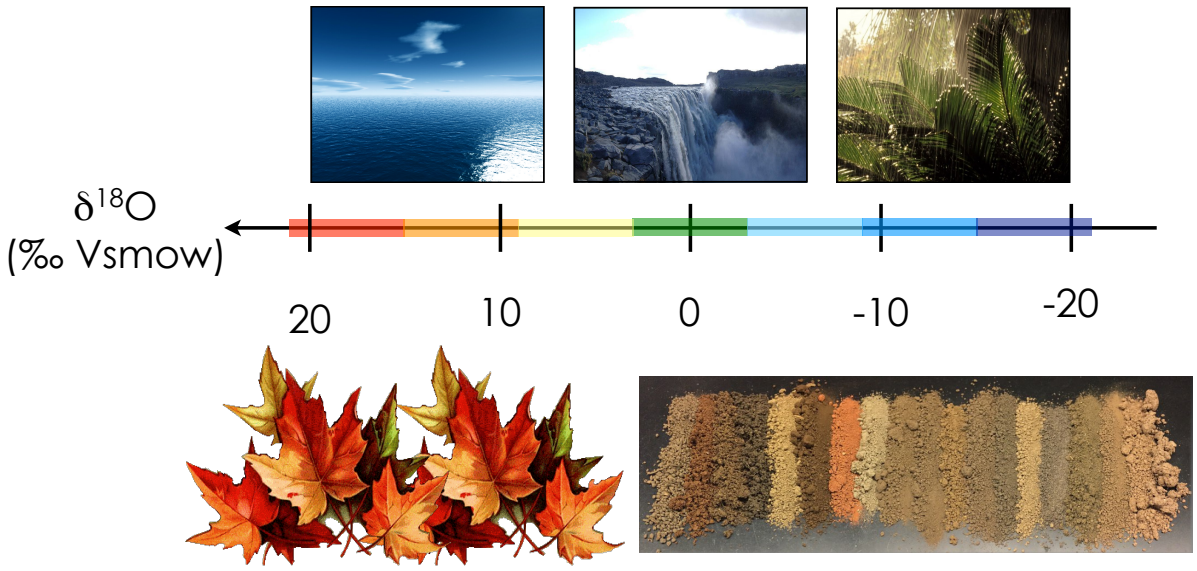

Figure 1.5 : Schéma récapitulatif des signatures de l'oxygène 18 de l'eau dans les feuilles et les sols.

1.2.2. L'oxysulfure de carbone (OCS)

1.2.2.1. Le cycle global de l'OCS

L'oxysulfure de carbone (OCS) est une molécule à structure linéaire (O=C=S). C'est le gaz soufré le plus abondant dans l'atmosphère avec un rapport de mélange relativement stable de nos jours, autour de 500 ppt. L'OCS est un gaz à effet de serre 700 fois plus puissant que le CO_2. Mais son potentiel est en partie compensé par la présence massive de dioxygène, qui dégrade rapidement l'OCS par photolyse, produisant des aérosols soufrés qui renvoient vers l'espace une partie du rayonnement infrarouge solaire (Brühl et al., 2012; Crutzen, 1976; Kettle, 2002).

L'océan est la principale source d'OCS, avec les rejets anthropiques, le volcanisme et les sols lorsqu'ils sont anoxiques (**Fig. 1.6**). L'OCS est également issu indirectement de l'oxydation dans l'atmosphère de sulfure de diméthyle (DMS) et de disulfure de carbone (CS_2) dégazés depuis l'océan. L'absorption de l'OCS atmosphérique se fait essentiellement par la végétation et les sols (**Fig. 1.6**).

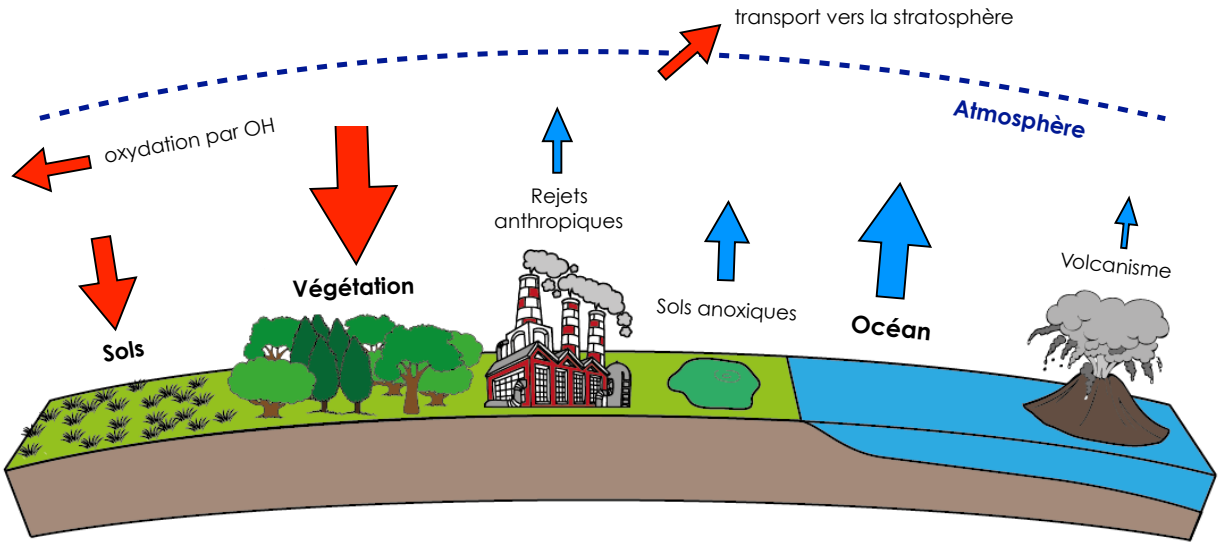

Figure 1.6 : Schéma récapitulatif des principales sources et principaux puits d'OCS.

1.2.2.2. Évolution de la concentration atmosphérique de l'OCS de l'Archéen à nos jours

A l'Archéen, une Terre « boule de neige » (*snowball Earth*) a été évitée essentiellement grâce aux teneurs importantes d'OCS dans l'atmosphère (Ueno et al., 2009). A cette époque, les concentrations en OCS étaient de l'ordre de 1 à 10 ppm, principalement du fait de l'intensité du volcanisme. A de telles concentrations l'OCS était alors le principal gaz à effet de serre et a permis le maintien d'eau liquide à la surface de la Terre. L'émission massive d'O_2 par les êtres vivants a plus tard été à l'origine de l'oxydation de l'OCS et donc de la forte diminution de sa concentration dans l'atmosphère.

Au cours des périodes plus récentes, le taux de mélange de l'OCS dans l'atmosphère a été relativement stable (Aydin et al., 2008). Cependant, depuis le milieu du 19^{ième} siècle et le début de l'ère industrielle, la concentration atmosphérique d'OCS a fortement augmenté (Montzka et al., 2004). Les rejets anthropiques d'OCS, mais aussi de disulfure de carbone (CS_2) qui peut s'oxyder en OCS, n'ont fait qu'augmenter la concentration et le rapport de mélange de l'OCS dans l'atmosphère (Stern et al., 2001).

Depuis les années 2000 le rapport de mélange de l'OCS dans l'atmosphère semble s'être stabilisé aux alentours de 500 ppt mais avec un cycle saisonnier dans l'hémisphère Nord encore plus marqué que pour le CO_2 (**Fig. 1.7**). Sur les quatre sites de mesure de la NOAA (*National Oceanic and Atmospheric Administration*) présentés **Figure 1.7**, ceux du Pôle Sud

et de *Mauna Loa* sont majoritairement sous l'influence océanique tandis que les stations de *MaceHead* et *Alert* sont plutôt sous influence continentale. Il en résulte que les teneurs en OCS dans les stations du Pôle Sud et de Mauna Loa sont plus élevées (car directement au contact de la principale source d'OCS) et que les cycles saisonniers sont plus marqués dans les stations de *MaceHead* et *Alert* du fait de l'impact de l'absorption d'OCS par la végétation et les sols.

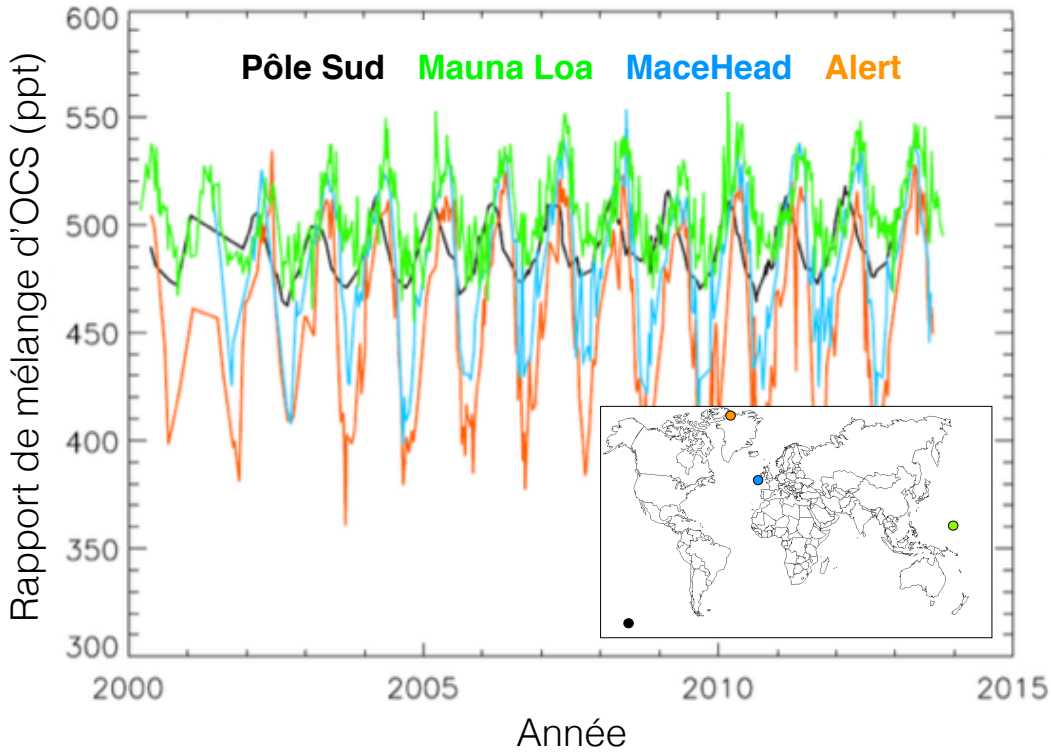

Figure 1.7 : Taux de mélange et cycles saisonniers de l'OCS de 2000 à 2013 relevés dans quatre stations de la NOAA. Les sites nommés Pôle Sud et Mauna Loa sont sous influence océanique tandis que ceux appelés MaceHead et Alert sont principalement sous influence continentale (cf. carte de localisation).

1.2.2.3. Pourquoi l'OCS pour contraindre les flux de photosynthèse ?

L'OCS est considéré comme un analogue du CO_2. En effet, dans l'hémisphère Nord les teneurs atmosphériques en OCS et CO_2 montrent une variabilité saisonnière quasiment en phase. La concentration en CO_2 montre cependant à long terme, une tendance à la hausse, alors que les teneurs en OCS restent plus ou moins constantes. Cette concordance entre les cycles saisonniers du CO_2 et de l'OCS provient du fait que ces deux molécules sont absorbées

par la biosphère. En effet toutes deux sont diffusées dans la plante au travers des stomates, et rencontrent la même première enzyme, l'anhydrase carbonique (AC), qui catalyse l'hydratation du CO_2 (Eq. 5) et l'hydrolyse de l'OCS (Eq. 6). La différence majeure entre ces deux réactions est que l'hydratation du CO_2 est une réaction réversible, une partie peut donc être renvoyée vers l'atmosphère, tandis que l'hydrolyse de l'OCS est irréversible.

$$CO_2 + H_2O \leftrightarrow H^+ + HCO_3^- \quad (5)$$

$$OCS + H_2O \rightarrow H_2S + CO_2 \quad (6)$$

Dans ce contexte, on comprend mieux que les variations spatiales et temporelles de la concentration atmosphérique d'OCS peuvent être utilisées comme une nouvelle contrainte pour améliorer la représentation actuelle de la GPP dans les modèles du cycle du carbone planétaire.

1.2.3. Adaptation des outils $CO^{18}O$ et OCS au sol

Si les mécanismes régissant les échanges de $CO^{18}O$ et d'OCS entre la végétation et l'atmosphère sont relativement bien compris (Barbour et al., 2007; Farquhar and Cernusak, 2005; Kesselmeier and Hubert, 2002; Lai et al., 2008; Sandoval-Soto et al., 2005; Seibt et al., 2009; Stimler et al., 2010; Welp et al., 2008), ceux régissant les échanges gazeux de CO_2 et d'OCS entre le sol et l'atmosphère sont encore mal connus (Van Diest and Kesselmeier, 2008; Kesselmeier et al., 1999; Maseyk et al., 2014; Seibt et al., 2006; Whelan et al., 2013; Wingate et al., 2008, 2009). Cette incertitude sur les flux de $CO^{18}O$ entre le sol et l'atmosphère est une limitation majeure pour quantifier les flux bruts de photosynthèse et de respiration (Francey and Tans, 1987; Cuntz et al. 2003; Hoag, 2005; Stern et al., 2001; Welp et al., 2011; Wingate et al., 2008, 2009, 2010; Buenning et al. 2011). Les connaissances sur les flux d'OCS par les sols sont encore plus disparates. Il s'est avéré que le sol pouvait aussi bien être un puits (Van Diest and Kesselmeier, 2008; Kesselmeier et al., 1999; Kettle, 2002; Kuhn et al., 1999) qu'une source d'OCS (Maseyk et al., 2014; Whelan et al., 2013; Yi et al., 2008). De ce fait les échanges d'OCS entre le sol et l'atmosphère sont décrits dans les modèles de manière encore assez grossière :

- Kesselmeier et al. (1999), Kettle et al. (2002) puis Van Diest & Kesselmeier. (2008) ont décrit l'absorption de l'OCS par les sols à l'aide d'une relation paramétrique où intervenait la teneur en eau et la température du sol. Si l'optimum

de teneur en eau semblait assez semblable entre les différents sols, l'optimum de température et l'amplitude du flux semblait varier fortement d'un sol à l'autre sans explication apparente, rendant l'utilisation du modèle à large échelle problématique.

- Belviso et al. (2013) puis Launois et al. (2015) ont proposé d'utiliser la proportionnalité entre les vitesses de dépôt au sol de l'OCS et de l'hydrogène (H_2) observé sur un site, qu'ils ont combiné à des cartes de dépôt d'H_2 à l'échelle planétaire. Cette approche souffre cependant de la généralité du coefficient de proportionnalité utilisé, et de la validité des cartes de dépôt d'H_2 disponibles.
- Yi et al. (2007) et Berry et al. (2013) ont corrélé les flux d'absorption d'OCS à la respiration hétérotrophe du sol, qui résulte de l'activité microbienne du sol. Cette relation de proportionnalité semble cependant varier d'un sol à l'autre, ce qui rend difficile son extrapolation à l'échelle planétaire.

Finalement, aussi bien pour le $CO^{18}O$ que pour l'OCS, une question fondamentale aujourd'hui consiste à comprendre et appréhender l'activité de l'anhydrase carbonique dans les sols et les raisons de sa variabilité.

1.3. L'anhydrase carbonique : une enzyme au cœur des questions

1.3.1. Les familles d'anhydrase carbonique

L'anhydrase carbonique (AC) est une enzyme connue depuis le début des années 1930. Une enzyme, de manière très générale, est une protéine qui agit comme catalyseur biochimique, un agent qui change la vitesse d'une réaction mais qui ne change pas avec la réaction. Purifiée pour la première fois à partir d'érythrocytes bovins (Stadie and O'Brien, 1933) l'AC est depuis l'une des enzymes les mieux caractérisées. On retrouve abondamment l'anhydrase carbonique à divers niveaux trophiques, autant chez les eucaryotes que les procaryotes. Il existe à ce jour trois grandes familles connues d'anhydrases carboniques appelées α, β, et Υ (Smith et Ferry 1999), mais il existe aussi d'autres familles plus rares appelées δ, ε, ζ. La classe α est principalement associée aux mammifères, néanmoins on la retrouve chez certaines plantes et procaryotes (Tripp et al., 2001). La famille d'anhydrases carboniques β se retrouve principalement chez les plantes, les algues, mais aussi chez la bactérie *E. coli* et chez certaines archéobactéries comme *Methanobacterium thermoautotrophicum* (Cronk et al., 2001; Mitra, 2004; Smith and Ferry, 1999). Les

anhydrases carboniques de type ϒ se retrouvent principalement dans le règne des archéobactéries. Il s'agirait de l'une des anhydrases carboniques les plus anciennes, datant d'au moins 3 milliards d'années (Liljas and Laurberg, 2000).

1.3.2. L'AC essentielle aux réactions d'hydratation du CO_2 et d'hydrolyse de l'OCS

Chez les mammifères, l'AC participe à de nombreux processus biologiques tels que la respiration ou l'acidification tubulaire rénale (Hewett-Emmett and Tashian, 1996). Chez la plante elle contribue activement au processus de photosynthèse, notamment en favorisant les transferts du CO_2 à travers les parois cellulaires (Fridlyand and Kaler, 1987). Derrière tous ces processus biologiques se cache en fait la catalyse de la réaction d'hydratation du CO_2 par l'AC (**Fig. 1.8**). Le cycle catalytique des différentes anhydrases repose toujours sur la présence d'un atome métallique au sein du site actif. Le principal atome est le zinc, bien qu'il puisse parfois être remplacé par d'autres métaux comme le cobalt ou le fer (Tripp, 2003; Tripp et al., 2001). La catalyse de la réaction d'hydratation d'une molécule de CO_2 débute par l'activation de l'atome de zinc de l'AC par une molécule d'eau ce qui engendre la formation d'un hydroxyde de zinc, un nucléophile plus puissant que le résidu d'histidine présent précédemment. Le carbone d'une molécule de CO_2, possédant une charge partielle positive subit par la suite une attaque nucléophile par l'oxygène du zinc activé. Le produit de l'attaque nucléophile n'est autre qu'un ion bicarbonate (HCO_3^-) lié au zinc métallique. Pour que cet ion bicarbonate diffuse hors du site actif il faut qu'une seconde molécule d'eau vienne prendre sa place, régénérant ainsi le site actif (Lindskog, 1997). Cette réaction est réversible et aboutit à un état d'équilibre que la catalyse enzymatique ne change pas

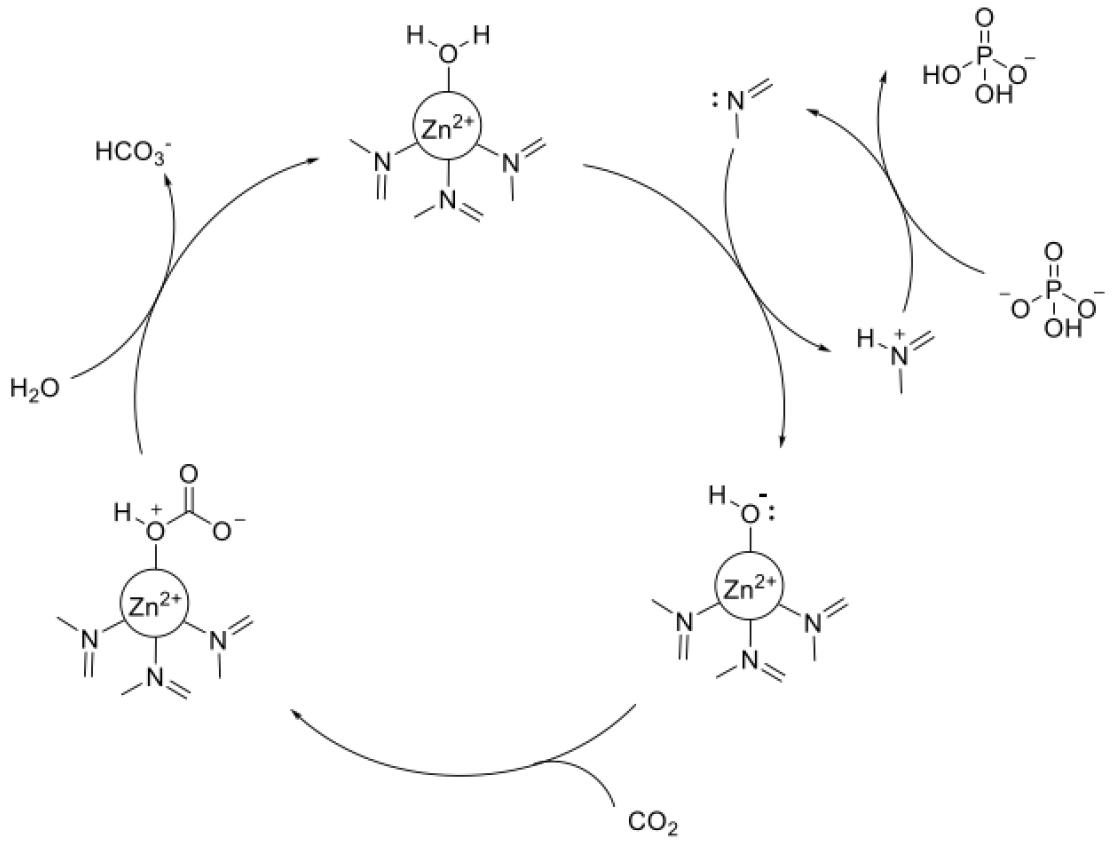

Figure 1.8 Cycle d'activation de l'anhydrase carbonique : dé-protonation de l'enzyme puis conversion du CO_2 en bicarbonate puis réactivation dite « active » via un ion extérieur.

Tout comme elle catalyse l'hydratation des molécules de CO_2, l'AC catalyse l'hydrolyse des molécules d'OCS suivant l'équation 4 décrite précédemment. Néanmoins les mécanismes d'activation de l'AC avec l'OCS ne sont à ce jour pas encore bien caractérisés, mais il semblerait que la régénération de l'enzyme se fasse comme pour le cas du CO_2 à l'aide d'une nouvelle molécule d'eau (Notni et al., 2007).

1.3.3. Quels moteurs pour expliquer les variations d'activité de l'AC ?

L'activité de l'AC d'un sol peut être estimée à l'aide de mesures des échanges $CO^{18}O$ et de la composition isotopique de l'eau du sol (Wingate et al., 2008, 2009, 2010). En effet lors des réactions d'hydratation du CO_2 avec les pools d'eau les isotopes de l'oxygène sont également échangés et ces échanges sont eux aussi catalysés par la présence d'AC. En pratique, les approches isotopiques utilisées pour estimer l'activité de l'AC du sol impliquent l'inversion de modèles des isotopologues du CO_2 dans la colonne de sol afin d'estimer le taux

d'échange isotopique pendant la réaction d'hydratation (Seibt et al., 2006; Wingate et al., 2009). Néanmoins, ce n'est que récemment que des études ont démontré la nécessité de tenir compte de l'activité de l'AC pour expliquer, et reproduire, les flux de $CO^{18}O$ observés *in situ* et/ou en laboratoire (**Figure 1.9** ; Seibt et al., 2006; Wingate et al., 2009, 2010). Les résultats des simulations ont aussi indiqué que la prise en compte de l'activité de l'AC pouvait fortement affecter les bilans globaux de $CO^{18}O$, les estimations de la GPP ainsi que le signal isotopique du CO_2 du sol (Wingate et al., 2009; Welp et al. 2011; Buenning et al. 2011). Pourtant actuellement la prévalence et la fonction de ces enzymes dans les sols sont mal comprises. Il a été montré que la distribution de l'activité de l'AC du sol sur le globe variait de manière non négligeable en fonction des environnement ou climat ou elle avait été mesurée. En effet, cette enzyme semble 15 fois moins active dans des environnements type tempérés et boréaux que des climats méditerranéens et subtropicaux (Wingate et al., 2009). Approfondir nos connaissances sur les paramètres responsables de la variabilité de l'activité de l'AC est une priorité pour mieux comprendre et contraindre les flux bruts de photosynthèse et de respiration et ainsi mieux appréhender le cycle mondial du carbone.

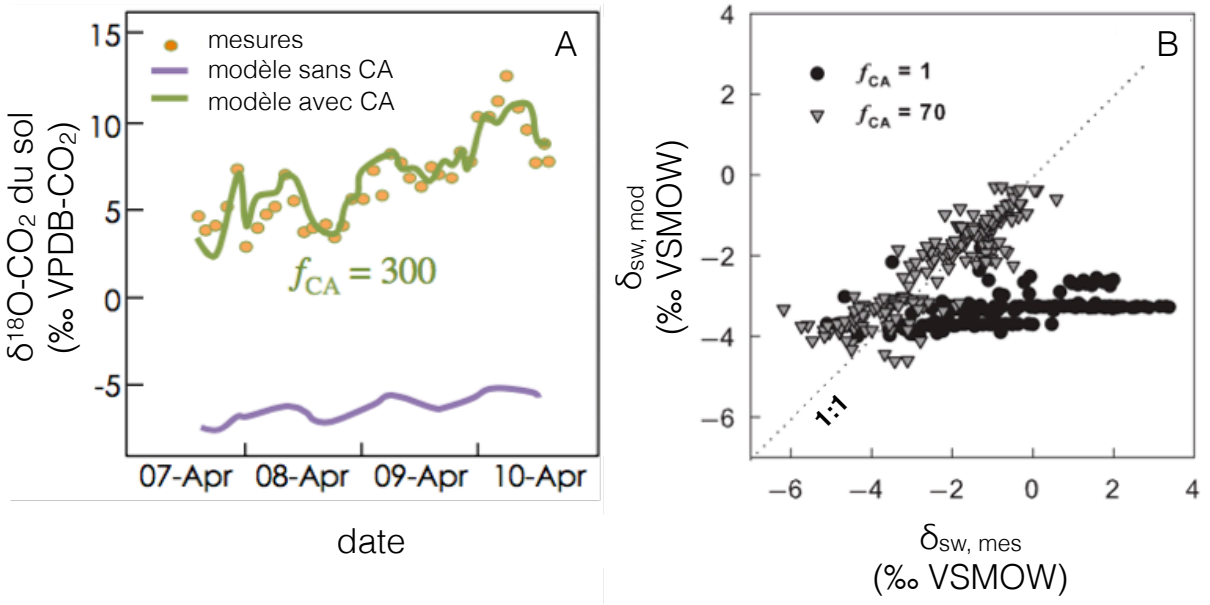

Figure 1.9 : A) Mesure in situ des flux de $CO^{18}O$ échangés entre le sol et l'atmosphère et modélisation de ce même signal avec (courbe verte) et sans (courbe violette) activité d'anhydrase carbonique dans le sol (modifiée d'après Wingate et al., 2008) B) Relation entre mesure et modélisation du signal isotopique de l'eau du sol pour une activité d'anhydrase carbonique de 1 (i.e. pas d'activité ; ronds noirs) et de 70 (triangles gris ; modifiée d'après Wingate et al., 2010).

1.3.3.1. Les rôles de la température et de la teneur en eau du sol

L'activité enzymatique généralement augmente avec la température car la chaleur du milieu apporte un supplément d'énergie qui facilite la réaction enzymatique. Cette réponse de l'activité enzymatique à la température est traduite dans la littérature par la notion de Q_{10}. Au-dessus d'une certaine température optimale (T_{opt}) l'activité enzymatique peut se mettre à décroitre car l'excès de chaleur dénature l'enzyme. Cette décroissance de l'activité peut aussi s'expliquer sans faire appel à la notion de dénaturation de l'enzyme mais par le fait que les enzymes sont des macromolécules dont la capacité calorifique est non négligeable (Alster et al., 2016; Schipper et al., 2014). La température a également un rôle indirect sur l'activité enzymatique en modifiant la solubilité du substrat (le CO_2 ou l'OCS en l'occurrence) et sa diffusivité en phase gazeuse (Bird et al., 2002) ou liquide (Ulshöfer et al., 1996).

L'activité enzymatique dépend aussi de la teneur en eau du sol. Le manque d'eau diminue l'activité ainsi que la croissance microbienne (Hueso et al., 2012; Sorensen et al., 2013). L'eau est également un support de transport essentiel pour les substrats. En effet, lorsque les sols se dessèchent l'approvisionnement en substrat devient de plus en plus limité car le drain des pores et les films d'eau autour des agrégats deviennent plus minces et se déconnectent (Ilstedt et al., 2000). L'humidité du sol a également un impact sur la diffusivité des gaz et des solutés. En conditions sèches, la diffusion des espèces solubles est moins importante en raison de la faible connectivité de l'eau porale. A l'inverse, la connectivité de pores non remplis par la solution du sol permettra une bonne diffusion des gaz (Moldrup et al., 2001; Moyano et al., 2013). La diffusion des gaz étant près de 10000 fois plus grande dans l'air que dans l'eau, un sol saturé en eau sera sujet à une réduction brutale de l'activité des microorganismes aérobies, et favorisera potentiellement les activités microbiennes anaérobies (**Fig.1.10** ; Moyano et al., 2013). En influençant l'abondance ainsi que la structure des communautés microbienne en place dans le sol, la teneur en eau modifie également probablement l'activité de l'AC du sol (Wingate et al., 2009), mais selon une relation qui reste encore à élucider.

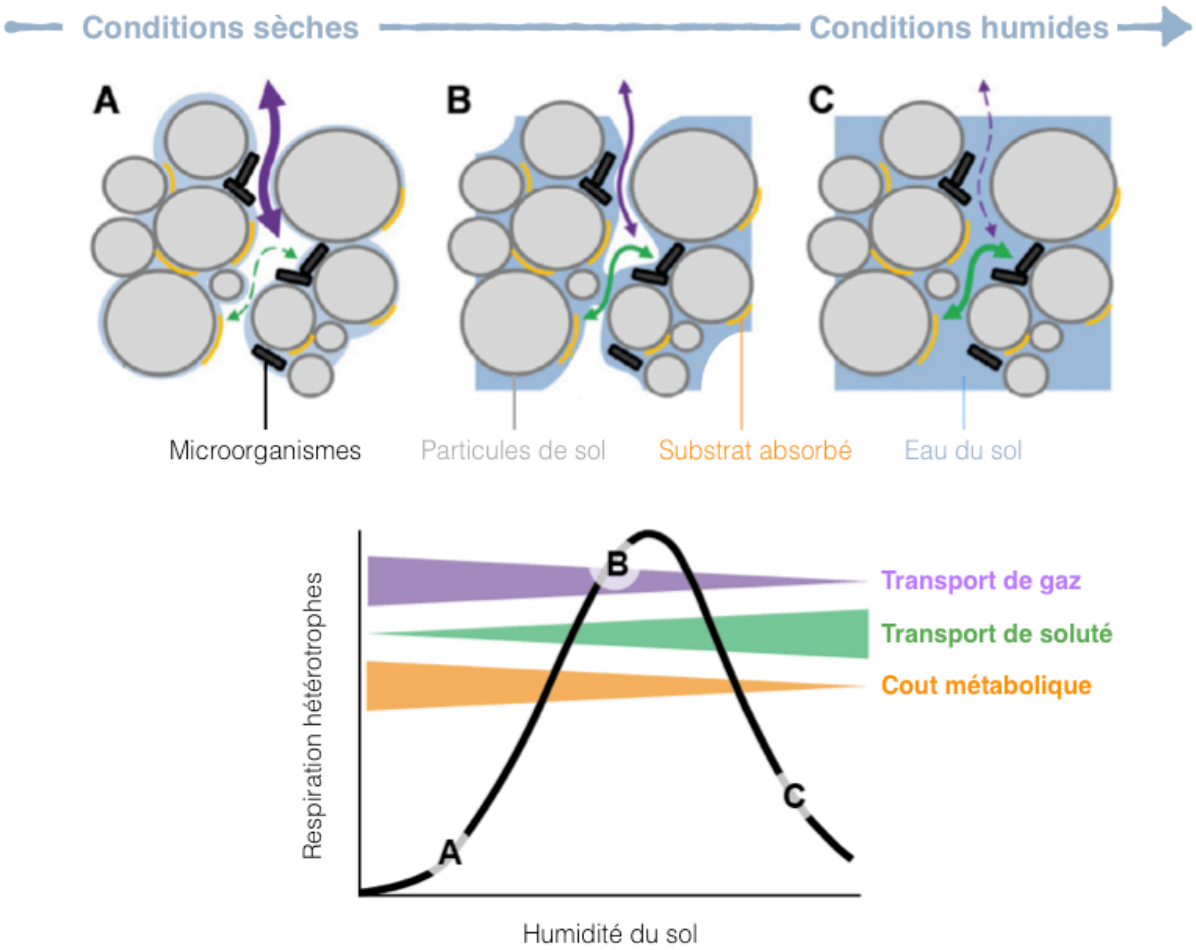

Figure 1.10 : Illustration des effets de l'humidité du sol sur l'activité microbienne. La relation entre la respiration hétérotrophique et la disponibilité de l'eau dans les sols est le résultat de plusieurs processus (modifiée d'après Moyano et al., 2013).

1.3.3.2. Influence du pH et des communautés microbiennes du sol sur l'activité de l'AC : ce que l'on sait

Le pH a un rôle central pour bien comprendre les mécanismes derrière l'activité de l'AC du sol. Tout d'abord car c'est un paramètre abiotique connu pour influencer de manière générale l'activité enzymatique, y compris de l'AC (Kernohan, 1965; Pocker and Deits, 1982; Roughton and Booth, 1946; Rowlett et al., 2002). La réponse de l'AC au pH est cependant complexe et dépend à la fois de la présence d'ions dans la solution tampon, et aussi du type d'AC étudié. De plus, ces réponses au pH des différentes ACs sont connues en partie pour le CO_2 mais, à notre connaissance, ne sont pas connues pour l'OCS. Concernant le CO_2, le pH est également un paramètre important du fait qu'il joue sur la spéciation du CO_2, qui est la

forme prédominante uniquement aux pH acides. En plus donc de jouer sur la disponibilité du substrat CO_2, le pH modifie donc le taux d'hydratation du CO_2 et joue sur le taux d'échange isotopique, qui est en cohérence plus élevé aux pH acides qu'alcalins.

A l'échelle d'un sol, l'effet direct du pH sur l'activité de l'AC est difficile à dissocier de celui sur les communautés microbiennes. En effet le pH est un facteur contrôlant à la fois la diversité et la richesse des communautés microbiennes présentes dans les sols (**Fig. 1.11** ; (Griffiths et al., 2011; Lauber et al., 2008, 2009; Rousk et al., 2010). L'abondance relative de nombreux phylums bactériens est par exemple fortement liée aux valeurs de pH. Il a été observé que les sols aux pH plutôt alcalins avaient de plus grandes abondances relatives en *Actinobacteria* et *Bacteroidetes* comparés aux sols aux pH plus acides. De même les sols avec un pH proche de la neutralité possèdent une plus grande diversité de bactéries que les sols à la fois très acides ou très alcalins (Griffiths et al., 2011; Lauber et al., 2009).

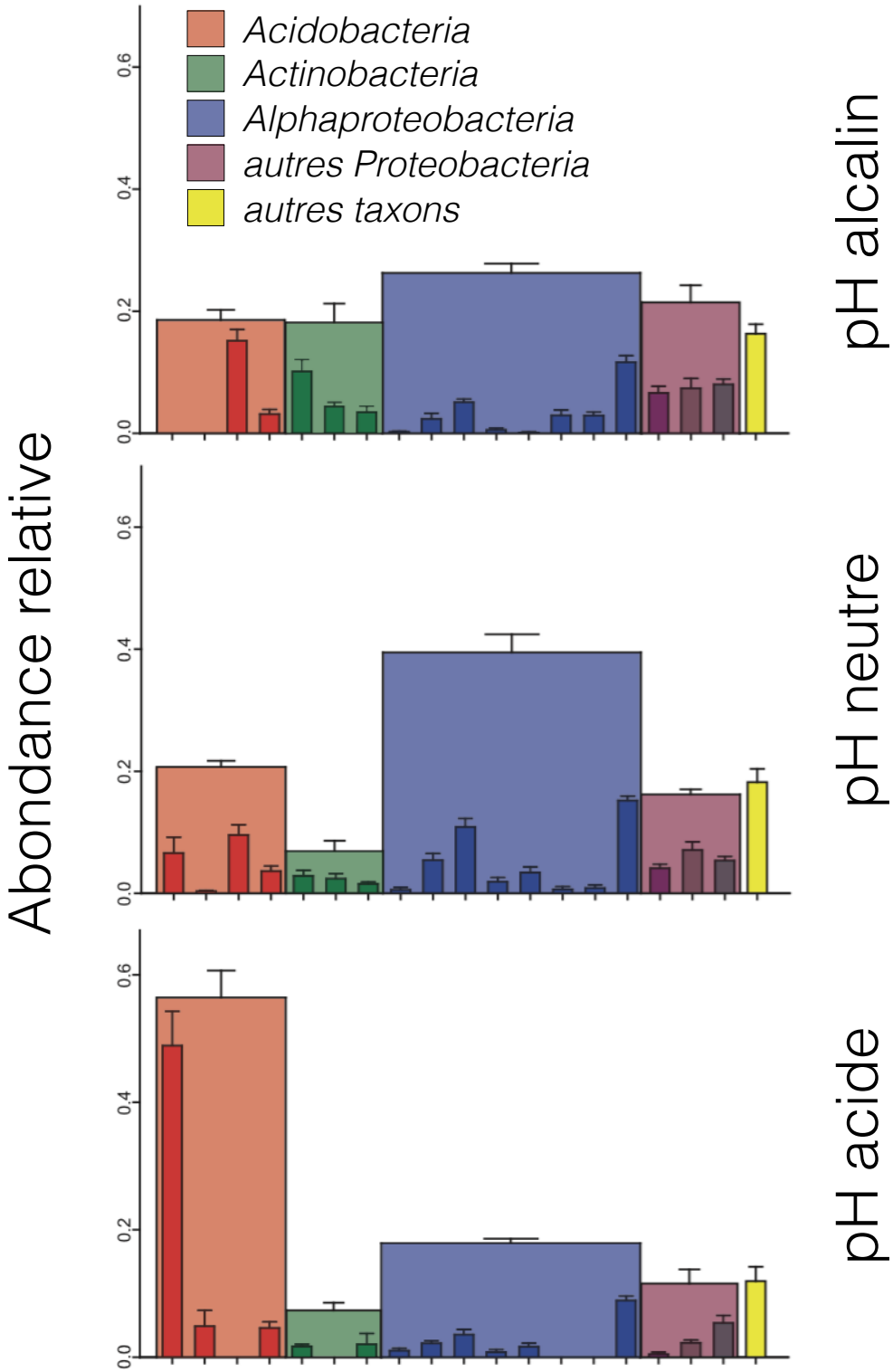

Figure 1.11 : Abondances relatives de différents taxons bactériens à pH faible, moyen et élevé. Les banques de clones ont été séquencées à partir d'une gamme de sols géographiquement dispersés (modifiée d'après Griffiths et al., 2011).

L'implication directe des communautés microbiennes, que ce soit en terme d'abondance ou de diversité, sur l'activité de l'AC des sols n'a, à ce jour, pas été clairement démontrée. Li et al. (2005) ont toutefois observé sur des systèmes karstiques que l'activité de l'AC était plus élevée dans les sols à proximité de racines. Ces auteurs ont aussi souligné que les variations d'activité de l'AC étaient généralement en accord avec les variations saisonnières qui contrôlent également d'autre part l'abondance des microorganismes présents dans les écosystèmes karstiques. Enfin Li et al. (2005) ont observé en isolant divers microorganismes des systèmes karstiques que les actinomycètes et les champignons pourraient produire respectivement une activité d'AC intracellulaire ou extracellulaire comparativement plus élevée par rapport aux autres micro-organismes étudiés. Ces faits suggèrent donc qu'à la fois l'abondance et la diversité des microorganismes pourraient expliquer les variations de l'activité de l'AC. Wingate et al. (2009) ont également proposé que l'abondance et la diversité des microorganismes du sol soient responsables des différences observées dans leurs taux catalysés de l'hydratation du CO_2 (de 20 à 300 fois plus élevé que le taux non catalysé). Ces auteurs ont également constaté que la présence d'algues à la surface d'un des sols étudiés a considérablement augmenté l'activité mesurée de l'AC.

1.4. Objectif de la thèse

L'anhydrase carbonique joue donc un rôle clé dans les échanges de CO_2, $CO^{18}O$ et OCS entre le sol et l'atmosphère. Sans une meilleure compréhension des facteurs biotiques et abiotiques régulant l'activité de l'AC des sols, l'utilisation du $CO^{18}O$ et de l'OCS pour étudier le cycle du carbone planétaire reste difficile. Mon travail de thèse a pour objectif d'apporter des éléments de réponses quant aux rôles respectifs du pH et des communautés microbiennes du sol sur les variations d'activité d'AC dans des sols. Pour répondre à cet objectif, et au vu de la littérature, nous avons formulés et testé quatre hypothèses.

Nous avons tout d'abord supposé que l'activité de l'AC serait inhibée dans les sols acides. Nous avons également fait l'hypothèse que les pH de sol *a contrario* alcalin affaibliraient significativement le flux de $CO^{18}O$. Dans un troisième temps nous avons présumé que l'activité de l'AC serait positivement corrélée à l'abondance des phototrophes, et enfin nous avons supposé que la structure des communautés affecterait différemment les flux de $CO^{18}O$ et d'OCS.

Une forte originalité de mon travail repose dans le fait que nous proposons de suivre l'impact de ces deux paramètres biotiques et abiotiques *via* une approche multi-traceurs,

combinant à la fois des mesures de $CO^{18}O$ et d'OCS, ce qui n'a encore jamais été fait. L'objectif est de disposer de contraintes complémentaires pour améliorer notre compréhension de l'activité de l'AC des sols et *in fine* sa représentation dans les modèles du cycle du carbone.

Références

Alster, C. J., Baas, P., Wallenstein, M. D., Johnson, N. G. and von Fischer, J. C.: Temperature Sensitivity as a Microbial Trait Using Parameters from Macromolecular Rate Theory, Front. Microbiol., 7(November), 1821, doi:10.3389/fmicb.2016.01821, 2016.

Anav, A., Friedlingstein, P., Beer, C., Ciais, P., Harper, A., Jones, C., Murray-Tortarolo, G., Papale, D., Parazoo, N. C., Peylin, P., Piao, S., Sitch, S., Viovy, N., Wiltshire, A. and Zhao, M.: Spatiotemporal patterns of terrestrial gross primary production: A review, Rev. Geophys., 53(3), 785–818, doi:10.1002/2015RG000483, 2015.

Aydin, M., Williams, M. B., Tatum, C. and Saltzman, E. S.: Carbonyl sulfide in air extracted from a South Pole ice core: a 2000 year record, Atmos. Chem. Phys. Discuss., 8(4), 16763–16788, doi:10.5194/acpd-8-16763-2008, 2008.

Baldocchi, D., Falge, E. and Wilson, K.: A spectral analysis of biosphere–atmosphere trace gas flux densities and meteorological variables across hour to multi-year time scales, Agric. For. Meteorol., 107(1), 1–27, doi:10.1016/S0168-1923(00)00228-8, 2001.

Barbour, M. M., Farquhar, G. D., Hanson, D. T., Bickford, C. P., Powers, H. and McDowell, N. G.: A new measurement technique reveals temporal variation in d18 O of leaf-respired CO2, Plant. Cell Environ., 30(4), 456–468, doi:10.1111/j.1365-3040.2007.01633.x, 2007.

Beer, C., Reichstein, M., Tomelleri, E., Ciais, P., Jung, M., Carvalhais, N., Rodenbeck, C., Arain, M. A., Baldocchi, D., Bonan, G. B., Bondeau, A., Cescatti, A., Lasslop, G., Lindroth, A., Lomas, M., Luyssaert, S., Margolis, H., Oleson, K. W., Roupsard, O., Veenendaal, E., Viovy, N., Williams, C., Woodward, F. I. and Papale, D.: Terrestrial Gross Carbon Dioxide Uptake: Global Distribution and Covariation with Climate, Science, 329(5993), 834–838, doi:10.1126/science.1184984, 2010.

Belviso, S., Schmidt, M., Yver, C., Ramonet, M., Gros, V. and Launois, T.: Strong similarities between night-time deposition velocities of carbonyl sulphide and molecular hydrogen inferred from semi-continuous atmospheric observations in Gif-sur-Yvette , Paris region, Tellus B, 1(65), 1–8, doi:10.3402/tellusb.v65i0.20719, 2013.

Berry, J., Wolf, A., Campbell, J. E., Baker, I., Blake, N., Blake, D., Denning, a. S., Kawa, S. R., Montzka, S. a., Seibt, U., Stimler, K., Yakir, D. and Zhu, Z.: A coupled model of the global cycles of carbonyl sulfide and CO 2 : A possible new window on the carbon cycle, J. Geophys. Res. Biogeosciences, 118(2), 842–852, doi:10.1002/jgrg.20068, 2013.

Bird R, Stewart W, Lightfoot E: Transport Phenomena. John Wiley, Hoboken, NJ, 2002

Bowling, D. R., Sargent, S. D., Tanner, B. D. and Ehleringer, J. R.: Tunable diode laser absorption spectroscopy for stable isotope studies of ecosystem–atmosphere CO_2 exchange, Agric. For. Meteorol., 118(1–2), 1–19, doi:10.1016/S0168-1923(03)00074-1, 2003.

Brühl, C., Lelieveld, J., Crutzen, P. J. and Tost, H.: The role of carbonyl sulphide as a source of stratospheric sulphate aerosol and its impact on climate, Atmos. Chem. Phys., 12(3), 1239–1253, doi:10.5194/acp-12-1239-2012, 2012.

Buenning, N., Noone, D., Randerson, J., Riley, W. J. and Still, C.: The response of the $^{18}O/^{16}O$ composition of atmospheric CO_2 to changes in environmental conditions, J. Geophys. Res. Biogeosciences, 119(1), 55–79, doi:10.1002/2013JG002312, 2014.

Ciais, P., Canadell, J. G., Luyssaert, S., Chevallier, F., Shvidenko, A., Poussi, Z., Jonas, M., Peylin, P., King, A. W., Schulze, E.-D., Piao, S., Rödenbeck, C., Peters, W. and Bréon, F.-M.: Can we reconcile atmospheric estimates of the Northern terrestrial carbon sink with land-based accounting?, Curr. Opin. Environ. Sustain., 2(4), 225–230, doi:10.1016/j.cosust.2010.06.008, 2010.

Cramer, W., Bondeau, A., Woodward, F. I., Prentice, I. C., Betts, R. a., Brovkin, V., Cox, P. M., Fisher, V., Foley, J. a., Friend, A. D., Kucharik, C., Lomas, M. R., Ramankutty, N., Sitch, S., Smith, B., White, A. and Young-Molling, C.: Global response of terrestrial ecosystem structure and function to CO_2 and climate change: Results from six dynamic global vegetation models, Glob. Chang. Biol., 7(4), 357–373, doi:10.1046/j.1365-2486.2001.00383.x, 2001.

Cronk, J. D., Endrizzi, J. a, Cronk, M. R., O'neill, J. W. and Zhang, K. Y. J.: Crystal structure of E. coli β-carbonic anhydrase, an enzyme with an unusual pH-dependent activity, Protein Sci., 10(5), 911–922, doi:10.1110/ps.46301, 2001.

Crutzen, P. J.: The possible importance of CSO for the sulfate layer of the stratosphere, Geophys. Res. Lett., 3(2), 73–76, 1976.

Cuntz, M.: A comprehensive global three-dimensional model of $\delta^{18}O$ in atmospheric CO_2 : 1. Validation of surface processes, J. Geophys. Res., 108(D17), 1–24, doi:10.1029/2002JD003153, 2003.

Denman, K.L., G. Brasseur, A. Chidthaisong, P. Ciais, P.M. Cox, R.E. Dickinson, D. Hauglustaine, C. Heinze, E. Holland, D. Jacob, U. Lohmann, S Ramachandran, P.L. da Silva Dias, S.C. Wofsy and X. Zhang, 2007: Couplings Between Changes in the Climate System and Biogeochemistry. In: Climate Change 2007: The Physical Science

Basis. Contribution of Working Group I to the Fourth Assessment Report of the Intergovernmental Panel on Climate Change [Solomon, S., D. Qin, M. Manning, Z. Chen, M. Marquis, K.B. Averyt, M.Tignor and H.L. Miller (eds.)]. Cambridge University Press, Cambridge, United Kingdom and New York, NY, USA.

Dongmann, G., Nürnberg, H. W., Förstel, H. and Wagener, K.: On the enrichment of $H_2{}^{18}O$ in the leaves of transpiring plants, Radiat. Environ. Biophys., 11(1), 41–52, doi:10.1007/BF01323099, 1974.

Dlugokencky, E. and Tans, P.: Trends in atmospheric carbon dioxide, National Oceanic & Atmo- spheric Administration, Earth System Research Laboratory (NOAA/ESRL), http://www.esrl. 5 noaa.gov/gmd/ccgg/trends, last access: 8 August 2014. Doney,

Farquhar, G. D. and Cernusak, L. A.: On the isotopic composition of leaf water in the non-steady state, Funct. Plant Biol., 32(4), 293, doi:10.1071/FP04232, 2005.

Farquhar, G. D., Lloyd, J., Taylor, J. A., Flanagan, L. B., Syvertsen, J. P., Hubick, K. T., Wong, S. C. and Ehleringer, J. R.: Vegetation effects on the isotope composition of oxygen in atmospheric CO_2, Nature, 363(6428), 439–443, doi:10.1038/363439a0, 1993.

Francey, R. J. and Tans, P. P.: Latitudinal variation in oxygen-18 of atmospheric CO_2, Nature, 327(6122), 495–497, doi:10.1038/327495a0, 1987.

Fridlyand, L. E. and Kaler, V. L.: Possible CO_2 concentrating mechanism in chloroplasts of C3 plants. Role of carbonic anhydrase., Gen. Physiol. Biophys., 6(6), 617–636, 1987.

Friedlingstein, P., Cox, P., Betts, R., Bopp, L., von Bloh, W., Brovkin, V., Cadule, P., Doney, S., Eby, M., Fung, I., Bala, G., John, J., Jones, C., Joos, F., Kato, T., Kawamiya, M., Knorr, W., Lindsay, K., Matthews, H. D., Raddatz, T., Rayner, P., Reick, C., Roeckner, E., Schnitzler, K.-G., Schnur, R., Strassmann, K., Weaver, A. J., Yoshikawa, C. and Zeng, N.: Climate–Carbon Cycle Feedback Analysis: Results from the C4 MIP Model Intercomparison, J. Clim., 19(14), 3337–3353, doi:10.1175/JCLI3800.1, 2006.

Griffiths, R. I., Thomson, B. C., James, P., Bell, T., Bailey, M. and Whiteley, A. S.: The bacterial biogeography of British soils, Environ. Microbiol., 13(6), 1642–1654, doi:10.1111/j.1462-2920.2011.02480.x, 2011.

Hewett-Emmett, D. and Tashian, R. E.: Functional Diversity, Conservation, and Convergence in the Evolution of the α-, β-, and γ-Carbonic Anhydrase Gene Families, Mol. Phylogenet. Evol., 5(1), 50–77, doi:10.1006/mpev.1996.0006, 1996.

Hoag, K. J.: Triple oxygen isotope composition of tropospheric carbon dioxide as a tracer of

terrestrial gross carbon fluxes, Geophys. Res. Lett., 32(2), L02802, doi:10.1029/2004GL021011, 2005.

Hueso, S., García, C. and Hernández, T.: Severe drought conditions modify the microbial community structure, size and activity in amended and unamended soils, Soil Biol. Biochem., 50, 167–173, doi:10.1016/j.soilbio.2012.03.026, 2012.

Ilstedt, U., Nordgren, A. and Malmer, A.: Optimum soil water for soil respiration before and after amendment with glucose in humid tropical acrisols and a boreal mor layer, Soil Biol. Biochem., 32(11–12), 1591–1599, doi:10.1016/S0038-0717(00)00073-0, 2000.

IPCC (2013). Changements Climatiques 2013. Les éléments scientifiques. Contribution du Groupe de travail I au cinquième Rapport d'Évaluation du Groupe d'experts intergouvernemental sur l'Évolution du climat. Équipe de rédaction principale, Stocker, T.F. et Qin, D.

Jacobson, M. Z.: Correction to "Control of fossil-fuel particulate black carbon and organic matter, possibly the most effective method of slowing global warming," J. Geophys. Res., 110(D14), D14105, doi:10.1029/2005JD005888, 2005.

Joos, F. and Spahni, R.: Rates of change in natural and anthropogenic radiative forcing over the past 20,000 years, Proc. Natl. Acad. Sci., 105(5), 1425–1430, doi:10.1073/pnas.0707386105, 2008.

Kernohan, J. C.: The pH-activity curve of bovine carbonic anhydrase and its relationship to the inhibition of the enzyme by anions, Biochim. Biophys. Acta - Enzymol. Biol. Oxid., 96(2), 304–317, doi:10.1016/0926-6593(65)90014-7, 1965.

Kesselmeier, J. and Hubert, A.: Exchange of reduced volatile sulfur compounds between leaf litter and the atmosphere, Atmos. Environ., 36(29), 4679–4686, doi:10.1016/S1352-2310(02)00413-2, 2002.

Kesselmeier, J., Teusch, N. and Kuhn, U.: Controlling variables for the uptake of atmospheric carbonyl sulfide by soil, J. Geophys. Res. Atmos., 104(D9), 11577–11584, doi:10.1029/1999JD900090, 1999.

Kettle, A., Kuhn, U., von Hope, M., Kesselmeier, J. and Andreae, O. J.: Global budget of atmospheric carbonyl sulfide: Temporal and spatial variations of the dominant sources and sinks, J. Geophys. Res., 107(D22), 4658, doi:10.1029/2002JD002187, 2002.

Krinner, G., Viovy, N., de Noblet-Ducoudré, N., Ogée, J., Polcher, J., Friedlingstein, P., Ciais, P., Sitch, S. and Prentice, I. C.: A dynamic global vegetation model for studies of the coupled atmosphere-biosphere system, Global Biogeochem. Cycles, 19(1), 1–33, doi:10.1029/2003GB002199, 2005.

Krulwich, T. A., Sachs, G. and Padan, E.: Molecular aspects of bacterial pH sensing and homeostasis, Nat. Rev. Microbiol., 9(5), 330–343, doi:10.1038/nrmicro2549, 2011.

Kuhn, U., Ammann, C., Wolf, A., Meixner, F. ., Andreae, M. . and Kesselmeier, J.: Carbonyl sulfide exchange on an ecosystem scale: soil represents a dominant sink for atmospheric COS, Atmos. Environ., 33(6), 995–1008, doi:10.1016/S1352-2310(98)00211-8, 1999.

Lai, C. T., Ometto, J. P. H. B., Berry, J. A., Martinelli, L. A., Domingues, T. F. and Ehleringer, J. R.: Life form-specific variations in leaf water oxygen-18 enrichment in Amazonian vegetation, Oecologia, 157(2), 197–210, doi:10.1007/s00442-008-1071-5, 2008.

Lauber, C. L., Hamady, M., Knight, R. and Fierer, N.: Pyrosequencing-Based Assessment of Soil pH as a Predictor of Soil Bacterial Community Structure at the Continental Scale, Appl. Environ. Microbiol., 75(15), 5111–5120, doi:10.1128/AEM.00335-09, 2009.

Lauber, C. L., Strickland, M. S., Bradford, M. A. and Fierer, N.: The influence of soil properties on the structure of bacterial and fungal communities across land-use types, Soil Biol. Biochem., 40(9), 2407–2415, doi:10.1016/j.soilbio.2008.05.021, 2008.

Launois, T., Peylin, P., Belviso, S. and Poulter, B.: A new model of the global biogeochemical cycle of carbonyl sulfide – Part 2: Use of OCS to constrain gross primary productivity of current vegetation models, Atmos. Chem. Phys. Discuss., 14(20), 27663–27729, doi:10.5194/acpd-14-27663-2014, 2015.

Li, W., Yu, L., Yuan, D., Wu, Y. and Zeng, X.: A study of the activity and ecological significance of carbonic anhydrase from soil and its microbes from different karst ecosystems of Southwest China, Plant Soil, 272(1–2), 133–141, doi:10.1007/s11104-004-4335-9, 2005.

Liljas, A. and Laurberg, M.: A wheel invented three times, EMBO Rep., 1(1), 16–17, doi:10.1093/embo-reports/kvd016, 2000.

Lindskog, S.: Structure and mechanism of carbonic anhydrase, Pharmacol. Ther., 74(1), 1–20, doi:10.1016/S0163-7258(96)00198-2, 1997.

Maseyk, K., Berry, J. a, Billesbach, D., Campbell, J. E., Torn, M. S., Zahniser, M. and Seibt, U.: Sources and sinks of carbonyl sulfide in an agricultural field in the Southern Great Plains., Proc. Natl. Acad. Sci. U. S. A., 111(25), 9064–9, doi:10.1073/pnas.1319132111, 2014.

Metzl, N., Tilbrook, B. and Poisson, A.: The annual CO_2 cycle and the air-sea CO_2 flux in the sub-Antarctic Ocean, Tellus B, 51(4), 849–861, doi:10.1034/j.1600-0889.1999.t01-3-

00008.x, 1999.

Mitra, M.: Identification of a New Chloroplast Carbonic Anhydrase in Chlamydomonas reinhardtii, Plant Physiol., 135(1), 173–182, doi:10.1104/pp.103.037283, 2004.

Moldrup, P., Olesen, T., Komatsu, T., P, S. and Rolston, D.: Tortuosity, diffusivity, and permeability in the soil liquid and gaseous phases, Soil Sci. Soc. Am. J., 65(3), 613–623, 2001.

Montzka, S. a., Aydin, M., Battle, M., Butler, J. H., Saltzman, E. S., Hall, B. D., Clarke, a. D., Mondeel, D. and Elkins, J. W.: A 350-year atmospheric history for carbonyl sulfide inferred from Antarctic firn air and air trapped in ice, J. Geophys. Res. Atmos., 109(D22), n/a-n/a, doi:10.1029/2004JD004686, 2004.

Moyano, F. E., Manzoni, S. and Chenu, C.: Responses of soil heterotrophic respiration to moisture availability: An exploration of processes and models, Soil Biol. Biochem., 59, 72–85, doi:10.1016/j.soilbio.2013.01.002, 2013.

Notni, J., Schenk, S., Protoschill-Krebs, G., Kesselmeier, J. and Anders, E.: The Missing Link in COS Metabolism: A Model Study on the Reactivation of Carbonic Anhydrase from its Hydrosulfide Analogue, ChemBioChem, 8(5), 530–536, doi:10.1002/cbic.200600436, 2007.

Ogée, J., Peylin, P., Cuntz, M., Bariac, T., Brunet, Y., Berbigier, P., Richard, P. and Ciais, P.: Partitioning net ecosystem carbon exchange into net assimilation and respiration with canopy-scale isotopic measurements: An error propagation analysis with $^{13}CO_2$ and $CO^{18}O$ data, Global Biogeochem. Cycles, 18(2), n/a-n/a, doi:10.1029/2003GB002166, 2004.

Pan, Y., Birdsey, R. a, Fang, J., Houghton, R., Kauppi, P. E., Kurz, W. a, Phillips, O. L., Shvidenko, A., Lewis, S. L., Canadell, J. G., Ciais, P., Jackson, R. B., Pacala, S. W., McGuire, a D., Piao, S., Rautiainen, A., Sitch, S. and Hayes, D.: A Large and Persistent Carbon Sink in the World's Forests, Science, 333(6045), 988–993, doi:10.1126/science.1201609, 2011.

Peylin, P., Ciais, P., Denning, A. S., Tans, P. P., A., B. J. and White, J. W. C.: A 3-dimensional study of $d^{18}O$ in atmospheric CO_2: contribution of different land ecosystems, Tellus B, 51(3), 642–667, doi:10.1034/j.1600-0889.1999.t01-2-00006.x, 1999.

Piao, S., Ciais, P., Friedlingstein, P., Peylin, P., Reichstein, M., Luyssaert, S., Margolis, H., Fang, J., Barr, A., Chen, A., Grelle, A., Hollinger, D. Y., Laurila, T., Lindroth, A., Richardson, A. D. and Vesala, T.: Net carbon dioxide losses of northern ecosystems in

response to autumn warming., Nature, 451(7174), 49–52, doi:10.1038/nature06444, 2008.

Piao, S., Sitch, S., Ciais, P., Friedlingstein, P., Peylin, P., Wang, X., Ahlström, A., Anav, A., Canadell, J. G., Cong, N., Huntingford, C., Jung, M., Levis, S., Levy, P. E., Li, J., Lin, X., Lomas, M. R., Lu, M., Luo, Y., Ma, Y., Myneni, R. B., Poulter, B., Sun, Z., Wang, T., Viovy, N., Zaehle, S. and Zeng, N.: Evaluation of terrestrial carbon cycle models for their response to climate variability and to CO_2 trends., Glob. Chang. Biol., 19(7), 2117–32, doi:10.1111/gcb.12187, 2013.

Pocker, Y. and Deits, T. L.: Effects of pH on anionic inhibition of carbonic anhydrase activities, J. Am. Chem. Soc., 104(9), 2424–2434, doi:10.1021/ja00373a016, 1982.

Le Quéré, C., Raupach, M. R., Canadell, J. G., Marland, G., Bopp, L., Ciais, P., Conway, T. J., Doney, S. C., Feely, R. A., Foster, P., Friedlingstein, P., Gurney, K., Houghton, R. A., House, J. I., Huntingford, C., Levy, P. E., Lomas, M. R., Majkut, J., Metzl, N., Ometto, J. P., Peters, G. P., Prentice, I. C., Randerson, J. T., Running, S. W., Sarmiento, J. L., Schuster, U., Sitch, S., Takahashi, T., Viovy, N., van der Werf, G. R. and Woodward, F. I.: Trends in the sources and sinks of carbon dioxide, Nat. Geosci., 2(12), 831–836, doi:10.1038/ngeo689, 2009.

Le Quéré, C., Moriarty, R., Andrew, R. M., Canadell, J. G., Sitch, S., Korsbakken, J. I., Friedlingstein, P., Peters, G. P., Andres, R. J., Boden, T. A., Houghton, R. A., House, J. I., Keeling, R. F., Tans, P., Arneth, A., Bakker, D. C. E., Barbero, L., Bopp, L., Chang, J., Chevallier, F., Chini, L. P., Ciais, P., Fader, M., Feely, R. A., Gkritzalis, T., Harris, I., Hauck, J., Ilyina, T., Jain, A. K., Kato, E., Kitidis, V., Klein Goldewijk, K., Koven, C., Landschützer, P., Lauvset, S. K., Lefèvre, N., Lenton, A., Lima, I. D., Metzl, N., Millero, F., Munro, D. R., Murata, A., Nabel, J. E. M. S., Nakaoka, S., Nojiri, Y., O'Brien, K., Olsen, A., Ono, T., Pérez, F. F., Pfeil, B., Pierrot, D., Poulter, B., Rehder, G., Rödenbeck, C., Saito, S., Schuster, U., Schwinger, J., Séférian, R., Steinhoff, T., Stocker, B. D., Sutton, A. J., Takahashi, T., Tilbrook, B., van der Laan-Luijkx, I. T., van der Werf, G. R., van Heuven, S., Vandemark, D., Viovy, N., Wiltshire, A., Zaehle, S. and Zeng, N.: Global Carbon Budget 2015, Earth Syst. Sci. Data, 7(2), 349–396, doi:10.5194/essd-7-349-2015, 2015.

Roughton, F. J. W. and Booth, V. H.: The effect of substrate concentration, pH and other factors upon the activity of carbonic anhydrase, Biochem. J., 40(2), 319–330, 1946.

Rousk, J., Bååth, E., Brookes, P. C., Lauber, C. L., Lozupone, C., Caporaso, J. G., Knight, R. and Fierer, N.: Soil bacterial and fungal communities across a pH gradient in an arable

soil, ISME J., 4(10), 1340–1351, doi:10.1038/ismej.2010.58, 2010.

Rowlett, R. S., Tu, C., McKay, M. M., Preiss, J. R., Loomis, R. J., Hicks, K. a., Marchione, R. J., Strong, J. a., Donovan, G. S. and Chamberlin, J. E.: Kinetic characterization of wild-type and proton transfer-impaired variants of β-carbonic anhydrase from Arabidopsis thaliana, Arch. Biochem. Biophys., 404(2), 197–209, doi:10.1016/S0003-9861(02)00243-6, 2002.

Sandoval-Soto, L., Stanimirov, M., von Hobe, M., Schmitt, V., Valdes, J., Wild, A. and Kesselmeier, J.: Global uptake of carbonyl sulfide (COS) by terrestrial vegetation: Estimates corrected by deposition velocities normalized to the uptake of carbon dioxide (CO_2), Biogeosciences, 2(2), 125–132, doi:10.5194/bg-2-125-2005, 2005.

Schipper, L. A., Hobbs, J. K., Rutledge, S. and Arcus, V. L.: Thermodynamic theory explains the temperature optima of soil microbial processes and high Q_{10} values at low temperatures, Glob. Chang. Biol., 20(11), 3578–3586, doi:10.1111/gcb.12596, 2014.

Schmid, H. P.: Source areas for scalars and scalar fluxes, Boundary-Layer Meteorol., 67(3), 293–318, doi:10.1007/BF00713146, 1994.

Schmidt, G. a., Ruedy, R. a., Miller, R. L. and Lacis, A. a.: Attribution of the present-day total greenhouse effect, J. Geophys. Res., 115(D20), D20106, doi:10.1029/2010JD014287, 2010.

Seibt, U., Kesselmeier, J., Sandoval-Soto, L., Kuhn, U. and Berry, J. A.: A kinetic analysis of leaf uptake of COS and its relation to transpiration, photosynthesis and carbon isotope fractionation, Biogeosciences Discuss., 6(5), 9279–9300, doi:10.5194/bgd-6-9279-2009, 2009.

Seibt, U., Wingate, L., Lloyd, J. and Berry, J. a.: Diurnally variable $\delta^{18}O$ signatures of soil CO_2 fluxes indicate carbonic anhydrase activity in a forest soil, J. Geophys. Res., 111(G4), G04005, doi:10.1029/2006JG000177, 2006.

Sellers, P. J., Tucker, C. J., Collatz, G. J., Los, S. O., Justice, C. O., Dazlich, D. A. and Randall, D. A.: A Revised Land Surface Parameterization (SiB2) for Atmospheric GCMS. Part II: The Generation of Global Fields of Terrestrial Biophysical Parameters from Satellite Data, J. Clim., 9(4), 706–737, doi:10.1175/1520-0442(1996)009<0706:ARLSPF>2.0.CO;2, 1996.

Smith, K. S. and Ferry, J. G.: A plant-type (beta-class) carbonic anhydrase in the thermophilic methanoarchaeon Methanobacterium thermoautotrophicum., J. Bacteriol., 181(20), 6247–6253 [online] Available from: http://www.pubmedcentral.nih.gov/articlerender.fcgi?artid=103756&tool=pmcentrez

&rendertype=abstract, 1999.

Sorensen, P. O., Germino, M. J. and Feris, K. P.: Microbial community responses to 17 years of altered precipitation are seasonally dependent and coupled to co-varying effects of water content on vegetation and soil C, Soil Biol. Biochem., 64, 155–163, doi:10.1016/j.soilbio.2013.04.014, 2013.

Stadie, W. and O'Brien, H.: The catalysis of hydration of carbon dioxide and dehydration of carbonic acid by enzyme isolated from red blood cells, J. Biol. Chem., 103, 521–529, 1933.

Stern, L. A., Amundson, R. and Baisden, W. T.: Influence of soils on oxygen isotope ratio of atmospheric CO_2, Global Biogeochem. Cycles, 15(3), 753–759, doi:10.1029/2000GB001373, 2001.

Stimler, K., Montzka, S. A., Berry, J. A., Rudich, Y. and Yakir, D.: Relationships between carbonyl sulfide (COS) and CO2 during leaf gas exchange, New Phytol., 186(4), 869–878, doi:10.1111/j.1469-8137.2010.03218.x, 2010.

Takahashi, T., Sutherland, S. C., Sweeney, C., Poisson, A., Metzl, N., Tilbrook, B., Bates, N., Wanninkhof, R., Feely, R. a, Sabine, C., Olafsson, J. and Nojiri, Y.: Global sea–air CO_2 flux based on climatological surface ocean pCO_2, and seasonal biological and temperature effects, Deep Sea Res. Part II Top. Stud. Oceanogr., 49(9–10), 1601–1622, doi:10.1016/S0967-0645(02)00003-6, 2002.

Tripp, B. C.: A Role for Iron in an Ancient Carbonic Anhydrase, J. Biol. Chem., 279(8), 6683–6687, doi:10.1074/jbc.M311648200, 2003.

Tripp, B. C., Smith, K. and Ferry, J. G.: Carbonic Anhydrase: New Insights for an Ancient Enzyme, J. Biol. Chem., 276(52), 48615–48618, doi:10.1074/jbc.R100045200, 2001.

Ueno, Y., Johnson, M. S., Danielache, S. O., Eskebjerg, C., Pandey, A. and Yoshida, N.: Geological sulfur isotopes indicate elevated OCS in the Archean atmosphere, solving faint young sun paradox, Proc. Natl. Acad. Sci., 106(35), 14784–14789, doi:10.1073/pnas.0903518106, 2009.

Ulshöfer, V. S., Flock, O. R., Uher, G. and Andreae, M. O.: Photochemical production and air-sea exchange of carbonyl sulfide in the eastern Mediterranean Sea, Mar. Chem., 53(1–2), 25–39, doi:10.1016/0304-4203(96)00010-2, 1996.

Van Diest, H. and Kesselmeier, J.: Soil atmosphere exchange of carbonyl sulfide (COS) regulated by diffusivity depending on water-filled pore space, Biogeosciences, 5(2), 475–483, doi:10.5194/bg-5-475-2008, 2008.

Wanninkhof, R.: Relationship between wind speed and gas exchange over the ocean, J.

Geophys. Res., 97(C5), 7373, doi:10.1029/92JC00188, 1992.

Welp, L. R., Keeling, R. F., Meijer, H. a J., Bollenbacher, A. F., Piper, S. C., Yoshimura, K., Francey, R. J., Allison, C. E. and Wahlen, M.: Interannual variability in the oxygen isotopes of atmospheric CO_2 driven by El Niño, Nature, 477(7366), 579–582, doi:10.1038/nature10421, 2011.

Welp, L. R., Lee, X., Kim, K., Griffis, T. J., Billmark, K. A. and Baker, J. M.: $\delta^{18}O$ of water vapour, evapotranspiration and the sites of leaf water evaporation in a soybean canopy, Plant, Cell Environ., 31(9), 1214–1228, doi:10.1111/j.1365-3040.2008.01826.x, 2008.

Whelan, M. E., Min, D.-H. and Rhew, R. C.: Salt marsh vegetation as a carbonyl sulfide (COS) source to the atmosphere, Atmos. Environ., 73, 131–137, doi:10.1016/j.atmosenv.2013.02.048, 2013.

Wingate, L., Ogée, J., Burlett, R. and Bosc, A.: Strong seasonal disequilibrium measured between the oxygen isotope signals of leaf and soil CO_2 exchange, Glob. Chang. Biol., 16(11), 3048–3064, doi:10.1111/j.1365-2486.2010.02186.x, 2010.

Wingate, L., Ogee, J., Cuntz, M., Genty, B., Reiter, I., Seibt, U., Yakir, D., Maseyk, K., Pendall, E. G., Barbour, M. M., Mortazavi, B., Burlett, R., Peylin, P., Miller, J., Mencuccini, M., Shim, J. H., Hunt, J. and Grace, J.: The impact of soil microorganisms on the global budget of ^{18}O in atmospheric CO_2, Proc. Natl. Acad. Sci., 106(52), 22411–22415, doi:10.1073/pnas.0905210106, 2009.

Wingate, L., Seibt, U., Maseyk, K., Ogée, J., Almeida, P., Yakir, D., Pereira, J. S. and Mencuccini, M.: Evaporation and carbonic anhydrase activity recorded in oxygen isotope signatures of net CO_2 fluxes from a Mediterranean soil, Glob. Chang. Biol., 14(9), 2178–2193, doi:10.1111/j.1365-2486.2008.01635.x, 2008.

Yakir, D. and Wang, X.-F.: Fluxes of CO_2 and water between terrestrial vegetation and the atmosphere estimated from isotope measurements, Nature, 380(6574), 515–517, doi:10.1038/380515a0, 1996.

Yi, Z., Wang, X., Sheng, G. and Fu, J.: Exchange of carbonyl sulfide (OCS) and dimethyl sulfide (DMS) between rice paddy fields and the atmosphere in subtropical China, Agric. Ecosyst. Environ., 123(1–3), 116–124, doi:10.1016/j.agee.2007.05.011, 2008.

Yi, Z., Wang, X., Sheng, G., Zhang, D., Zhou, G. and Fu, J.: Soil uptake of carbonyl sulfide in subtropical forests with different successional stages in south China, J. Geophys. Res., 112(D8), D08302, doi:10.1029/2006JD008048, 2007.

Chapitre 2 : Modélisation mécaniste des échanges d'OCS entre le sol et l'atmosphère

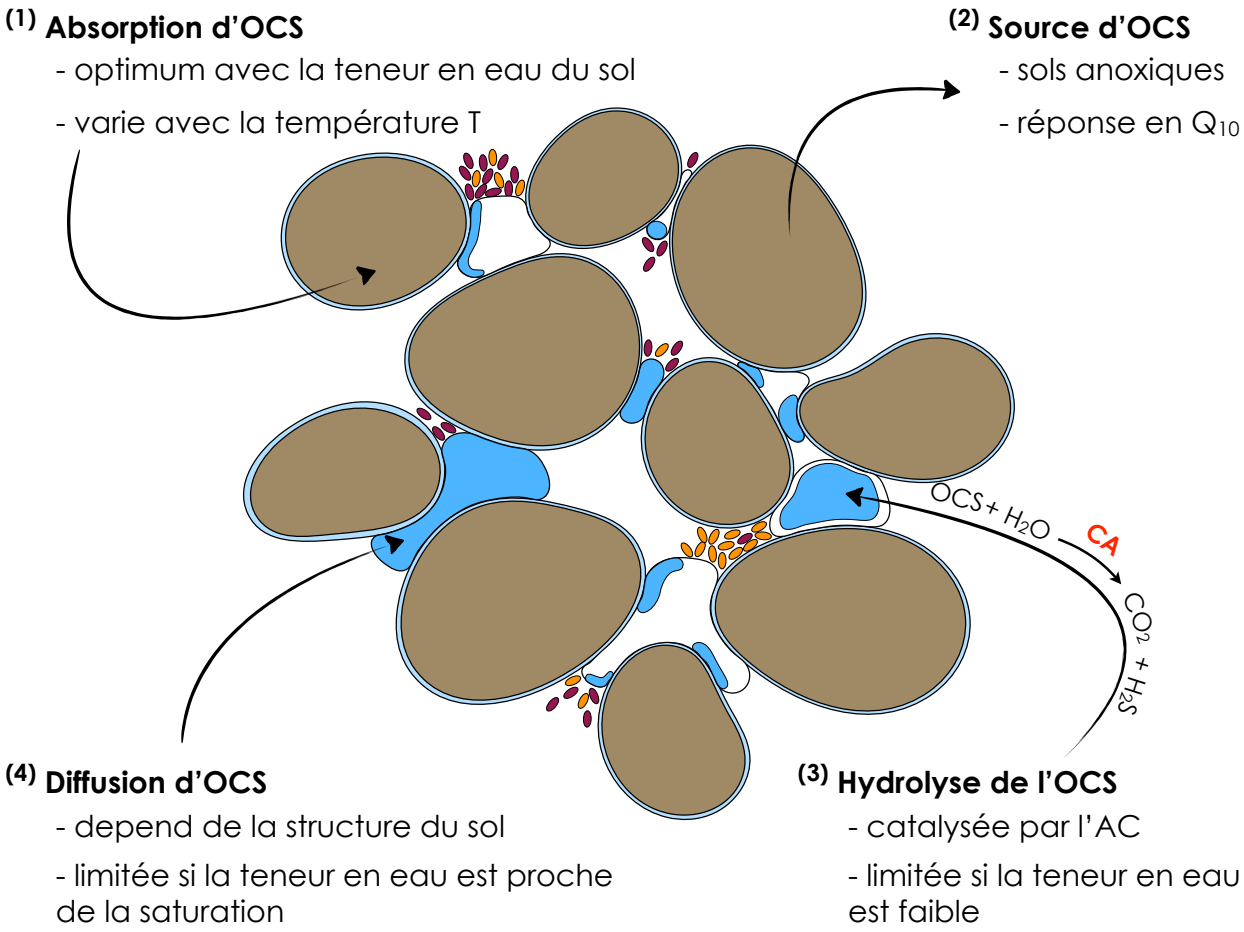

Figure 2.1: Schéma illustrant les différents processus dans le sol pris en compte pour modéliser les flux d'OCS.

Introduction au chapitre 2

Ce chapitre fait l'état des lieux des approches mécanistes décrivant les échanges d'OCS entre le sol et l'atmosphère. De telles approches n'ont été proposées que très récemment par deux études indépendantes (Sun et al. 2015 ; Ogée et al. 2016). Établissant un parallèle avec les processus responsables des transferts du CO_2 (ou d'autres gaz traces) dans les sols, ces deux études ont proposé des formulations relativement proches du flux d'OCS et de sa dépendance à plusieurs variables environnementales telle que la température, la teneur en eau ou la porosité du sol. Si l'approche de Sun et al. (2015) reste fortement empirique dans le choix de certaines formulations du modèle, nous nous sommes efforcés de relier le taux d'hydrolyse de l'OCS à l'activité et la biomasse microbienne et d'établir un lien direct entre les activités d'AC vis-à-vis de l'OCS et du CO_2. Ceci nous a permis d'introduire le pH et le potentiel redox du sol comme nouvelles variables environnementales à considérer. Ce travail a été publié dans le journal *Biogeosciences* en avril 2016 (Ogée et al., 2016).

L'approche que nous avons utilisée reste en plusieurs points similaire à celle développée pour représenter les échanges isotopiques CO_2-H_2O dans les sols, afin de faciliter les comparaisons entre les deux traceurs. Brièvement, notre modèle tient compte à la fois des processus de diffusion et d'advection de l'OCS dans la matrice du sol, ainsi que des réactions de dissolution et d'hydrolyse dans l'eau du sol. Enfin nous avons également intégré la possible production d'OCS par le sol. Nous avons exploré la réponse théorique des flux d'OCS à la teneur en eau et à la température du sol, deux paramètres déjà mentionnés pour expliquer les variations observées de flux d'OCS entre le sol et l'atmosphère (Van Diest et al., 2008), ainsi qu'au pH, au potentiel redox et à la taille de la colonne de sol. Une place particulière a été consacrée à l'activité microbienne du sol qui contribue à l'hydrolyse de l'OCS en régulant la concentration d'AC du sol qui joue ensuite sur le taux de catalyse de cette réaction chimique. La catalyse de la réaction d'hydrolyse de l'OCS est fonction à la fois de la température et de l'humidité du sol, du pH et de la concentration d'AC. La production d'OCS par le sol est quant à elle prise en compte en utilisant une réponse à la température de type Q_{10} modulée toutefois par le potentiel redox du sol. Dans ce modèle nous ne faisons donc pas de différence entre une émission d'OCS d'origine biotique ou abiotique.

S'appuyant sur un jeu de données en grande partie publié (Van Diest et al. 2008) que j'ai récupéré auprès de ses auteurs et mis en forme pour cette étude, nous avons testé les capacités de notre modèle à reproduire les réponses des flux d'OCS observés à la température

et la teneur en eau du sol. Enfin, nous avons montré que l'optimum en température pouvait être déplacé vers des températures plus froides en présence d'une émission d'OCS par le sol.
La suite de ce chapitre n'est autre que l'article lui-même qui décrit de manière détaillée le modèle mécaniste d'échange d'OCS entre le sol et l'atmosphère, modèle que je vais systématiquement utiliser dans les chapitres suivants.

A new mechanistic framework to predict OCS fluxes from soils

Jérôme Ogée[1], Joana Sauze[1], Jürgen Kesselmeier[2], Bernard Genty[3], Heidi Van Diest[2], Thomas Launois[1] and Lisa Wingate[1]

[1]INRA, UMR 1391 ISPA, F-33140 Villenave d'Ornon, France
[2]Max Planck Institute for Chemistry, Biogeochemistry Department, Mainz, Germany
[3]CNRS/CEA/Aix-Marseille University, UMR 6191 BVME, Saint-Paul-lez-Durance, France

Abstract

Estimates of photosynthetic and respiratory fluxes at large scales are needed to improve our predictions of the current and future global CO_2 cycle. Carbonyl sulphide (OCS) is the most abundant sulphur gas in the atmosphere and has been proposed as a new tracer of photosynthesis (GPP), as the uptake of OCS from the atmosphere is dominated by the activity of carbonic anhydrase (CA), an enzyme abundant in leaves that also catalyses CO_2 hydration during photosynthesis. But soils also exchange OCS with the atmosphere which complicates the retrieval of GPP from atmospheric budgets. Indeed soils can take up large amounts of OCS from the atmosphere as soil microorganisms also contain CA, and OCS emissions from soils have been reported in agricultural fields or anoxic soils. To date no mechanistic framework exists to describe this exchange of OCS between soils and the atmosphere but empirical results, once upscaled to the global scale, indicate that OCS consumption by soils dominates over production and its contribution to the atmospheric budget is large, at about one third of the OCS uptake by vegetation, with also a large uncertainty. Here, we propose a new mechanistic model of the exchange of OCS between soils and the atmosphere that builds on our knowledge of soil CA activity from CO_2 oxygen isotopes. In this model the OCS soil budget is described by a first-order reaction-diffusion-production equation, assuming that the hydrolysis of OCS by CA is total and irreversible. Using this model we are able to explain the observed presence of an optimum temperature for soil OCS uptake and show how this optimum can shift to cooler temperatures in the presence of soil OCS emissions. Our model can also explain the observed optimum with soil moisture content previously described in the literature as a result of diffusional constraints on OCS hydrolysis. These diffusional constraints are also responsible for the response of OCS uptake to soil weight and depth observed previously. In order to simulate the exact OCS uptake rates and patterns observed on several soils collected from a range of biomes, different CA activities had to be invoked in

each soil type, coherent with expected physiological levels of CA in soil microbes and with CA activities derived from CO_2 isotope exchange measurements, given the differences in affinity of CA for both trace gases. Our model can also be used to help upscale laboratory measurements to the plot or the region. Several suggestions are given for future experiments in order to test the model further and allow a better constraint on the large-scale OCS fluxes from both oxic and anoxic soils.

2.1. Introduction

The terrestrial biosphere is, with the ocean, the largest sink in the global atmospheric CO_2 budget, with a very large year-to-year variability (*e.g.*, Gurney and Eckels, 2011). Yet there is a scarcity of observations on how photosynthesis (GPP) and respiration over land respond individually to warmer temperatures, increasing atmospheric CO_2 mixing ratios and changes in water availability (Beer et al., 2010; Frankenberg et al., 2011; Welp et al., 2011; Wingate et al., 2009). Obtaining new observational constraints of these two opposing land CO_2 gross fluxes at large scales is key to improve our models of the land C sink and provide robust projections of the atmospheric CO_2 budget and future climate (Friedlingstein et al., 2006; Piao et al., 2013).

In this context, additional tracers such as carbonyl sulphide (OCS), an analogue of CO_2 in many respects, could be very useful (Berry et al., 2013; Campbell et al., 2008; Kettle et al., 2002; Montzka et al., 2007). Indeed, the uptake rate of OCS by foliage is strongly related to GPP (Sandoval-Soto et al., 2005; Stimler et al., 2010), or more generally to the rate of CO_2 transfer into foliage (*e.g.*, Seibt et al., 2010; Wohlfahrt et al., 2011). This is because both OCS and CO_2 molecules diffuse into foliage through the same stomatal pores and through mesophyll cells where they get rapidly hydrated in an enzymatic reaction with carbonic anhydrase (CA) (Protoschill-Krebs and Kesselmeier, 1992). However, unlike CO_2 that is reversibly hydrated and converted into bicarbonate, OCS molecules are irreversibly hydrolysed (Elliott et al., 1989) and are not expected to diffuse back to the atmosphere, given the high affinity of CA towards OCS and the high activity of CA usually found in leaves (Protoschill-Krebs et al., 1996; Stimler et al., 2012).

Carbonic anhydrase is also widespread in diverse species from the Archaea, Bacteria, Fungi and Algae domains (Smith et al., 1999), so that OCS uptake can theoretically take place in soils. Several field studies provide support for this by showing that soils generally act as an OCS sink when measured at ambient concentrations (Castro and Galloway, 1991; Kuhn et al., 1999; Liu et al., 2010a; Steinbacher et al., 2004; White et al., 2010; Yi et al., 2007) and that the uptake rate is reduced when the soil is autoclaved (Bremner and Banwart, 1976). Kesselmeier et al. (1999) also observed a significant (>50%) reduction of the OCS uptake rate in soil samples after adding ethoxyzolamide, one of the most efficient known CA inhibitors (*e.g.*, Isik et al., 2009; Syrjänen et al., 2013). This finding strongly supports the idea that OCS uptake by soils is dominated by soil CA activity.

Soils can also emit OCS into the atmosphere as reported in some agricultural fields (Maseyk et al., 2014; Whelan and Rhew, 2015) or in anoxic soils (Devai and Delaune, 1995; Mello and Hines, 1994; Whelan et al., 2013; Yi et al., 2008) but the exact mechanisms for such emissions are still unclear (Mello and Hines, 1994; Whelan and Rhew, 2015). At the global scale, OCS consumption by soils seems to dominate over production and its contribution to the atmospheric budget is large, at about one third of the OCS uptake by vegetation, but with a large uncertainty (Berry et al., 2013; Kettle et al., 2002; Launois et al., 2015).

This large uncertainty in the OCS exchange rate from soils is partly caused by the variety of approaches used to obtain a global estimate of this flux. Kettle et al. (2002) assumed soil OCS fluxes responded to soil surface temperature and moisture only and used a parameterisation derived by Kesselmeier et al. (1999) from incubation measurements performed on a single agricultural soil in Germany. They recognised the limitation of such parameterisation and also noted the important role of some intrinsic properties of the soil and particularly its redox potential (Devai and Delaune, 1995) but did not account for it in their analysis. More recent approaches have assumed that the OCS flux from soils is proportional to other soil-air trace gas fluxes, such as heterotrophic (microbial) respiration (Berry et al., 2013) or the H_2 deposition rate (Launois et al., 2015). Experimental evidence that supports such scaling between different trace gas fluxes is however scarce and with mixed results. In summary, all the approaches to estimate soil OCS fluxes at large scales remain essentially empirical or based on hypotheses that are largely un-validated. Given the supposedly important contribution of soils in the global OCS atmospheric budget, it becomes apparent that a deeper understanding of this flux and its underlying mechanisms is urgently needed. Until then estimating global GPP using OCS as an additional tracer of the carbon cycle remains elusive.

A plethora of process-based models exist that describe the transport and fate of trace gases in porous media (Falta et al., 1989; Olesen et al., 2001). Transport processes are fairly well understood and similar between different trace gases. On the other hand the processes responsible for the emission or destruction are usually quite unique, *i.e.*, specific to each trace gas. The main difficulty then resides in understanding these emission and destruction processes. Very recently Sun et al. (2015) proposed parameterisations of OCS emission and destruction in soils. However their parameterisations remain largely empirically-based and lack important drivers such as soil pH or redox potential. In this paper we propose a mechanistic framework to describe OCS uptake and release from soil surfaces, based on our current understanding of OCS biogeochemistry in soils. Our model includes OCS diffusion and advection through the soil matrix, OCS dissolution and hydrolysis in soil water and OCS

production. Soil microbial activity contributes to OCS hydrolysis, through a pseudo first order CA-catalysed chemical reaction rate that varies with soil temperature and moisture, pH and CA concentration. OCS production, either abiotic or biotic, is also accounted for using a simple Q_{10}–type temperature response modulated by the soil redox potential. Using the model we explore the theoretical response of OCS fluxes to soil water content, soil temperature, soil depth and soil pH. We also evaluate our model against observed soil OCS uptake rates and patterns from the literature and discuss how the CA-catalysed reaction rates for each soil type can be reconciled with those typically observed for CO_2 hydration, given the differences in affinity of CA for OCS and CO_2.

2.2. Model description

2.2.1. Partitioning of OCS in the different soil phases

Carbonyl sulphide, like any other trace gas, can be present in the soil matrix in three forms: (1) vaporised in the air-filled pore space, (2) dissolved in the water-filled pore space or (3) adsorbed on the surface of the soil matrix (mineral and organic matter solid particles). The total OCS concentration C_{tot} (mol m^{-3} soil) is thus the sum of the OCS concentration in each phase weighted by their volumetric content: $C_{tot} = \varepsilon_a C + \theta C_l + \rho_b C_s$ where ε_a (m^3 air m^{-3} soil) is the volumetric air content, θ (m^3 water m^{-3} soil) is the volumetric water content, ρ_b (kg m^{-3}) is soil bulk density, C (mol m^{-3} air) and C_l (mol m^{-3} water) denote OCS concentration in soil air and liquid water respectively and C_s (mol kg^{-1} soil) denotes the OCS concentration adsorbed on the soil matrix.

In the following we will assume full equilibrium between the three phases. We will also assume linear sorption/desorption behaviour (a fair assumption at ambient OCS concentrations), so that C_l and C_s can be linearly related to C: $C_l = BC$ where B (m^3 water m^{-3} air) is the solubility of OCS in water and $C_s = (K_{sg} + BK_{sw})C$ where K_{sg} (m^3 air kg^{-1} soil) and K_{sw} (m^3 water kg^{-1} soil) are the solid/vapour and solid/liquid partitioning coefficients, respectively (Olesen et al., 2001). The solubility B is related to Henry's law constant K_H (mol m^{-3} Pa^{-1}): $B = K_H RT$ where $R = 8.31446$ J mol^{-1} K^{-1} is the ideal gas constant and T (K) is soil water temperature. It has been shown that K_H is fairly independent of pH (at least for pH below 9, see De Bruyn et al., 1995; Elliott et al., 1989) but decreased with temperature and salinity (De Bruyn et al., 1995; Elliott et al., 1989). In the following we will use the parameterisation of Wilhelm et al. (1977) assuming low salinity levels in the soil:

$K_H = 0.021\exp[24900/R\ (1/T - 1/298.15)]$.

We prefered this expression rather than the more recent expression proposed by DeBruyn et al. (1995) that was based on one single dataset rather than a compilation of multiple datasets. The difference between the two expressions is shown in **Fig. 2.2a**.

Expressions of K_{sg} and K_{sw} for OCS are currently not available. For organic vapours it has been shown that K_{sw} is well correlated with soil characteristics such as C content (Petersen et al., 1995), specific surface area or clay content (Yamaguchi et al., 1999), and that K_{sg} is usually significant at soil water contents corresponding to less than five molecular layers of water coverage (Petersen et al., 1995). In this range of soil moisture, direct chemical adsorption onto dry mineral surfaces dominates and can increase the adsorption capacity of soils by several orders of magnitude. For these organic vapours the relationship of K_{sg} with soil moisture can be related to soil specific surface area (Petersen et al., 1995) or clay content (Yamaguchi et al., 1999). However these relationships obtained for organic vapours are unlikely applicable for OCS because the adsorption mechanisms may be completely different. Liu and colleagues have estimated OCS adsorption capacities of several mineral oxides and found that quartz (SiO_2) and anatase (TiO_2) did not adsorb OCS but other oxides with higher basicity adsorbed, reversibly or not, rather large quantities of OCS (Liu et al., 2008; 2010b; 2009). They also recognised that these estimates of the adsorption capacity of the minerals were an upper limit owing to the competitive adsorption of other gases such as CO_2, H_2O and NO_x that occur in the real Earth's atmosphere (Liu et al., 2009; 2010b) and the somewhat lower OCS partial pressure in ambient air compared to that used in their experimental setup. Also, at steady state, adsorption should have little influence on the soil-air OCS exchange rate, unless heterogeneous (surface) reactions occur and continuously remove OCS from the adsorbed phase (Liu et al., 2010b). In the following we will neglect adsorption of OCS on solid surfaces but we recognise that this assumption might be an over-simplification.

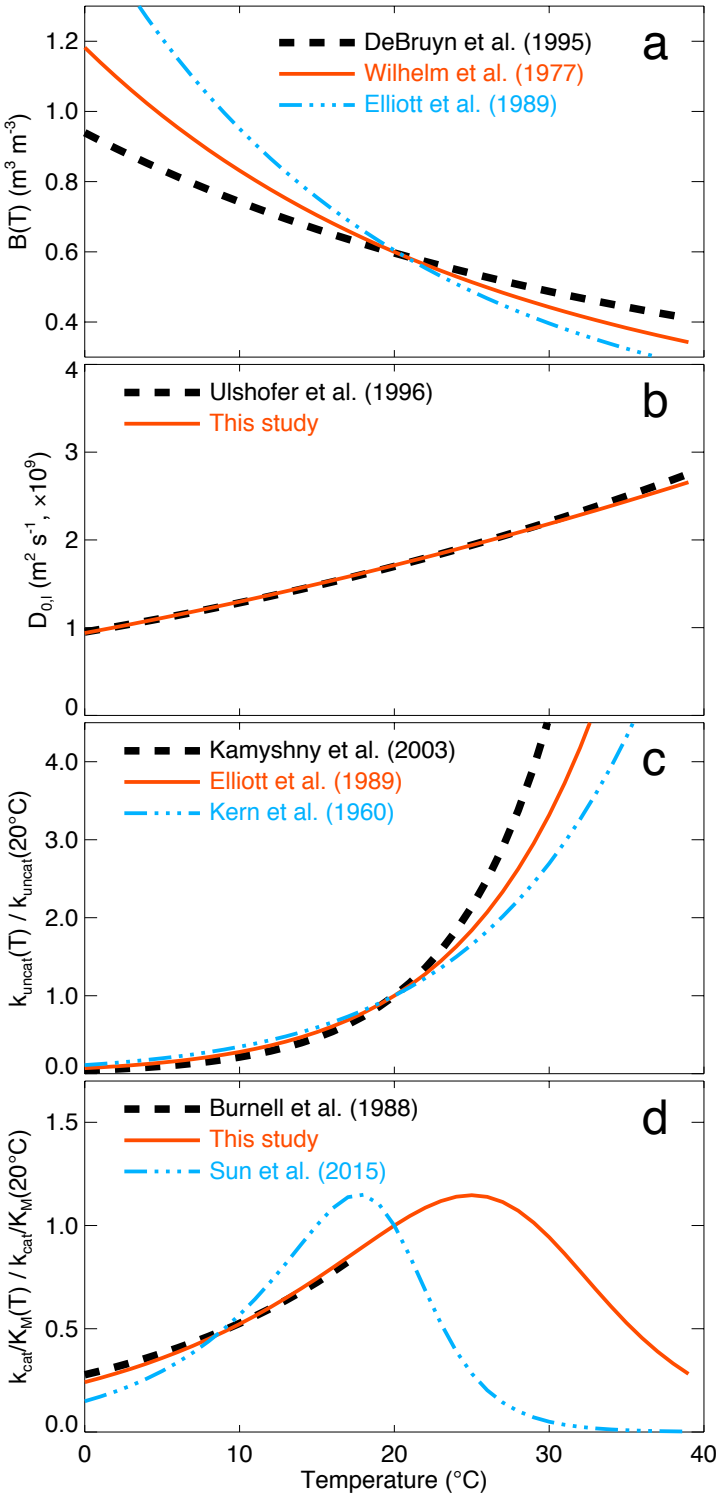

Figure 2.2: Temperature response of (a) the OCS solubility in water, (b) the OCS diffusivity in liquid water and (c) the uncatalysed and (d) CA-catalysed OCS hydrolysis rates. Red lines indicate the parameterisation used for this study.

2.2.2. Mass balance equation

The transport of OCS through the soil matrix occurs by either pressure-driven (advective-dispersive) or concentration-driven (diffusive) fluxes. Carbonyl sulphide can also be destroyed or emitted, owing to abiotic and/or biotic processes. The general mass balance equation for OCS in a small soil volume can then be written:

$$\frac{\partial \varepsilon_{\text{tot}} C}{\partial t} = -\nabla F_{\text{diff}} - \nabla F_{\text{adv}} + P - S, \quad (1)$$

where $\varepsilon_{\text{tot}} = \varepsilon_a + \theta B + \rho_b(K_{sg} + BK_{sw}) \approx \varepsilon_a + \theta B$ (m^3 air m^{-3} soil) is total OCS soil porosity, F_{diff} (mol m^{-2} s^{-1}) represents the diffusional flux of OCS through the soil matrix, F_{adv} (mol m^{-2} s^{-1}) is the advective flux of OCS, P (mol m^{-3} s^{-1}) the OCS production rate and S (mol m^{-3} s^{-1}) the OCS consumption rate and $\nabla = \partial/\partial x + \partial/\partial y + \partial/\partial z$ denotes the differential operator, *i.e.*, the spatial gradient in all three directions x, y and z.

If the soil is horizontally homogeneous (that is, the soil properties are independent of x and y) and the soil lateral dimensions are much larger than its total depth (minimal edge effects), the OCS concentration is only a function of soil depth z and time t and Eq. (1) simplifies to:

$$\frac{\partial \varepsilon_{\text{tot}} C}{\partial t} = -\frac{\partial F_{\text{diff}}}{\partial z} - \frac{\partial F_{\text{adv}}}{\partial z} + P - S. \quad (2)$$

2.2.3. Diffusive fluxes

Diffusion in the gas phase is commonly described by Fick's first law (Bird et al., 2002; Scanlon et al., 2002):

$$F_{\text{diff,a}} = -D_{\text{eff,a}} \frac{\partial C}{\partial z}, \quad (3)$$

where $F_{\text{diff,a}}$ (mol m^{-2} s^{-1}) is the diffusive flux of gaseous OCS and $D_{\text{eff,a}}$ (m^3 air m^{-1} soil s^{-1}) is the effective diffusivity of gaseous OCS through the soil matrix. The latter is commonly expressed relative to the binary diffusivity of OCS in free air $D_{0,a}$ (m^2 air s^{-1}): $D_{\text{eff,a}}/D_{0,a} = \tau_a \varepsilon_a$ where τ_a is the so-called air tortuosity factor that accounts for the tortuosity of the air-filled pores, as well as their constrictivity and water-induced disconnectivity (*e.g.*, Moldrup et al., 2003). The air-filled porosity (ε_a) appears in this equation to account for the reduced cross-sectional area in the soil matrix relative to free air, although the effective porosity for diffusion could be smaller if the soil contains small pores that do not contribute to the overall transport such as dead end or blind pores. Expressions for τ_a differ depending on whether the soil is repacked or undisturbed (Moldrup et al., 2003). For undisturbed soils the most

commonly used equations are those of Penman ((1940); $\tau_a = 0.66$, hereafter referenced as Pen40) and Millington and Quirk ((1961); $\tau_a = \varepsilon_a^{7/3}/\varphi^2$, where f is total soil porosity, hereafter referred to as MQ61). For repacked soils, equations proposed by Moldrup et al. ((2003); $\tau_a = \varepsilon_a^{3/2}/\varphi$, hereafter referred as Mol03r) are preferred. For undisturbed soils with high porosity such as volcanic ash, the expression proposed by Moldrup et al. ((2003); $\tau_a = \varepsilon_a^{1+3/b}/\varphi^{3/b}$, where *b* is the pore-size distribution parameter) seems a better predictor (Moldrup et al., 2003). Recently a new density-corrected expression for undisturbed soils has also been proposed by Deepagoda et al. ((2011); $\tau_a = [0.2(\varepsilon_a/\varphi)^2 + 0.004]/\varphi$) that seems to be superior to previous formulations and has the advantage of not requiring knowledge of the pore-size distribution parameter *b*. A summary of these different formulations of the tortuosity factor and their range of application is given in **Table 2.1**.

Notation	t_a	t_l	Soil treatment	Reference
Pen40	0.66	0.66	NA	Penman (1940)
MQ61	$\varepsilon_a^{7/3}/\varphi^2$	$\theta^{7/3}/\varphi^2$	NA	Millington et al. (1961)
Mol03r	$\varepsilon_a^{3/2}/\varphi$	$\theta^{b/3}/\varphi^{b/3-1}$	repacked	Moldrup et al. (2003)
Mol03u	$\varepsilon_a^{1+3/b}/\varphi^{3/b}$	$\theta^{b/3}/\varphi^{b/3-1}$	undisturbed	Moldrup et al. (2003)
Deepa11	$[0.2(\varepsilon_a/\varphi)^2 + 0.004]/\varphi$	NA	undisturbed	Deepagoda et al. (2011)

Table 2.1: Summary of tortuosity factor formulations for gaseous (τ_a) and liquid (τ_l) diffusion from the literature. ε_a: air porosity; φ: total porosity; θ: soil water content; b: pore-size distribution parameter; NA: data not available.

Diffusion in the liquid phase is described in a similar fashion to the gas phase (Olesen et al., 2001):

$$F_{\text{diff,l}} = -D_{\text{eff,l}}\frac{\partial C_l}{\partial z} = -D_{\text{eff,l}}\left\{B\frac{\partial C}{\partial z} + C\frac{dB}{dT}\frac{\partial T}{\partial z}\right\}, \quad (4)$$

where $F_{\text{diff,l}}$ (mol m^{-2} s^{-1}) is the diffusive flux of dissolved OCS in soil water and $D_{\text{eff,l}}$ (m^3 water m^{-1} soil s^{-1}) is the effective diffusivity of dissolved OCS through the soil matrix. As for gaseous diffusion $D_{\text{eff,l}}$ is commonly expressed relative to the binary diffusivity of OCS in free water $D_{0,l}$ (m^2 water s^{-1}): $D_{\text{eff,l}}/D_{0,l} = \tau_l\,\theta$ where τ_l is the tortuosity factor for solute diffusion. Different expressions for τ_l can also be found in the literature (**Table 2.1**).

Diffusion of OCS in the adsorbed phase can also theoretically occur and can be described in a similar fashion to other trace gases (*e.g.*, see Choi et al., 2001 for ozone). However we will

neglect such a diffusion flux in the adsorbed phase because it is expected to be orders of magnitude smaller than in the two other phases. Also the binary diffusivity of any trace gas is several orders of magnitude higher in the air than it is for its dissolved counterpart in liquid water so that, in unsaturated (oxic) soils, $F_{diff} = F_{diff,a} + F_{diff,l}$ is dominated by the gas-phase OCS diffusion flux $F_{diff,a}$. The role of $F_{diff,l}$ in the OCS transport equations becomes significant only when the soil is water-logged.

The binary diffusivity $D_{0,a}$ depends on pressure and temperature and is assumed here to follow the Chapman-Enskog theory for ideal gases (*i.e.*, Bird et al., 2002): $D_{0,a}(T,p) = D_{0,a}(T_0,p_0)\,(T/T_0)^{1.5}\,(p_0/p)$. A value for $D_{0,a}$(25°C, 1atm) of 1.27 10^{-5} m^2 s^{-1} is used and derived from the value for the diffusivity of water vapour in air at 25°C (2.54 10^5 m^2 s^{-1}, see Massman (1998)) and the CO_2/OCS diffusivity ratio of 2.0±0.2 derived from the Chapman-Enskog theory and the difference in molar masses of OCS and CO_2 (Seibt et al., 2010). The binary diffusivity $D_{0,l}$ also depends on temperature (Ulshöfer et al., 1996). Because the Stokes-Einstein equation only applies to spherical suspended particles we prefered to use an empirical equation that works well for both the self-diffusivity of water and the diffusivity of dissolved CO_2 in liquid water (Zeebe, 2011): $D_{0,l}(T) = D_{0,l}(T_0)\,(T/T_0 - 1)^2$, with $D_{0,l}$(25°C) = 1.94 10^{-9} m^2 s^{-1} (Ulshöfer et al., 1996) and T_0 = 216K. This value of T_0 was chosen to be intermediate between the value used for water (215.05K) and dissolved CO_2 (217.2K) (Zeebe, 2011) and results in a temperature dependency of $D_{0,l}$ for OCS in water in very good agreement with relationships found in other studies (**Fig. 2.2b**).

2.2.4. Advective fluxes

Advection of OCS can occur in both the liquid and gas phases when the carrier fluid (water or air) moves relative to the soil matrix:

$$F_{adv,l} = q_l C_l = q_l B C\,, \tag{5a}$$

$$F_{adv,a} = q_a C\,, \tag{5b}$$

where q_l (m s^{-1}) and q_a (m s^{-1}) are the velocity fields for liquid water and air respectively. If the flow in the porous soil is laminar these velocity fields are given by Darcy's law (Massman et al., 1997; Scanlon et al., 2002):

$$q_l = -\frac{k_l}{\mu_l}\frac{\partial \Psi_l}{\partial z} = -K_l\left(\frac{\partial h_l}{\partial z} + 1\right), \tag{6a}$$

$$q_a = -\frac{k_a}{\mu_a}\left(\frac{\partial p_a}{\partial z} + \rho_a g\right). \tag{6b}$$

In Eqs. (6a) and (6b) k_l and k_a (m^2) denote soil permeabilities for liquid water and air respectively, μ_l and μ_a (kg m^{-1} s^{-1}) are water and air dynamic viscosities, $\psi_l = \rho_l g(h_l + z)$ is total soil water potential (Pa), ρ_l is water density (1000 kg m^{-3}), h_l (m) is matric potential height, g is gravitational acceleration (9.81 m s^{-2}), ρ_a is air density (ca. 1.2 kg m^{-3}) and p_a (Pa) is air pressure. We also defined the soil hydraulic conductivity K_l (m s^{-1}): $K_l = k_l \rho_l g/\mu_l$. In practice p_a can be expressed as the sum of the hydrostatic pressure ($p_{ah} = -\rho_a g z$) and a fluctuating (non-hydrostatic) part: $p_a = -\rho_a g z + p'_a$ so that Eq. (6b) can be replaced by:

$$q_a = -\frac{k_a}{\mu_a}\frac{\partial p'_a}{\partial z}. \tag{6c}$$

From Eq. (6c) we can see that advection in the gas phase can result from pressure fluctuations, caused by, *e.g.*, venting the soil surface (according to Bernouilli's equation) or turbulence above the soil surface. Typical air pressure fluctuations are of the order of 10 Pa (Maier et al., 2012; Massman et al., 1997). Pressure fluctuations can also result from non-hydrostatic density fluctuations caused by a change in the air composition with gas species of different molar mass as air or by temperature gradients, but the resulting flux is significant only in highly permeable (*i.e.* fractured) soils.

When averaged over a long enough timescale (>1h) the advective flux starts to become negligible compared to the diffusive flux (*e.g.*, Massman et al., 1997). Integration timescales of a few minutes were already assumed to allow liquid-vapour equilibration in Eq. (5a). In the following we will thus neglect advective fluxes in the OCS budget equation, keeping in mind that such an assumption is valid only for time scales of about 1h or longer.

Even when advective fluxes are negligible, advection through porous media generates a diffusive-like flux called mechanical dispersion that reflects the fact that not everything in the porous medium travels at the average water or gas flow speed. Some paths are faster, some slower, some longer and some shorter, leading to a net spreading of the gas or solute plume that looks very much like diffusive behaviour. Since mechanical dispersion depends on the flow, it is expected to increase with increasing flow speed and is usually expressed as:

$$F_{disp,l} = -D_{disp,l}\frac{\partial C_l}{\partial z} = -\alpha_l |q_l| \frac{\partial BC}{\partial z}, \tag{7a}$$

$$F_{disp,a} = -D_{disp,a}\frac{\partial C}{\partial z} = -\alpha_a |q_a| \frac{\partial C}{\partial z}, \tag{7b}$$

where α_l (m) and α_a (m) are the longitudinal dynamic dispersivity of liquid water and air flow respectively and $D_{disp,l}$ (m^2 s^{-1}) and $D_{disp,a}$ (m^2 s^{-1}) are the corresponding dispersive

diffusivities. Transverse dispersion (*i.e.* in a plane perpendicular to the flow) can also occur but will be neglected here.

In practice, because of advective-dispersive fluxes, we must know the liquid water and air velocity fields q_l and q_a in order to solve the trace gas OCS mass budget Eq. (2). This requires solving the total mass balance equations for liquid water and air separately. However, except during rain infiltration and immediate redistribution, q_l rarely exceeds a few mm per day while the drift velocity, defined as the ratio $F_{diff,a}/C$, is typically of the order of a few mm per minute. For this reason, advection fluxes are generally neglected in soil gas transport models. Dispersive fluxes can still be accounted for as a correction factor to true diffusion, provided we have parameterisations of the dispersion diffusivities that are independent of the advective flux (*e.g.*, expressions for $D_{disp,a}$ independent of q_a). For example Maier et al. (2012) proposed expressions of $D_{disp,a}/D_{0,a}$ that rely on the air-filled porosity (ε_a) and permeability (μ_a) of the soil and the degree of turbulence above the soil surface (characterised by the friction velocity u_*).

2.2.5. Consumption and production rates

The processes of consumption or production of OCS in a soil are not fully understood. Carbonyl sulphide can be consumed through hydrolysis in the bulk soil water at an un-catalysed rate k_{uncat} (s^{-1}) that depends mostly on temperature T and pH (Elliott et al., 1989). In the following we will use the expression proposed by Elliott et al. (1989) because it covers the widest range of temperature and pH:

$$k_{uncat} = 2.15 \cdot 10^{-5} \exp\left(-10450\left(\frac{1}{T} - \frac{1}{298}\right)\right) + 12.7 \cdot 10^{-pK_w + pH} \exp\left(-6040\left(\frac{1}{T} - \frac{1}{298}\right)\right), \quad (8)$$

where pK_w is the dissociation constant of water. Other expressions are available in the literature and compared to Eq. 8 for both temperature (**Fig. 2.2c**) and pH (**Fig. 2.3a**) responses. Using Eq. 8 the uncatalysed OCS uptake rate is then computed as $S_{uncat} = k_{uncat} B \theta C$. The volumetric soil water content θ appears in this equation to convert the hydration rate from mol m^{-3} water s^{-1} to mol m^{-3} soil s^{-1}.

This uncatalysed rate is rather small and cannot explain the large OCS uptake rates observed in oxic soils (Kesselmeier et al., 1999; Liu et al., 2010a; Van Diest and Kesselmeier, 2008). The main consumption of OCS is thought to be enzymatic and governed by soil micro-organisms' CA activity (Kesselmeier et al., 1999; Liu et al., 2010a; Van Diest and Kesselmeier, 2008). We will assume that such a catalysed reaction by CA-containing

organisms can be described by Michaelis-Menten kinetics, as was observed for OCS in several marine algae species (Blezinger et al., 2000; Protoschill-Krebs et al., 1995) and one flour beetle (Haritos and Dojchinov, 2005). Because of the low concentrations of OCS in ambient air (500ppt) and the comparatively high values of the Michaelis-Menten coefficient for OCS (K_m, see Ogawa et al., 2013; Protoschill-Krebs et al., 1995; 1996) the catalysed uptake rate S_{cat} (mol m^{-3} s^{-1}) can be approximated:

$$S_{cat} = \theta k_{cat}[CA]\frac{BC}{K_m + BC} \approx \frac{k_{cat}}{K_m}[CA]B\theta C\,, \qquad (9)$$

where k_{cat} (s^{-1}) and K_m (mol m^{-3}) are the turnover rate and the Michaelis-Menten constant of the enzymatic reaction, respectively and $[CA]$ (mol m^{-3}) is the total CA concentration in soil water. We recognise that Eq. 9 is an over-simplification of the reality in the sense that k_{cat} and K_m are not true kinetic parameters but rather volume-averaged parameters for the entire soil microbial community. Also Eq. 9 neglects the competition for CA by CO_2 molecules and the co-limitation of the uptake by diffusional constraints. Given the Michaelis-Menten constant of CA for CO_2 ($K_{m,CO2}$, of the order of 3mM at 25°C and *pH* 8-9) and the range of CO_2 mixing ratios encountered in soil surfaces (300-5000 ppm or 0.01-0.15 mM at 25°C and 1atm) we can conclude that the competition with CO_2 is negligible (*i.e.* the denominator in Eq. 9 would need to be mutliplied by a factor $1 + [CO_2]/K_{m,CO2}$ which would be less than 5%). We recognise that the CO_2 concentration inside microbial cells (*i.e.* at the CA sites) must be somewhat larger than in the surrounding soil water but certainly not to an extent to justify accounting for competition between the two substrates. Also, using typical values of transfer conductance across cell wall and plasma membrane (Evans et al., 2009), we can show that the limitation of OCS uptake by diffusion into the microbial cells is negligible for calculating the OCS uptake rate (see Appendix A for a derivation). In the following we will therefore assume Eq. 9 to be valid.

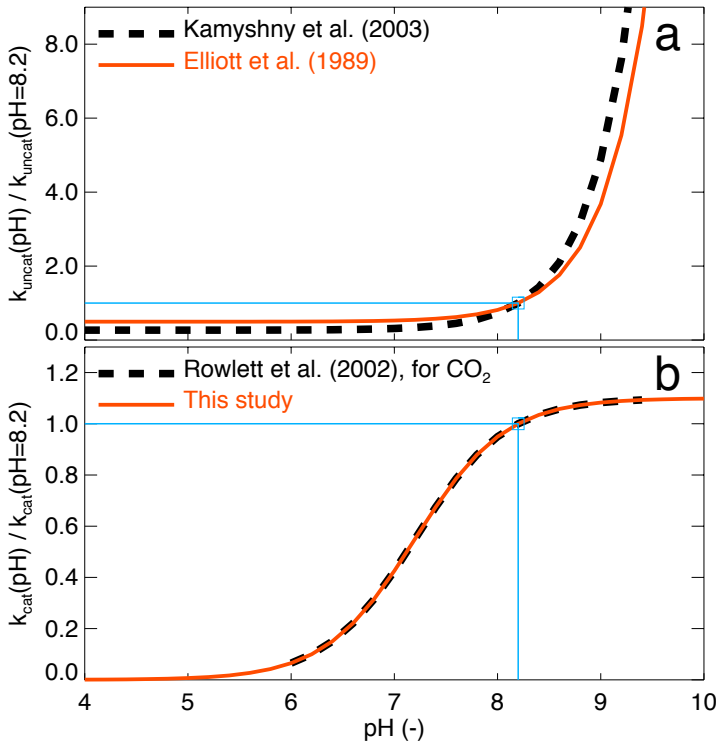

Figure 2.3: Response of the normalised (a) uncatalysed and (b) CA-catalysed OCS hydrolysis rates to changes in soil pH. Red lines indicate the parameterisation used for this study. The blue lines indicate the normalisation at pH = 8.2.

As found for any enzymatic reaction, k_{cat} and K_m depend on temperature and internal *pH* (pH_{in}). In the following we will assume that the ratio k_{cat}/K_m has a temperature dependency that can be approximated as:

$$\frac{k_{cat}}{K_m} \propto x_{CA}(T) = \frac{\exp(-\Delta H_a / RT)}{1+\exp(-\Delta H_d / RT + \Delta S_d / R)}, \quad (10a)$$

where DH_a, DH_d and DS_d are thermodynamic parameters. In the following we will take DH_a = 40 kJ mol^{-1}, DH_d = 200 kJ mol^{-1} and DS_d = 660 J mol^{-1} K^{-1}, that leads to a temperature optima $T_{opt,CA}$ = 25°C and reproduces well the temperature response of β-CA found on maize leaf extracts observed in the range 0-17°C by Burnell et al. (1988) (**Fig. 2.2d**). To our knowledge this is the only study that reports the temperature response of β-CA, the dominant CA class expected in soils (Smith et al., 1999). Interestingly our parameterisation of $x_{CA}(T)$, based on direct measurements on β-CA from Burnell et al. (1988), is very different from the one used by Sun et al. (2015), especially at temperatures above 20°C (**Fig. 2.2d**).

The *pH* response of CA activity for OCS hydrolysis was described by a monotonically decreasing function towards more acidic pH_{in}, as observed in plant β-CA for both OCS (Protoschill-Krebs et al., 1996) and CO_2 (Rowlett et al., 2002). In the following we will use the expression proposed by Rowlett et al. (2002) for CO_2:

$$\frac{k_{cat}}{K_m} \propto y_{CA}(pH_{in}) = \frac{1}{1+10^{-pH_{in}+pK_{CA}}}. \quad (10b)$$

A value of $pK_{CA} = 7.2$ was used that corresponds to the CA response of the wild-type *Arabidopsis thaliana* (Rowlett et al., 2002). The shape of the function y_{CA} is shown in **Fig. 2.3b**.

A β-CA K_M value for OCS (39 mM at 20°C and *pH* 8.2) was estimated on pea (*Pisum sativum*) by Protoschill-Krebs et al. (1996). From a re-analysis of the same dataset we also estimated a k_{cat} of 93 s^{-1} at the same temperature and *pH*, leading to a k_{cat}/K_m value of 2.39 s^{-1} mM^{-1}. To our knowledge this is the only report of k_{cat} and K_m values for OCS in β-CA.

The breaking of water film continuity that occurs at low soil water content leads to a reduction in microbial activity owing to the spatial separation of the microbes and their respiratory substrates (Manzoni and Katul, 2014). In our case soil water discontinuity should not affect OCS supply as gaseous OCS should be equally available in all soil pores. On the other hand different organisms may have different k_{cat}/K_m values so that the spatially-averaged k_{cat}/K_m could vary with drought-induced changes in microbial diversity. However our knowledge of how k_{cat}/K_m for OCS varies amongst different life forms is too scarce to know if it should increase or decrease during drought stress. We will therefore assume that soil water discontinuity does not affect k_{cat}/K_m directly. CA concentration ([CA]) could also vary during drought stress, although it is not clear in which direction. During water stress microbial activity such as respiration or growth is usually reduced, but slow growth rates and heat stress have been shown to cause an up-regulation of CA-gene expression in *Escherichia coli* (Merlin et al., 2003), probably because of a need of bicarbonate for lipid synthesis. For this study we thus make the simplifying assumption that CA concentration does not vary with soil water content. The catalysed OCS uptake rate S_{cat} is then simply proportional to soil water content (Eq. 9).

Destruction of OCS can also occur in the solid phase and was observed on pure mineral oxides with high basicity (Liu et al., 2008; 2009; 2010b). However, such catalytic reaction should be significant only in very dry soils (with only a few molecular layers of water) and in

the absence of other competitive adsorbants such as CO_2 (Liu et al., 2008; 2010c) and is therefore neglected in our model. The total soil OCS uptake rate is thus computed as $S = kB\theta C$ with:

$$k = k_{\text{uncat}}(T, pH) + \frac{x_{\text{CA}}(T)}{x_{\text{CA}}(20°C)} \frac{y_{\text{CA}}(pH_{\text{in}})}{y_{\text{CA}}(8.2)} 2390[CA]. \quad (11a)$$

Following common practice in the CO_2 literature we will also express k with respect to the unctalysed rate at 25°C and pH 4.5, *i.e.*:

$$k = f_{\text{CA}}\, k_{\text{uncat}}(25°\text{C}, pH = 4.5)\, x_{\text{CA}}(T) / x_{\text{CA}}(25°\text{C}) , \quad (11b)$$

where f_{CA} is the so-called soil CA enhancement factor. We can see from Eqs. (11a-b) that f_{CA} is not an intrinsic property of the soil and will vary with temperature, and pH, even at constant CA concentration. In the case where the catalysed rate dominates k in Eq. (11a) and the internal pH in close to 8.2 we have: $f_{\text{CA}} \approx 127\ [CA]$, where $[CA]$ is in nM.

In some situations the OCS uptake rates can be overridden by OCS production. This is the case when soil temperature rises above 25°C (Maseyk et al., 2014; Whelan and Rhew, 2015) or soil redox potential falls below -100mV (Devai and Delaune, 1995). Light has also been proposed as an important trigger of OCS production, assuming photoproduction processes similar to those observed in ocean waters can occur (Whelan and Rhew, 2015). However the literature and data on this possible mechanism is still too scarce and not quantitative enough to be accounted for in our model.

The soil redox potential (E_{h}) is a very dynamic variable that is not easily measured in the field, especially in unsaturated soils (*e.g.*, van Bochove et al., 2002). Although E_{h} and pH are linked, their relationship is not unique and depends on the set of oxidants and reductants present in the soil solution (*e.g.*, Delaune and Reddy, 2005). Also the soil redox potential is probably a more direct trigger for OCS production as it defines when sulfate ions start to become limiting for the plants or the soil microbes (Husson, 2012). For this study we thus consider that, for anoxic soils at least, E_{h} is the primary driver of OCS production, independently of pH:

$$P = P_{\text{ref}}\, y_{\text{P}}(E_{\text{h}})\, Q_{10}^{(T - T_{\text{ref}})/10} , \quad (12a)$$

where P_{ref} (mol m^{-3} s^{-1}) is the production rate at temperature T_{ref} (K) and low E_{h} (typically -200mV) and Q_{10} is the multiplicative factor of the production rate for a 10°C temperature rise. Because soil OCS emission, when observed in oxic soils, usually occurs at temperature around 25°C or higher, we will set $T_{\text{ref}} = 25°\text{C}$ and thus $P_{\text{ref}} = P_{25}$. According to results from Devai and DeLaune (1995), the function $y_{\text{P}}(E_{\text{h}})$ may be expressed as:

$$y_P(E_h) = \frac{1}{1+\exp\left(-(E_h - 100mV)/20mV\right)}, \quad (12b)$$

For oxic soils, Eq. 12a would probably need to be modified to incorporate the effect of light on the OCS production rate (Whelan and Rhew, 2015) and the function $y_P(E_h)$ given by Eq. 12b may not hold and in any case would be difficult to evaluate. Whether we should use UV light only or total solar radiation could also be debated. For all these reasons we decided for this study to only look at the effect of temperature on the OCS production rate and its consequences on the total OCS deposition rate.

2.2.6. Steady-state solution

The one-dimensional mass balance equation (Eq. (2)) can be re-written as:

$$\frac{\partial \varepsilon_t C}{\partial t} = \frac{\partial}{\partial z}\left\{\left(D_{eff,a} + \alpha_a |q_a|\right)\frac{\partial C}{\partial z} + \left(D_{eff,l} + \alpha_l |q_l|\right)\frac{\partial BC}{\partial z}\right\} + P - kB\theta C . \quad (13)$$

Assuming steady-state conditions and isothermal and uniform soil moisture and porosity through the soil column, this simplifies to:

$$D\frac{d^2C}{dz^2} - kB\theta C = -P , \quad (14)$$

with:

$$D = D_{eff,a} + \alpha_a |q_a| + \left(D_{eff,l} + \alpha_l |q_l|\right)B . \quad (15)$$

Boundary conditions are $C(z{=}0) = C_a$, the OCS concentration in the air above the soil column and $dC/dz(z{=}z_{max}) = 0$, *i.e.*, zero flux at the bottom of the soil column, located at depth z_{max} (the case for laboratory measurements). With such boundary conditions, the solution of Eq. (14) is:

$$C(z) = \frac{z_l^2}{D}P + (C_a - \frac{z_l^2}{D}P)\frac{e^{-z/z_l} + \xi^2 e^{+z/z_l}}{1+\xi^2}, \quad (16a)$$

with $z_l^2 = D/kB\theta$ and $\xi = e^{-z_{max}/z_l}$. This leads to an OCS efflux at the soil surface:

$$F = \sqrt{kB\theta D}\left(C_a - \frac{z_l^2 P}{D}\right)\frac{1-\xi^2}{1+\xi^2}, \quad (16b)$$

from which we can deduce the deposition velocity $V_d = -F/C_a$.

For field datasets, the condition at the lower boundary should be modified to $dC/dz(z\rightarrow\infty) = 0$ and the production rate P should be positive and uniform only over a certain depth z_P below the surface. In this case the steady-state solution becomes:

$$F = \sqrt{kB\theta D}\cdot\left(C_a - \frac{z_1^2 P}{D}(1-\exp(-z_P/z_1))\right). \quad (17)$$

We can verify that both equations give the same results if $z_{max}\rightarrow\infty$ and $z_P\rightarrow\infty$, and also that Eq. (17) leads to $F\rightarrow -Pz_P$ when $k\rightarrow 0$.

2.2.7. Soil incubation datasets used for model validation

The steady-state OCS deposition model presented here (Eq. (16b)) was evaluated against measurements performed on different soils in the laboratory. For this purpose we revisited the dataset presented in Van Diest and Kesselmeier (2008). Volumetric soil moisture content (θ, in $m^3(H_2O)\ m^{-3}(soil)$) was converted from gravimetric soil water content data ($M_{w,soil}$, in $g(H_2O)\ g(soil)^{-1}$) by means of the bulk density of the soil inside the chamber (ρ_b, in $g\ cm^{-3}$): $\theta = M_{w,soil}\rho_b/\rho_w$, where $\rho_w = 1 g\ cm^{-3}$ is the density of liquid water. The soil bulk density was itself estimated from the maximum soil moisture content after saturation ($\theta_{max} = M_{w,soil,max}\rho_b/\rho_w$), assuming the latter corresponded to soil porosity ($\phi = 1 - \rho_b/2.66$), *i.e.*, ($\rho_b = 1/(M_{w,soil,max}/\rho_w + 1/2.66)$. Soil thickness ($z_{max}$) was further estimated using ρ_b, soil dry weight (200g for the German soil, 80g for the other soils) and soil surface area ($165.1\ cm^2$) assuming soil density was uniform. Air porosity was calculated as: $\varepsilon_a = \varphi - \rho$. These estimates of ρ, φ, and ε_a where then used to compute D (Eq. 15, assuming $|\rho_a| = |\rho_l| = 0$) and F (Eq. 16b, with $P = 0$ and k estimated using Eq. 11b, with different f_{CA} values for each soil temperature incubation). Note that, in these experiments, the air in the chamber headspace was stirred with fans above the soil surface so that dispersion fluxes may be large (*i.e.* $|\rho_a|$ may not be zero). Without any more information about turbulence intensity at the soil surface in these experiments we had to neglect this possible complication. We will discuss below how this simplification may affect the results of our simulations of these experiments.

2.3. Results

2.3.1. Sensitivity to diffusivity model

Given the large diversity of expressions for the air tortuosity factor (τ_a) used to compute the effective diffusivity of OCS through the soil matrix, we felt it important to perform a sensitivity analysis of the model to different formulations available in the literature for τ_a. In **Fig. 2.4** we show how the steady-state soil OCS deposition velocity model (Eq. (16b)) responds to soil moisture or soil temperature for three different formulations of τ_a: Pen40

($\tau_a = 0.66$), MQ61 ($\tau_a = \varepsilon_a^{7/3}/\varphi^2$) and Mol03r ($\tau_a = \varepsilon_a^{3/2}/\varphi$). We also indicate the optimal soil moisture (θ_{opt}) and temperature ($T_{opt,Vd}$) for each formulation.

We found that the optimal temperature and the general shape of the response to temperature were not affected by the choice of the diffusivity model (**Fig. 2.4**, right panel). On the other hand the optimal soil moisture and the general shape of the response to soil moisture strongly depended on the choice made for τ_a (**Fig. 2.4**, left panel). In particular the model of Penman (1940) gives a perfectly symmetric response to soil moisture with an optimal value at $\theta_{opt} = 0.50\varphi$, unlike other formulations: $\theta_{opt} \approx 0.23\varphi$ for Millington and Quirk (1961) and $\theta_{opt} \approx 0.29\varphi$ for Moldrup et al. (2003).

It is also noticeable on the right panel of **Fig. 2.4** that the optimal temperature for V_d ($T_{opt,Vd}$) is actually lower than the prescribed optimal temperature for the catalysed OCS hydrolysis rate ($T_{opt,CA} = 25$°C in this case), even in the absence of an OCS source term. This is because $T_{opt,Vd}$ integrates other temperature responses, from the total effective diffusivity (D) and the OCS solubility (B). Although these variables do not exhibit a temperature optimum, their temperature responses affect the overall value of $T_{opt,Vd}$. It can be shown analytically that this leads to $T_{opt,Vd} < T_{opt,CA}$.

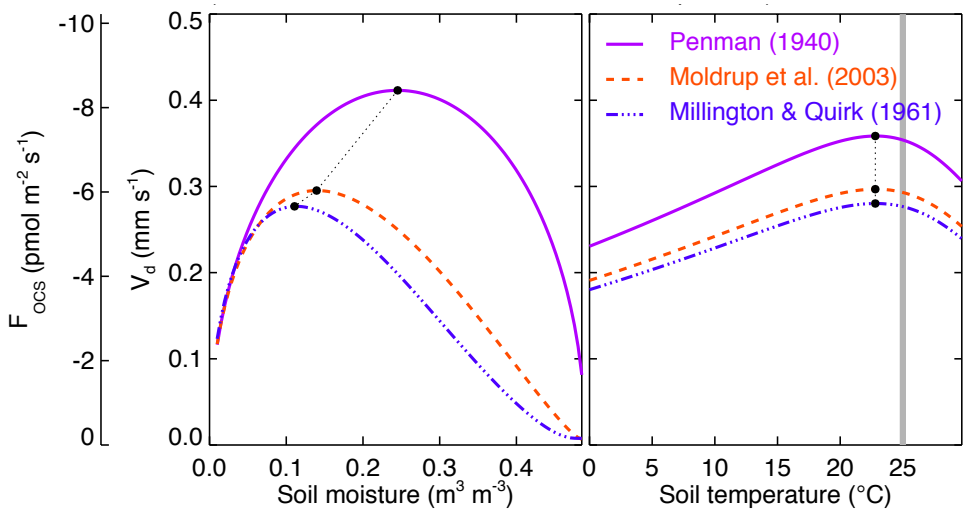

Figure 2.4: Sensitivity of the modelled OCS flux (F_{OCS}) and deposition velocity (V_d) to the formulation used to describe gaseous and solute diffusion. The soil moisture and temperature response curves shown here were obtained assuming no source term, a soil depth and pH of 1m and 7.2 respectively and a CA enhancement factor for OCS hydrolysis of 30000. Closed circles indicate the temperature or soil moisture optimum of each response curve and the grey thick line in right panel indicates the set optimal temperature for CA activity (25°C in this case).

2.3.2. Sensitivity to soil depth

Laboratory-based measurements of soil-air OCS fluxes are generally performed on small soil samples whose thickness are no more than a few centimetres. In contrast flux measurements performed in the field account for the entire soil column beneath the chamber enclosure. In order to see whether results from laboratory measurements could be directly applied to field conditions we performed a sensitivity analysis of the model to soil thickness (**Fig. 2.5**). We found that the responses to both soil moisture and soil temperature were affected by maximum soil depth (z_{max}), at least when z_{max} was below a few centimetres. Thin soils lead to lower maximum deposition rates but higher values of θ_{opt} and $T_{opt,Vd}$. In **Fig. 2.5** this is true mostly for $z_{max} = 1$ cm, and as soon as z_{max} reaches values above or equal to 3 cm, the response curve becomes almost indistinguishable from that obtained with $z_{max} = 100$ cm.

However this threshold on z_{max} also depends on soil CA activity. Results shown in **Fig. 2.5** were obtained with an enhancement factor for OCS hydrolysis f_{CA} of only 10000. An even smaller enhancement factor would have led to a deeper transition zone (*e.g.* about 10 cm with f_{CA} of 1000). This is because in Eq. (16b), the steady-state model of OCS deposition is proportional to $\tanh(z_{max}/z_1)$. Given the shape of the hyperbolic tangent function, we expect our steady-state OCS deposition velocity model to become insensitive to z_{max} as soon as $z_{max}/z_1 \geq 2$. With $z_1 = \sqrt{D/kB\theta}$ and because k is proportional to f_{CA} we can see that this condition on z_{max}/z_1 will depend on f_{CA}. At $f_{CA} = 1000$, we have $z_1(\theta_{opt}) \sim 5$ cm while at $f_{CA} = 10000$ we have $z_1(\theta_{opt}) \sim 1.5$ cm.

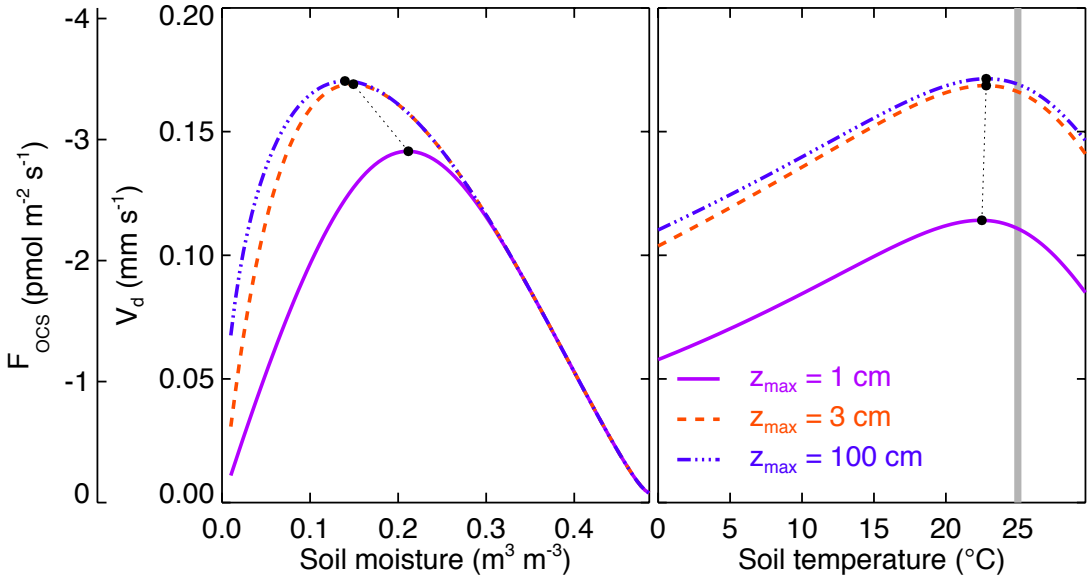

Figure 2.5: Sensitivity of the modelled OCS flux (F_{OCS}) and deposition velocity (V_d) to soil column depth. The soil moisture and temperature response curves shown here were obtained using the diffusivity model of Moldrup et al. (2003) and assuming no source term, a soil pH of 7.2 and a CA enhancement factor for OCS hydrolysis of 10000. Closed circles indicate the temperature or soil moisture optimum of each response curve and the grey thick line in right panel indicates the set optimal temperature for CA activity (25°C in this case).

This response to soil depth was already observed by Kesselmeier et al. (1999) who reported measurements of OCS deposition velocity that increased linearly with the quantity of soil in their soil chamber enclosure up to 200g of soil and then reached a plateau at around 400g. Because their soil samples were evenly spread inside the soil chamber, an increase in the quantity of soil directly translates into an increase in soil thickness. Using an enhancement factor f_{CA} of 27000 we were able to reproduce their saturation curve with soil weight using our steady-state model (**Fig. 2.6**). A lower f_{CA} value would have reduced the curvature of the model but would have also lowered the maximum V_d (not shown, but see **Fig. 2.7**). A value for f_{CA} of 27000 was the best compromise to match the observed saturation curve. Because different soil weights were measured at different times with new soil material each time, it is possible that they would correspond to slightly different f_{CA} values and this could explain the slight mismatch between the model and the fitted curve on the observations.

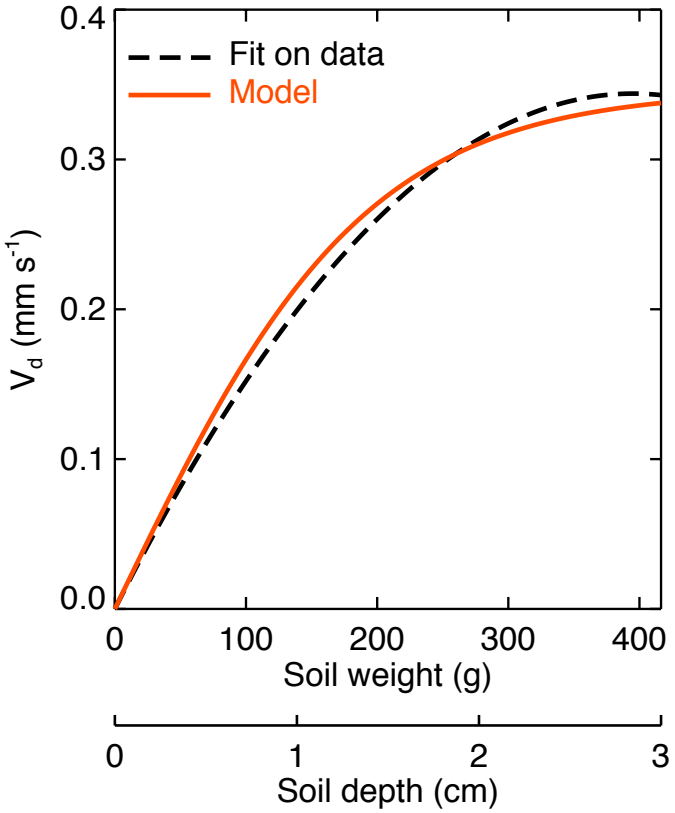

Figure 2.6: Modelled (solid line) and observed (dotted line) response of the modelled OCS deposition velocity (V_d) to soil column depth. Soil column depth is also converted into soil weight assuming a soil surface area of 165.1 cm^2 and a soil bulk density and pH of 0.85 kg m^3 and 7.2, respectively, to be comparable with the experimental setup used in Kesselmeier et al. (1999) to derive the observed response curve. Model results shown here were obtained using the diffusivity model of Moldrup et al. (2003) and assuming an enhancement factor and an optimum temperature for OCS hydrolysis of 26000 and 25°C, respectively and no source term. Soil water content and temperature were also set to 11% weight and 17°C, respectively, to be comparable with the experimental data, while the fit on observed uptake rates that was originally reported were converted into deposition velocities assuming a constant mixing ratio of 600 ppt (Kesselmeier et al., 1999).

2.3.3. Sensitivity to soil CA activity and OCS emission rates

Our model has two main parameters that need to be constrained by observations: these are the CA concentration (or conversely the CA enhancement factor f_{CA}) and the OCS production rate at 25°C (P_{25}). A sensitivity analysis of our steady-state OCS deposition model to these two parameters is shown in **Fig. 2.7** and **Fig. 2.8**. Both parameters affect the maximum

deposition rates but in opposite directions, with high f_{CA} values leading to higher V_d and high P_{25} values leading to lower V_d. This was expected from Eq. (16b) as V_d is proportional to $\sqrt{f_{CA}}$ and is linearly and negatively related to P_{25}.

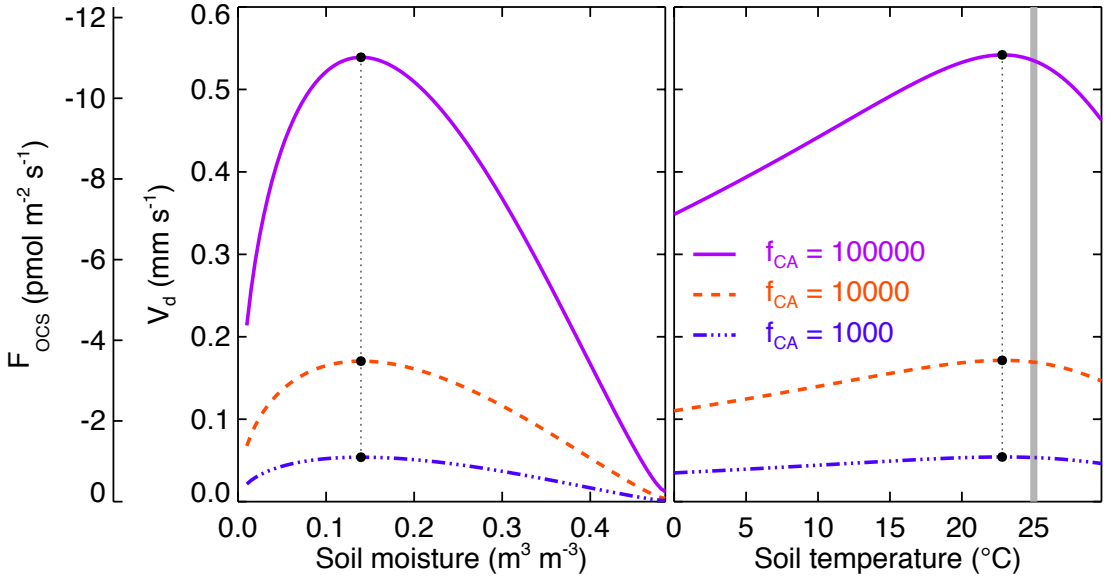

Figure 2.7: Sensitivity of the modelled OCS flux (F_{OCS}) and deposition velocity (V_d) to soil CA activity. The soil moisture and temperature response curves shown here were obtained using the diffusivity model of Moldrup et al. (2003) and assuming no source term, a soil pH of 7.2 and a soil depth of 1 m. Closed circles indicate the temperature or soil moisture optimum of each response curve and the grey thick line in right panel indicates the set optimal temperature for CA activity (25°C in this case).

Interestingly, the optimal soil moisture is not modified by changes in f_{CA} (**Fig. 2.7**, left panel) and only slightly by P_{25} (**Fig. 2.8**, left panel). This means that, provided that z_{max} is known precisely (or larger than $2z_1$, see section 2.3.2), the overall shape of the response to soil moisture (as typically measured during a drying cycle) and the exact value of θ_{opt} are indicative solely of the diffusivity model to be used (**Fig. 2.4**). This result is important and should help us to, at least, decide whether the Pen40 formulation for τ_a must be used instead of a more asymmetrical one (the Mol03r and MQ61 formulations are harder to distinguish, see **Fig. 2.4**).

The value of $T_{opt,Vd}$ is also insensitive to changes in f_{CA} (**Fig. 2.7**, right panel) but diminishes when P_{25} increases (**Fig. 2.8**, right panel). This means that very low optimal temperature

values $T_{opt,Vd}$ (*i.e.* unusually low compared to expected values for enzymatic activities and $T_{opt,CA}$) should be indicative of an OCS emission term, even if the values of V_d remain positive (*i.e.* the soil acts as a sink) in the temperature range explored. Of course at higher temperature, and because in our model the OCS source term responds exponentially with temperature (Q_{10} response) while k exhibits an optimal temperature ($T_{opt,CA}$), the V_d should reach negative values if the value of P_{25} is large and f_{CA} is low. In some extreme cases where P_{25} fully dominates over f_{CA}, our model could even predict OCS fluxes close to zero at temperatures below ~10°C that would increase exponentially at warmer temperatures, as it has been observed in some agricultural soils (Liu et al., 2010a; Maseyk et al., 2014; Whelan and Rhew, 2015).

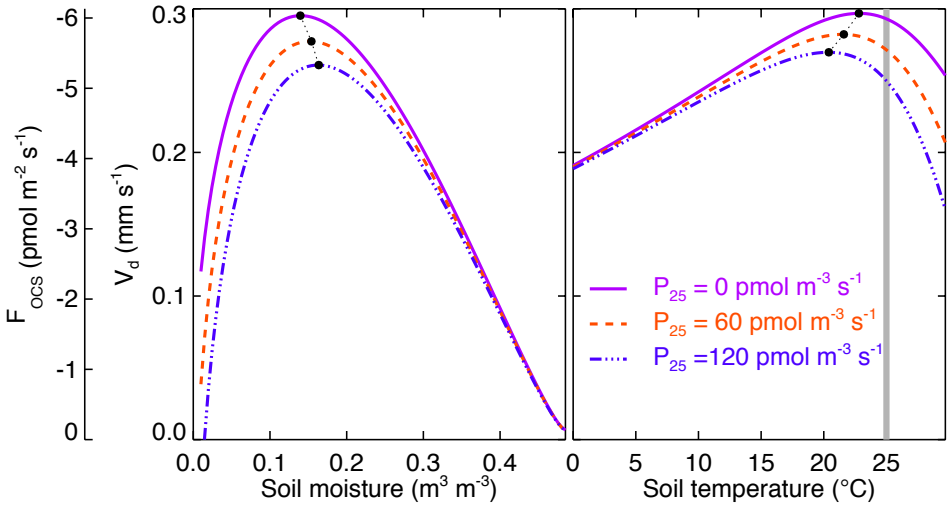

Figure 2.8: Sensitivity of the modelled OCS flux (F_{OCS}) and deposition velocity (V_d) to soil OCS emission rate. The soil moisture and temperature response curves shown here were obtained using the diffusivity model of Moldrup et al. (2003) and assuming a CA enhancement factor of 30000, a soil pH of 7.2 and a soil depth of 1 m. OCS source is assumed to occur only in the top 5cm. Closed circles indicate the temperature or soil moisture optimum of each response curve and the grey thick line in right panel indicates the set optimal temperature for CA activity (25°C in this case).

2.3.4. Sensitivity to soil pH

The sensitivity of our model to different soil *pH* was also tested. Because the effect of soil *pH* is mostly to modify the hydration rate *k*, we could not set a constant value of f_{CA}. Instead we fixed the CA concentration in the soil (330nM) and also adjusted the internal *pH* assuming partial homeostasis with changes in soil *pH*, as observed in bacteria (Krulwich et al., 2011): $pH_{in} = 6 + 0.25pH$ (**Fig. 2.9**). By assuming pH_{in} to vary with changes in soil *pH* we changed k_{cat} (Eq. (11a)) and this was equivalent to changing f_{CA}. Indeed results shown in **Fig. 2.9** are very similar to those shown in **Fig. 2.7** where low *pH* (and pH_{in}) correspond to low f_{CA} values. If we had assumed that pH_{in} was not modified by soil *pH* (and fixed at 8.2) no change in k_{cat} would have been observed and the change in *k* would have only been caused by the effect of soil *pH* on k_{uncat} (Eq. 11a). Unless the soil contains very little CA or the soil *pH* moves to very alkaline values (**Fig. 2.3**), this change in k_{uncat} would have been too small to significantly affect V_d. Indeed at a CA concentration of 330nM and with a pH_{in} maintained at 8.2 our model Eq. (16b) gives exactly the same values for soil *pH* ranging from 4 to 9. In summary, within the range of soil *pH* found in nature, the response of V_d to this environmental factor is only happening through its influence on pH_{in} and hence on k_{cat} (Eq. 10b and **Fig.2.3 b**).

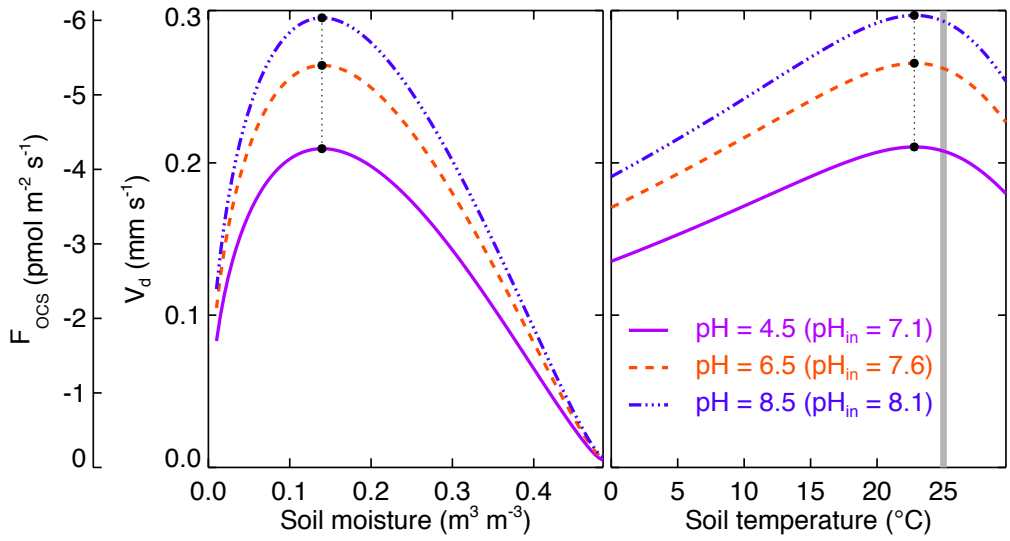

Figure 2.9: Sensitivity of the modelled OCS flux (F_{OCS}) and deposition velocity (V_d) to soil pH. The soil moisture and temperature response curves shown here were obtained using the diffusivity model of Moldrup et al. (2003) and assuming no source term, a CA concentration in the soil of 330nM and a soil depth of 1 m. Closed circles indicate the temperature or soil moisture optimum of each response curve and the grey thick line in right panel indicates the set optimal temperature for CA activity (25°C in this case).

2.3.5. Model evaluation against lab-based drying curves

Our steady-state OCS deposition model was further evaluated against experimental data from Van Diest and Kesselmeier (2008) and results are shown in **Figs. 2.10-2.13** for different soils. Because OCS deposition values observed by Van Diest and Kesselmeier (2008) were all positive we set the source term to zero ($P_{25} = 0$) although we recognise that this may be an oversimplification. We also set the optimum temperature for the catalysed OCS hydration rate to 25°C. A value for f_{CA} was then manually adjusted for each soil and each temperature, between 21600 and 336000, depending on the soil origin and temperature (**Figs. 2.10-2.13**). Once this adjustment on f_{CA} was done, our model, with the diffusivity formulation of Moldrup et al. (2003), was able to reproduce most observed response curves to soil drying (**Figs. 2.10-2.13**, left and middle panels). The model was also able to reproduce, within the measurement uncertainties, the temperature dependency of V_d at a soil moisture level of 0.12 m^3 m^{-3} (far right panels in **Figs. 2.10-2.13**).

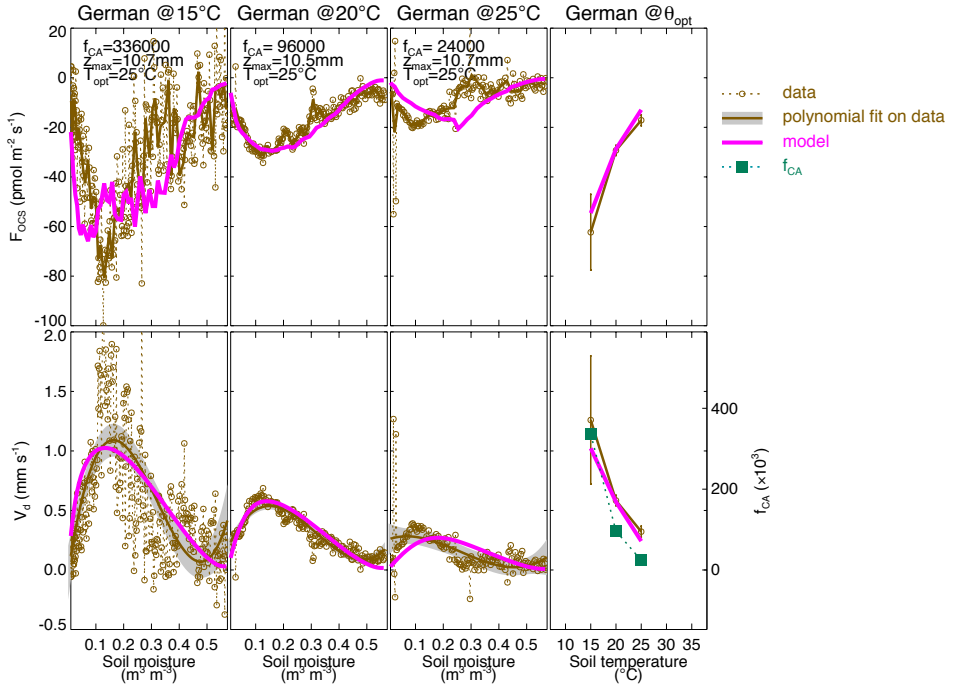

Figure 2.10: Observed and modelled soil-air OCS flux (F_{OCS}) and deposition velocity (V_d) during soil drying at different incubation temperatures (indicated above each panel) and their value at a soil moisture content W_{opt} = 0.12 m^3 m^{-3} (far right panels). The soil moisture and temperature response curves shown here were recalculated from data of Van Diest and Kesselmeier (2008) (open circles and brown line) or computed with our model (thick pink line) using the diffusivity model of Moldrup et al. (2003). For each incubation temperature, a

different set of model parameters (f_{CA}, z_{max}, T_{opt}) was used as indicated in each panel. The data shown here are representative of an agricultural soil near Mainz in Germany (soil weight is 200g).

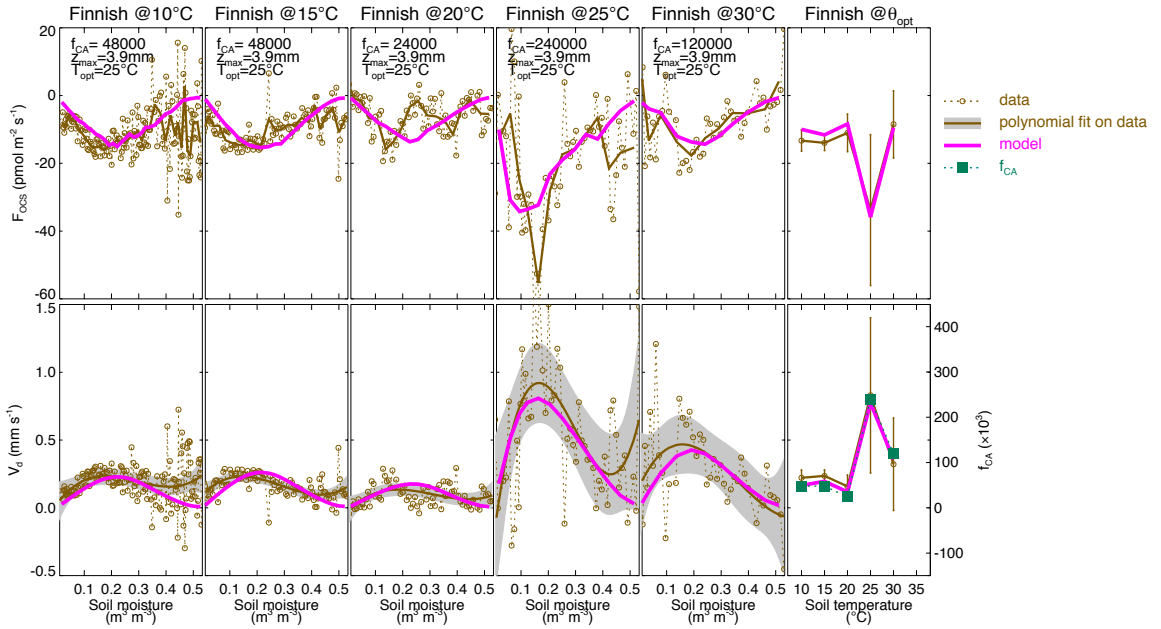

Figure 2.11: Same as Fig. 9 but for an agricultural soil near Hyytiala in Finland (soil weight is 80g).

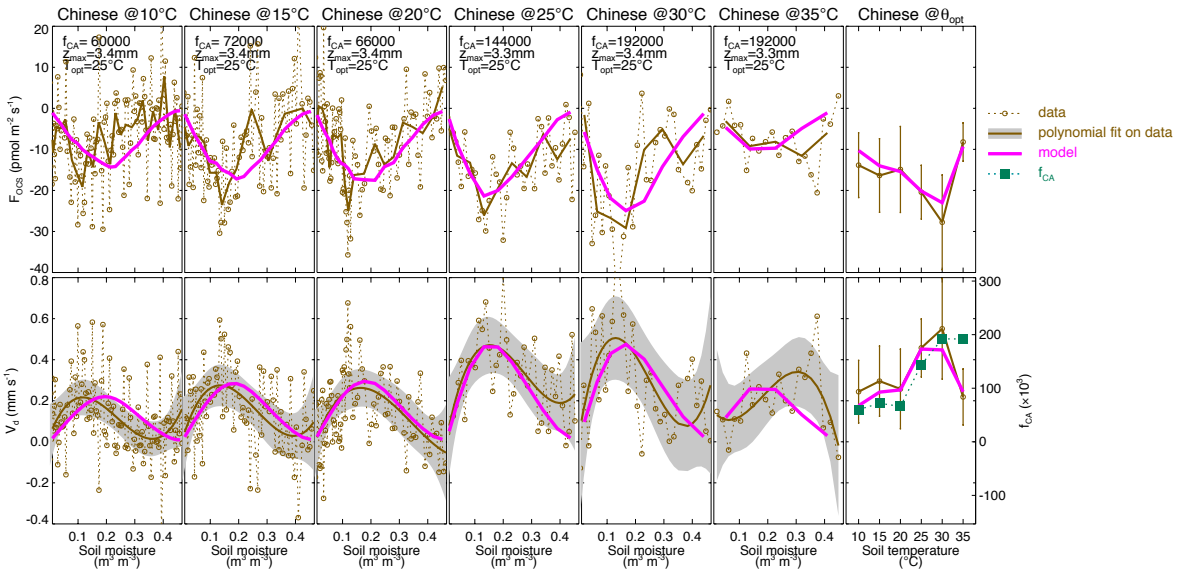

Figure 2.12: Same as Fig. 9 but for an agricultural soil from north-eastern China (soil weight is 80g).

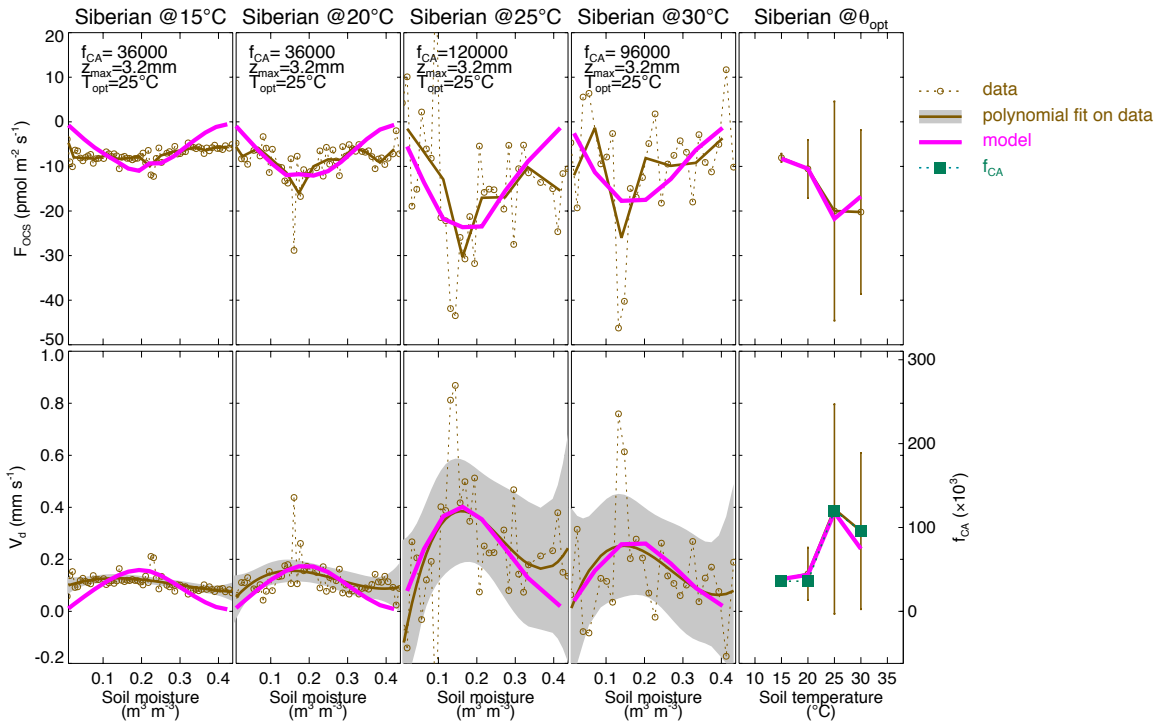

Figure 2.13: Same as Fig. 9 but for an agricultural soil from Siberia (soil weight is 80g).

2.4. Discussion

2.4.1. Can the proposed model explain observations realistically?

Many studies have clearly demonstrated that soil moisture strongly modulates OCS uptake by soils, with an optimal soil moisture content usually around 12% of soil weight (Kesselmeier et al., 1999; Liu et al., 2010a; Van Diest and Kesselmeier, 2008). As noted in some of these studies, such a bell-shape response is indicative of reactional and diffusional limitations at low and high soil moisture contents, respectively. Using our steady-state formulation for shallow soils (Eq. (16b)) we were able to reproduce the soil moisture response observed experimentally (**Fig. 2.10-2.13**). We also found that the observed asymmetric response to soil moisture was best captured by the soil diffusivity model of Moldrup et al. (2003) or Millington and Quirk (1961) and showed that the optimum soil moisture could be related to soil porosity: $\theta_{opt} = 0.3\varphi/1.3$ for MQ61 and $\theta_{opt} = 2\varphi/7$ for Mol03r. Using our model we were also able to explain the response of OCS uptake to soil weight (*i.e.* soil thickness) observed by Kesselmeier et al. (1999) (**Fig. 2.6**).

We also tested our model against observations of the temperature response of V_d. Empirical studies showed that, for a given soil, the maximum OCS uptake rate was modulated by

incubation temperature, with an optimal temperature ranging from 15°C to 35°C (Kesselmeier et al., 1999; Liu et al., 2010a; Van Diest and Kesselmeier, 2008). This temperature response was interpreted as an enzymatically catalysed process, governed by soil micro-organisms' CA activity (Kesselmeier et al., 1999; Liu et al., 2010a; Van Diest and Kesselmeier, 2008). To reproduce this response of V_d to incubation temperature using our steady-state model, we had to manually adjust f_{CA} for each incubation temperature. We will argue here that using different f_{CA} values on the same soil is justified given the way measurements were performed. Van Diest and Kesselmeier (2008) wanted to characterise the V_d response to soil drying at a set temperature and for this, they saturated a soil sample with water and acclimated it to a given temperature (between 5°C and 35°C), they then recorded the OCS exchange immediately and continued to measure until the soil was completely dry, which usually lasted 1 to 2 days. The same soil sample, or a different one from the same geographical location, was then re-watered and re-acclimated to a different temperature and another cycle of measurements started. Sometimes several months separated measurements at two different temperatures but storage time (at 5°C) did not seem to affect the soil CA activity (measurements on the same soil and incubation temperature were reproducible). On the other hand incubation temeprature clearly differ and, at least for the German soil, samples were not collected all at the same season. This means that, for a given soil origin, the microbial community was experiencing different environmental conditions and history between each drying curve. Thus, the size and diversity of the microbial population were likely different for each incubation temperature, thus justifying the use of different enhancement factors at each temperature. Interestingly f_{CA} tends to increase with incubation temperature, as we would expect for the microbial biomass. Only the German soil has a higher f_{CA} at low temperature (15°C) and this corresponds to a soil sampled at a different period (March) than the other two incubation temperatures (June).

Following this argument it seems that the optimum temperatures observed by Van Diest and Kesselmeier (2008) for different soil types are not a good proxy for the optimal temperature of CA activity ($T_{opt,CA}$). Using our model we already showed that the optimum temperature for V_d ($T_{opt,Vd}$) was different from $T_{opt,CA}$, at least for deep soils (**Fig. 2.5**). A closer inspection of the results shown in **Figs. 2.10-2.13** also show that the adjusted f_{CA} values closely follow the patterns of the maximum V_d at θ_{opt} (see right panels in **Figs. 2.10-2.13**). This means that the optimum temperature observed by Van Diest and Kesselmeier (2008) is a better indicator of maximum f_{CA} or equivalently maximum CA concentration (assuming all the CAs in the soil have similar k_{cat}/K_M as the pea extracts measured by Protoschill-Krebs et al. (1996). This

could explain why the optimum for the German soil was so low (around 15°C), *i.e.*, lower than expected for $T_{opt,CA}$. The presence of a competing enzymatic process, such as OCS emission, could have explained this low $T_{opt,Vd}$ value (**Fig. 2.8**) but it is more likely that the soil sample studied at 15°C contained more CA than those used for other incubation temperatures. Measurements on microbial biomass could have helped confirm this hypothesis but were unfortunately not made.

Because f_{CA} is a fitting parameter in our model, it is important to see if the values that we derived for the different soils are realistic. There are two ways to do so. First, we have a relatively good idea of how much CA is needed inside the cytosol of leaf mesophyll cells or in unicellular algae, which is of the order of 100 mM (Tholen and Zhu, 2011). Assuming this CA concentration value is also applicable to microbial cells, and using estimates of the soil microbial population size we can convert this physiological CA concentration ($[CA]_{in}$) into a CA concentration in the soil matrix ([CA]): $[CA]\theta = [CA]_{in}\rho_{mic}$, where ρ_{mic} (m^3 microbes m^{-3} soil) denotes the volumetric microbial content of the soil. Using a typical microbial population size of $3 \cdot 10^9$ cm^{-3} and an average cell size of 1 mm^3 (Wingate et al., 2009), we obtain a microbial content of $\rho_{mic} = 0.003$ m^3 m^{-3} and a soil CA content of about 1000 nM (we used $\theta = 0.3$). Using this value of [CA] and the k_{cat}/K_M value for OCS (2.39 s^{-1} mM^{-1} at 20°C and pH_{in} 8.2) this leads to an f_{CA} value of about 127000 for OCS, which is in the same order of magnitude as those found for the different soils in this study (between 21600 and 336000, with a median value at 66000). From this crude calculation we can conclude that our f_{CA} estimates are physiologically meaningful.

Another way of checking if our f_{CA} estimates are meaningful is to convert them into f_{CA} equivalents for soil CO_2 isotope fluxes, for which we have a better idea of what the expected values should be (Seibt et al., 2006; Wingate et al., 2009; 2010; 2008). The k_{cat}/K_M value for CO_2 in pea extracts has been measured for a *pH* range of 6-9 and at 25°C (Bjorkbacka et al., 1999). The *pH* response described a similar pattern as the one found for *Arabidopsis* by Rowlett et al. (2002) (**Fig. 2.3**) with a pK_a of 7.1. Using $x_{CA}(T)$ and $y_{CA}(pH_{in})$ to convert those values to pH_{in} 8.2 and 20°C, we obtain a k_{cat}/K_M value for CO_2 of 50 s^{-1} mM^{-1}, *i.e.*, about 20 times greater than the k_{cat}/K_M for OCS. Given the difference in uncatalysed hydration rates between the two gas species (12000 ms^{-1} for CO_2 and 21.5 ms^{-1} for OCS at 25°C and $pH = 4.5$) this means that at equal soil CA concentration, the f_{CA} for CO_2 should be about 30 times smaller than that derived for OCS. This corresponds to a median f_{CA} value of 2200 for CO_2, *i.e.*, at the higher end of values observed in different soils (Wingate et al., 2009).

The calculation above considers only β-CA kinetic parameters to relate the soil CA enhancement factor for OCS to the f_{CA} for CO_2. However other enzymes can catalyse OCS hydrolysis and not have a strong affinity to CO_2. For example Smeulders et al. (2012) found a carbon disulphide hydrolase from an acido-thermophilic archaeon that was very efficient at catalysing OCS hydrolysis but did not have CO_2 as one of its substrates (Smeulders et al., 2012). More recently, Ogawa et al. (2013) found in *Thiobacillus thioparus*, a sulfur-oxidizing bacterium widely distributed in soils and freshwaters, an enzyme that shared a high similarity with β-CAs and was able to catalyse OCS hydrolysis with a similar efficiency (K_M = 60mM, k_{cat} = 58 s^{-1} at *pH* 8.5 and 30°C) but whose CO_2 hydration activity was 3-4 orders of magnitude smaller than that of β-CAs. For this reason they called this enzyme carbonyl sulphide hydrolase (COSase). The carbon disulphide hydrolase identified by Smeulders et al. (2012) may only be present in extremely acidic environments such as volcanic solfataras, but the COSase found in *T. thioparus* may be more ubiquitous in soils. If this was the case this would imply that the f_{CA} ratio of OCS to CO_2 is not unique and could, in some soils, be higher than the same ratio derived from β-CA kinetic parameters only. This could partly explain the highest f_{CA} values obtained here for OCS.

Higher-than-expected values of f_{CA} could also be explained by the fact that we neglected dispersion fluxes when we compared the model against observations. Indeed dispersion fluxes would enhance OCS diffusion (Eq. (15)) and result in larger deposition velocities (Eq. (16b)) for the same level of CA concentration. Results from Maier et al. (2012) show that the diffusivity D could be easily doubled by the presence of turbulence above the soil surface, which would be equivalent to a doubling of k (D and k appear as a product in the sink term of Eq. (16b)). This means that, if dispersion occurred in the experiments (a possibility that we cannot rule out), the f_{CA} values that we derived from them may be overestimated by a factor two, bringing them closer to values compatible with CO_2 studies.

To conclude, the f_{CA} values derived here for OCS seem compatible with physiological CA contents and also compatible with f_{CA} values reported in CO_2 isotope studies, given possible affinity differences of some CAs towards OCS and CO_2 and possible artefacts of mechanical dispersion caused by fans in some laboratory experiments.

2.4.2. Can we transpose laboratory data to field conditions?

Response curves of OCS deposition rates to soil moisture and temperature have been derived from laboratory experiments similar to those presented here (Kesselmeier et al., 1999) and the derived equations have been used to estimate the OCS uptake by soils at the global scale (Kettle et al., 2002). Also Van Diest and Kesselmeier have proposed that the optimum (gravimetric) soil moisture content for OCS deposition was around 0.12 g g^{-1}, independently of soil type (Van Diest and Kesselmeier, 2008). Our model allows us to verify if such simplification or extrapolation is justified, on a theoretical point of view at least. For semi-infinite soil columns we showed that θ_{opt} varied with soil porosity from 0.23φ to 0.5φ, depending on the soil diffusivity model used. Assuming soil bulk density is 2.66(1 - φ), this leads to gravimetric soil moisture contents of between 0.61φ(1 - φ) and 1.33φ(1 - φ), which is clearly dependent on soil type. Also from **Fig. 2.5** we can see that the general shape of the soil moisture response and θ_{opt} strongly depend on the exact soil depth used during the experiment, at least for soil less than 3cm thick (or more if the CA activity is lower). For thicker soils the deepest soil layers do not contribute to the exchange and we reach the saturation point with soil weight shown in **Fig. 2.6**. However in both aforementioned studies (Kesselmeier et al., 1999; Van Diest and Kesselmeier, 2008), care was taken not to reach the saturation point (using soil weights of about 80g). From our model results we can see that this would lead to an overestimation of θ_{opt} and an overall understimation of V_d (**Fig. 2.5**). Thus based on this observation we would recommend to use soil depths of at least 5-6 cm in future studies so that the results can be more readily extrapolated to field conditions.

Another difficulty when we want to extrapolate laboratory data to the natural environment is that soil disturbance prior to the experiment (sieving, repacking…) strongly modifies the gas diffusivity properties of the soil. Our results show that OCS deposition rates can be extremely sensitive to the choice of the diffusvity model used (**Fig. 2.4**). In highly compacted, highly aggregated soils the gas diffusivity response to soil moisture content can even become bi-modal (Deepagoda et al., 2011) that would certainly have a strong impact on the V_d-θ relationship. Even without such a complication our results suggest that deposition rate measurements on repacked soils may not be representative of field conditions because the soil treatment would modify the diffusivity properties of the soil and alter the soil moisture response of the OCS deposition rate. On the other hand applying our model (Eq. 17, for semi-infinite soil column) with a soil diffusivity formulation applicable to undisturbed soils (*i.e.* Mol03u or Deepa11, see **Table 2.1**) should work for interpreting field measurements.

2.5. Perspectives

Our model so far has been tested under steady state conditions and with fairly uniform soil properties (temperature, moisture, *pH*…). In the natural environment such conditions are the exception rather than the rule. The model has not been tested either on true temperature response curves as happens in nature with strong diurnal variations of temperature at nearly constant soil moisture content. Indeed data from Van Diest and Kesselmeier (2008) have been collected at constant incubation temperatures and are therefore more indicative of the range of f_{CA} and V_d values one would expect over a growing season for a given soil type. Suprisingly we could not find published laboratory measurements of V_d where soil temperature was varied diurnally.

Another point that should be addressed in future studies is the characterisation of the soil microbial community size and structure, that should be done systematically with the soil OCS deposition measurements. This would allow us to test whether our upscaling of CA activity to the soil level (Eq. (11a)) is correct or not, and compatible with physiologically realistic CA contents in soil microbes. Our results so far suggest that the CA contents that we derive seem physiologically meaningful and also compatible with CO_2 isotope studies, given the uncertainties in the k_{cat}/K_M values of different CAs for the two substrates and in the diffussivity model formulation for different experimental setup (see above). Concurrent microbial data on the soil samples could have greatly constrained our downscaling exercise and lead to a more precise picture of possible mismatch between our model and the observations. When combined with both OCS and CO_2 isotope gas exchange measurements, it could also help identify the microbial communities that are more prone to express specific CAs which favor OCS uptake such as the COSase found in *T. thioparus*.

Finally our study mostly focused on the temperature response of the OCS production term, but there is a growing body of evidence that other environmental variables trigger OCS production from soils, independently of temperature. In oxic soils, light-induced OCS emissions have been observed (Whelan and Rhew, 2015) whereas in anoxic soils, redox potential seems to be the main trigger (Devai and Delaune, 1995). The mechanisms leading to these OCS emission rates should be better understood before we can incorporate them into a modelling framework and estimate OCS fluxes at large scales. For this reason we strongly suggest to systematically report measurements of light and soil redox potential (and/or S speciation) in future soil OCS flux studies.

References

Beer, C., Reichstein, M., Tomelleri, E., Ciais, P., Jung, M., Carvalhais, N., Rödenbeck, C., Arain, M. A., Baldocchi, D., Bonan, G. B., Bondeau, A., Cescatti, A., Lasslop, G., Lindroth, A., Lomas, M., Luyssaert, S., Margolis, H., Oleson, K. W., Roupsard, O., Veenendaal, E., Viovy, N., Williams, C., Woodward, F. I. and Papale, D.: Terrestrial Gross Carbon Dioxide Uptake: Global Distribution and Covariation with Climate, Science, 329(5993), 834–838, doi:10.1126/science.1184984, 2010.

Berry, J. A., Wolf, A., Campbell, J. E., Baker, I., Blake, N., Blake, D., Denning, A. S., Kawa, S. R., Montzka, S. A., Seibt, U., Stimler, K., Yakir, D. and Zhu, Z.: A coupled model of the global cycles of carbonyl sulfide and CO_2: A possible new window on the carbon cycle, J. Geophys. Res. Biogeosci., 118(2), 842–852, doi:10.1002/jgrg.20068, 2013.

Bird, R. B., Stewart, W. E. and Lightfoot, E. N.: Transport phenomena, John Wiley & Sons. 2002.

Bjorkbacka, H., Johansson, I.-M. and Forsman, C.: Possible Roles for His 208 in the Active-Site Region of Chloroplast Carbonic Anhydrase from *Pisum sativum*, Arch. Biochem. Biophys., 361(1), 17–24, 1999.

Blezinger, S., Wilhelm, C. and Kesselmeier, J.: Enzymatic consumption of carbonyl sulfide (COS) by marine algae, Biogeochemistry, 48(2), 185–197, 2000.

Bremner, J. M. and Banwart, W. L.: Sorption of sulfur gases by soils, Soil Biology and Biochemistry, 8(2), 79–83, 1976.

Burnell, J. N. and Hatch, M. D.: Low bundle sheath carbonic anhydrase is apparently essential for effective C_4 pathway operation, Plant Physiology, 86(4), 1252–1256, 1988.

Campbell, J. E., Carmichael, G. R., Chai, T., Mena-Carrasco, M., Tang, Y., Blake, D. R., Blake, N. J., Vay, S. A., Collatz, G. J., Baker, I., Berry, J. A., Montzka, S. A., Sweeney, C., Schnoor, J. L. and Stanier, C. O.: Photosynthetic Control of Atmospheric Carbonyl Sulfide During the Growing Season, Science, 322(5904), 1085–1088, doi:10.1126/science.1164015, 2008.

Castro, M. S. and Galloway, J. N.: A comparison of sulfur-free and ambient air enclosure techniques for measuring the exchange of reduced sulfur gases between soils and the atmosphere, Journal of Geophysical Research: Atmospheres (1984–2012), 96(D8), 15427–15437, 1991.

Choi, J.-G., Do, D. D. and Do, H. D.: Surface Diffusion of Adsorbed Molecules in Porous Media: Monolayer, Multilayer, and Capillary Condensation Regimes, Ind. Eng. Chem.

Res., 40(19), 4005–4031, doi:10.1021/ie010195z, 2001.

De Bruyn, W. J., Swartz, E., Hu, J. H., Shorter, J. A., Davidovits, P., Worsnop, D. R., Zahniser, M. S. and Kolb, C. E.: Henry's law solubilities and Śetchenow coefficients for biogenic reduced sulfur species obtained from gas-liquid uptake measurements, Journal of Geophysical Research: Atmospheres (1984–2012), 100(D4), 7245–7251, 1995.

Deepagoda, T. K. K. C., Moldrup, P., Schjønning, P., Jonge, L. W. de, Kawamoto, K. and Komatsu, T.: Density-Corrected Models for Gas Diffusivity and Air Permeability in Unsaturated Soil, Vadose Zone Journal, 10(1), 226–238, doi:10.2136/vzj2009.0137, 2011.

Delaune, R. D. and Reddy, K. R.: Redox Potential, edited by D. Hillel, pp. 366–371, Encyclopedia of Soils in the Environment. 2005.

Devai, I. and Delaune, R. D.: Formation of volatile sulfur compounds in salt marsh sediment as influenced by soil redox condition, Organic Geochemistry, 23(4), 283–287, 1995.

Elliott, S., Lu, E. and Rowland, F. S.: Rates and mechanisms for the hydrolysis of carbonyl sulfide in natural waters, Environ. Sci. Technol., 23(4), 458–461, doi:10.1021/es00181a011, 1989.

Evans, J. R., Kaldenhoff, R., Genty, B. and Terashima, I.: Resistances along the CO_2 diffusion pathway inside leaves, Journal of Experimental Botany, 60(8), 2235–2248, doi:10.1093/jxb/erp117, 2009.

Falta, R. W., Javandel, I., Pruess, K. and Witherspoon, P. A.: Density-Driven Flow of Gas in the Unsaturated Zone Due to the Evaporation of Volatile Organic-Compounds, Water Resources Research, 25(10), 2159–2169, 1989.

Frankenberg, C., Fisher, J. B., Worden, J., Badgley, G., Saatchi, S. S., Lee, J.-E., Toon, G. C., Butz, A., Jung, M., Kuze, A. and Yokota, T.: New global observations of the terrestrial carbon cycle from GOSAT: Patterns of plant fluorescence with gross primary productivity, Geophysical research Letters, 38(17), L17706, doi:10.1029/2011GL048738, 2011.

Friedlingstein, P., Bopp, L., Rayner, P., Cox, P. M., Betts, R., Jones, C., Bloh, Von, W., Brovkin, V., Cadule, P. and Doney, S. C.: Climate-carbon cycle feedback analysis: Results from the C4MIP model intercomparison, Journal of Climate, 19(14), 3337–3353, 2006.

Gurney, K. R. and Eckels, W. J.: Regional trends in terrestrial carbon exchange and their seasonal signatures, Tellus B, 63(3), 328–339, doi:10.1111/j.1600-0889.2011.00534.x, 2011.

Haritos, V. S. and Dojchinov, G.: Carbonic anhydrase metabolism is a key factor in the toxicity of CO_2 and COS but not CS_2 toward the flour beetle *Tribolium castaneum* [Coleoptera: Tenebrionidae], Comparative Biochemistry and Physiology Part C: Toxicology & Pharmacology, 140(1), 139–147, doi:10.1016/j.cca.2005.01.012, 2005.

Husson, O.: Redox potential (Eh) and pH as drivers of soil/plant/microorganism systems: a transdisciplinary overview pointing to integrative opportunities for agronomy, Plant Soil, 362(1-2), 389–417, doi:10.1007/s11104-012-1429-7, 2012.

Isik, S., Kockar, F., Aydin, M., Arslan, O., Guler, O. O., Innocenti, A., Scozzafava, A. and Supuran, C. T.: Carbonic anhydrase inhibitors: inhibition of the beta-class enzyme from the yeast *Saccharomyces cervevisiae* with sulfonamides and sulfamates, Bioorganic & Medicinal Chemistry, 17(3), 1158–1163, doi:10.1016/j.bmc.2008.12.035, 2009.

Kesselmeier, J., Teusch, N. and Kuhn, U.: Controlling variables for the uptake of atmospheric carbonyl sulfide by soil, J. Geophys. Res, 104(D9), 11,577–11,584, 1999.

Kettle, A. J., Kuhn, U., Hobe, von, M., Kesselmeier, J. and Andreae, M. O.: Global budget of atmospheric carbonyl sulfide: Temporal and spatial variations of the dominant sources and sinks, J. Geophys. Res, 107(D22), 4658, doi:10.1029/2002JD002187, 2002.

Krulwich, T. A., Sachs, G. and Padan, E.: Molecular aspects of bacterial pH sensing and homeostasis, Nature Reviews Microbiology, 9(5), 330–343, doi:10.1038/nrmicro2549, 2011.

Kuhn, U., Ammann, C., Wolf, A., Meixner, F., Andreae, M. and Kesselmeier, J.: Carbonyl sulfide exchange on an ecosystem scale: soil represents a dominant sink for atmospheric COS, Atmospheric Environment, 33(6), 995–1008, 1999.

Launois, T., Peylin, P., Belviso, S. and Poulter, B.: A new model of the global biogeochemical cycle of carbonyl sulfide – Part 2: Use of OCS to constrain gross primary productivity of current vegetation models, Atmos. Chem. Phys., 15(20), 9285–9312, doi:10.5194/acp-15-9285-2015, 2015.

Liu, J., Geng, C., Mu, Y., Zhang, Y., Xu, Z. and Wu, H.: Exchange of carbonyl sulfide (COS) between the atmosphere and various soils in China, Biogeosciences, 7(2), 753–762, 2010a.

Liu, Y., He, H. and Ma, Q.: Temperature Dependence of the Heterogeneous Reaction of Carbonyl Sulfide on Magnesium Oxide, J. Phys. Chem. A, 112(13), 2820–2826, doi:10.1021/jp711302r, 2008.

Liu, Y., Ma, J. and He, H.: Heterogeneous reactions of carbonyl sulfide on mineral oxides: mechanism and kinetics study, Atmospheric Chemistry and Physics, 10(21), 10335–

10344, doi:10.5194/acp-10-10335-2010-supplement, 2010b.

Liu, Y., Ma, J., Liu, C. and He, H.: Heterogeneous uptake of carbonyl sulfide onto kaolinite within a temperature range of 220–330K, J. Geophys. Res, 115(D24), D24311, doi:10.1029/2010JD014778, 2010c.

Liu, Y., Ma, Q. and He, H.: Comparative study of the effect of water on the heterogeneous reactions of carbonyl sulfide on the surface of α-Al_2O_3 and MgO, Atmospheric Chemistry and Physics, 9, 6273–6286, 2009.

Maier, M., Schack-Kirchner, H., Aubinet, M., Goffin, S., Longdoz, B. and Parent, F.: Turbulence Effect on Gas Transport in Three Contrasting Forest Soils, Soil Science Society of America Journal, 76(5), 1518, doi:10.2136/sssaj2011.0376, 2012.

Manzoni, S. and Katul, G. G.: Invariant soil water potential at zero microbial respiration explained by hydrological discontinuity in dry soils, Geophysical research Letters, 41, 7151–7158, doi:10.1002/2014GL061467, 2014.

Maseyk, K., Berry, J. A., Billesbach, D., Campbell, J. E., Torn, M. S., Zahniser, M. and Seibt, U.: Sources and sinks of carbonyl sulfide in an agricultural field in the Southern Great Plains, Proceedings of the National Academy of Sciences, 111(25), 9064–9069, doi:10.1073/pnas.1319132111, 2014.

Massman, W. J.: A review of the molecular diffusivities of H_2O, CO_2, CH_4, CO, O_3, SO_2, NH_3, N_2O, NO, and NO_2 in air, O_2 and N_2 near STP, Atmospheric Environment, 32(6), 1111–1127, 1998.

Massman, W. J., Sommerfeld, R. A., Mosier, A. R., Zeller, K. F., Hehn, T. J. and Rochelle, S. G.: A model investigation of turbulence-driven pressure-pumping effects on the rate of diffusion of CO_2, N_2O, and CH_4 through layered snowpacks, Journal of Geophysical Research: Atmospheres (1984–2012), 102(D15), 18851–18863, 1997.

Mello, W. Z. and Hines, M. E.: Application of static and dynamic enclosures for determining dimethyl sulfide and carbonyl sulfide exchange in *Sphagnum* peatlands: Implications for the magnitude and direction of flux, J. Geophys. Res, 99(D7), 14–601–14–607, 1994.

Merlin, C., Masters, M., McAteer, S. and Coulson, A.: Why Is Carbonic Anhydrase Essential to *Escherichia coli*, Journal of Bacteriology, 185(21), 6415–6424, doi:10.1128/JB.185.21.6415-6424.2003, 2003.

Millington, R. J. and Quirk, J. P.: Permeability of porous solids, Transactions of the Faraday Society, 57, 1200–1207, 1961.

Moldrup, P., Olesen, T., Komatsu, T., Yoshikawa, S., Schjønning, P. and Rolston, D. E.:

Modeling diffusion and reaction in soils: X. A unifying model for solute and gas diffusivity in unsaturated soil, Soil science, 168(5), 321–337, doi:10.1097/00010694-200305000-00002, 2003.

Montzka, S. A., Calvert, P., Hall, B. D., Elkins, J. W., Conway, T. J., Tans, P. P. and Sweeney, C.: On the global distribution, seasonality, and budget of atmospheric carbonyl sulfide (COS) and some similarities to CO_2, J. Geophys. Res, 112(D9), D09302, doi:10.1029/2006JD007665, 2007.

Ogawa, T., Noguchi, K., Saito, M., Nagahata, Y., Kato, H., Ohtaki, A., Nakayama, H., Dohmae, N., Matsushita, Y., Odaka, M., Yohda, M., Nyunoya, H. and Katayama, Y.: Carbonyl Sulfide Hydrolase from *Thiobacillus thioparus* Strain THI115 Is One of the β-Carbonic Anhydrase Family Enzymes, Journal of the American Chemical Society, 135(10), 3818–3825, doi:10.1021/ja307735e, 2013.

Ogée, J., Sauze, J., Kesselmeier, J., Genty, B., Van Diest, H., Launois, T. and Wingate, L.: A new mechanistic framework to predict OCS fluxes from soils, Biogeosciences, 13(8), 2221–2240, doi:10.5194/bg-13-2221-2016, 2016.

Olesen, T., Gamst, J., Moldrup, P., Komatsu, T. and Rolston, D.: Diffusion of sorbing organic chemicals in the liquid and gaseous phases of repacked soil, Soil Sci. Soc. Am. J, 65, 1585–1593, 2001.

Penman, H.: Gas and vapour movements in the soil: I. The diffusion of vapours through porous solids, The Journal of Agricultural Science, 30(03), 437–462, 1940.

Petersen, L. W., Moldrup, P., Elpharan, Y. H., Jacobsen, O. H., Yamaguchi, T. and Rolston, D. E.: The Effect of Moisture and Soil Texture on the Adsorption of Organic Vapors, J. Environ. Qual., 24(4), 752–759, 1995.

Piao, S., Sitch, S., Ciais, P., Friedlingstein, P., Peylin, P., Wang, X., Ahlström, A., Anav, A., Canadell, J. G., Cong, N., Huntingford, C., Jung, M., Levis, S., Levy, P. E., Li, J., Lin, X., Lomas, M. R., Lu, M., Luo, Y., Ma, Y., Myneni, R. B., Poulter, B., Sun, Z., Wang, T., Viovy, N., Zaehle, S. and Zeng, N.: Evaluation of terrestrial carbon cycle models for their response to climate variability and to CO_2 trends, Global Change Biol, 19(7), 2117–2132, doi:10.1111/gcb.12187, 2013.

Protoschill-Krebs, G. and Kesselmeier, J.: Enzymatic pathways for the consumption of carbonyl sulphide (COS) by higher plants, Botanica Acta, 105(3), 206–212, 1992.

Protoschill-Krebs, G., Wilhelm, C. and Kesselmeier, J.: Consumption of Carbonyl Sulphide by *Chlamydomonas reinhardtii* with Different Activities of Carbonic Anhydrase (CA) Induced by Different CO_2 Growing Regimes, Botanica Acta, 108(5), 445–448, 1995.

Protoschill-Krebs, G., Wilhelm, C. and Kesselmeier, J.: Consumption of carbonyl sulphide (COS) by higher plant carbonic anhydrase (CA), Atmospheric Environment, 30(18), 3151–3156, 1996.

Rowlett, R. S., Tu, C., McKay, M. M., Preiss, J. R., Loomis, R. J., Hicks, K. A., Marchione, R. J., Strong, J. A., Donovan, G. S., Jr and Chamberlin, J. E.: Kinetic characterization of wild-type and proton transfer-impaired variants of β-carbonic anhydrase from *Arabidopsis thaliana*, Arch. Biochem. Biophys., 404, 197–209, 2002.

Sandoval-Soto, L., Stanimirov, M., Hobe, M. V., Schmitt, V., Valdes, J., Wild, A. and Kesselmeier, J.: Global uptake of carbonyl sulfide (COS) by terrestrial vegetation: Estimates corrected by deposition velocities normalized to the uptake of carbon dioxide (CO_2), Biogeosciences, 2(2), 125–132, 2005.

Scanlon, B. R., Nicot, J. P. and Massmann, J. W.: Soil gas movement in unsaturated systems, in Soil Physics Companion, pp. 297–341, CRC Press: Boca Raton, FL. 2002.

Seibt, U., Kesselmeier, J., Sandoval-Soto, L., Kuhn, U. and Berry, J. A.: A kinetic analysis of leaf uptake of COS and its relation to transpiration, photosynthesis and carbon isotope fractionation, Biogeosciences, 7, 333–341, 2010.

Seibt, U., Wingate, L., Lloyd, J. and Berry, J. A.: Diurnally variable $\delta^{18}O$ signatures of soil CO_2 fluxes indicate carbonic anhydrase activity in a forest soil, J. Geophys. Res, 111(G4), G04005, doi:10.1029/2006JG000177, 2006.

Smeulders, M. J., Barends, T. R. M., Pol, A., Scherer, A., Zandvoort, M. H., Udvarhelyi, A., Khadem, A. F., Menzel, A., Hermans, J., Shoeman, R. L., Wessels, H. J. C. T., van den Heuvel, L. P., Russ, L., Schlichting, I., Jetten, M. S. M. and Op den Camp, H. J. M.: Evolution of a new enzyme for carbon disulphide conversion by an acidothermophilic archaeon, Nature, 478(7369), 412–416, doi:10.1038/nature10464, 2012.

Smith, K., Jakubzick, C., Whittam, T. and Ferry, J.: Carbonic anhydrase is an ancient enzyme widespread in prokaryotes, Proceedings of the National Academy of Sciences, 96(26), 15184–15189, 1999.

Steinbacher, M., Bingemer, H. and Schmidt, U.: Measurements of the exchange of carbonyl sulfide (OCS) and carbon disulfide (CS_2) between soil and atmosphere in a spruce forest in central Germany, Atmospheric Environment, 38(35), 6043–6052, doi:10.1016/j.atmosenv.2004.06.022, 2004.

Stimler, K., Berry, J. A. and Yakir, D.: Effects of Carbonyl Sulfide and Carbonic Anhydrase on Stomatal Conductance, Plant Physiology, 158(1), 524–530, doi:10.1104/pp.111.185926, 2012.

Stimler, K., Montzka, S. A., Berry, J. A., Rudich, Y. and Yakir, D.: Relationships between carbonyl sulfide (COS) and CO_2 during leaf gas exchange, New Phytologist, 186(4), 869–878, doi:10.1111/j.1469-8137.2010.03218.x, 2010.

Sun, W., Maseyk, K., Lett, C. and Seibt, U.: A soil diffusion-reaction model for surface COS flux: COSSM v1, Geosci. Model Dev. Discuss., 8(7), 5139–5182, doi:10.5194/gmdd-8-5139-2015, 2015.

Syrjänen, L., Vermelho, A. B., de Almeida Rodrigues, I., Corte-Real, S., Salonen, T., Pan, P., Vullo, D., Parkkila, S., Capasso, C. and Supuran, C. T.: Cloning, Characterization, and Inhibition Studies of a β-Carbonic Anhydrase from Leishmania donovani chagasi, the Protozoan Parasite Responsible for Leishmaniasis, J. Med. Chem., 56(18), 7372–7381, doi:10.1021/jm400939k, 2013.

Tholen, D. and Zhu, X.-G.: The Mechanistic Basis of Internal Conductance: A Theoretical Analysis of Mesophyll Cell Photosynthesis and CO_2 Diffusion, Plant Physiology, 156(1), 90–105, doi:10.1104/pp.111.172346, 2011.

Ulshöfer, V. S., Flock, O. R., Uher, G. and Andreae, M. O.: Photochemical production and air-sea exchange of carbonyl sulfide in the eastern Mediterranean Sea, Marine chemistry, 53, 25–39, 1996.

van Bochove, E., Beauchemin, S. and Thériault, G.: Continuous multiple measurement of soil redox potential using platinum microelectrodes, Soil Science Society of America Journal, 66, 1813–1820, 2002.

Van Diest, H. and Kesselmeier, J.: Soil atmosphere exchange of carbonyl sulfide (COS) regulated by diffusivity depending on water-filled pore space, Biogeosciences, 5(2), 475–483, 2008.

Welp, L. R., Keeling, R. F., Meijer, H. A. J., Bollenbacher, A. F., Piper, S. C., Yoshimura, K., Francey, R. J., Allison, C. E. and Wahlen, M.: Interannual variability in the oxygen isotopes of atmospheric CO_2 driven by El Niño, Nature, 477(7366), 579–582, doi:10.1038/nature10421, 2011.

Whelan, M. E. and Rhew, R. C.: Carbonyl sulfide produced by abiotic thermal and photodegradation of soil organic matter from wheat field substrate, J. Geophys. Res. Biogeosci., 120, 54–62, doi:10.1002/2014JG002661, 2015.

Whelan, M. E., Min, D.-H. and Rhew, R. C.: Salt marsh vegetation as a carbonyl sulfide (COS) source to the atmosphere, Atmospheric Environment, 73, 131–137, doi:10.1016/j.atmosenv.2013.02.048, 2013.

White, M., Zhou, Y., Russo, R., Mao, H., Talbot, R., Varner, R. and Sive, B.: Carbonyl

sulfide exchange in a temperate loblolly pine forest grown under ambient and elevated CO_2, Atmospheric Chemistry and Physics, 10, 547–561, 2010.

Wilhelm, E., Battino, R. and Wilcock, R. J.: Low-pressure solubility of gases in liquid water, Chemical Reviews, 77, 219–262, 1977.

Wingate, L., Ogée, J., Burlett, R. and Bosc, A.: Strong seasonal disequilibrium measured between the oxygen isotope signals of leaf and soil CO_2 exchange, Global Change Biol, 16(11), 3048–3064, doi:10.1111/j.1365-2486.2010.02186.x, 2010.

Wingate, L., Ogée, J., Cuntz, M., Genty, B., Reiter, I., Seibt, U., Yakir, D., Maseyk, K., Pendall, E. G., Barbour, M. M., Mortazavi, B., Burlett, R., Peylin, P., Miller, J., Mencuccini, M., Shim, J. H., Hunt, J. and Grace, J.: The impact of soil microorganisms on the global budget of $\delta^{18}O$ in atmospheric CO_2, Proceedings of the National Academy of Sciences, 106(52), 22411–22415, doi:10.1073/pnas.0905210106, 2009.

Wingate, L., Seibt, U., Maseyk, K., Ogée, J., Almeida, P., Yakir, D., Pereira, J. S. and Mencuccini, M.: Evaporation and carbonic anhydrase activity recorded in oxygen isotope signatures of net CO_2 fluxes from a Mediterranean soil, Global Change Biol, 14(9), 2178–2193, doi:10.1111/j.1365-2486.2008.01635.x, 2008.

Wohlfahrt, G., Wohlfahrt, G., Brilli, F., Brilli, F., Hörtnagl, L., Hörtnagl, L., XU, X., XU, X., Bingemer, H., Bingemer, H., Hansel, A., Hansel, A., Loreto, F. and Loreto, F.: Carbonyl sulfide (COS) as a tracer for canopy photosynthesis, transpiration and stomatal conductance: potential and limitations, Plant Cell and Environment, 35(4), 657–667, doi:10.1111/j.1365-3040.2011.02451.x, 2011.

Yamaguchi, T., Poulsen, T., Moldrup, P. and Fukushima, T.: Predictive model for adsorption of volatile organic chemicals on soils, Environmental Engineering Research, 36, 477–482, 1999.

Yi, Z., Wang, X., Sheng, G. and Fu, J.: Exchange of carbonyl sulfide (OCS) and dimethyl sulfide (DMS) between rice paddy fields and the atmosphere in subtropical China, Agriculture, Ecosystems & Environment, 123(1-3), 116–124, doi:10.1016/j.agee.2007.05.011, 2008.

Yi, Z., Wang, X., Sheng, G., Zhang, D., Zhou, G. and Fu, J.: Soil uptake of carbonyl sulfide in subtropical forests with different successional stages in south China, J. Geophys. Res, 112(D8), D08302, doi:10.1029/2006JD008048, 2007.

Zeebe, R. E.: On the molecular diffusion coefficients of dissolved CO_2, HCO_3^- and CO_3^{2-} and their dependence on isotopic mass, Geochimica et Cosmochimica Acta, 75(9), 2483–2498, doi:10.1016/j.gca.2011.02.010, 2011.

Appendix

Here we derive an equation for the catalysed OCS sink term (S_{cat}) that accounts for the co-limitation between the enzymatic reaction that takes place inside the micro-organisms (at pH_{in} and with an OCS concentration C_{in}) and the OCS diffusion through the cell wall of the microbes. In this situation, Eq. 9 needs to be re-written as:

$$S_{cat} = \theta k_{cat}[CA]\frac{BC_{in}}{K_m + BC_{in}} \approx \frac{k_{cat}}{K_m}[CA]B\theta C_{in}. \quad \text{(A1)}$$

The OCS uptake can also be written in terms of transport across the cell wall and the plasma membrane of the microbial cell (see for example Tholen and Zhu (2011), their Eqs. 8-9):

$$S_{cat} = G_{wall}V_{mol}(C - C_{in})S_{wall}, \quad \text{(A2)}$$

where G_{wall} (mol(air) m^{-2} wall s^{-1}) is the cell wall and plasma membrane aggregated conductance to OCS, V_{mol} (m^3 air mol(air)$^{-1}$) is the molar volume of air and S_{wall} (m^2 wall m^{-3} soil) is the microbial cell wall surface density in the soil. Combining Eqs. A1-2 we can eliminate C_{in} and express S as a function of C only:

$$S_{cat} = \frac{B\theta k_{cat}[CA]}{K_m + B\theta k_{cat}[CA]r_{wall}}C, \quad \text{(A3)}$$

where we defined $1/r_{wall} = G_{wall}V_{mol}S_{wall}$. Equation A3 simplifies to Eq. 9 under the condition that:

$$B\theta k_{cat}[CA]r_{wall} << K_m. \quad \text{(A4)}$$

Accounting for the dilution of CA in soils, *i.e.* $[CA]\theta = [CA]_{in}\rho_{mic}$, where ρ_{mic} (m^3 microbes m^{-3} soil) is the volumetric density of the soil microbes (that can be expressed as $\nu_{mic}V_0$ in which ν_{mic} is the number of microbes per soil volume and V_0 the volume of a single microbial cell), the condition (A4) also writes:

$$\frac{Bk_{cat}[CA]_{in}}{G_{wall}V_{mol}}\frac{V_0}{S_{wall0}} << K_m, \quad \text{(A5)}$$

where S_{wall0} is the single cell wall surface area. If the microbes are spherical with diameter D_0, we have $V_0/S_{wall0} = D_0/6$. With typical values of $D_0 = 1$ mm, $B = 0.5$ m^3 m^{-3}, $V_{mol} = 0.025$ m^3 mol^{-1}, $k_{cat} = 93$ s^{-1} and $G_{wall} = 0.14$ mol m^{-2} s^{-1} (*i.e.* 0.35 cm s^{-1}, see the note under Table 2 in Evans et al. (2009)) the left-hand side of Eq. (A5) equals 0.22 mM, which is much smaller than K_m (39 mM at 20°C, Protoschill-Krebs et al., 1996). In this situation the transport of OCS through the membrane is not a co-limiting factor to the OCS uptake (for CO_2 it is less true because the left-hand side of Eq. A5 is around 0.57 mM for a K_m around

3 mM). Note also that CA is not spread in the entire cell volume so that the cell volume appearing in Eq. A5 should be somewhat smaller. Although there are large uncertainties on the value of cytoplasmic CA concentration or k_{cat}/K_M, our derivation indicates that these parameter would need to be much higher (by two orders of magnitude) to justify the need to account for the transport of OCS into the cell during microbial consumption. In this study we assumed Eq. 9 to be valid, bearing in mind that the CA concentration we derived from it remains sensitive to the k_{cat}/K_M value we use.

Chapitre 3 : Le rôle du pH sur l'activité de l'anhydrase carbonique du sol

Introduction au chapitre 3

Nous avons évoqué en introduction l'existence et l'utilisation de deux traceurs complémentaires du cycle du carbone (l'OCS et le $CO^{18}O$) pour affiner nos représentations respectives des flux de photosynthèse et de respiration. Dans le chapitre précédent nous avons proposé un modèle décrivant le flux sol-atmosphère d'OCS en fonction de différentes proprietés du sol (*i.e.* la porosité, la teneur en eau, la profondeur, le pH et la température du sol) que nous avons ensuite évalué sur des jeux de données de la littérature. Avec ce nouveau modèle, les descriptions des échanges d'OCS et $CO^{18}O$ partagent désormais les mêmes concepts (tortuosité, diffusion, solubilité, réaction en phase liquide…) ce qui renforce la complémentarité des deux traceurs. Nous proposons dans ce chapitre 3 d'évaluer plus amplement la dépendance des deux modèles au pH du sol. Dans le cas du $CO^{18}O$ la dépendance des échanges isotopiques CO_2-H_2O au pH est connue depuis l'article fondateur de Mills et Urey (1940) et est largement utilisée en paléo-océanographie (Mills and Urey, 1940; Rollion-Bard et al., 2011; Uchikawa and Zeebe, 2012, Usdowski et al. 1991). Cette dépendance au pH des échanges isotopiques CO_2-H_2O (notée k_{iso} par la suite) n'a cependant jamais été évaluée dans les sols. Nous avons souhaité dans ce chapitre tester la relation entre activité d'AC vis-à-vis de l'OCS (notée k_h par la suite) et du CO_2 (k_{iso}), concentration en AC et pH du sol. Pour cela nous avons artificiellement modifié la concentration en α-AC de six sols présentant une large gamme de pH. Pour estimer cette activité enzymatique nous utilisons une nouvelle approche expérimentale, non destructive, qui a l'avantage de ne pas dépendre de la mesure de la composition isotopique de l'eau du sol et donc sujette à moins de biais expérimentaux. Ce chapitre est rédigé sous la forme d'un article qui sera prochainement soumis au journal *Biogeosciences* de la société européenne de geophysique (*European Geophysical Union* ou EGU). Ma contribution à cet article a consisté à co-construire les expériences, réaliser les mesures d'échanges gazeux et isotopiques, co-executer les extractions et les mesures isotopiques de l'eau du sol, analyser les résultats et écrire une première version de l'article. Une partie de l'analyse et la version finale de l'article ont été rendus possibles grâce aux co-auteurs de l'article.

The role of pH on soil carbonic anhydrase activity

J. Sauze[1*], S.P. Jones[1], L. Wingate[1], S. Wohl[1] and J. Ogée[1*]

[1]INRA, UMR 1391 ISPA, F-33140 Villenave d'Ornon, France

* Author(s) for correspondence: J. Sauze (joana.sauze@inra.fr) and J. Ogée (jerome.ogee@inra.fr)

Abstract

Carbonic anhydrases (CAs) are metalloenzymes present in plants and microorganisms that catalyse the interconversion of CO_2 and water to bicarbonate and protons. Because oxygen isotopes are also exchanged during this reaction, the presence of CA also modifies the contribution of soils and plants to the global budget of atmospheric $CO^{18}O$. The isotopic signatures ($\delta^{18}O$) of these contributions differ as leaf water pools are usually more enriched than soil water pools, and this difference is used to partition the net CO_2 flux over land into soil respiration and plant photosynthesis. However, the use of atmospheric $CO^{18}O$ as a tracer of the land CO_2 fluxes requires a good knowledge of soil CA activity. Previous studies have shown that significant differences in soil CA activity are found in different biomes and seasons but our understanding of the environmental and ecological drivers responsible for the spatial and temporal patterns observed in soil CA activity is still limited. One factor that has been overlooked so far is pH. Soil pH is known to strongly influence microbial community composition, richness and diversity and it also governs the speciation of CO_2 between the different carbonate forms. In this study we investigated the CO_2-H_2O isotopic exchange rate (k_{iso}) in six soils with pH varying from 4.5 to 8.5. We also artificially increased the soil CA concentration to test how pH and other soil properties (texture, phosphate content…) affected the relationship between k_{iso} and CA concentration. We found that soil pH seemed to be the primary driver of k_{iso} after CA addition and that the chemical composition (i.e. phosphate content) played only a secondary role. We also found an offset between the $\delta^{18}O$ of the water pool with which CO_2 equliibrates and total soil water (i.e. water extracted by vacuum distillation) that varied with soil texture. The reasons for this offset are still unknown.

3.1. Introduction

The emission of carbon dioxide (CO_2) into the atmosphere by anthropogenic activities is happening at unprecedented rates (IPCC, 2013). The terrestrial biosphere currently absorbs and stores about 25% of these anthropogenic CO_2 emissions as a result of a small disequilibrium between plant photosynthesis and soil respiration. The amplitude of this disequilibrium, also called the land CO_2 sink strength, is also highly variable (Ballantyne et al., 2012; Gurney and Eckels, 2011; Poulter et al., 2014) because the processes driving photosynthesis and respiration over land are very sensitive to changes in climate. For example, microbial mineralisation of soil organic carbon is highly sensitive to temperature so that soil emissions of CO_2 to the atmosphere are expected to increase as global warming proceed (Reynolds et al., 2015). Currently the land CO_2 sink strength is monitored through atmospheric budgets of CO_2 that do not allow the separation of gross photosynthesis and respiration, making it difficult to evaluate coupled climate-carbon models and their projections. Approaches that allow the contributions of gross carbon fixation and mineralisation to the atmospheric CO_2 budget to be partitioned are required.

One such approach takes advantage of the difference in the oxygen isotope signatures ($d^{18}O$) of CO_2 molecules that have interacted with leaf or soil water pools (Ciais et al., 1997; Cuntz, 2003; Farquhar et al., 1993; Welp et al., 2011; Wingate et al., 2009). This difference in isotopic signatures occurs as oxygen atoms are exchanged between CO_2 and water during CO_2 hydration because soil and leaf water pools usually differ in their oxygen isotope composition. The hydration of CO_2 is catalysed by carbonic anhydrases (CAs), a widespread class of metallo-enzymes ubiquitous in plants and algae (Badger, 2003; Moroney et al., 2001), but also in bacteria and fungi (Smith and Ferry, 2000). In leaves CAs are abundant enough that CO_2 diffusing out of the leaf is expected to be in full isotopic equilibrium with leaf water (Farquhar and Cernusak, 2012; Gillon and Yakir, 2001). In soils full isotopic equilibration between CO_2 and water also occurs but above a certain depth, CO_2 diffusion through the soil matrix becomes too fast to allow for further equilibration. Given the high degree of isotopic enrichment of top soil water during evaporation, soil CA activity will dictate the shallowest depth of full isotopic equilibration between CO_2 and water and will have a profound effect on the $d^{18}O$ of soil respiration, and thus on the partitioning of the land CO_2 gross fluxes using atmospheric $CO^{18}O$ budget.

Wingate et al. (2009) compiled datasets of depth-resolved soil water and CO_2 oxygen isotope exchange in a range of biomes and found a tendency to larger soil CA activity in warmer and

drier regions. Welp et al. (2011) used the lower range of these CA activity estimates to retrieve a global, mean annual land photosynthesis rate of *ca*. 175 GtC yr^{-1} over the period 1980-2010, and also noted that it was largely dependent on the assumptions made on soil CA activity. Seasonal changes in soil CA activity also occur, as shown by Seibt et al. (2006) and Wingate et al. (2010) in two temperate forests. Unfortunately, our current understanding of the environmental and ecological drivers of these spatiotemporal variations in soil CA activity is too fragmented to be able to use $CO^{18}O$ as an additional tracer of the highly dynamic land CO_2 sink.

Changes in the abundance and diversity of soil microbial communities were proposed as possible drivers of the observed spatial and temporal changes in soil CA activity (Wingate et al., 2008, 2009). Because soil pH is known to strongly influence microbial community composition, richness and diversity (Fierer and Jackson, 2006; Hartman et al., 2008; Lauber et al., 2009) it could be an important driver of soil CA activity *via* direct changes in the microbial populations, with different CA requirements and isoforms. Soil pH should also directly influence CA-driven CO_2 hydration kinetics as CA reactivation is known to be limited by its de-protonation with a pK_a around 7.2 (Rowlett et al., 2002). Because micro-organisms have the ability to regulate and maintain their intracellular pH within one pH unit near neutral (Krulwich et al., 2011), the influence of soil pH on intra-cellular CA activity might not be so critical. However, because CO_2 hydration converts CO_2 into bicarbonate, and mostly CO_2 can diffuse across cell membranes, one of the main roles of CA *in vivo* is actually to regulate this intracellular pH as well as to facilitate the transport of CO_2 across cell membranes (Badger, 2003). In certain micro-organisms, extracellular CAs have also been found (*e.g*. Hopkinson et al., 2013) whose activity should be directly affected by external (soil) pH. We should therefore expect a direct link between soil CA activity and soil pH.

Actually, part of the reported variations in soil CA activity derived from the isotopic exchange rates between soil water and CO_2 could also be explained by differences in soil pH. Indeed these soil CA activity are often reported against the un-catalysed CO_2-H_2O isotopic exchange rate ($k_{iso,uncat}$), usually assumed equal to *ca*. 0.012 s^{-1} at 25°C. But because soil pH governs the speciation of CO_2 between the different carbonate forms, with dissolved CO_2 being predominant only in acidic environments (pH < 6), $k_{iso,uncat}$ is not the same for all soils and is strongly reduced in alkaline conditions (Mills and Urey, 1940; Uchikawa and Zeebe, 2012). Thus for the same soil CA activity – or more rightly for the same soil CO_2-water isotopic exchange rate (k_{iso}) – the enhancement factor relative to the *true* un-catalysed rate would be much greater in alkaline soils than in acidic ones.

The chemical composition of the soil is another potentially important factor that should be considered when reporting soil CA activity. Several studies have shown that some anions commonly found in soils could act as CA inhibitors or activators, depending on their ability to exchange protons. For example, at neutral pH, phosphate ions were reported as CA activators with a maximum of 6.5-fold increase in CO_2 hydration rates compared to a solution without phosphates, while sulphate ions act as a weak inhibitor (Rowlett et al., 1991). The presence of these ions also modifies, sometimes dramatically, the pH response of CA activity *in vitro* (Rowlett et al., 1991), questioning the idea that pH would be the only chemical factor controlling soil CA activity.

The aim of this study was to investigate the relationship between soil CA activity and soil pH. For this we used a setup that allowed us to retrieve simultaneously the soil CA activity and the $d^{18}O$ of the soil water pool with which CO_2 equilibrates, without destructive sampling. Using six different soils differing in pH by almost 4 pH units, we investigated the influence of soil pH on the CO_2 hydration rate (k_h) and CO_2-H_2O equilibration (k_{iso}). We also artificially increased the CA concentration in each soil by adding solutions of bovine CA. This CA isoform was chosen because it is well characterised in terms of enzymatic activity (Uchikawa and Zeebe, 2012) and pH response (Rowlett et al., 1991). This way we could investigate whether CA concentrations and soil pH were the only factors affecting the activity of this exogenous CA. Following the arguments given above, we hypothesised that exogenous CA activity should be inhibited in acidic soils, but that the soil chemical composition could also influence the CA activity at different pHs.

3.2. Material and methods

3.2.1. Soil sampling

The soils that we investigated differed in terms of pH, but also texture, land use and chemical composition (**Table 3.1**). Soil samples from Le Bray, a maritime pine forest located at about 20km southwest of Bordeaux (France), were collected in November 2014 (LeBray1) and April 2016 (LeBray2). The four other soils were taken in croplands. The soils from Planguenoual (France, 95km northwest of Rennes) and Grignon-Folleville (France, 20km southwest of Paris) were collected in May 2013. More details about these soils can be found in Achat et al. (2014). The soil from Pierrelaye (France, 30km northwest of Paris) was

sampled in October 2014 and May 2016 but mixed in one batch and the soil from and the soil from Toulouse was sampled once in May 2016.

Table 3.1: Main characteristics of the soils investigated in this study. Numbers in italics indicate literature data.

	Le Bray1	**Le Bray2**	**Planguenoual**	**Pierrelaye**	**Grignon-Folleville**	**Toulouse**
Land use	pine plantation	pine plantation	cropland	cropland	cropland	cropland
Coordinates	44°42'N 0°46'W	44°42'N 0°46'W	48°32'N 02°34'W	49°02'N 02°13'E	48°50'N 01°56'E	43°32'N 01°30'E
pH	4.1 (*4.1*)	4.8 (*4.1*)	6.3 (*6.3*)	7.6 (*7.8*)	8.2 (*8.1*)	8.5 (*8.5*)
Sand content %	*94.7*	*94.7*	*43.7*	*82.2*	*11*	*43.8*
Silt content %	*2.6*	*2.6*	*41.5*	*8.7*	*60.3*	*38.2*
Clay content %	*2.7*	*2.7*	*14.8*	*9.1*	*28.7*	*18*
Total N (g kg^{-1})	*31.2*	*31.2*	*16.6*	*11.5*	*14.3*	*7.5*
Total C (g kg^{-1})	*1.2*	*1.2*	*1.6*	*0.83*	*1.2*	*0.59*
Phosphates (mg kg^{-1})	4.85	6.93	2.88 (*3.0*)	13.6	0.53 (*0.5*)	1.4

All soil samples were taken from the soil surface (0-15cm) after removal of the coarse litter elements. They were sieved with a 4mm mesh, homogenised and air-dried for several weeks in the laboratory. A first set of experiments was conducted in March 2015 with the soils from LeBray1, Planguenoual and Grignon-Folleville. Prior to gas exchange measurements, 330 to 440 g of soils were inserted into a 500-mL Teflon pot in order to obtain a common soil depth (*ca*. 7 cm). Each soil pot was then irrigated with 125 mL of water and let to drain for 12 to 24h at room temperature and light conditions. A small hole had been drilled at the bottom of the pot to avoid the accumulation of water and anoxic conditions in deeper soil layers. Preliminary results from this first set of experiments indicated substantial evaporation-induced isotopic enrichment of soil water in the top layer, as well as soil-to-soil variations in water-filled pore space (WFPS), which could complicate the interpretation of the results. A second set of experiments was then conducted in June 2016 where WFPS was better controlled and soil evaporation was minimised by letting the soils acclimate prior to the measurements inside a dark chamber at 21°C with saturating water vapour generated from evaporation of the same water as that used for soil irrigation. The soils from LeBray2, Pierrelaye and Toulouse were chosen for this second set of experiments, to also minimise differences between soil texture, while keeping a large range of pH (**Table 3.1**). Prior to gas exchange measurements, 280 to 300 g of soils were inserted into a 500-mL Teflon pot up to a common soil depth of *ca*. 5-6 cm. Each soil pot was then irrigated in order to reach a WFPS

of 25% and left in the dark chamber for 24h. All Teflon pots used for the experiments had a constant surface area of 41.85 cm^2.

3.2.2. Carbonic anhydrase addition

For some experiments lyophilised α-CA powder from bovine erythrocytes (C3934-100MG, Sigma-Aldrich, France) was diluted into the water used for irrigation. For each set of experiment CA concentrations of *ca*. 24 and 80 mg L^{-1} were used. Apart from this addition of CA into the irrigation water, all other steps were kept identical as for the measurement of the soil without any CA addition.

3.2.3. Experimental setup and working sequence

Prior to gas exchange measurements, each soil pot was sealed and used as a flow-through gas exchange chamber. An acclimation time of at least 20 minutes was used to let the soil column to re-equilibrate to the new air supply CO_2 composition. The soil CO_2 efflux and its oxygen isotopic composition were then measured using the experimental setup illustrated in **Fig. 3.1**.
To simultaneously retrieve soil CA activity, reported here as the CO_2-H_2O isotopic exchange rate k_{iso}, and the $\delta^{18}O$ of the soil water pools with which CO_2 equilibrates (δ_{eq}), we designed a system that allowed us to measure CO_2 isotope fluxes under two, quasi-simultaneous isotopic steady states that only differ in the isotopic composition of the CO_2 entering the soil chamber (**Fig. 3.1**, Jones et al., in prep). The air supplied to the chamber came directly from a compressed air tank during the first steady state (SS1) and from a mix between dry, CO_2-free air (from a synthetic air generator) and a tank of pure CO_2 during the second state (SS2). During SS2 mixing valves allowed to adjust the CO_2 concentration of the inlet air to maintain it close to the value of the inlet air used in SS1 within acceptable error (423 ± 5 ppm), while their oxygen isotopic composition differed markedly (**Fig. 3.2**). The transition between SS1 and SS2 was operated by means of a three-way valve (**Fig. 3.1**) and a transition period of 20 minutes was necessary to let the new steady state to be reached (**Fig. 3.2**). During each steady state, the by-pass (*i.e.* the air entering the soil chamber) and the outlet of the chamber were alternately recorded *via* a manifold connected to the stable isotope CO_2 analyser (**Fig. 3.2**). During the first set of experiment each working sequence was repeated three times on each soil and CA treatment (pseudo-replication) at a temperature of 25°C. During the second set of experiment each soil and CA treatment were made in triplicates but measured only once over a single working sequence (true replication) at a temperature of 21°C.

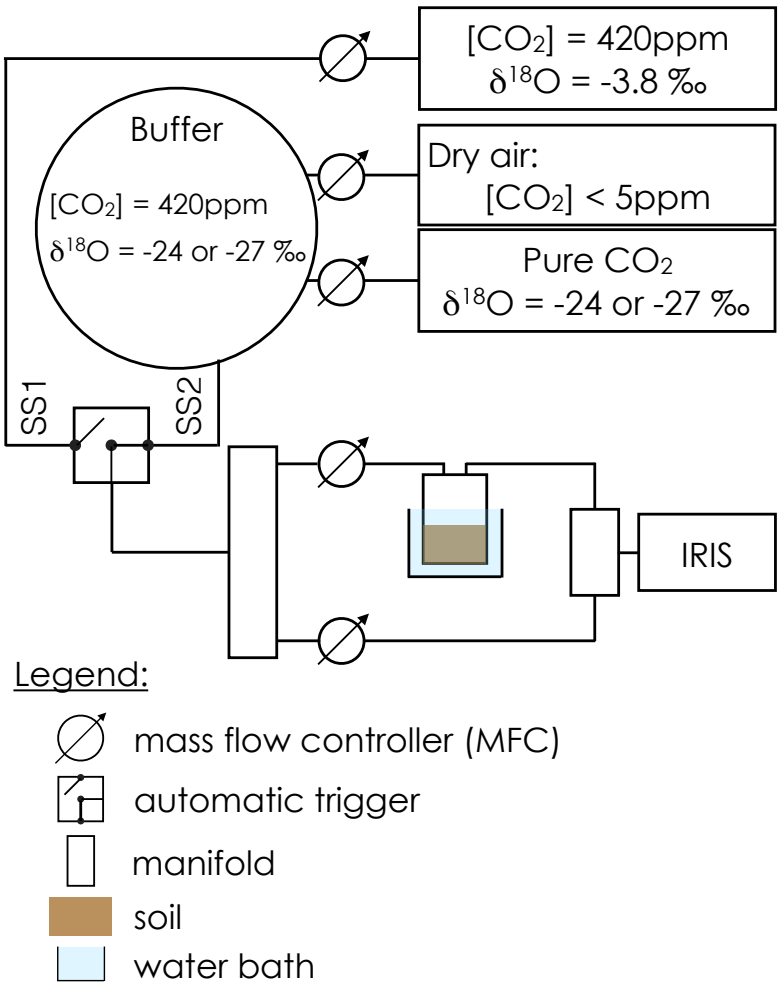

Figure 3.1: Schematic of the experimental setup used here to estimate simultaneously the CO_2-H_2O isotopic exchange rate (k_{iso}) in a soil microcosm and the oxygen isotopic composition of the soil water pool with which the CO_2 equilibrates ($\delta_{sw\text{-}eq}$). The soil microcosm is thermally regulated using a water bath and flushed with CO_2 in dry air whose oxygen isotopic composition is either enriched (around -4‰ $VPDB_g$) or depleted (between -24‰ and -27‰ $VPDB_g$).

To account for possible non-linearity and drift of the stable isotope analyser during the experiments, gas from two calibration tanks of known CO_2 concentration and isotopic composition were regularly recorded in-between sample measurements (**Fig. 3.2**). For both sets of experiments the calibration tanks, whose $^{12}C^{16}O_2$ and $^{12}C^{16}O^{18}O$ mixing ratios bracketed our measurements, were measured at approximately 16 min intervals, consistent with the expected stability of the analyser (see next section).

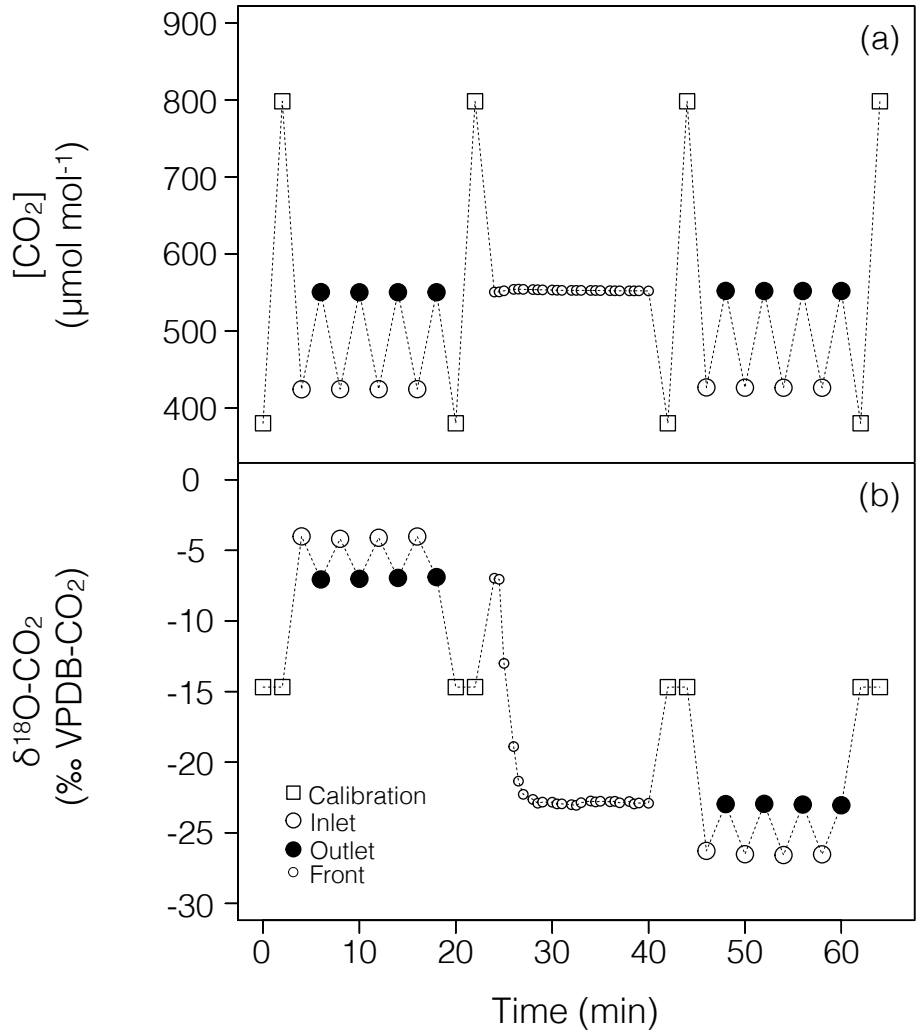

Figure 3.2: Typical time-series of CO_2 mixing ratio and isotope composition ($\delta^{18}O$) as measured by the analyser over the course of a working sequence. The sequence is composed of 7 steps: (1) two calibration bottles spanning the expected range of CO_2 mixing ratios, (2) inlet and outlet lines of the soil microcosm, measured 3 times consecutively, using a high $\delta^{18}O$ ratio (steady state 1), (3) calibration bottles, (4) the outlet of the chamber during the switch of the air supplying the soil chamber (front), (5) calibration bottles, (6) inlet and outlet lines of the soil chamber, measured 3 times consecutively, using a low $\delta^{18}O$ ratio (steady state 2) and (7) calibration bottles.

3.2.4. CO_2 mixing ratio and stable isotope measurements

Mixing ratios of $^{12}C^{16}O_2$, $^{13}C^{16}O_2$ and $^{12}C^{16}O^{18}O$ were measured using an Isotope Ratio Infrared Spectrometer (IRIS, Delta Ray, Thermo Fisher Scientific, USA). The cell pressure was controlled and maintained at 100 mbar throughout the experiment. The air sample passed

through a multi-pass Herriot cell at a flow of 85 mL min^{-1} with a total path length of 5m, leading to a theoretical residence time in the analyser of *ca*. 35 seconds. To minimise carry-over effect caused by this residence time, each line (inlet or chamber air or calibration tanks) were measured for 2 minutes and only the last 40 s of measurements were averaged to provide a single mean and standard deviation.

Calibration tank mixing ratios for the different isotopologues ($^{12}CO_2$, $^{13}CO_2$ and $CO^{18}O$) were averaged as described above, and interpolated in time using a spline function. These interpolated time-series were then used to perform a two-point calibration regression on the mixing ratios for each sample measurement. Total CO_2 mixing ratio was computed as in Wingate et al. (2010):

$$[CO_2]=\frac{[^{12}C^{16}O^{16}O]+[^{13}C^{16}O^{16}O]+[^{12}C^{16}O^{18}O]}{0.999179} \quad (1)$$

where the factor 0.999179 accounts for the presence of $^{12}C^{16}O^{17}O$ in the gas mixture. The $\delta^{18}O$ of CO_2 was expressed on the VPDB-CO_2 scale using the formula:

$$\delta^{18}O\text{-}CO_2=0.5\frac{[^{12}C^{16}O^{18}O]/[^{12}C^{16}O_2]}{0.00208835}-1 \quad (2)$$

where 0.0020835 is the $^{18}O/^{16}O$ isotope ratio of the VPDB-CO_2 reference standard (Allison et al., 1995) and the factor 0.5 accounts for the fact that there is two oxygen atoms per molecule of CO_2 but only one ^{18}O atom in $^{12}C^{16}O^{18}O$.

Standard deviations on CO_2 mixing ratios of the different isotopologues were propagated using Eq. 1 to provide a measurement error on total CO_2. In contrast measurement error on the isotope ratios were not calculated using Eq. 2 but computed from the standard deviation over the last 40 s of measurements of the instantaneous ratio $[^{12}C^{16}O^{18}O]/[^{12}C^{16}O^{16}O]$. This is because fluctuations in one CO_2 isotopologue was always highly correlated with fluctuations in the other CO_2 isotopologue leading to much smaller fluctuations in their ratios than the one calculated from simple error propagation using Eq. 2 (Jones et al. in prep). With such analysis, typical errors on $[CO_2]$ and $\delta^{18}O\text{-}CO_2$ values were around 0.1 ppm and 0.3‰, respectively.

Under steady state conditions (*i.e.* during SS1 or SS2 in **Fig. 3.2**), and according to the mass balance of total CO_2 in the chamber headspace, the soil CO_2 efflux is proportional to the total CO_2 concentration difference between the inlet and outlet airstreams:

$$F = \frac{u_{in}}{S}\left(c_{out} - c_{in}\right) \quad (3)$$

where u_{in} (mol s^{-1}) is the flow rate of dry air on the inlet of the chamber, S is soil surface (m^2) and c_{in} and c_{out} are the mixing ratios of total CO_2 (mol mol^{-1}) in the air entering and leaving

the chamber respectively. Because these mixing ratios were determined on a dry air basis (due to the Nafion dryer upstream of the CO_2 isotope analyser) only the flow of dry air on the inlet of the chamber was needed to perform the mass balance.

The fluxes of $^{12}C^{16}O_2$ (^{16}F) and $^{12}CO^{18}O$ (^{18}F) can be computed using Eq. 3, and the oxygen isotopic signature of the soil CO_2 flux ($\delta_F = 0.5\,^{18}F/^{16}F/0.00208835 - 1$, also expressed on the VPDB-CO_2 scale) can thus be calculated from the $^{12}C^{16}O_2$ concentrations and $\delta^{18}O$ of the inlet ($^{16}C_{in}$, $^{18}\delta_{in}$) and outlet ($^{16}C_{out}$, $^{18}\delta_{out}$) air:

$$\delta_F = \frac{^{16}c_{out}\,^{18}\delta_{out} - {}^{16}c_{in}\,^{18}\delta_{in}}{^{16}c_{out} - {}^{16}c_{in}} \quad (4)$$

For each steady state, 3 or 4 inlet/outlet measurements were performed leading to 3 or 4 individual values of δ_F from which a mean and standard deviation could be computed.

3.2.5. Theoretical retrieval of soil CA activity and δ_{eq}

Assuming uniform soil properties (*i.e.* uniform soil porosity, moisture and temperature), δ_F can also be computed as (Tans, 1998; Wingate et al., 2010):

$$\delta_F = \delta_{eq} - a + \frac{V_{inv} C_a}{F}\left(\delta_{eq} - \delta_a\right) \quad (5)$$

where δ_{eq} (‰ VPDB-CO_2) is the CO_2 oxygen isotopic composition in equilibrium with soil water, a (8.8‰) is the oxygen isotope fractionation factor during diffusion of CO_2 in air, C_a (mol m^{-3}) and δ_a (‰VPDB-CO_2) are the concentration and $\delta^{18}O$ of CO_2 in the air at the soil-air interface, respectively, F is the soil CO_2 efflux (μmol m^{-2} s^{-1}) and V_{inv} (m s^{-1}) is the so-called piston velocity. In the following we will assume full mixing inside the chamber so that $\delta_a = \delta_{out}$ and $C_a = c_{out}\,p/8.3144/T$ where p (Pa) and T (K) are air pressure and temperature inside the chamber headspace. The piston velocity is a function of soil moisture and temperature and soil CA activity only (Tans, 1998; Wingate et al., 2010) so that it should be the same between the two steady states. Because c_{out} and F were also maintained constant between the two steady states it was possible to retrieve δ_{eq} and V_{inv} from the two steady-state measurements (Jones et al. in prep):

$$\delta_{eq} = \frac{a\left(\delta_{a,1} - \delta_{a,2}\right) + \delta_{F,2}\delta_{a,1} - \delta_{F,1}\delta_{a,2}}{\delta_{a,1} - \delta_{a,2} + \delta_{F,2} - \delta_{F,1}} \quad (6a)$$

$$V_{inv} = \frac{F}{C_{out}}\frac{\delta_{F,2} - \delta_{F,1}}{\delta_{out,1} - \delta_{out,2}} \quad (6b)$$

where $\delta_{a,1}$ and $\delta_{a,2}$ are δ_a during steady states 1 and 2 and $\delta_{F,1}$ and $\delta_{F,2}$ are δ_F (computed from Eq. 4) during steady states SS1 and SS2.

The soil CO_2–H_2O isotopic exchange rate (k_{iso}, in s^{-1}) was then derived from the piston velocity according to:

$$k_{iso} = \frac{V_{inv}^2}{D_{iso} B \theta} \quad (7)$$

where B ($m^3\ m^{-3}$) is the solubility coefficient for CO_2 in water (Weiss, 1974), θ ($m^3\ m^{-3}$) is the volumetric soil water content, $D_{iso} = D_{eff} / (1 + a)$ and D_{eff} ($m^2\ s^{-1}$) is the effective diffusivity of gaseous CO_2 through the soil matrix (Tans, 1998; Wingate et al., 2010). The latter was computed using the formulation of Moldrup et al. (2003) for repacked soils: $D_{eff} = (\phi - \theta)^{2.5}/\phi\ D_0$, where ϕ ($m^3\ m^{-3}$) is total soil porosity and D_0 ($m^2\ s^{-1}$) is the molecular diffusivity of CO_2 in soil air at temperature T_s (K): $D_0 = 1.381\ 10^{-5}\ (T_s/273.15)^{1.81}$ (Massman, 1998).

Strictly speaking Eq. 5 is valid only for a semi-infinite soil column. In our experiments the soil depths were of only a few centimetres only and mass transport was not possible at the bottom of the soil column (*i.e.*, zero CO_2 flux), because the microcosms were closed at the bottom. With this new boundary condition, Eq. 5 should be slightly modified:

$$\delta_F = \delta_{eq} - \tilde{a} + \frac{\tilde{V}_{inv} C_a}{F}\left(\delta_{eq} - \delta_a\right) \quad (8)$$

with $\tilde{a} = a\left(1 - z_1/z_{max}\tanh\left(z_{max}/z_1\right)\right)$ and $\tilde{V}_{inv} = V_{inv}\tanh\left(z_{max}/z_1\right)$, where $z_1 = D_{iso}/V_{inv}$ and z_{max} is soil depth. The right-hand side of Eq. 6b was then used to estimate $\tilde{V}_{inv}$ and V_{inv} was solved iteratively to satisfy the equation $\tilde{V}_{inv} = V_{inv}\tanh\left(V_{inv} z_{max}/D_{iso}\right)$, from which z_1 and then $\tilde{a}$ and δ_{eq} could be deduced.

The soil CO_2–H_2O isotopic exchange rate k_{iso} was further converted into a CO_2 hydration rate (k_h). Following Uchikawa and Zeebe (2012) we have:

$$k_h = 2k_{iso}\left\{1 + \frac{C}{S} - \sqrt{1 + \frac{2}{3}\frac{C}{S} + \left(\frac{C}{S}\right)^2}\right\}^{-1} \quad (9)$$

where C ($mol\ m^{-3}$) is the CO_2 concentration in soil water and $S = [H_2CO_3] + [HCO_3^-] + [CO_3^{2-}]$. Assuming that the ratio C/S is close to its equilibrium value (this assumption is actually required to derive Eq. 9), the ratio k_h/k_{iso} is only a function of temperature and pH (Uchikawa and Zeebe, 2012). In acidic soils, this ratio approaches 3 at any temperature, because there are three oxygen atoms in the CO_2-H_2O system and in this pH range, CO_2 is the dominant dissolved inorganic carbon species.

Following the same reasoning as in Ogée et al. (2016) for OCS hydrolysis, the soil CO_2 hydration rate can also be expressed as a function of bulk CA concentration [CA] ($mol\ m^{-3}$):

$$k_h = k_{h,uncat}(T, pH) + \frac{k_{cat}}{K_m}(T, pH)[CA] \quad (10)$$

where $k_{h,uncat}$ (s^{-1}) is the un-catalysed CO_2 hydration rate at a given temperature T (K) and pH and k_{cat} and K_M are the (spatially-averaged) CA-catalysed maximum hydration rate and Michaelis-Menten constant at the same temperature and pH. The expected pH dependency of k_h and k_{iso} for different levels of CA concentrations are shown in **Fig. 3.3**.

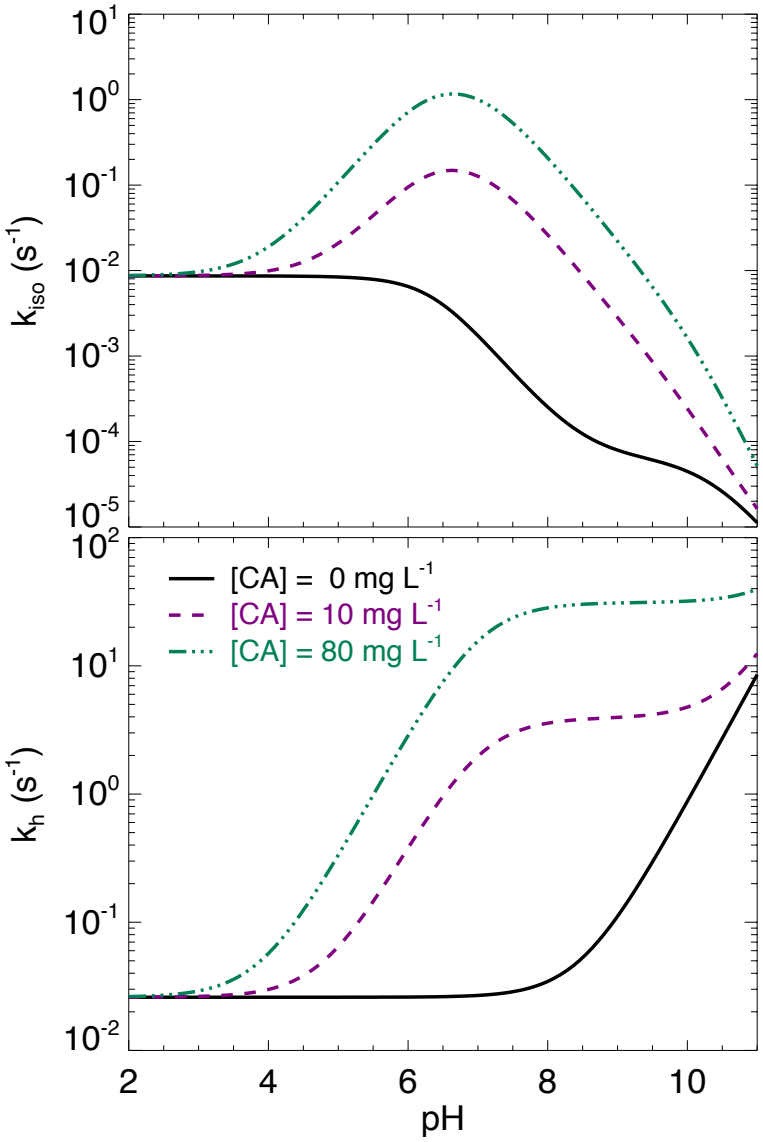

Figure 3.3: Theoretical rates of CO_2 hydration (k_h) and CO_2-H_2O oxygen isotopic exchange (k_{iso}) as a function of pH, for 3 levels of carbonic anhydrase concentration. These theoretical curves have been obtained using enzymatic parameters of k_{cat}/K_M = 70 s^{-1} μM^{-1} and pK_a = 7, which are typical of β-CAs, the expected most abundant CA isoform in soils.

Values of δ_{eq} were converted into a soil water isotope composition equivalent ($\delta_{sw\text{-}eq}$, in ‰VSMOW) according to (Brenninkmeijer et al., 1983): $\delta_{sw\text{-}eq} = \delta_{eq} + 0.20(T_s - 297.15)$. According to Wingate et al. (2009) this $\delta_{sw\text{-}eq}$ should correspond to the soil water $\delta^{18}O$ at a depth z_{eq} (m) given by:

$$z_{eq} \approx 2\sqrt{2\ln 2}z_1 \quad (11)$$

3.2.6. Water extraction and isotopic signature measurement

These estimated profiles of soil water $\delta^{18}O$ were further compared to $\delta^{18}O$ measurements of soil water extracts (δ_{sw}). For this, after completion of the full gas exchange sequence shown in **Fig. 3.2**, soil samples were collected at 1, 2 and 4 cm below the soil surface and stored in Weaton glass jar with parafilm in a fridge. Water from these soil samples was extracted by vacuum distillation and the extracted water was analysed for stable isotope composition using a Triple Isotope Water Analyser (TIWA 45EP; Los Gatos Research Inc., CA, USA) coupled to a liquid auto sampler (PAL System, Switzerland). The $\delta^{18}O$ values of soil water samples were calibrated using three internal laboratory water standards that covered the expected range of $\delta^{18}O$ in soil water (-10.16 ± 0.10 ‰, -5.56 ± 0.18 ‰ and +5.18 ± 0.18 ‰ on the VSMOW-SLAP scale). Two internal standards (the most depleted and more enriched ones) were used for calibration whilst the third internal standard was used for quality check.

Both soil water samples and internal working standards were transferred into 2mL glass vials and the vials were then closed with pre-pierced PTFE caps and silicone septa. Vials with internal standard waters were interspaced every five sample vials following the International Atomic Energy Agency (IAEA) recommendations. A small water volume (0.2-1.0 µL) from each vial was sampled using a 5-µL syringe (SGE, Milton Keynes, Great Britain) and injected through a septum in a vaporiser unit maintained at 80°C to help vaporise the water under vacuum immediately upon injection. The vapour was then transferred through a Teflon tube to the pre-evacuated optical cavity of the water isotope analyser. Before each measurement the syringe was rinsed three times in deionised water. Each vial was then measured five times and averaged. The accuracy (the mean absolute difference between calibrated and true $\delta^{18}O$ values) and reproducibility (the standard deviation of these means) on the $\delta^{18}O$ measurements of this internal standard used for quality check were always below 0.15 ‰ and 0.1 ‰ respectively.

3.2.7. Phosphate concentration measurements

Because phosphate ions can act either as strong CA activators (Rowlett et al., 1991) or CA inhibitors (Rusconi et al., 2004), total phosphate concentration in the different soils was also measured using the water extraction and colorimetric method (Van Veldhoven and Mannaerts, 1987). On 10 g of dry soil we added 99 mL of deionised water and 1 ml of a biocide (Toluene) to stop any microbial activity. Soil suspensions were left at 20°C for 16 h on an agitating roller, then sampled with plastic syringes and filtered through 0.2 mm membrane filters. The filtered solutions were analysed for phosphate concentrations (mg(P) L^{-1}) using a malachite green colorimetric method (Van Veldhoven and Mannaerts, 1987). Results were then expressed on a dry soil mass basis (mg(P) $kg(soil)^{-1}$).

3.3. Results

3.3.1. Illustration of the non destructive soil CA activity measurement method

A full sequence of measurements lasted about 1h (**Fig. 3.2**) and consisted of 2 steady states. For each sequence and each steady state, we were able to compute a k_{iso} *vs*. $\delta_{sw\text{-}eq}$ relationship combining Eqs. 7 and 8, leading up to six curves in the k_{iso}-$\delta_{sw\text{-}eq}$ space (3 for each steady state, see **Fig. 3.4**). Combining the two steady states of a same sequence and using the iterative procedure described above, we were also able to estimate separately k_{iso} and $\delta_{sw\text{-}eq}$. As expected, their values correspond closely to the intersection points of the two curves for each steady state in the k_{iso}-$\delta_{sw\text{-}eq}$ space (**Fig. 3.4**). Errors on the CO_2 isotope measurements were also algebraically propagated into the equations in order to estimate uncertainties on k_{iso} and $\delta_{sw\text{-}eq}$. The repeatability of the measurements between the three sequences was very good with a standard deviation equal or lower than the propagated error on individual estimates (*i.e.*, the spread of the squares in **Fig. 3.4** was always smaller than the error bars on each individual square). Sometimes the intersection between the two lines was not as clearly defined as the one shown in **Fig. 3.4** but the combination of the two steady states always provided very consistent and repeatable estimates of both k_{iso} and $\delta_{sw\text{-}eq}$ between the different sequences.

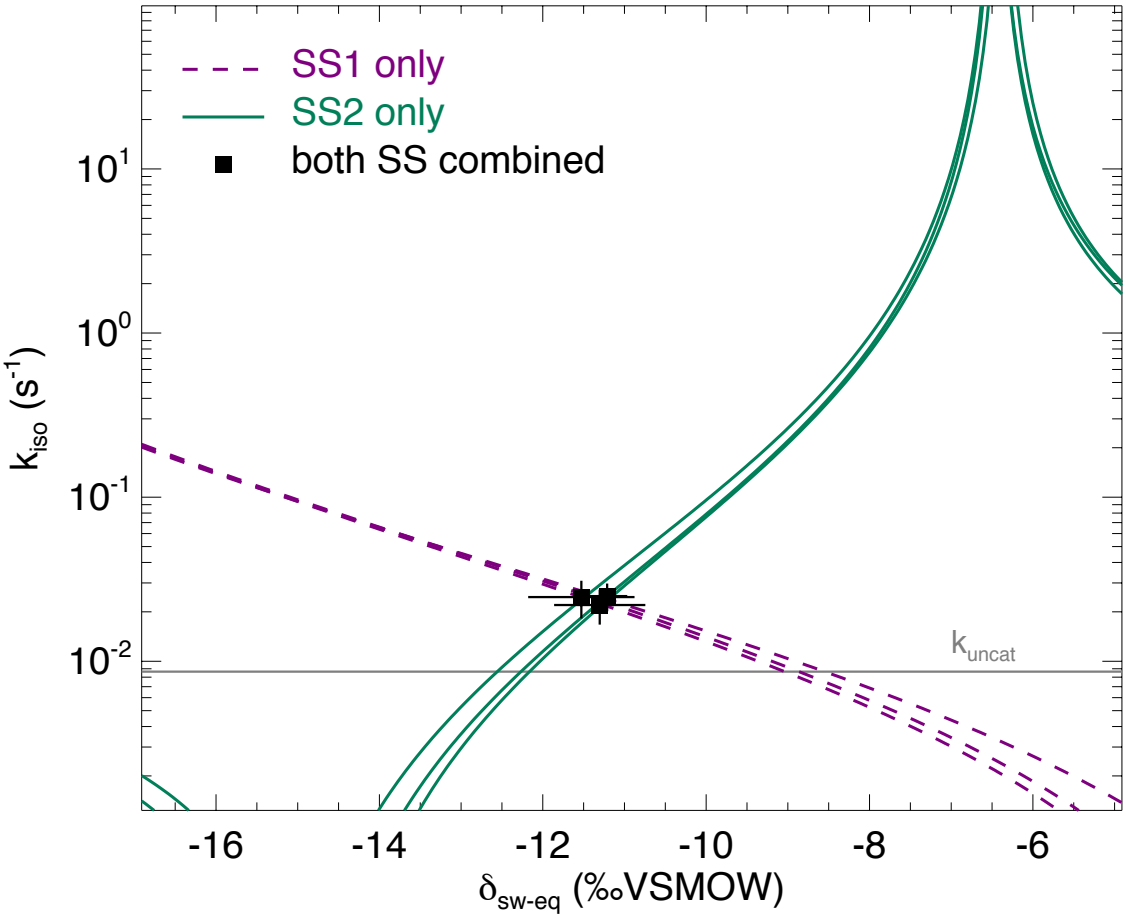

Figure 3.4: CO_2-H_2O isotopic exchange rate (k_{iso}) and isotopic composition of the soil water with which CO_2 equilibrates ($\delta_{sw\text{-}eq}$) retrieved using the two-steady-state approach described in the main text, for LeBray1 soil and an α-CA addition of 24 mg L^{-1}. Are also shown the relationships between k_{iso} and $\delta_{sw\text{-}eq}$ for steady-state 1 (dotted lines) and steady-state 2 (solid lines). In this example 3 sequences as shown in Fig. 3.2 were used, resulting in 3 curves for each steady state and 3 intersection points. The pH-dependent, un-catalysed CO_2-H_2O isotopic exchange rate is also indicated by a grey horizontal line.

For example, in the experiment shown in **Fig. 3.4**, we obtained for the three sequences k_{iso} values of 0.022 ± 0.005 s^{-1}, 0.025 ± 0.006 s^{-1} and 0.025 ± 0.005 s^{-1} and $\delta_{sw\text{-}eq}$ values of -11.3 ± 0.6, -11.5± 0.7 and -11.2± 0.3 ‰VSMOW. The estimated value of $\delta_{sw\text{-}eq}$ was in this case depleted compared to the $\delta^{18}O$ of irrigation water (-10.1 ‰VSMOW) and that of soil water at the equilibration depth z_{eq} (**Fig. 3.5**). Similar results were also observed on LeBray2 where the water pool "seen" by CO_2 had an isotopic composition ($\delta_{sw\text{-}eq}$, black circles in **Fig. 3.5**) that was strongly depleted (by about 4‰) compared to the cryogenically-extracted

soil water pool (blue squares in **Fig. 3.5**). In contrast, more enriched CO_2-derived δ_{sw} values and shallower z_{eq} were found in more clayey soils (*i.e.* Planguenoual and Folleville, see **Table 3.1**), also in much better agreement with the $\delta^{18}O$ profile of cryogenically-extracted soil water (**Fig. 3.5**).

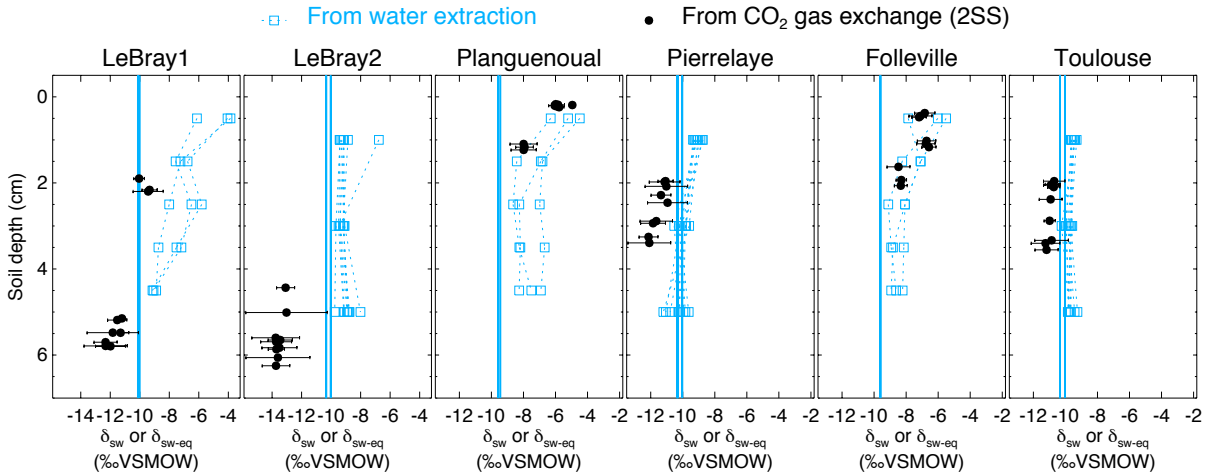

Figure 3.5: Isotopic composition of soil water at different depths in the different soil microcosms, estimated either by vacuum distillation and water isotope analysis (blue squares) or online CO_2-H_2O isotopic exchange using the two steady-state approach (black circles, see text). Profiles for the different CA treatment are plotted together without distinction. The blue vertical line also indicates the isotopic composition of the water used for the re-wetting of the air-dried soils.

3.3.2. Effect of soil pH on soil CA activity

The native (*i.e.* without any addition of exogenous α-CA during irrigation) isotopic exchange rates ($k_{iso,native}$) of the six soils were always higher than the un-catalysed rate and tended to increase slightly with more alkaline conditions (**Fig. 3.6**). These values of native isotopic exchange rates are consistent with what we would theoretically predict using β-CA concentrations between 10 and 80 mg L^{-1} (**Fig. 3.3**).

As expected, the addition of exogenous CA generally led to higher k_{iso} values compared to the native rates, and also enhanced CO_2 hydration rates k_h, with marked differences depending on the pH range (**Fig. 3.6**). On the most acidic soils, the addition of exogenous α-CA barely increased k_h above its native rate ($k_{h,native}$), by 0.1 s^{-1} or less (the native rate being already at

around 0.06 s^{-1}), *i.e.*, within the uncertainties on the measurements. On the other hand on the most alkaline soils (Toulouse, Folleville) k_h was enhanced by about 20 s^{-1} with 24 mg L^{-1} of CA added to the irrigation water and up to 65-100 s^{-1} at 80 mg L^{-1}. Results from the soils with more neutral pH (Planguenoual, Pierrelaye) were intermediate between these two cases with enhancement hydration rates of the order of 10 s^{-1} or less.

This influence of soil pH on the enhancement of k_h by exogenous CA was expected as the k_{cat}/K_M value of α-CA is known to be strongly reduced in acidic pH with a pH response of the form (Rowlett et al., 1991):

$$\frac{k_{cat}}{K_m} = \left(\frac{k_{cat}}{K_m}\right)_{max} \frac{1}{1+10^{pK_a - pH}} \quad (11)$$

To test whether our results only reflected the pH response of the exogenous α-CA, we rewrote Eq. 9 as follows:

$$k_h = k_{h,native} + \frac{k_{cat}}{K_m}[CA]_{exogenous} \quad (10)$$

where $k_{h,native}$ (s^{-1}) represents the native value of k_h and $[CA]_{exogenous}$ (mol m^{-3}) is the concentration of exogenous CA in soil water. For a given pH (and temperature) the difference $\Delta k_h = k_h - k_{h,native}$ should then be proportional to $[CA]_{exogenous}$ and the slope of the relationship should be given by k_{cat}/K_M and thus be influenced by soil pH. The theoretical pH response of Δk_h at the two CA concentration values used in this study (24 and 80mg L^{-1}) is shown in **Fig. 3.6b**, using Eq. 11 with $pK_a = 7.1 \pm 0.5$ and $(k_{cat}/K_M)_{max} = 30 \pm 7$ s^{-1} mM^{-1} and a molar mass of 30 kg mol^{-1}, which are typical values for bovine α-CA (Lindskog and Coleman, 1973; Rowlett et al., 1991; Uchikawa and Zeebe, 2012). For LeBray1, Folleville and Toulouse, our results were in very close agreement with Eq. 11 for the two different CA concentrations we tested, but this was not the case for the other soils. For LeBray2 and Pierrelaye, the observed enhanced hydration rates were smaller than the ones predicted by Eq. 11 while for Planguenoual, they were higher.

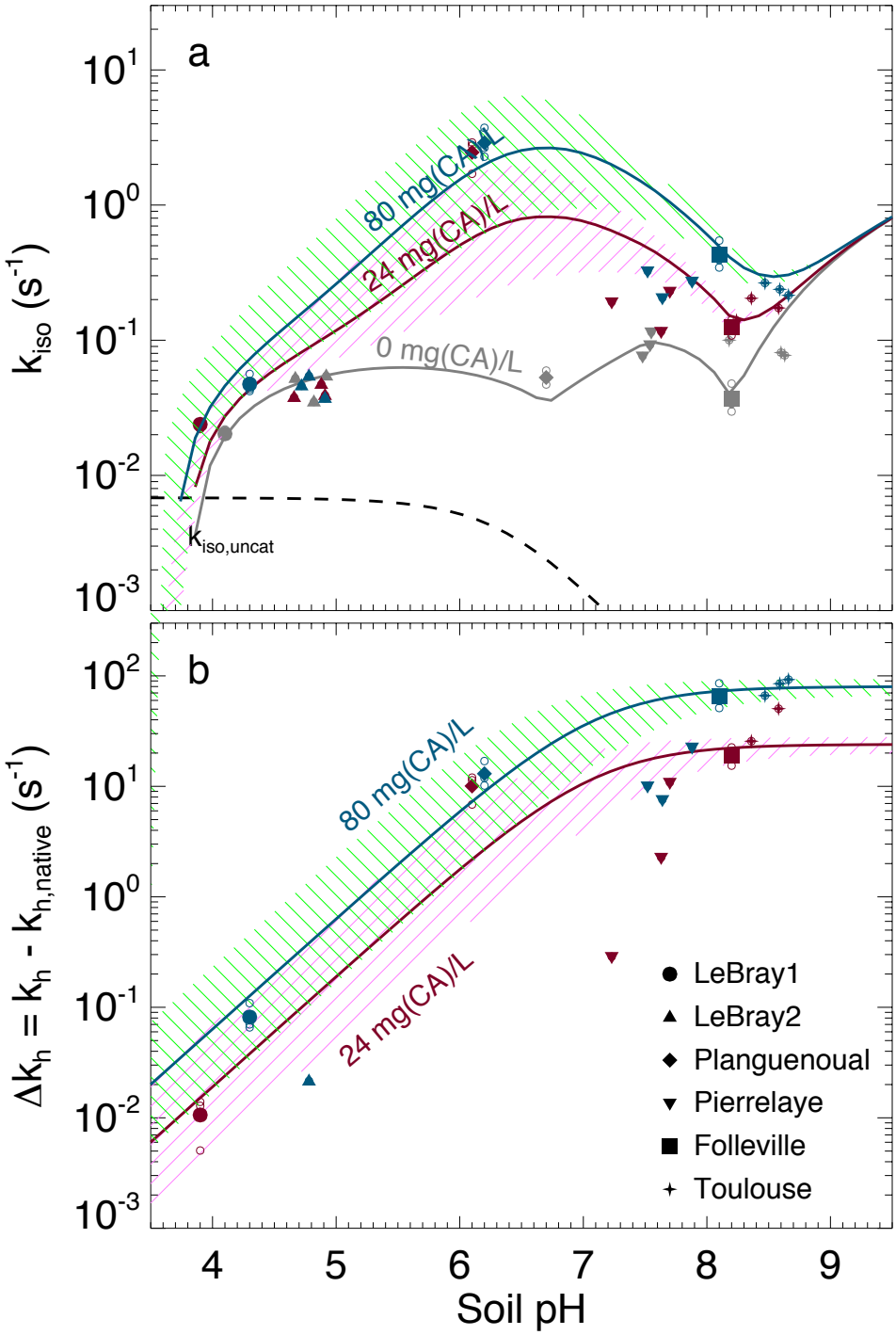

Figure 3.6: Measured CO_2-H_2O isotopic exchange rates (k_{iso}) in the different soils for different levels of α-CA addition (top) and associated enhancement hydration rates (k_h - $k_{h,native}$) caused by the α-CA addition (bottom). In the top panel, the un-catalysed isotope exchange rate ($k_{iso,uncat}$) is shown for reference (black dotted curve). Native rate (grey curve in top panel) and theoretical rates above the native rate (green and purple curves) are also shown, using $k_{cat}/K_M = 30 \pm 5\ s^{-1}\ \mu M^{-1}$ and $pK_a = 7.1 \pm 0.5$.

3.4. Discussion

3.4.1. Can we predict the enhancement in soil CA activity with exogenous CA?

Results shown in **Fig. 3.6b** indicate that soil pH is certainly the primary driver of the enhancement in the hydration rates as a result of exogenous CA addition. Our data from three soils agreed remarkably well with a pH response given by Eq. 11 and k_{cat}/K_M and pK_a values estimated by independent studies on the same CA (Uchikawa and Zeebe, 2012). This indicates that our method to estimate the CO_2 hydration rates in soil water is robust, despite the complications caused by CO_2 diffusion through the soil matrix, the possible heterogeneity in soil water content and pore space and the fact that we also had to subtract the native hydration rate from our Δk_h calculations.

Regarding this last point, a possible bias in our Δk_h calculations could arise if the native hydration rates were markedly different between the soils with and without CA addition, *i.e.*, if the addition of water with exogenous CA over the 12h-24h prior to our gas exchange measurements was enough to induce changes in microbial growth and diversity compared to what we would expect in soils where only water was added. To explore this possibility we analysed by qPCR some of our microcosms and could not find any clear trend in the number of 16S and 18S gene copies with the amount of exogenous CA added to the soil (not shown). These results, although only preliminary, suggest that exogenous CA addition should not affect the native CO_2 hydration rates and our Δk_h estimations should not be biased.

Some discrepancies between observed and predicted Δk_h values remained however for 3 of the soils tested (LeBray2, Pierrelaye and Planguenoual). One possible reason for these discrepancies could be that the model we are using to derive k_{iso} and thus k_h from our gas exchange data (Eq. 8) assumes that the soil column is homogeneous in terms of soil water content, temperature, porosity, CA concentration and respiration rate (Tans, 1998). Care was taken to get as close as possible from these conditions: the soils had been sieved and homogenised before being placed into the soil chambers, the irrigation of the soil was performed at least 12h prior to the gas exchange measurements and the soil microcosms were immersed in a water bath to minimise temperature gradients during the gas exchange measurements. In 2016 we also increased the preparation time to 24h and minimised soil water evaporation and isotopic enrichment (see Material and Methods). Despite these precautions, soil water content and its isotopic composition was not always homogeneous throughout the soil column (**Fig. 3.5**).

Also, on the most alkaline soils, we noticed that the CO_2 mixing ratio on the outlet of the soil microcosm was not always stable, indicating that steady state was not reached. This could be explained by the fact that these alkaline soils contain a large pool of total dissolved inorganic carbon that takes much longer to re-equilibrate after a change in the CO_2 concentration in the microcosm headspace, especially if that concentration differed markedly from the CO_2 concentration seen by the soil prior to the measurements. On these soils, the acclimation time of 20 minutes was certainly too short but was chosen as a compromise to also minimise possible artefacts caused by soil evaporation as the microcosm was flushed with dry air during the measurements.

In order to explore the possible consequences of non-steadiness and soil water inhomogeneity on our k_{iso} estimates, we also used a numerical model that simulates explicitly the transport and rate of change of the different CO_2 isotopologues throughout the soil column and inside the chamber headspace. The model was ran over the entire sequence shown in **Fig. 3.2** and three model parameters were optimised in order to find the best match between the modelled and observed time-series of CO_2 mixing ratio and its carbon and oxygen isotopic composition in the chamber headspace. These model parameters were the ratio $k_{iso}/k_{iso,uncat}$ (assumed constant through the soil column), the CO_2 mixing ratio of the air prior to connecting the microcosm to the air supply and a possible offset between δ_{sw} and $\delta_{sw,eq}$ (also assumed constant throughout the soil column). The latter parameter seemed necessary given the results shown in **Fig. 3.5**. Soil CO_2 production rate was assumed uniformed throughout the soil column and iteratively computed to match the observed CO_2 efflux. Soil temperature was set constant to the temperature of the water bath and vertical profiles of soil water content and isotopic composition (δ_{sw}) were prescribed from depth-resolved measurements (**Fig. 3.5**). Surprisingly, the results from this numerical model differed only marginally from those shown in **Fig. 3.5** and **Fig. 3.6** (not shown). Δk_h values were slightly affected by non-steady-state effects, but either positively (Toulouse) or negatively (Planguenoual). Soil water inhomogeneity could also slightly affect Δk_h values but both positively (Folleville) or negatively (LeBray1). Overall the discrepancies between Δk_h estimates and the theoretical predictions (Eq. 11) remained, even once non-steadiness and soil water inhomogeneity had been accounted for.

Another factor that could explain the deviation of Δk_h from theory is the presence of phosphate ions in the soil solution that could either activate or inhibit CA compared to its activity in absence of such anion (Rowlett et al., 1991; Rusconi et al., 2004). We tested this

hypothesis by exploring how the ratio between Δk_h predicted by Eq. 11 ($\Delta k_{h,theory}$) and the observed Δk_h varied with total phosphate concentration (P_i), as well as with the concentrations in mono- and di-hydrogen phosphate ions (HPO_4^{2-} and $H_2PO_4^-$ respectively). Although the relationships between $\Delta k_{h,theory}/\Delta k_h$ and the different phosphate ion concentrations were quite spread, we could observe a positive trend. Also two soils with the highest total P_i and $H_2PO_4^-$concentrations (LeBray2 and Pierrelaye, once expressed on a molar basis) had also the largest $\Delta k_{h,theory}/\Delta k_h$ ratio, corresponding to an inhibitory factor of about 10 in Pierrelaye and even higher in LeBray2. This could indicate that phosphate ions act as an inhibitor of the exogenous CA used in our experiments, explaining the reduced response to CA addition in these two soils (**Fig. 3.6**).

3.4.2. With which soil water pool does the CO_2 equilibrate?

Our results also revealed large differences between the isotopic composition of the water pool "seen" by the CO_2 (δ_{sw-eq}) and that of total (*i.e.* cryogenically extracted) soil water (δ_{sw}), with more depleted δ_{sw-eq} values compared to δ_{sw} (**Fig. 3.5**). Interestingly very similar "offsets" between δ_{sw} and $\delta_{sw,eq}$ were also predicted by the numerical model (not shown), except for LeBray1 where even larger offsets were found. For a given soil the offset did not seem to vary with soil CA activity (*i.e.* the difference between δ_{sw} and $\delta_{sw,eq}$ was the same for soils with and without CA addition) and, at least for the only soil tested, did not seem to be affected by soil water content (similar offsets were observed between LeBray1 and LeBray2).

The exact reason for this offset between δ_{sw} and $\delta_{sw,eq}$ is still unknown. Noting that δ_{sw} and $\delta_{sw,eq}$ are estimated from measurements coming from different analysers, we verified that the calibrations of the two analysers were consistent with one another. We thus pressurised pure CO_2 into a keg partially full of water of known isotopic composition and let the water-CO_2 mixture equilibrate for several weeks. The pure CO_2 was then diluted into CO_2-free air to reach ambient CO_2 concentrations and the air mixture was analysed with our CO_2 isotope analyser. We found a small difference of about -0.4‰ between the $\delta^{18}O$ of the equilibrated CO_2 and the $\delta^{18}O$ of the water in the keg. We suspect that this difference is caused by our calibration scheme on the CO_2 isotope analyser because a similar offset of -0.4‰ was also systematically found on the $\delta^{18}O$ of the CO_2 in the gas bottle used for steady state 2 (**Fig. 3.1**), between our calibrated value during online measurements and the value estimated independently by mass spectroscopy. This bias could be caused by the small non-linearity response of the analyser to CO_2 concentration and could be reduced by increasing the number

of calibration bottles and narrowing their CO_2 concentration range but in any case, it could only explain a small fraction of the offset between δ_{sw} and $\delta_{sw,eq}$ (down to -6‰ on some soils). A possible explanation for the offset between δ_{sw} and $\delta_{sw,eq}$ could be that, at any given depth, soil water is not isotopically homogeneous and that CO_2 "sees" a different water pool to that extracted during cryogenic distillation, with different thermodynamic and chemical properties between the different soil water pools. This idea has been proposed by several studies already. For example Hsieh et al. (1998) let pure CO_2 to equilibrate for several weeks with different soils at different water contents and found that the isotopic composition of equilibrated CO_2 could differ by several ‰ compared to the $\delta^{18}O$ of the soil water extracted by vacuum distillation, even at relatively high (*i.e.* 32%) gravimetric water contents. They explained this difference by recognising that soil surfaces contain a lot of ions that could modify the isotopic composition of the "bound" water pool and also the CO_2-H_2O isotopic fractionation factor.
More recently, Chen et al. (2016) performed laboratory experiments that suggest the existence of two isotopically distinct pools of water around hydrophilic materials such as silage, litter or soil organic matter. They found a negative apparent isotopic fractionation between total water (extracted by cryogenic distillation) and unconfined water (estimated by water liquid-vapour equilibration), suggesting a depletion of the water bound to the hydrophilic material. They also found that the magnitude of this apparent fractionation increased with the solid to water ratio. To reconcile these results with ours, we would need to assume that CO_2 equilibrates with bound water, even when exogenous CA is added to the soil. This is somewhat surprising, because once in solution we would expect the exogenous CA to be equally spread between bound and unbound water. Another explanation would be that water around the CA reaction sites is depleted. Chen et al. (2016) found large apparent fractionation factors with water adsorbed to casein, another protein found in milk. However according to their theory, at high water contents (or low solid-to-water ratios), the fractionation factor should vanish. In addition Uchikawa and Zeebe (2012) found that the isotopic equilibration between $BaCO_3$ and water was not affected by the presence of CA in the solution, thus rejecting the hypothesis of different water composition around the CA reaction sites.

3.5. Conclusion

Currently we do not have an explanation for the observed offset between δ_{sw} and $\delta_{sw,eq}$. However our results demonstrate that our two steady-state approach was robust to retrieve CO_2-H_2O isotopic exchange rates in soils and the associated CA activity. We also found that soil pH was the primary driver of the differences in soil CA activity after α-CA addition to a variety of soils, and that the chemical composition of the soil such as its phosphate ion concentration seemed to play only a secondary role. These results will help understand better the spatio-temporal variations observed in CO_2-H_2O isotopic exchange rates acrross different biomes, and improve our understanding of $CO^{18}O$ as an atmospheric tracer of CO_2 fluxes over land.

Résultats, conclusions et perspectives additionnelles

En complément de l'étude précédente, nous avons conduit une expérience similaire en mesurant la réponse de l'α-AC au pH du sol en utilisant cette fois les flux sol-atmosphère d'OCS. Nous avons ajouté des quantités connues de la même α-AC à trois des sols précédemment utilisés (LeBray2, Pierrelaye et Toulouse) afin d'atteindre les même concentrations d'AC, *i.e.* 0, 24 et 80 $mg.L^{-1}$. Le système de mesure utilisé pour mesurer ces échanges d'OCS est décrit en détails dans le Chapitre 4. Le point important que nous souhaitons souligner ici est que, malgré des sols et des concentrations d'α-AC identiques entre les deux expériences, nous avons retrouvé deux réponses différentes de l'α-AC au pH du sol. D'un part, l'activité de l'AC, estimée avec les flux d'OCS, varie peu avec le pH du sol mais varie aussi peu avec la quantité d'α-AC ajoutée (**Fig. 3.7**).

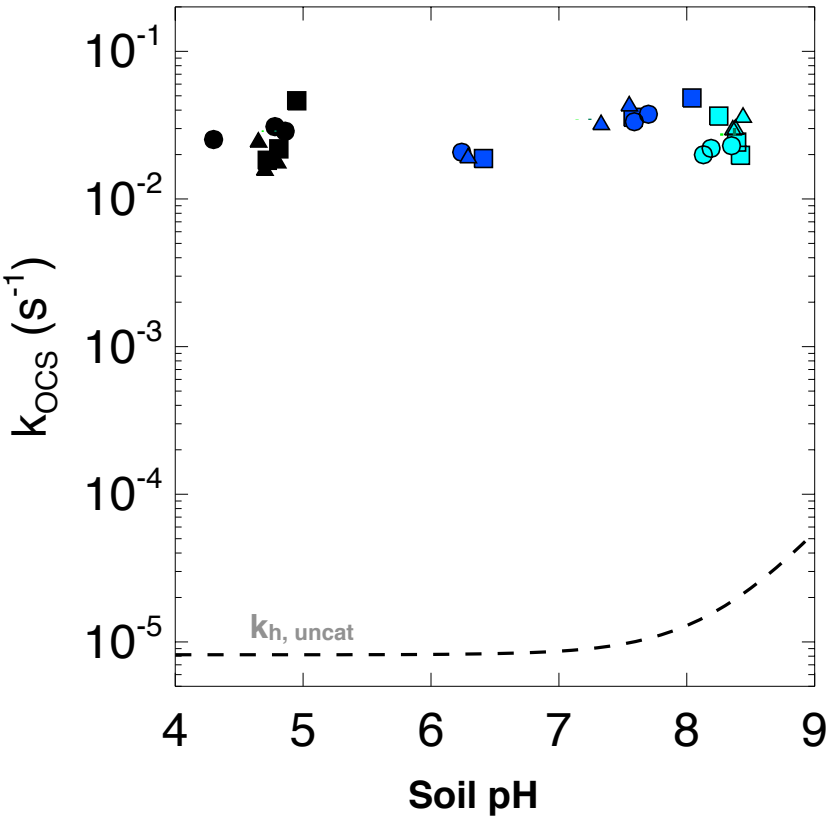

Figure 3.7 : Réponse de l'activité d'AC au pH du sol obtenue via la mesure des flux d'OCS. Les différentes couleurs représentent les différents sols (noir = LeBray2, bleu foncé = Pierrelaye et bleu ciel = Toulouse) et les différents symboles représentent les différentes concentrations d' α-AC ajoutées (cercle = 0, carré = 24 et triangle = 80 $mg.L^{-1}$).

Cette différence dans la réponse à l'ajout d'AC de l'activité enzymatique estimée en utilisant les isotopes du CO_2 (k_{iso}) ou les flux d'OCS (k_{OCS}) peut s'expliquer par la différence d'affinité de l'AC bovine ici utilisée vis à vis de chacun de ces deux substrats. Haritos and Dojchinov, (2005) ont montré que pour une AC bovine identique à celle nous avons utilisée, les paramètres cinétiques associés au taux d'hydratation du CO_2 d'une part et au taux d'hydrolyse de l'OCS d'autre part étaient très différents. Le ratio k_{cat}/K_M associé à la réaction d'hydratation du CO_2 est supérieur à celui associé à l'hydrolyse de l'OCS de plus de trois ordres de grandeurs (respectivement k_{cat}/K_M égal 8.3 10^7 et 2.2 10^4 s^{-1} M^{-1}). A notre connaissance, il s'agit de la seule étude reportant des paramètres enzymatiques de l'AC bovine vis-à-vis de l'OCS.

Il est également ici intéressant de noter que, bien que l'ajout d'α-AC soit sans effet sur k_{OCS}, le taux d'hydrolyse natif se trouve largement au-dessus de la valeur du taux non catalysé, indiqué par la courbe en pointillés sur la **Figure 3.7**. Une explication possible est que les sols que nous avons ici mesurés aient une teneur native en β-AC élevée, car les paramètres enzymatiques de cette classe d'enzyme, bien qu'encore peu documentés (Ogée et al. 2016), semblent plus favorables à des taux d'hydrolise élevés. Smeulders et al. (2011) ont par ailleurs identifié une enzyme à la structure proche d'une β-AC qui serait très efficace pour catalyser la réaction d'hydrolyse de l'OCS et qui n'utiliserait pas (ou peu) le CO_2 comme substrats. Il est pourtant peu probable de trouver cette enzyme dans nos sols puisqu'elle serait spécifique aux organismes extrêmophiles (type acidothermophiles). Ogawa et al. (2013) ont également découvert dans *Thiobacillus thioparus*, une bactérie de type Gram-négative bien connue pour oxyder le soufre présent dans les sols. Cette bactérie contiendrait une enzyme dont la séquence d'acides aminés partage de grandes similitudes avec celle des enzymes de types β-AC. Cette enzyme a été nommée COSase puisqu'elle catalyse l'hydrolyse de l'OCS de la même manière qu'une β-AC et possède aussi une très faible affinité pour le CO_2 (taux d'hydratation 3-4 fois plus faible qu'une β-AC). Ces résultats montrent clairement que CO_2 et OCS répondent différemment au pH du sol et possiblement aux familles d'AC, et ouvrent la porte à de nouvelles questions sur les réelles similitudes à considérer pour décrire les mécanismes contrôlant les flux sol-atmosphère de CO_2 et d'OCS.

References

Achat, D. L., Daumer, M.-L., Sperandio, M., Santellani, A.-C. and Morel, C.: Solubility and mobility of phosphorus recycled from dairy effluents and pig manures in incubated soils with different characteristics, Nutr. Cycl. Agroecosystems, 99(1–3), 1–15, doi:10.1007/s10705-014-9614-0, 2014.

Allison, C. E., Francey, R. J. and Meijer, H. A. J.: Recommendations for the reporting of stable isotope measurements of carbon and oxygen in CO gas, Ref. Intercomp. Mater. Stable Isot., 24(IAEA-TECDOC), 155–162, doi:10.1016/0020-708X(73)90108-7, 1995.

Badger, M.: The roles of carbonic anhydrases in photosynthetic CO_2 concentrating mechanisms, Photosynth. Res., 77(2/3), 83–94, doi:10.1023/A:1025821717773, 2003.

Ballantyne, A. P., Alden, C. B., Miller, J. B., Tans, P. P. and White, J. W. C.: Increase in observed net carbon dioxide uptake by land and oceans during the past 50 years, Nature, 488(7409), 70–72, doi:10.1038/nature11299, 2012.

Brenninkmeijer, C. a. M., Kraft, P. and Mook, W. G.: Oxygen isotope fractionation between CO_2 and H_2O, Chem. Geol., 41, 181–190, doi:10.1016/S0009-2541(83)80015-1, 1983.

Chen, G., Auerswald, K. and Schnyder, H.: ^{2}H and ^{18}O depletion of water close to organic surfaces, Biogeosciences, 13(10), 3175–3186, doi:10.5194/bg-13-3175-2016, 2016.

Ciais, P., Denning, A. S., Tans, P. P., Berry, J. A., Randall, D. A., Collatz, G. J., Sellers, P. J., White, J. W. C., Trolier, M., Meijer, H. A. J., Francey, R. J., Monfray, P. and Heimann, M.: A three-dimensional synthesis study of $\delta^{18}O$ in atmospheric CO_2 1. Surface fluxes, J. Geophys. Res., 102, 5857–5872, 1997.

Cuntz, M.: A comprehensive global three-dimensional model of $\delta^{18}O$ in atmospheric CO_2 : 1. Validation of surface processes, J. Geophys. Res., 108(D17), 1–24, doi:10.1029/2002JD003153, 2003.

Farquhar, G. D., Lloyd, J., Taylor, J. A., Flanagan, L. B., Syvertsen, J. P., Hubick, K. T., Wong, S. C. and Ehleringer, J. R.: Vegetation effects on the isotope composition of oxygen in atmospheric CO_2, Nature, 363(6428), 439–443, doi:10.1038/363439a0, 1993.

Fierer, N. and Jackson, R. B.: The diversity and biogeography of soil bacterial communities, Proc. Natl. Acad. Sci., 103(3), 626–631, doi:10.1073/pnas.0507535103, 2006.

Gillon, J. and Yakir, D.: Influence of Carbonic Anhydrase Activity in Terrestrial Vegetation on the ^{18}O Content of Atmospheric CO_2, Science, 291(5513), 2584–2587,

doi:10.1126/science.1056374, 2001.

Gurney, K. R. and Eckels, W. J.: Regional trends in terrestrial carbon exchange and their seasonal signatures, Tellus B, 328–339, doi:10.1111/j.1600-0889.2011.00534.x, 2011.

Haritos, V. S. and Dojchinov, G.: Carbonic anhydrase metabolism is a key factor in the toxicity of CO_2 and COS but not CS_2 toward the flour beetle Tribolium castaneum [Coleoptera: Tenebrionidae], Comp. Biochem. Physiol. Part C Toxicol. Pharmacol., 140(1), 139–147, doi:10.1016/j.cca.2005.01.012, 2005.

Hartman, W. H., Richardson, C. J., Vilgalys, R. and Bruland, G. L.: Environmental and anthropogenic controls over bacterial communities in wetland soils, Proc. Natl. Acad. Sci., 105(46), 17842–17847, doi:10.1073/pnas.0808254105, 2008.

Hopkinson, B. M., Meile, C. and Shen, C.: Quantification of Extracellular Carbonic Anhydrase Activity in Two Marine Diatoms and Investigation of Its Role, Plant Physiol., 162(2), 1142–1152, doi:10.1104/pp.113.217737, 2013.

Hsieh, J. C. C., Savin, S. M., Kelly, E. F. and Chadwick, O. A.: Measurement of soil-water $\delta^{18}O$ values by direct equilibration with CO_2, Geoderma, 82(1–3), 255–268, doi:10.1016/S0016-7061(97)00104-3, 1998.

IPCC (2013). Changements Climatiques 2013. Les éléments scientifiques. Contribution du Groupe de travail I au cinquième Rapport d'Évaluation du Groupe d'experts intergouvernemental sur l'Évolution du climat. Équipe de rédaction principale, Stocker, T.F. et Qin, D.

Jones, S. P., Sauze, J., Ogée, J., , Wohl, S., Fernandez-Prado, N., Saavedra-Belanga, N., Sajus, T., Bosc, A., and Wingate, L.: Non-destructive estimates of soil carbonic anhydrase activity and soil water oxygen isotope composition, in prep

Krulwich, T. A., Sachs, G. and Padan, E.: Molecular aspects of bacterial pH sensing and homeostasis, Nat. Rev. Microbiol., 9(5), 330–343, doi:10.1038/nrmicro2549, 2011.

Lauber, C. L., Hamady, M., Knight, R. and Fierer, N.: Pyrosequencing-Based Assessment of Soil pH as a Predictor of Soil Bacterial Community Structure at the Continental Scale, Appl. Environ. Microbiol., 75(15), 5111–5120, doi:10.1128/AEM.00335-09, 2009.

Li, W., Yu, L., Yuan, D., Wu, Y. and Zeng, X.: A study of the activity and ecological significance of carbonic anhydrase from soil and its microbes from different karst ecosystems of Southwest China, Plant Soil, 272(1–2), 133–141, doi:10.1007/s11104-004-4335-9, 2005.

Lindskog, S. and Coleman, J. E.: The catalytic mechanism of carbonic anhydrase, Proc. Natl. Acad. Sci., 70(9), 2505–2508 [online] Available from:

http://linkinghub.elsevier.com/retrieve/pii/S0020169300950588, 1973.

Massman, W. J.: A review of the molecular diffusivities of H_2O, CO_2, CH_4, CO, O_3, SO_2, NH_3, N_2O, NO, and NO_2 in air, O_2 and N_2 near STP, Atmos. Environ., 32(6), 1111–1127, doi:10.1016/S1352-2310(97)00391-9, 1998.

Moldrup, P., Olesen, T., Komatsu, T., Yoshikawa, S., Schjønning, P. and Rolston, D. E.: Modeling Diffusion and reaction in soils: X. A unifying model for solute and gas diffusivity in unsaturated soil, Soil Sci., 168(5), 321–337, doi:10.1097/01.ss.0000070907.55992.3c, 2003.

Moroney, J. V., Bartlett, S. G. and Samuelsson, G.: Carbonic anhydrases in plants and algae, Plant, Cell Environ., 24(2), 141–153, doi:10.1046/j.1365-3040.2001.00669.x, 2001.

Ogawa, T., Noguchi, K., Saito, M., Nagahata, Y., Kato, H., Ohtaki, A., Nakayama, H., Dohmae, N., Matsushita, Y., Odaka, M., Yohda, M., Nyunoya, H. and Katayama, Y.: Carbonyl Sulfide Hydrolase from Thiobacillus thioparus Strain THI115 Is One of the β-Carbonic Anhydrase Family Enzymes, J. Am. Chem. Soc., 135(10), 3818–3825, doi:10.1021/ja307735e, 2013.

Ogée, J., Sauze, J., Kesselmeier, J., Genty, B., Van Diest, H., Launois, T. and Wingate, L.: A new mechanistic framework to predict OCS fluxes from soils, Biogeosciences, 13(8), 2221–2240, doi:10.5194/bg-13-2221-2016, 2016.

Poulter, B., Franck, D., Ciais, P., Myneni, R. B., Andela, N., Bi, J., Broquet, G., Canadell, J. G., Chevallier, F., Liu, Y. Y., Running, S. W., Sitch, S. and van der Werf, G. R.: Contribution of sem-arid ecosystems to interannual variability of the global carbon cycle, Nature, 509(7502), 600–603, doi:10.1038/nature13376, 2014.

Reynolds, L. L., Johnson, B. R., Pfeifer-Meister, L. and Bridgham, S. D.: Soil respiration response to climate change in Pacific Northwest prairies is mediated by a regional Mediterranean climate gradient, Glob. Chang. Biol., 21(1), 487–500, doi:10.1111/gcb.12732, 2015.

Rollion-Bard, C., Chaussidon, M. and France-Lanord, C.: Biological control of internal pH in scleractinian corals: Implications on paleo-pH and paleo-temperature reconstructions, Comptes Rendus Geosci., 343(6), 397–405, doi:10.1016/j.crte.2011.05.003, 2011.

Rowlett, R. S., Gargiulo, N. J., Santoli, F. A., Jackson, J. M. and Corbett, A. H.: Activation and Inhibition of Bovine Carbonic Anhydrase III by Dianions, J. Biol. Chem., 266(2), 933–941, 1991.

Rowlett, R. S., Tu, C., McKay, M. M., Preiss, J. R., Loomis, R. J., Hicks, K. a., Marchione, R. J., Strong, J. a., Donovan, G. S. and Chamberlin, J. E.: Kinetic characterization of

wild-type and proton transfer-impaired variants of β-carbonic anhydrase from Arabidopsis thaliana, Arch. Biochem. Biophys., 404(2), 197–209, doi:10.1016/S0003-9861(02)00243-6, 2002.

Rusconi, S., Innocenti, A., Vullo, D., Mastrolorenzo, A., Scozzafava, A. and Supuran, C. T.: Carbonic anhydrase inhibitors. Interaction of isozymes I, II, IV, V, and IX with phosphates, carbamoyl phosphate, and the phosphonate antiviral drug foscarnet, Bioorg. Med. Chem. Lett., 14(23), 5763–5767, doi:10.1016/j.bmcl.2004.09.064, 2004.

Seibt, U., Wingate, L., Lloyd, J. and Berry, J. a.: Diurnally variable $\delta^{18}O$ signatures of soil CO_2 fluxes indicate carbonic anhydrase activity in a forest soil, J. Geophys. Res., 111(G4), G04005, doi:10.1029/2006JG000177, 2006.

Smeulders, M. J., Barends, T. R. M., Pol, A., Scherer, A., Zandvoort, M. H., Udvarhelyi, A., Khadem, A. F., Menzel, A., Hermans, J., Shoeman, R. L., Wessels, H. J. C. T., van den Heuvel, L. P., Russ, L., Schlichting, I., Jetten, M. S. M. and Op den Camp, H. J. M.: Evolution of a new enzyme for carbon disulphide conversion by an acidothermophilic archaeon., Nature, 478(7369), 412–6, doi:10.1038/nature10464, 2011.

Smith, K. . and Ferry, J. G.: Prokaryotic carbonic anhydrases, FEMS Microbiol. Rev., 24(4), 335–366, doi:10.1016/S0168-6445(00)00030-9, 2000.

Tans, P.: Oxygen isotopic equilibrium between carbon dioxide and water in soils, Tellus B, 50(2), 163–178, doi:10.1034/j.1600-0889.1998.t01-1-00004.x, 1998.

Uchikawa, J. and Zeebe, R. E.: The effect of carbonic anhydrase on the kinetics and equilibrium of the oxygen isotope exchange in the CO_2–H_2O system: Implications for $\delta^{18}O$ vital effects in biogenic carbonates, Geochim. Cosmochim. Acta, 95, 15–34, doi:10.1016/j.gca.2012.07.022, 2012.

Usdowski, E., Michaelis, J., Bottcher, M. E., and Hoefs, J. : Factors for the oxygen isotope equilibrium fractionation between aqueous and gaseous CO_2, carbonic-acid, bicarbonate, carbonate, and water (19-degrees-C)., *Zeitschrift fur Physikalische Chemie-International Journal of Research in Physical Chemistry & Chemical physics*, *170*, 237-249, 1991.

Van Veldhoven, P. P. and Mannaerts, G. P.: Inorganic and organic phosphate measurements in the nanomolar range, Anal. Biochem., 161(1), 45–48, doi:10.1016/0003-2697(87)90649-X, 1987.

Weiss, R. F.: Carbon dioxide in water and seawater: the solubility of a non-ideal gas, Mar. Chem., 2(3), 203–215, doi:10.1016/0304-4203(74)90015-2, 1974.

Welp, L. R., Keeling, R. F., Meijer, H. a J., Bollenbacher, A. F., Piper, S. C., Yoshimura, K., Francey, R. J., Allison, C. E. and Wahlen, M.: Interannual variability in the oxygen isotopes of atmospheric CO_2 driven by El Niño, Nature, 477(7366), 579–582, doi:10.1038/nature10421, 2011.

Wingate, L., Ogée, J., Burlett, R. and Bosc, A.: Strong seasonal disequilibrium measured between the oxygen isotope signals of leaf and soil CO_2 exchange, Glob. Chang. Biol., 16(11), 3048–3064, doi:10.1111/j.1365-2486.2010.02186.x, 2010.

Wingate, L., Ogee, J., Cuntz, M., Genty, B., Reiter, I., Seibt, U., Yakir, D., Maseyk, K., Pendall, E. G., Barbour, M. M., Mortazavi, B., Burlett, R., Peylin, P., Miller, J., Mencuccini, M., Shim, J. H., Hunt, J. and Grace, J.: The impact of soil microorganisms on the global budget of ^{18}O in atmospheric CO_2, Proc. Natl. Acad. Sci., 106(52), 22411–22415, doi:10.1073/pnas.0905210106, 2009.

Wingate, L., Seibt, U., Maseyk, K., Ogée, J., Almeida, P., Yakir, D., Pereira, J. S. and Mencuccini, M.: Evaporation and carbonic anhydrase activity recorded in oxygen isotope signatures of net CO_2 fluxes from a Mediterranean soil, Glob. Chang. Biol., 14(9), 2178–2193, doi:10.1111/j.1365-2486.2008.01635.x, 2008.

Chapitre 4 : Contribution des communautés photosynthétiques et des champignons du sol aux flux de CO_2 et d'OCS et à l'activité d'anhydrase carbonique associée

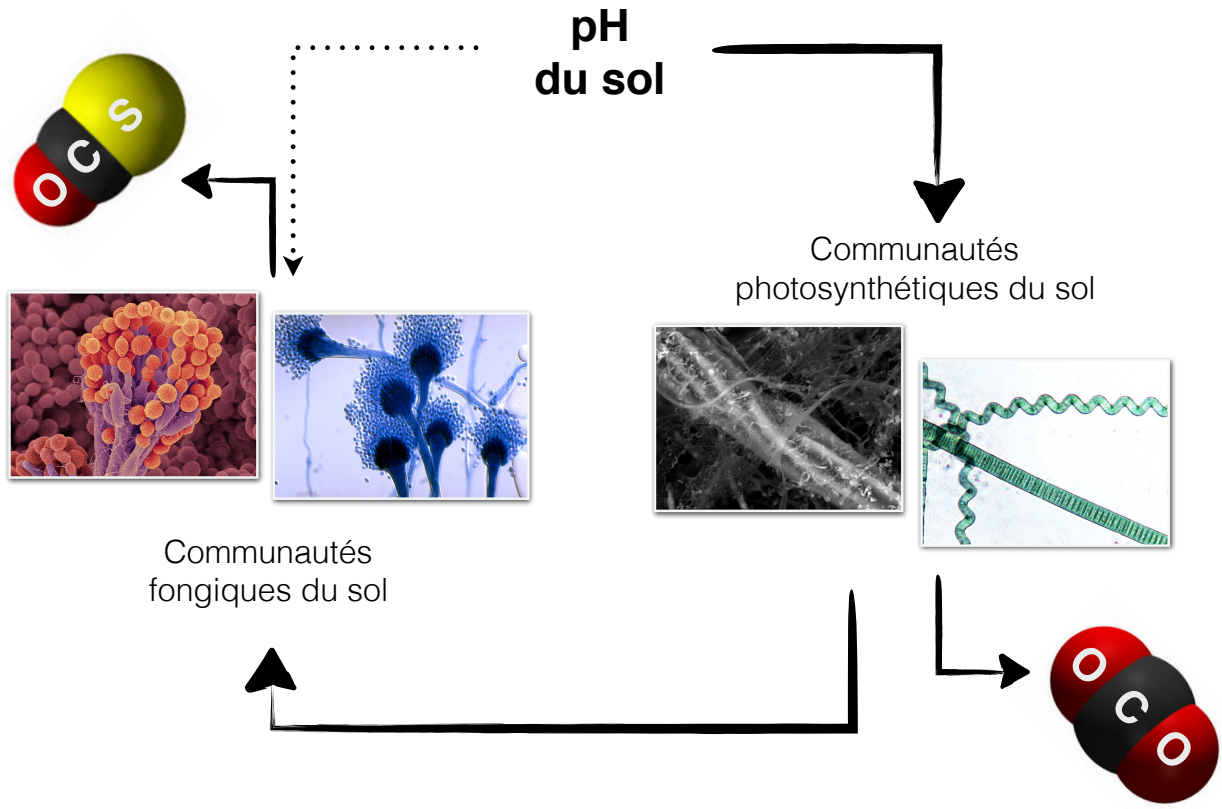

Figure 4.1: schéma synthétique des interactions observées entre le pH, le développement des différentes communautés microbiennes du sol et les flux sol-atmosphère de CO_2 et d'OCS.

Introduction au chapitre 4

Dans le chapitre précédent nous avons étudié la réponse à un ajout d'α-AC exogène du taux d'échanges isotopiques CO_2-H_2O (k_{iso}) et du taux d'hydrolyse de l'OCS (k_h). Nous avons montré que k_{iso} répondait à cet ajout de manière différenciée suivant le pH du sol tandis que la réponse de k_h semblait faible ou indissociable de l'erreur de mesure, quelque soit le pH du sol. Dans ce nouveau chapitre nous nous sommes intéressés à d'autres familles d'anhydrases naturellement présentes dans les cellules des communautés microbiennes du sol. Plus précisément, nous avons manipulé les communautés microbiennes indigènes du sol en jouant sur le cycle lumière/obscurité et l'humidité afin de favoriser le développement de communautés phototrophes, et indirectement jouer sur l'abondance et la diversité des différentes classes d'AC dans les sols. Nous avons ensuite testé si l'activité de l'AC « native » de ces différents microcosmes répondait (ou pas) au pH du sol et de manières différentes dans le cas de mesures effectuées avec le $CO^{18}O$ et l'OCS. L'*a priori* pris sur le pH du sol comme facteur de modulation dans ce travail se justifiait à la fois en raison de son impact démontré sur l'activité de l'AC, mais aussi sur la diversité et l'abondance des communautés microbiennes du sol, que nous avons quantifiées par qPCR en termes de bactéries, de champignons et d'organismes phototrophes.

Contrairement à l'expérience présentée dans le chapitre précédent, nous avons travaillé ici directement avec des microorganismes indigènes à différents sols, et non à partir d'une enzyme préalablement purifiée et réintroduite dans le sol. Ceci présentait l'avantage de nous placer dans des conditions plus réalistes pour étudier les paramètres de modulation de l'AC dans son environnement cellulaire.

A défaut de pouvoir identifier les différentes anhydrases présentes pendant nos expériences, ce chapitre ouvre la discussion sur le rôle potentiellement important des différentes famille d'AC sur les échanges isotopiques CO_2–H_2O et l'hydrolyse de l'OCS par les sols. Ce chapitre est rédigé sous la forme d'un article qui sera prochainement soumis au journal *Soil Biology and Biochemistry*. Pour cet article j'ai co-construit les expériences, conduit les mesures d'échanges gazeux et isotopiques, analysé les résultats et écrit une première version de l'article. Les outils et données qPCR, une partie de l'analyse et la version finale de l'article ont été rendus possibles grâce aux co-auteurs de l'article.

The contribution of soil phototrophs and fungi to soil CO_2 and OCS exchange and the associated carbonic anhydrase activity

Joana Sauze[1,*], Jérôme Ogée[1], Pierre-Alain Maron[2], Virginie Nowak[2], Steven Wohl[1], Aurore Kaisermann[1], Sam P. Jones[1], Olivier Crouzet[3], Lisa Wingate[1]

[1] ISPA, INRA-Bordeaux Science Agro, 33140 Villenave d'Ornon, France

[2] Agroécologie, INRA-AgroSup Dijon-Université de Bourgogne Franche-Comté, 21000 Dijon, France

[3] ECOSYS, INRA-AgroParisTech, 78026 Versailles, France

[*] Corresponding author: joana.sauze@inra.fr

Abstract

The stable oxygen isotope composition of atmospheric CO_2 and the mixing ratio of carbonyl sulphide (OCS) are potential tracers of biospheric CO_2 fluxes at large scales. However, the use of these tracers hinges on our ability to understand and predict better the activity of the enzyme carbonic anhydrase (CA) in different soil microbial groups including phototrophs. Soils were incubated in the dark or with a diurnal cycle for forty days to vary the abundance of native phototrophs. Fluxes of CO_2, $CO^{18}O$ and OCS were measured to estimate CA activity alongside the abundance of bacteria, fungi and phototrophs. The abundance of soil phototrophs increased most at higher soil pH. In the light, the soil CO_2 sink strength and the CA-driven CO_2-H_2O isotopic exchange rates correlated with phototrophs. OCS uptake rates were associated to fungi whose abundance was positively enhanced in alkaline soils but only in the presence of increased phototrophs. Our findings demonstrate that soil-atmosphere CO_2, OCS and $CO^{18}O$ fluxes are strongly regulated by the microbial community structure in response to changes in soil pH and light availability. This could be explained by different members of the microbial community expressing different classes of CA, with different affinities to CO_2 and OCS.

Keywords: carbonic anhydrase, fungi, micro-algae, OCS, pH, respiration

4.1. Introduction

The majority of the Earth's terrestrial carbon (C) is stored in soils. However, changes in climate and land use could lead to a rapid release of this C back to the atmosphere in the near future, setting up a positive feedback of uncertain magnitude (Carvalhais et al., 2014; Heimann and Reichstein, 2008). In order to constrain some of the uncertainties surrounding the fate of the C sink from the terrestrial biosphere, it is necessary to improve the representation of soil processes in land surface models. For this the C cycle research community is developing novel tools and independent tracers that will enable the detection of changes in carbon emissions and soil community function at large scales.

The oxygen stable isotope composition of atmospheric CO_2 ($\delta^{18}O_a$) is one such tracer of biosphere fluxes at large scales (Cuntz, 2003; Francey and Tans, 1987; Welp et al., 2011; Wingate et al., 2009). This is because soil and leaf water pools carry very different isotopic compositions that are transferred to the CO_2 fluxes during leaf photosynthesis and soil respiration under the action of the enzyme carbonic anhydrase (CA), ubiquitous in plants and soil micro-organisms (Badger, 2003; Moroney et al., 2001; Smith and Ferry, 2000). However, the partitioning of leaf and soil CO_2 fluxes using $\delta^{18}O_a$ hinges on our understanding of how CA activity varies in different members of the soil community and across the land surface (Welp et al., 2011; Wingate et al., 2009). Wingate et al. (2009) demonstrated that the CA-catalysed oxygen isotope exchange rate in soils from different biomes was between 20 to 300 times faster than the un-catalysed rate. These rates of soil CA activity have recently been supported by another study modelling the hydrolysis of carbonyl sulphide (OCS) by CA and the net exchange of OCS between different soil types and the atmosphere (Ogée et al., 2016). This is an important and promising finding as OCS has also emerged recently as another independent and promising tracer of gross CO_2 fluxes at large scales (Campbell et al., 2008; Montzka et al., 2004; Sandoval-Soto et al., 2005).

Wingate et al. (2009) hypothesised that spatial variability in CA activity could be caused either by variations in the intrinsic activity of certain soil community members and/or linked to shifts in soil community structure between biomes. For example, soil micro-algae are generally much larger organisms ($100\mu m^3$) than bacteria ($1\mu m^3$) and are likely to contain higher concentrations of both intra- and extra-cellular CA (Coleman et al., 1984; Hopkinson et al., 2013; Moroney et al., 2001; Palmqvist and Badger, 1996; Sültemeyer, 1998). Micro-

algae are also most abundant at the soil surface (Bristol-Roach, 1927; John, 1942; Metting, 1981) where rapid equilibration of $\delta^{18}O_a$ with soil water also occurs (Wingate et al., 2008, 2009, 2010). On the other hand, the number of micro-algae (10^6 g^{-1} dry soil) found at the soil surface is still generally out-numbered by the size of bacterial and fungal populations (typically 10^9 g^{-1} dry soil). Soil pH is an important controlling factor of the abundance and diversity of micro-algal (Lund, 1947; Shields and Durrell, 1964; Stokes, 1940), bacterial (Griffiths et al., 2011; Lauber et al., 2009) and fungal (Tedersoo et al., 2014) communities, thus the variations in CA activity observed by Wingate et al. (2009) may also partially reflect pH-driven variations in the relative abundance of community members at the soil surface.

Irrespective of their role in the atmospheric $\delta^{18}O_a$ signal, photoautotrophic micro-organisms (*i.e.* micro-algae and cyanobacteria referred to hereon as phototrophs) are important players in the C and nitrogen (N) cycles. For example it has been known for some time that variations in the abundance of phototrophs in soil can set-up ecological ripples by improving soil fertility and crop productivity (Montgomery & Biklé, 2016; Shields and Durrell, 1964) at the same time as contributing an important role to the sequestration of soil C and N at the global scale (Elbert et al., 2012). A number of recent studies have also indicated that soils from a range of biomes are capable of fixing CO_2 at different depths in the soil profile (Goyal, 1997; Hart et al., 2013; Nowak et al., 2015; Šantrůčková et al., 2005; Yuan et al., 2012). So far the attribution of CO_2 fixation in soils by phototrophic organisms is currently supported by observed changes in the abundance of marker genes encoding for RuBISCO (Nowak et al., 2015) but heterotrophic CO_2 fixation by bacteria and micro-algae may also occur (Šantrůčková et al., 2005). Indeed complex relationships between phototrophs and other microbial partners often arise as phototrophs can excrete a large variety of substances including enzymes, organic acids and polysaccharides (Metting, 1981) into their surroundings that allow bacterial and fungal partners to grow. Phototrophs also contribute to the initiation of microbial mats that develop over time by recruiting other microbial partners (Flemming et al., 2016; Konopka et al., 2015; Thompson et al., 2015). However, as far as we are aware, no study to date has determined how changes in the net soil CO_2 efflux and other GHG tracers such as OCS are regulated by changes in the abundance of phototrophic (algae and bacteria) and heterotrophic community members in natural soils varying in pH. This is mainly because the tools to address these functional relationships are generally time-consuming (dilution counts) or indirect (pigment analysis). Moreover, the development of molecular tools to study

the abundance and diversity of algae present in natural soils has been somewhat overlooked in the field of metagenomics, despite growing evidence for the important ecological and biogeochemical role of soil dwelling phototrophs as natural improvers of soil fertility and plant growth.

In this study, we investigated how the contribution of soil phototrophs and heterotrophs impacted the net exchange of atmospheric CO_2 and OCS with soils. We questioned how changes in the abundance of community members altered the CA activity of soils, and how changes in the soil community structure and function would be altered by soil pH and texture. In particular, we set out to test the hypothesis that, as the abundance of phototrophs increased in soils, the sink strength for CO_2 and OCS as well as the CA activity of the soil would increase. However, we hypothesised that the behaviour of the two trace gases across all soil types would diverge between light and dark periods as emissions of CO_2 would increase in the dark because of an increase in respiratory metabolism, whilst OCS exchange rates would remain unchanged as CA is considered to be a light-independent enzyme (Gimeno et al., submitted; Protoschill-Krebs et al., 1996). We also tested the hypothesis that increasing soil pH would favour the development of soil phototrophs and increase the sink strength for both CO_2 and OCS and lead to larger estimates of CA activity derived from the two tracers.

4.2. Material and methods

4.2.1. Soil sampling and conditioning

Four soils with differing characteristics were sampled from field sites across France ensuring a wide range of pH values (4.6 to 8.1). Le Bray (LB) is a podzol with an organic, sandy A horizon that was sampled from a coniferous forest located 20km southwest of Bordeaux during February 2016. La Cage (LG) is a luvisol with a silty loam A horizon that was sampled from an INRA experimental field growing a wheat-wheat-alfalfa-alfalfa rotation located in Versailles during April 2016. Pierrelaye (DBZ) is a luvisol with a sandy A horizon that was sampled from an INRA experimental field growing a corn/wheat rotation located 30km northwest of Paris during December 2015. Finally Toulenne (TL) is a fluviosol sampled from an INRA experimental orchard field growing cherry and peach trees located 50km southeast of Bordeaux during February 2016. A brief summary of the different soil properties for each site is presented in **Table 4.1**.

Table 4.1: Main characteristics of the different soils used for the study.

	Le Bray (LB)	**La Cage (LG)**	**Pierrelaye (DBZ)**	**Toulenne (TL)**
Land use	pine plantation	cropland	cropland	cropland
pH	4.6	6.3	7	8.1
Sand content (%)	94.7	18.4	82.2	16.7
Silt content (%)	2.6	64.7	8.7	52.3
Clay content (%)	2.7	16.9	9.1	31.0
C/N ratio	26.0	10.4	13.9	10.4

At each location three spatially-independent soil samples were taken from the surface horizon 0-10cm. Composite soil samples for each location were then sieved with a 5mm mesh and mixed together to reconstitute one homogenised soil sample. For each soil the maximum water holding capacity (WHC) was estimated on three replicates. Thereafter for each soil, six microcosms were prepared, consisting of 350 to 400g of fresh soil re-packed in a 0.825dm^3 glass jar. Each soil was then weighed and maintained at 80% of its maximum WHC to encourage the development of native soil algae. Each microcosm was then sealed with Parafilm M© to minimise evaporation, and incubated in a climate-controlled room at 20°C for forty days. At the start of the incubation three of the six microcosms were coated with aluminium foil (Dark Conditioning or DC) to inhibit the development of phototrophic organisms whilst the other three microcosms were conditioned under a day/night cycle (Light Conditioning or LC) consisting of a 16h light/8h dark photoperiod using LED lighting with an intensity of about 500 μmol(photons) m^{-2} s^{-1} in the visible range to promote the growth of the native phototrophic flora (**Fig. 4.2a**). During the incubation period the jars were periodically opened two times a week to refresh the air in the microcosm headspace.

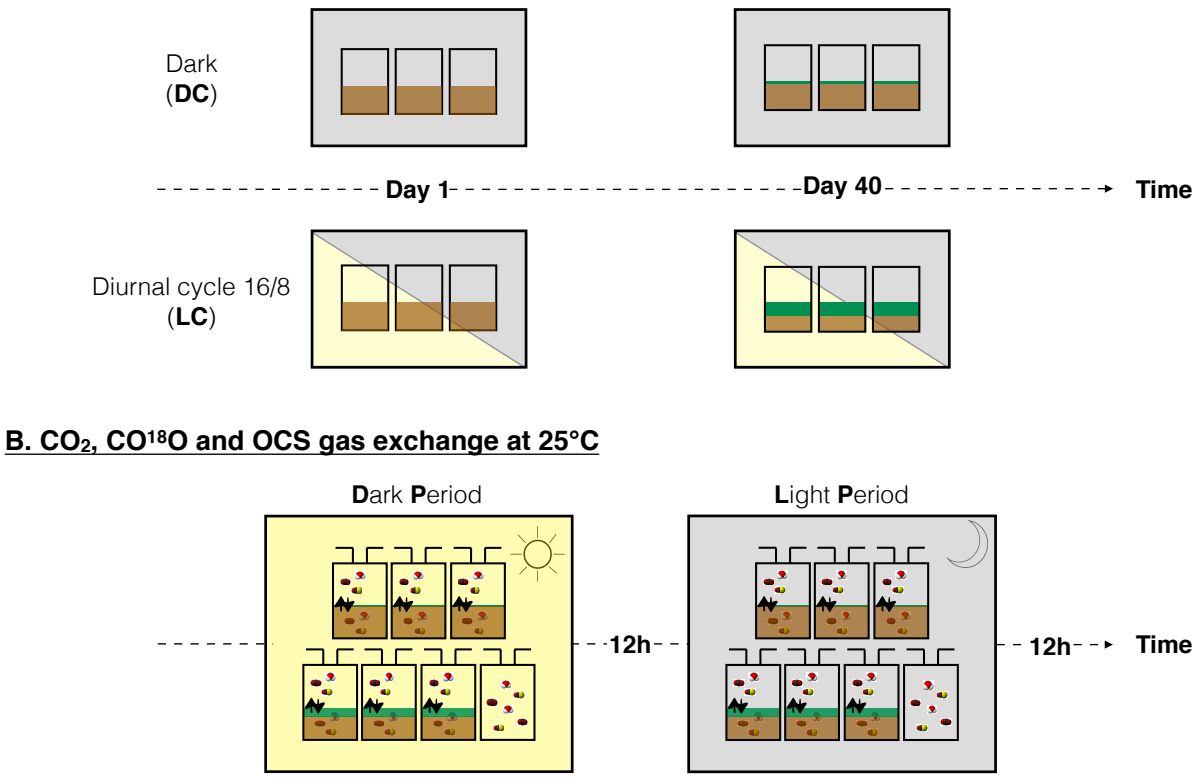

Figure 4.2: Diagram illustrating the incubation and gas exchange measurements of the six microcosms from a given soil. DC: Dark Conditioning, LC: Light Conditioning, DP: Dark Period, LP: Light Period, WHC: Water Holding Capacity.

4.2.2. Gas exchange experimental setup

After forty days, the aluminium covers were removed from the three dark conditioned microcosms and a self-contained thermocouple datalogger (iButton, DS1923, Embedded Data Systems, Lawrenceburg, KY, US) was positioned at the top of each soil column to measure the humidity and temperature at the soil surface. Each microcosm was then sealed with a customised glass lid fitted with two stainless steel Swagelok® bulkhead fittings connected to 0.25 inch (3.175 mm) Teflon™ inlet and outlet lines to form a flow-through gas exchange chamber. The six soil microcosms were then placed in a customised climate-control chamber (MD1400, Snijders, Tillburg, NL) to acclimate at 25°C with the lights on. An additional soil-free glass jar containing an iButton was also sealed and connected to a set of lines in the climate-control chamber in order to check that our setup was free of any OCS contamination.

During the gas exchange measurements, air was supplied to each of the microcosms using a compressor (FM2 Atlas Copto, Nacka, Sweden), coupled to a chemical scrub column (Ecodry K-MT6, Parker Hannifin, Cleveland, OH, US) that first removed water vapour, CO_2 and OCS from ambient air in the lab. Concentrations in the scrubbed airstream were typically less than 5 μmol(CO_2) mol^{-1}, 7 pmol(OCS) mol^{-1} and -40°C dew point. A set of individual mass flow controllers (MFC, EL-Flow® Select, Bronkhorst, Ruurlo, NL) and stainless steel cylinders containing either pure CO_2 or CO_2-free dry air with 500 nmol(OCS) mol^{-1} (Linde, France) were then used to supply CO_2 and OCS to the air stream in a 4L aluminium buffer and reach concentrations around 420 μmol(CO_2) mol^{-1} (420 ppm) and 1000 pmol(OCS) mol^{-1} (1000 ppt). The (dry) air supplied to the inlet of each microcosm was taken from this buffer volume at a flow rate of 0.25 dm^3 min^{-1} (**Fig. S1**). The flow from the buffer volume to the microcosms was driven by a slight overpressure in the buffer of 20-30 mbar above atmosphere. Within a single flux measurement, the standard deviation on the inlet was less than 0.03 ppm(CO_2) and 1.5 ppt(OCS).

4.2.3. CO_2 mixing ratio and stable isotope measurements (TDLAS)

The inlet or outlet airstream of a given microcosm was selected for CO_2 measurements by means of an 8-way solenoid (BX 758.8E1C312, 0-4 bar, Matrix, Italy). The selected airstream passed through a Nafion dryer (MD-40 Perma pure Inc., NJ, USA) before being analysed for its $^{12}C^{16}O_2$, $^{13}C^{16}O_2$ and $^{12}C^{18}O^{16}O$ concentrations using a tuneable diode laser absorption spectrometer (TGA100A, Campbell Scientific Inc., Logan Utah, USA) configured to scan the three absorption lines quasi simultaneously. Laser emission on the absorption lines was maintained using a reference gas of 25% CO_2-in-air (Linde, France). Flow through the instrument was maintained with a diaphragm vacuum pump (KNF N940, Neuberger, UK Ltd, UK) connected to the TGA100A *via* a vacuum line and the excess air was exhausted to the atmosphere *via* the solenoid, together with the other outlet lines of the other chambers that were not measured (**Fig. S1**). Calibration of the instrument was performed every 16 minutes using 3 aluminium calibration tanks containing CO_2-in-air mixtures (Deuste-Steininger, Germany) spanning the CO_2 concentration range of our measurements (374.9 ± 1.9, 474.6 ± 2.4 and 687.1 ± 4.0 ppm) and with similar $\delta^{18}O$ values (-14.68 ± 0.01, -14.70 ± 0.03 and -14.68 ± 0.03 ‰ VPDB-CO_2). CO_2 concentrations and the carbon and oxygen isotope ratios of calibration tank gas were precisely characterised at the

MPI for Biogeochemistry (Jena, Germany). A series of Allan variances performed over 24h continuous measurement of compressed air indicated a standard deviation of 0.1 μmol(CO_2) mol^{-1} and 0.3‰ for $\delta^{13}C$ and $\delta^{18}O$ after 10s of averaging time, that increased after 900s averaging time for $\delta^{18}O$ only (between 0.5 and 0.8‰), indicating departure from pure white noise. To address this issue, we assumed that instrument drift was linear in time over the 16-min sequence. Calibration tank measurements were then linearly interpolated in time and a calibration regression was performed for each chamber inlet or outlet measurement, as described in Wingate et al. (2010).

4.2.4. OCS mixing ratio measurement (QCLS)

The inlet or outlet airstream of a given microcosm was selected for OCS measurements by means of a 12-way rotary valve (EUTA-SD16WE VICI® 16 positions two way valve, Valco Instruments Co. Inc, Texas, USA). The selected airstream was pre-dried with a Nafion™ drier (MD-070-24-S-2, Perma Pure LLC, NJ, USA) before being measured with a mid-infrared quantum cascade laser spectrometer (QCLS, Aerodyne Research Inc. Billerica, MA, USA). Flow through the instrument was maintained with a TriScroll 600 pump (Agilent Technolgies, Santa Clara, CA, USA) connected to the QCLS *via* a vacuum line and excess air was exhausted to atmosphere. Instrument drift was corrected with frequent (every 16 minutes) background calibrations (with dry N_2) in all runs. After 12 minutes of measurements, a 4-min, two-point standard calibration was also implemented using the same dry N_2 bottle and compressed dry air from an Aculife®-treated cylinder with a known OCS concentration (524.8 ± 2.2 ppt) that had been prepared and calibrated for OCS by the NOAA Global Monitoring Division. This 2-point calibration allowed us to estimate instrument drift over the last 16 minutes and also account for possible span corrections. An Allan variance calculated from a 24h continuous measurement on tank air indicated a standard deviation of 2.1 ppt(OCS) after 10 s averaging time, a deviation from pure white noise after more than 400s and a standard deviation still below 1 ppt(OCS) after 900s integration time. Although the instrument stability was very good, we implemented a 2-point calibration scheme using the same approach described for the CO_2 isotopes, *i.e.*, by interpolating in time calibration measurements and computing a calibration regression for each chamber inlet or outlet measurement.

4.2.5. Sampling sequence

Each component of the system (inlet and outlet of each microcosm and the calibration tanks) were scanned at 1 Hz over 2 minutes and only the last 20s were used to compute the mean gas concentrations, accounting for the flushing time of the tubes and analysers' cells (less than 30s). In a given sequence, seven chambers (the six microcosms from a given soil and a blank chamber) were scanned sequentially by the OCS and CO_2 isotope analysers and, when not measured, were continuously flushed through at the same constant flow rate. The full sequence of gas exchange measurements lasted 24h and combined light (LP) and dark (DP) periods and two different CO_2 isotopic compositions of the supplied air (using two different pure CO_2 bottles, see **Fig. S1**). The first 12hrs of gas exchange were done with the lights on (LP) providing a light intensity of 500 μmol(photons) m^{-2} s^{-1} in the visible range (**Fig. 4.2b**). The subsequent 12hrs of gas exchange were completed in the dark (DP). No measurement was performed during the first hour following the change in light intensity or CO_2 isotopic composition to ensure that measurements were always performed under steady state conditions. To summarise, for each soil we had 4 treatments (LC-LP, LC-DP, DC-LP and DC-DP) represented by a set of 3 microcosms, all measured at two different CO_2 isotopic compositions (SS1 and SS2).

4.2.6. Calculating fluxes and CA activity

The OCS and CO_2 fluxes were computed assuming steady-state conditions:

$$F = \frac{u_{\text{in}}}{S}(c_{out} - c_{in}) \quad (1)$$

where u_{in} is the flow rate of dry air through the chamber (mol s^{-1}), S is the soil surface (m^2) and c_{in} and c_{out} are the mixing ratios of OCS or total CO_2 (mol mol^{-1}) in the air entering and leaving the chamber respectively. Because these mixing ratios were determined on a dry air basis (because of Nafion dryer upstream of each analyser) only the flow of dry air on the inlet of the chamber was needed. For each microcosm, the three replicates of inlet/outlet pairs gave three individual values of the OCS and CO_2 fluxes from which a mean and standard deviation could be computed. The mean OCS flux from the blank (empty) chamber was always not significantly different from zero (**Fig. S2**), indicating that our experimental setup was free of any OCS contamination.

Under steady-state conditions, the fluxes of $^{12}C^{18}O_2$ (^{16}F) and $^{12}CO^{18}O$ (^{18}F) can also be computed using Eq. 1, and the oxygen isotopic signature of the soil CO_2 flux ($^{18}\delta_F = 0.5\,^{18}F/^{16}F/R_{std} - 1$, expressed relative to the isotope ratio R_{std} of the VPDB-CO_2 standard) can thus be calculated from the $^{12}C^{16}O_2$ mixing ratios and $\delta^{18}O$ of the inlet ($^{16}c_{in}$, $^{18}\delta_{in}$) and outlet ($^{16}c_{out}$, $^{18}\delta_{out}$) air:

$$^{18}\delta_F = \frac{^{16}c_{out}\,^{18}\delta_{out} - {}^{16}c_{in}\,^{18}\delta_{in}}{^{16}c_{out} - {}^{16}c_{in}} \quad (2)$$

For each steady-state three replicates of the inlet and outlet were obtained leading to three individual values of $^{18}\delta_F$ from which a mean and standard deviation could be computed.

Soil carbonic anhydrase activity was then calculated for the two independent tracers, either in the form of OCS hydrolysis rate (k_h) or CO_2-H_2O isotopic exchange rate (k_{iso}). The OCS hydrolysis rate k_h was estimated following Ogée et al. (2016). According to their Eq. 16b, and assuming no OCS source from the soil microcosm, the OCS flux F_S estimated with Eq. 1 is directly related to k_h:

$$F_S = \sqrt{k_h B_S \theta D_S}\, C_S \tanh\left(\frac{z_S}{2z_{max}}\right) \quad (3)$$

where B_S, D_S, C_S represent respectively the OCS solubility in soil water ($m^3\ m^{-3}$), the OCS effective diffusivity through the soil column ($m^2\ s^{-1}$) and the gaseous OCS concentration at the soil-air interface ($mol\ m^{-3}$), z_{max} is maximum soil depth and z_S is a characteristic depth above which diffusion of OCS out of the soil becomes faster than OCS hydrolysis: $z_S = \sqrt{D_S/k_h B_S \theta}$ (Ogée et al., 2016). The solubility B_S is only a function of temperature while D_S is a function of temperature, soil moisture and porosity, and the formulation of Moldrup et al. (2003) for repacked soils was used. Assuming well-mixed conditions in the chamber we have $C_s = c_{out}\,p$ / 8.31441 / T where p (Pa) and T (K) are the air pressure and temperature inside the headspace. Equation 3 was then solved iteratively for the OCS hydrolysis rate k_h.

Using a similar approach as in Tans (1998) or Wingate et al. (2010) but accounting for the finite depth z_{max} of our soil microcosms, we were also able to relate the CO_2-H_2O isotopic exchange rate k_{iso} (s^{-1}) to $^{18}\delta_F$ (for a full derivation, see Sauze et al., submitted):

$$^{18}\delta_F = \delta_{eq} + \varepsilon_D\left(1 - \frac{z_C}{z_{max}}\tanh\left(\frac{z_{max}}{z_C}\right)\right) + \frac{\sqrt{k_{iso}B_C\theta D_C C_C}}{F_C}\left(\delta_{eq} - \delta_a\right)\tanh\left(\frac{z_{max}}{z_C}\right) \quad (4)$$

where B_C, D_C, C_C, F_C and z_C are the counterparts of B_S, D_S, C_S, F_S and z_S for CO_2, δ_a is the $\delta^{18}O$ of CO_2 at the soil-air interface (assumed equal to $^{18}\delta_{out}$) and δ_{eq} is the CO_2 isotopic composition of CO_2 in equilibrium with soil water. The latter was measured after each gas exchange measurement (see below) so that Eq. 4 could be solved iteratively to retrieve k_{iso} from $^{18}\delta_F$ measurements. Note that Eq. 4 is not strictly valid in our case because it assumes uniformity of CO_2 production, soil moisture, porosity, temperature, k_{iso} and δ_{eq} throughout the soil column, and no CO_2 consumption. Care was taken to homogenise the soil microcosms prior to their incubation and to maintain a constant soil water content during the incubation but the day/night cycle imposed on half of them helped developed soil phototrophs at the soil surface that clearly challenged the validity of Eq. 4. Theoretically we could account for their presence and derive another equation but, in practice, this would introduce extra parameters that would be difficult to estimate. We thus preferred to use Eq. 4 for all our microcosms and the retrieved k_{iso} will be considered below as an apparent CO_2-H_2O isotopic exchange rate, related to some extent to soil CA activity for CO_2.

4.2.7. Soil community analyses

The abundance of bacterial, fungal and photosynthetic microbial communities was assessed by targeting these microbial groups with specific quantitative PCR. Immediately after gas exchange measurements were completed, soil material from the soil surface (0-2cm) was sampled from each microcosm and initially stored in the dark at -80°C before being freeze-dried. Microbial DNA was extracted from 1g of soil from each triplicate microcosm of each treatment using a single procedure standardized by the GenoSol platform (http://www.dijon.inra.fr/plateforme_genosol) (Plassart et al., 2012; Terrat et al., 2012). DNA concentrations of crude extracts were determined by electrophoresis in a 1% agarose gel using a calf thymus DNA standard curve, and used as estimates of microbial molecular biomass (Dequiedt et al., 2011). After quantification, DNA was purified using a MinElute gel extraction kit (Qiagen, Courtaboeuf, France). Bacterial, fungal and photosynthetic microorganism (algae and cyanobacteria) abundances were estimated using the number of copies measured for 16S-, 18S- and plastidial 23S-rDNA genes, respectively, by quantitative polymerase chain reaction (qPCR) using a StepOne® Real-Time PCR System (Applied Biosystems, Courtaboeuf, France) with a SYBRGreen® detection system (Chemidlin Prévost-Bouré et al., 2011; Plassart et al., 2012; Sherwood and Presting, 2007). Estimates of total

chlorophyll and carotenoids were also assessed from 2.5 g of fresh soil from each triplicate microcosm of each treatment using a plate reader spectrophotometer (SAFAS MC1, SAFAS Monaco, France).

4.2.8. Soil water oxygen isotopes composition

Immediately after the gas exchange measurements additional soil material from different soil depths (0-2, 2-4 and 4-6cm depth) was sampled from each microcosm and stored at 5°C before cryogenic vacuum distillation. Distilled waters were then analysed on a laser spectrometer to measure the deuterium and oxygen stable isotope composition of water vapour (LWIA-45EP, Los Gatos Research Inc., San Jose, California, USA).

4.2.9. Statistical analyses

All statistical analyses were performed with the R software package (R3.1.3, R Core Team, 2015). In particular we used mixed effect linear models (lme in nlme package, Pinheiro *et al.*, 2015) to assess how soil conditioning (DC or LC) and physicochemical properties (texture and pH) influenced the bacterial, fungal, cyanobacterial and eukaryotic algal abundances. Soil conditioning (DC or LC) and measurement type (DP or LP), soil type (LB, LG, DBZ, TL) and their interactions were taken as fixed effects and replicates as a random effect. Mixed effects linear models were also used to test whether the CO_2 and OCS fluxes as well as their associated CA activity (k_{iso} and k_h) were related to the abundance of photosynthetic microorganisms. Soil conditioning and measurement type, soil type and their interactions were taken as fixed effects and replicates as a random effect. Simple t-tests were used to determine the treatment effects (DC/LC and DP/LP). When the variances between the groups were too different, we also used a modification of the t-test, known as the Welch's t-test, that adjusts the number of degrees of freedom.

4.3. Results

4.3.1. Effect of conditioning on the abundances of microbial groups

The development of green mats in the microcosms incubated under a diurnal cycle (LC treatment) were observed by the naked eye after forty days on three of our soils (LG, DBZ and TL), but not on the most acidic soil (LB) or any soil that had been incubated in the dark (DC treatment) (see photos in **Fig. S3**). These green mats were indicative of the presence of chlorophyll pigments (Chl) at the soil surface, as confirmed qualitatively by our pigment data (**Fig. S3**). However our pigment data indicated a larger increase of chlorophyll pigments induced by the LC treatment on the acidic soil (LB) than on the most alkaline soil (TL) which seemed counter-intuitive from visual inspection. We believe this is because Chl estimates were based on equations designed for plants and algae, but not for soil solutions. The high organic contents in LB soil made the solution much darker (browner) than the other soil solutions, which could have induced a bias in the Chl estimation.

The qualitative indications of the visual observations were also supported by the qPCR data (**Fig. 4.3**). An overall increase in the number of 23S rDNA gene copies, a proxy for the abundance of photosynthetic microorganisms, was found in all the LC-incubated microcosms relative to the DC-incubated microcosms, but not significantly in the most acidic soil (LB). The largest increases in phototrophs abundance were observed on the high pH soils (DBZ and TL), whereas the smallest change in abundance occurred on the acidic, and less green, soil (LB). In all soils where algal abundance increased significantly (*i.e.* all soils except LB), an increase in the number of bacterial and fungal gene copies was also found using LME analysis, indicating that the LC treatment also promoted bacterial and fungal growth (**Fig. 4.3**). Interestingly, although increases in bacteria and fungi gene copies were also observed with LC in these soils, there was an overall shift in the community composition, with algal gene copies increasing in relative abundance to the bacterial and fungal members (**Fig. 4.4**). Such a shift was also found in the LB soil, because of a decrease of bacterial and fungal gene copies induced by the LC treatment (**Figs. 4.3 and 4.4**).

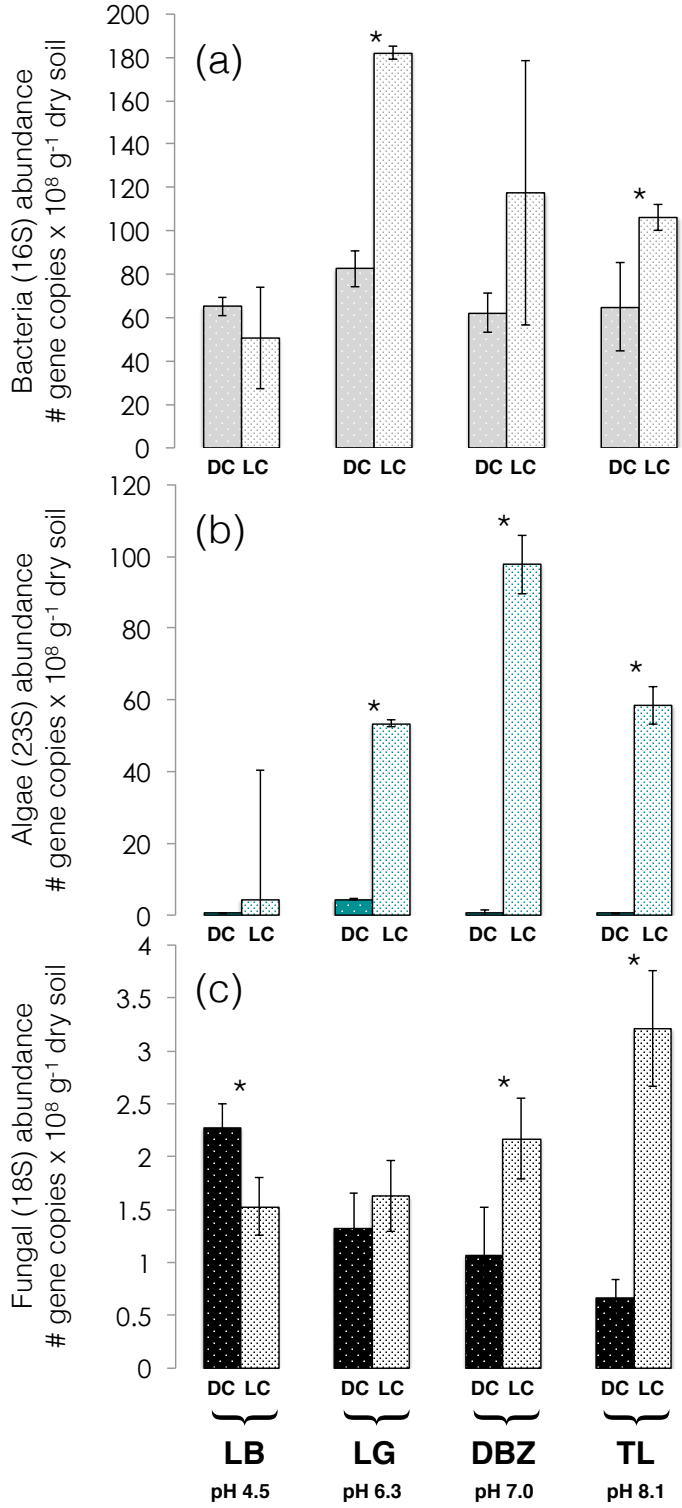

Figure 4.3: Relative number of bacterial (16S), fungal (18S) and algal (23S) gene copies (± SD, n=3) for the four soils (LB, LG, DBZ & TL) incubated in the dark (DC) and light (LC) after 40 days. Asterisks indicate soils incubation treatment (DC/LC) effect were significant ($p < 0.01$).

The number of fungal gene copies was always relatively smaller than the algal and bacterial number across all soil treatments (**Fig. 4.3**). In soils conditioned in the dark (DC treatment), the highest abundance of fungal gene copies was found in the most acidic soil, but the trend was opposite in soils conditioned to a day-night cycle (LC treatment). However in terms of relative abundance, their overall contribution within the community generally decreased with the LC treatment (**Fig. 4.4**).

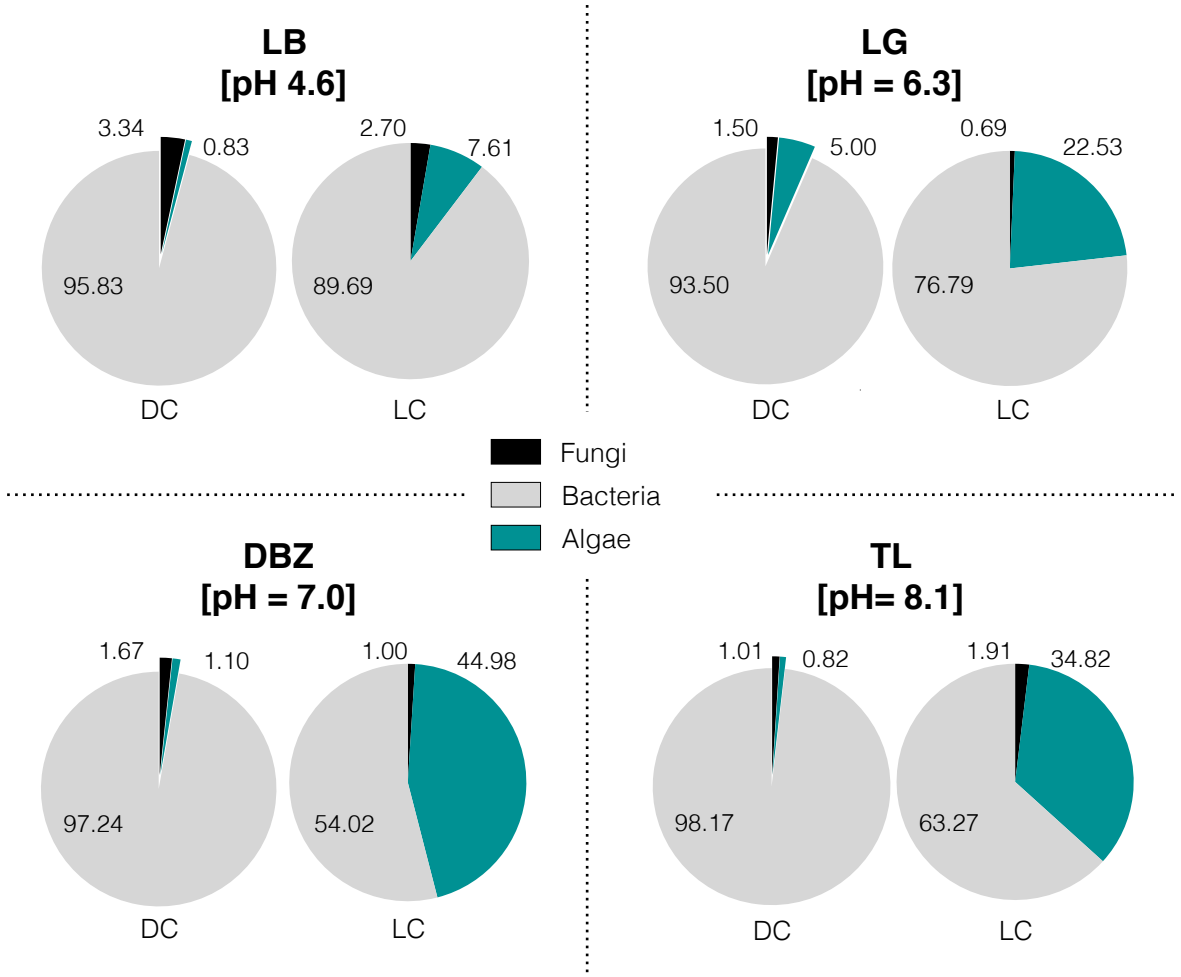

Figure 4.4: Variations in the relative abundance of community members in the different soils after dark (DC) and light incubations (LC).

4.3.2. CO_2 flux

In all soils that had been conditioned to darkness (DC treatment) there was no significant change in net observed CO_2 fluxes with light availability (**Fig. 4.5a**, compare DC-DP and DC-LP). In addition, these dark-conditioned soils were always a source of CO_2 to the atmosphere irrespective of whether they were measured in the light or in the dark. In contrast, the net CO_2 fluxes from soil microcosms conditioned to a day-night cycle (LC treatment) always differed significantly between the dark and light measurement periods, with reduced CO_2 emissions to the atmosphere or even CO_2 uptake in the light (**Fig. 4.5a**, compare LC-DP and LC-LP). The strength of this light response, characterised by the difference in the net CO_2 fluxes measured between light and dark periods ($\Delta F_{C,light-dark}$), partly reflected the changes in the abundance of 23S gene copies g^{-1} of dry soil in the LC treatments (**Fig. 4.3**) but was best captured by differences in soil pH, with the largest light response occurring in the most alkaline soil (**Fig. 4.6a**).

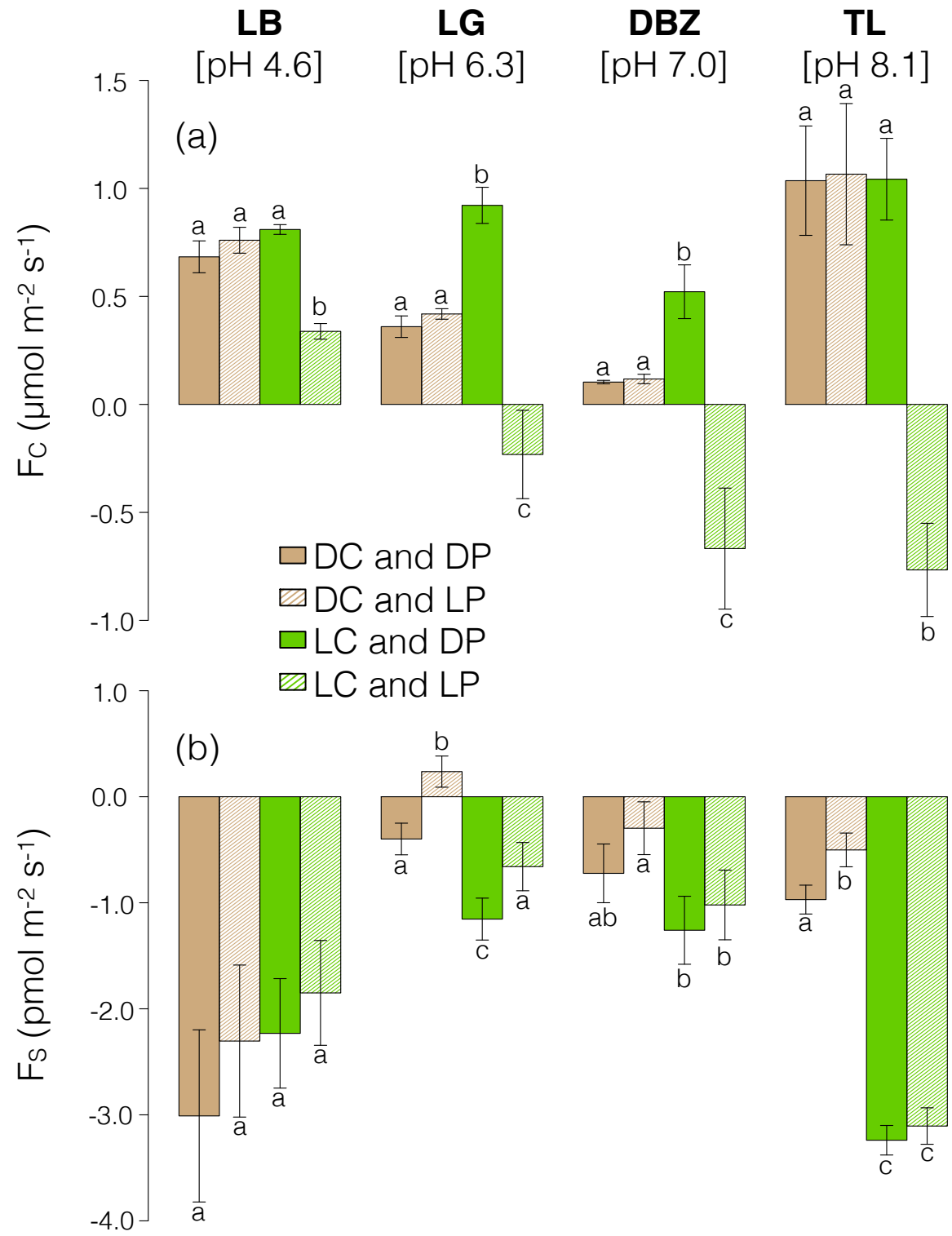

Figure 4.5: Mean variations (± SD, n=3) in the net soil (a) CO_2 and (b) OCS fluxes for four different soils measured in the light (LP) and the dark (DP) after incubation for 40 days in the light (LC) or the dark (DC). a, b and c indicate significant effects of both treatment ($p < 0.05$).

Dark respiration rates from LC-incubated soils were generally the same or larger than DC-incubated soils (**Fig. 4.5a**, compare LC-DP and DC-DP). This difference was qualitatively reflected by the changes in the number of algal, fungal and bacterial gene copies caused by the conditioning treatment (**Fig. 4.3**), except in the most alkaline soil where the increase in gene copies did not translate into larger dark respiration rates.

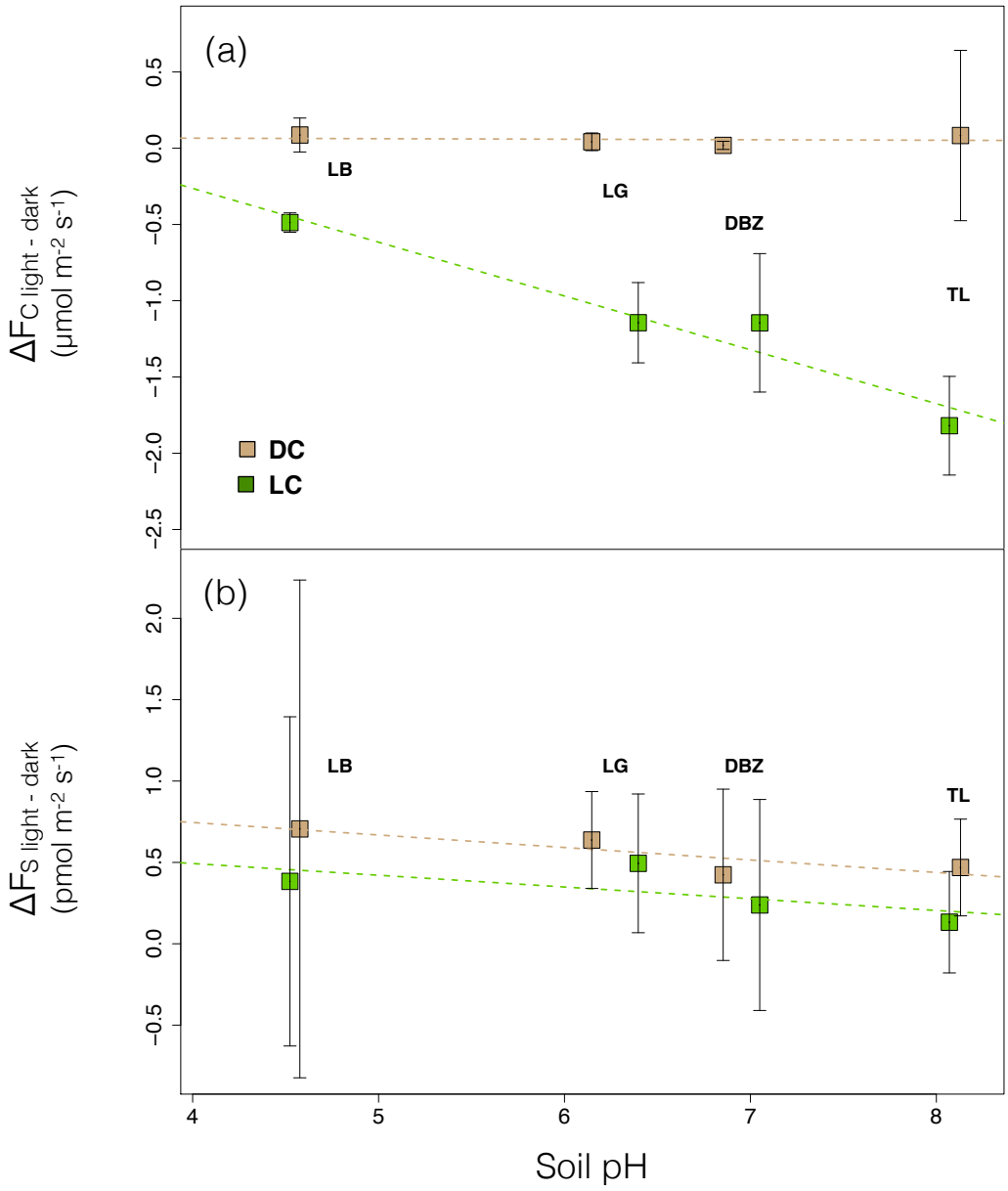

Figure 4.6: Mean differences (± SD, n=3) in the net soil (a) CO_2 and (b) OCS fluxes measured during the light (LP) and the dark (DP) period for four soils of different pH incubated in the light (LC) or the dark (DC) for ~40 days.

4.3.3. OCS flux

Nearly all soil types and treatments were sinks for OCS (**Fig. 4.5b**). Only the dark conditioned soil from Le Cage (LG) emitted OCS to the atmosphere when measured in the light. In both the DC- and LC-incubated soils there was an overall trend for the net OCS flux to decrease when measured in light and thus become a weaker OCS sink (**Fig. 4.5b**). However, this difference in sink strength ($\Delta F_{S,light-dark}$) was not statistically significant from zero for the majority of soils (**Fig. 4.6b**).

Apart from the most acidic soil (LB), the effect of the incubation treatment was statistically significant, with light-conditioned soil microcosms acting as larger OCS sinks than dark-conditioned ones (**Fig. 4.5b**). This effect of the incubation treatment on the soil OCS fluxes seems to follow changes in the number of fungal gene copies between the two treatments (**Fig. 4.3**).

4.3.4. Relationship between gas exchange and microbial communities

To assess more quantitatively the link between microbial community members and gas exchange rates, we performed different tests on the DC- and LC-incubated datasets. This was necessary to avoid conflicting results that would arise by mixing together data with either photosynthetic or respiratory metabolism caused by measurements performed in the light or the dark. With this approach we found that the net soil CO_2 flux was only correlated with the number of phototrophs (23S gene copies g^{-1} of dry soil) and only during the light measurement periods (**Fig. 4.7c**). This correlation was negative and consistent with an increase in light-induced CO_2 uptake from the atmosphere as the number of phototrophs increased. In contrast, we found that the net soil OCS flux was only correlated with the soil fungal abundance (18S gene copies g^{-1} of dry soil) with almost similar responses between light and dark measurements (**Fig. 4.7e**). Thus although the number of fungal gene copies was extremely low compared with either the bacterial or algal abundance, even a small increase in fungal abundance within the community significantly increased the OCS sink strength.

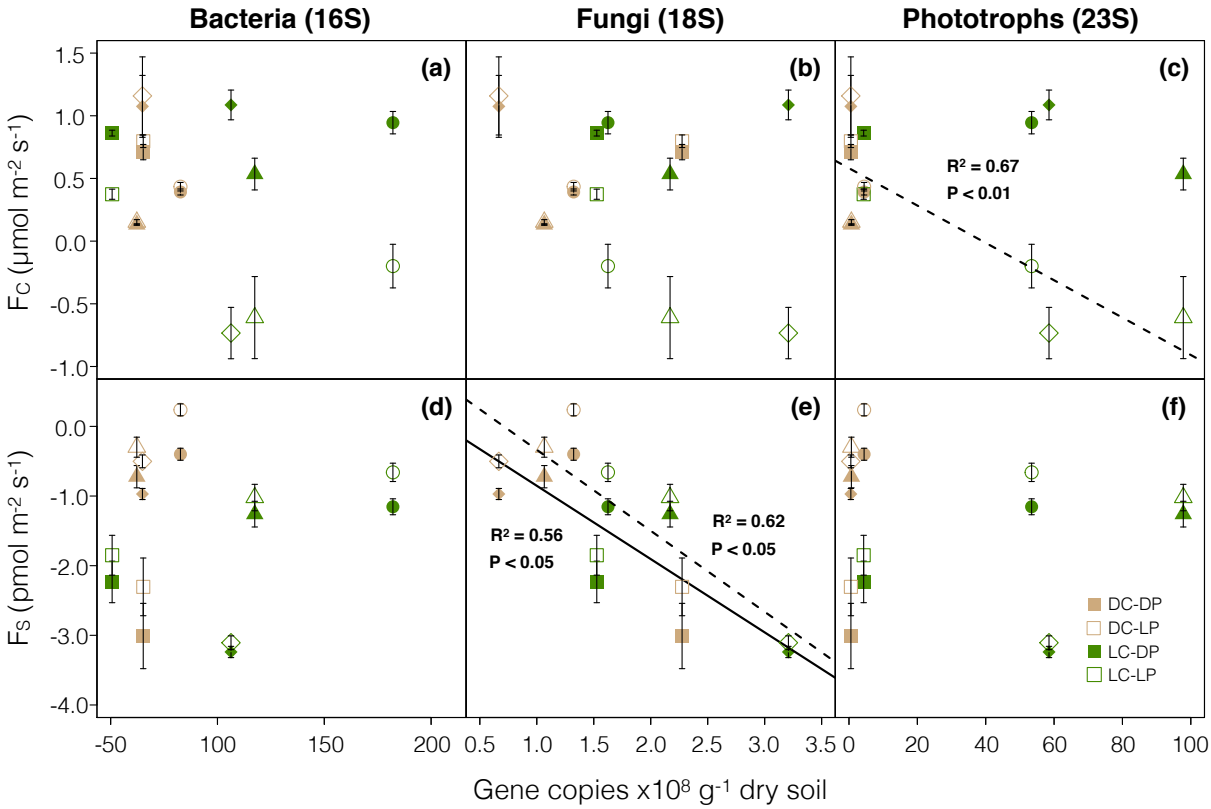

Figure 4.7: Relationship between the net soil CO_2 and OCS fluxes for four soils (LB: squares, LG: circles, DBZ: triangles, TL: lozanges) against the number of gene copies per gram of dry soil for bacteria (16S), fungi (18S) and algae (23S) measured in the light (LP) and the dark (DP) after incubation for ~40 days in the light (LC) or the dark (DC). Significant linear model results are also displayed (solid lines for dark periods and dashed lines for light periods).

Estimations of microcosm carbonic anhydrase activity were made using either the enzyme-catalysed rate of CO_2-H_2O isotope exchange (k_{iso}) or the enzyme-catalysed OCS hydrolysis rate (k_h). Generally we found that k_{iso} varied between 0.01 and 0.75 s^{-1}, and was higher in the LC treatments compared to DC treatment (**Fig. 4.8a**), although not significantly on the acidic soil (LB) that exhibited very little difference in algal abundance (**Fig 4.8a**). We also found that k_{iso} was positively correlated to the abundance of soil algae irrespective of the measurement period (LP or DP) (**Fig 4.8a**). The shift in k_{iso} between DC and LC treatments on the different soils was however more directly related to differences in soil pH than algal DNA counts (**Fig. 4.8b**), with a clear monotonic increase of k_{iso} in LC treatments with more

alkaline conditions. Estimated k_h varied between 0.002 and 0.028 s^{-1} and was positively correlated to fungal abundance across all soil treatments, but not other variables such as algal or bacterial counts or soil pH. As a consequence, and contrarily to what we expected, no significant relationship was found between k_{iso} and k_h in this dataset.

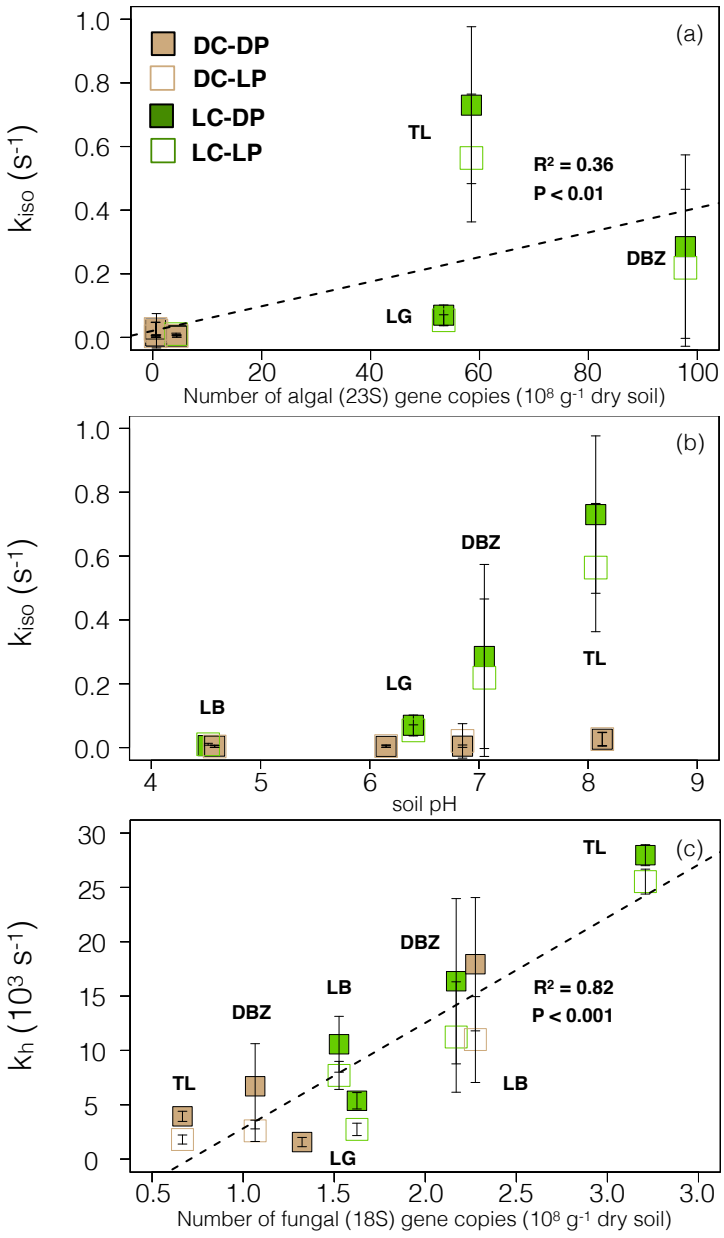

Figure 4.8: Significant relationship found between CA-catalysed activity and (a) algal gene copies using the oxygen isotopic exchange, (b) soil pH also using the oxygen isotopic exchange and (c) fungal gene copies using the OCS hydrolysis rates for the four different soils measured in the light (open; LP) and the dark (close; DP) after ~40 days of incubation in the dark (brown symbols; DC) or the light (green symbols; LC).

4.4. Discussion

4.4.1. Light and pH as driver of soil community structure

Rapid advances in the measurement of soil biodiversity have been made in the past decade using a suite of novel molecular techniques (Bardgett and Van Der Putten, 2014). Despite this progress however, little effort has been made to assemble the necessary databases required to identify the diversity of photosynthetic organisms in soils so that the use of next generation sequencing (NGS) to study soil phototroph ecology and function has been somewhat lagging within the field of metagenomics. For instance, major progress has been made recently in describing how bacterial and fungal diversity varies with pH and land management (Dequiedt et al., 2011; Griffiths et al., 2011; Lauber et al., 2008; Leff et al., 2015; Tedersoo et al., 2014). However, as far as we are aware, no study using molecular tools such as qPCR or NGS has been used to explore the interactions between the phototrophic and heterotrophic soil microbial community members. There are however several studies from the past that have made attempts to study the ecology of soil algae and bacteria but using manual and time-consuming approaches such as soil slurry dilutions combined with identification and count techniques (Lund, 1947; Shields and Durrell, 1964; Stokes, 1940; Zancan et al., 2006). From these early studies it was shown that the number of soil algae also varies strongly with soil pH (Lund, 1947; Stokes, 1940). This finding is consistent with the results of our study using a novel qPCR approach showing that algal abundance increased positively on alkaline soils when incubated in the light and at optimum water content.

Previous studies have also shown that the growth of soil algal populations is often accompanied by increases in bacterial populations (Ramanan et al., 2016; Stokes, 1940). This was also found to be the case in our study and might be partially explained by an increase in the cyanobacteria community in response to light and pH. For example, previous studies have shown that alkaline soils tend to promote the development of diatom and cyanobacterial species whilst acidic soils tend to favour green alga species from the chlorophyta (Metting, 1981; Shields and Durrell, 1964; Starks and Shubert, 1982). It has also been hypothesised that the development of algal communities may also be tracked by an increase in the number of nitrogen-fixing bacteria such as the *Azotobacter* (Reay, 2015; Stokes, 1940). These bacteria have evolved to grow rapidly (so-called *r*-strategists) in aerobic conditions and fix nitrogen from the atmosphere at optimal pH values of 7-7.5 (Garrity, 2005). It is widely known that

many soil microbes benefit from the soluble organic compounds secreted into the soil by phototrophs (Brock and Clyne, 1984; Cole et al., 1982; Larsson and Hagström, 1982). Indeed, fungal abundance was also related positively with phototroph abundance and pH but only in the LC treatments. In contrast, microcosms incubated in the dark showed a decrease in fungal abundance with pH, demonstrating that a strong positive interaction between algal and fungal abundance exists. This is in some respects consistent with other studies that have found variations in fungal abundance and diversity with pH (Tedersoo et al., 2014), although other studies have found that plant community composition seemed a better predictor of fungal community composition over pH (Leff et al., 2015). Our results indicate that the relationships between different members of the microbial community and pH may be conditional on the presence of certain phototrophs. Investigating these differences in community member interactions were beyond the scope of our present study. However, on-going development of our molecular method should render a novel tool and dataset in the near future to explore and understand better these finer ecological scale relationships within the community network.

4.4.2. The influence of soil community composition on CO_2 uptake

Most soils in the world emit CO_2 to the atmosphere (Bond-Lamberty and Thomson, 2010; Raich and Schlesinger, 1992). However, there are a number of studies showing that some alkaline soils and also ecosystems such as dry-land biocrusts remove CO_2 from the atmosphere (Elbert et al., 2012; Jasoni et al., 2005; Schlesinger et al., 2009; Wohlfahrt et al., 2008). This is typically explained by abiotic mechanisms such as thermally-induced pressure pumping or carbonate dissolution and CO_2 transport to groundwater (Schlesinger, 2017; Schlesinger et al., 2009). Recent studies have also shown that the process of carbonate formation is often microbially-induced and linked to CA activity (Benzerara et al., 2014; Couradeau et al., 2012; Kupriyanova et al., 2007; Thaler et al., 2017), highlighting the potential of microbial communities in calcareous soils to enhance CO_2 uptake. Our study also demonstrated that soil phototrophs have the potential to adapt rapidly to seasonal changes in light. Our experiment also highlighted that the extent of the community response to light is strongly controlled by soil pH as discussed above. We showed that an increase in the abundance of native phototrophs has the potential to convert soils rapidly from a net source to a net sink of CO_2 during daylight hours. However, we also observed that soils containing more phototrophs generally respired more CO_2 than dark-conditioned soils during the dark

period. Thus, on balance over a 24hr period with a 12h/12h day/night cycle, most soils (with the exception of DBZ at pH 7) remained a net source of CO_2 to the atmosphere.

Interestingly it is worth noting that variations in the abundance of soil phototrophs may introduce noise in diurnal and seasonal measurements of soil CO_2 respiration. For example, an important parameter in land surface models is the Q_{10} that describes how the sensitivity of the soil CO_2 efflux is driven by soil temperature (Lloyd and Taylor, 1994; Mahecha et al., 2010). There is a general tendency to have a higher Q_{10} in winter than in summer and macro-molecular rate theory has been evoked to help explain this pattern (Alster et al., 2016; Schipper et al., 2014). However, the presence of phototrophic organisms could also lower estimates of Q_{10} by reducing the CO_2 efflux during the day when temperatures are high and increasing it at night when temperatures are lower. Future studies exploring the link between phototrophic abundance for different biomes and soil CO_2 efflux are now possible with our new qPCR tool and could help explain some of the emergent patterns observed in key C cycle model parameters and improve our ability to predict how they interplay with climate, soil and vegetation composition.

4.4.3. The influence of soil pH and community structure on CA activity

The enzyme carbonic anhydrase catalyses both the reversible hydration of CO_2 and the irreversible hydrolysis of OCS in algae (Gries et al., 1994; Protoschill-Krebs and Kesselmeier, 1992), bacteria (Kamezaki et al., 2016; Kesselmeier et al., 1999; Ogawa et al., 2013) and fungi (Elleuche and Poggeler, 2010; Masaki et al., 2016). The activity of this enzyme is essential for the homeostatic regulation of intra-cellular pH in organisms (Smith and Ferry, 2000). Most organisms strive to maintain a physiologically optimal pH of around 7. However many organisms and indeed many bacterial and fungal genus have developed metabolic traits for surviving in extreme acidic and alkaline environments (Hesse et al., 2002; Krulwich et al., 2011; Mortenson et al., 2008; Slonczewski et al., 2009), and the enzyme CA seems to play a central role in this survival. The results from our study confirmed that soil pH not only had a strong influence on algal abundance but also on the strength of the photosynthetic CO_2 sink and associated CA activity (k_{iso}). This result was unsurprising as it is well known that unicellular green algae, such *as Chlamydomonas,* typically exhibit CA activities as high as those found in animals or higher plants and can express different classes of CA in a range of organelles including the periplasmic membrane (Moroney et al., 2001; Palmqvist and Badger,

1996). It has also been shown for β-CA, the most abundant class of CA in soil bacteria and fungi, the catalysed CO_2 hydration is maximal in the pH range above 8 (Rowlett et al., 2002). The results from our study showing a monotonous increase in k_{iso} with increasing pH on the light-acclimated soils (**Fig. 4.8b**) are entirely consistent with the study of Rowlett et al. (2002).

More surprisingly our CA activity estimates for CO_2 and OCS did not co-vary between the different treatments. The rate of enzyme-catalysed OCS hydrolysis (k_h) was surprisingly not significantly related to the abundance of algae or soil pH but seemed only explained by the absolute abundance of fungi (**Fig 4.8c**). This was even more surprising given that the relative abundance of fungi to the overall soil microbial community was the smallest (**Fig. 4.4**). Most fungi, including the basidiomycetes and hemiascomycetes, contain only β-CA, although some filamentous ascomycetes and basal fungi also contain genes for encoding α-CA or γ-CA (Elleuche, 2011; Elleuche and Poggeler, 2010). In contrast, all three classes of CA seem rather common in bacteria (Smith et al., 1999) and algae (Moroney et al., 2001), although α-CA seem more abundant in algae whilst γ-CA are often found in bacteria. Thus a relative increase in fungal populations could be accompanied by a relative increase in β-CA expression. Little is known regarding the affinity of these different CA classes to OCS but a few studies seem to indicate that β-CAs have a much higher affinity to OCS than α-CA, leading to OCS hydrolysis rates up to 1000 times faster (Haritos and Dojchinov, 2005; Ogawa et al., 2013, 2016; Ogée et al., 2016). If γ-CAs behave towards OCS as α-CA, the OCS uptake by soils should be mostly responsive to changes in β-CA expression. This may indicate that the relationship we found between k_h and fungal abundance is possibly dominated by the expression of β-CA that dominates in fungi. This would be consistent with a recent study on forest soil fungal isolates that demonstrated that a number of key species exhibited a strong uptake of OCS (Masaki et al., 2016). These species included *Scytalidium* sp. THIF03, *Trichoderma* spp. THIF08, THIF17, THIF21, THIF23 and THIF26 with *Trichoderma* species known to contain only β-CA (Elleuche and Poggeler, 2010). Thus future NGS on our experimental soils will aim to investigate whether changes in OCS flux can be associated with changes in these key fungal OCS degraders.

Alternatively, changes in OCS flux could have been driven by a shift in the community structure towards fungal species that emit OCS such as *Umbelopsis* and *Mortierella* spp. THIF09 and THIF13 (Masaki et al., 2016) in soils with lower fungal abundance. Addressing

this hypothesis is unfortunately impossible in this study. However, what is clear, is that when light and moisture were not limiting, phototroph populations bloomed. This increase in phototrophs then caused fungal, and to a lesser extent, bacterial numbers to increase as well leading to a greater OCS uptake rate (and an exactly opposite response in the most acidic soil). Thus the presence of the phototrophs conferred some benefit to the fungal population in non-acidic soils either by providing organic compounds to the fungi in a similar manner to the situation in lichens or by constituting prey to the fungi. For example some fungi such as the *Chytridiomycota* are parasites of micro-algae and are known to contain two β-CAs and one α-CA in secretions (Elleuche, 2011). This hypothesis should be tested in the near future using NGS. This would help characterise the importance of OCS producing metabolic pathways in soil organisms and improve our ability to model the emission of OCS from soils at larger scales.

4.5. Conclusion

Using novel molecular tools our study could reveal the interplay between soil pH and light in determining changes in the abundance of soil phototrophs, bacteria and fungi. This additional information helped us interpret the fluxes of two key tracers in the global C cycle. Interestingly, our study showed for the first time that the magnitude of each of these fluxes was regulated differently, with pH and algal abundance driving more strongly the CO_2 flux and CO_2-H_2O isotopic exchange rate, whilst fungal populations are driving more strongly the OCS uptake rates. Our study also demonstrates that the new qPCR tool for identifying phototrophic organisms has the potential to open new avenues of ecological and agronomical research, such as in the use of 'biofertilisers' composed of phototrophic organisms to promote soil fertility and plant health. Finally our study demonstrates that, by combining such molecular tools with soil gas exchange measurements, it will soon be possible to assess the impact of soil phototrophic abundance and diversity on the atmosphere through their ability to sequester both C, N and S in soils.

References

Alster, C. J., Baas, P., Wallenstein, M. D., Johnson, N. G. and von Fischer, J. C.: Temperature Sensitivity as a Microbial Trait Using Parameters from Macromolecular Rate Theory, Front. Microbiol., 7(November), 1821, doi:10.3389/fmicb.2016.01821, 2016.

Badger, M.: The roles of carbonic anhydrases in photosynthetic CO_2 concentrating mechanisms, Photosynth. Res., 77(2/3), 83–94, doi:10.1023/A:1025821717773, 2003.

Bardgett, R. D. and Van Der Putten, W. H.: Belowground biodiversity and ecosystem functioning, Nature, 515(7528), 505–511, doi:10.1038/nature13855, 2014.

Benzerara, K., Skouri-Panet, F., Li, J., Ferard, C., Gugger, M., Laurent, T., Couradeau, E., Ragon, M., Cosmidis, J., Menguy, N., Margaret-Oliver, I., Tavera, R., Lopez-Garcia, P. and Moreira, D.: Intracellular CA-carbonate biomineralization is widespread in cyanobacteria, Proc. Natl. Acad. Sci., 111(30), 10933–10938, doi:10.1073/pnas.1403510111, 2014.

Bond-Lamberty, B. and Thomson, A.: A global database of soil respiration data, Biogeosciences, 7(6), 1915–1926, doi:10.5194/bg-7-1915-2010, 2010.

Bristol-Roach, M.: On the algae of some normal English soils, J. Agric. Sci., 17(4), 563, doi:10.1017/S0021859600018839, 1927.

Brock, T. D. and Clyne, J.: Significance of algal excretory products for growth of epilimnetic bacteria., Appl. Environ. Microbiol., 47(4), 731–734, 1984.

Campbell, J. E., Carmichael, G. R., Chai, T., Mena-Carrasco, M., Tang, Y., Blake, D. R., Blake, N. J., Vay, S. A., Collatz, G. J., Baker, I., Berry, J. A., Montzka, S. A., Sweeney, C., Schnoor, J. L. and Stanier, C. O.: Photosynthetic Control of Atmospheric Carbonyl Sulfide During the Growing Season, Science, 322(5904), 1085–1088, doi:10.1126/science.1164015, 2008.

Carvalhais, N., Forkel, M., Khomik, M., Bellarby, J., Jung, M., Migliavacca, M., Mu, M., Saatchi, S., Santoro, M., Thurner, M., Weber, U., Ahrens, B., Beer, C., Cescatti, A., Randerson, J. T. and Reichstein, M.: Global covariation of carbon turnover times with climate in terrestrial ecosystems, Nature, 514(7521), 213–217, doi:10.1038/nature13731, 2014.

Chemidlin Prévost-Bouré, N., Christen, R., Dequiedt, S., Mougel, C., Lelièvre, M., Jolivet, C., Shahbazkia, H. R., Guillou, L., Arrouays, D. and Ranjard, L.: Validation and

Application of a PCR Primer Set to Quantify Fungal Communities in the Soil Environment by Real-Time Quantitative PCR, PLoS One, 6(9), e24166, doi:10.1371/journal.pone.0024166, 2011.

Cole, J. J., Likens, G. E. and Strayer, D. L.: Photosynthetically produced dissolved organic carbon: An important carbon source for planktonic bacteria1, Limnol. Oceanogr., 27(6), 1080–1090, doi:10.4319/lo.1982.27.6.1080, 1982.

Coleman, J. R., Berry, J. A., Togasaki, R. K. and Grossman, A. R.: Identification of Extracellular Carbonic Anhydrase of Chlamydomonas reinhardtii, Plant Physiol., 76(2), 472–477, doi:10.1104/pp.76.2.472, 1984.

Couradeau, E., Benzerara, K., Gerard, E., Moreira, D., Bernard, S., Brown, G. E. and Lopez-Garcia, P.: An Early-Branching Microbialite Cyanobacterium Forms Intracellular Carbonates, Science, 336(6080), 459–462, doi:10.1126/science.1216171, 2012.

Cuntz, M.: A comprehensive global three-dimensional model of $\delta^{18}O$ in atmospheric CO_2 : 1. Validation of surface processes, J. Geophys. Res., 108(1-24), 4527, doi:10.1029/2002JD003153, 2003.

Dequiedt, S., Saby, N. P. A., Lelievre, M., Jolivet, C., Thioulouse, J., Toutain, B., Arrouays, D., Bispo, A., Lemanceau, P. and Ranjard, L.: Biogeographical patterns of soil molecular microbial biomass as influenced by soil characteristics and management, Glob. Ecol. Biogeogr., 20(4), 641–652, doi:10.1111/j.1466-8238.2010.00628.x, 2011.

Elbert, W., Weber, B., Burrows, S., Steinkamp, J., Büdel, B., Andreae, M. O. and Pöschl, U.: Contribution of cryptogamic covers to the global cycles of carbon and nitrogen, Nat. Geosci., 5(7), 459–462, doi:10.1038/ngeo1486, 2012.

Elleuche, S.: Carbonic Anhydrase in Fungi and Fungal-Like Organisms - Functional Distribution and Evolution of a Gene Family, Mycota, 14, 257–274, doi:10.1007/978-3-540-87407-2, 2011.

Elleuche, S. and Poggeler, S.: Carbonic anhydrases in fungi, Microbiology, 156(1), 23–29, doi:10.1099/mic.0.032581-0, 2010.

Flemming, H.-C., Wingender, J., Szewzyk, U., Steinberg, P., Rice, S. A. and Kjelleberg, S.: Biofilms: an emergent form of bacterial life, Nat. Rev. Microbiol., 14(9), 563–575, doi:10.1038/nrmicro.2016.94, 2016.

Francey, R. J. and Tans, P. P.: Latitudinal variation in oxygen-18 of atmospheric CO_2, Nature, 327(6122), 495–497, doi:10.1038/327495a0, 1987.

Garrity, G. M., Brenner, D.J. Krieg, N.R. and Staley, J.R., Bergey's Manual of Systematic Bacteriology, Volume Two, Springer – Verlag, 2005.

Gimeno, T.E., Ogée, J., Royles, J., Gibon, Y., West, J., Burlett, R., Jones, S.P., Sauze, J., Wohl, S., Griffiths, H., Benard, C. and Wingate, L.: Bryophyte gas-exchange dynamics along varying hydration status reveal a significant COS sink in the dark and COS source in the light, New Phytol, submitted.

Goyal, S. .: Algae and the soil environment, Phykos, 36(1), 1–13, 1997.

Gries, C., Nash, T. H. and Kesselmeier, J.: Exchange of reduced sulfur gases between lichens and the atmosphere, Biogeochemistry, 26(1), 25–39, doi:10.1007/BF02180402, 1994.

Griffiths, R. I., Thomson, B. C., James, P., Bell, T., Bailey, M. and Whiteley, A. S.: The bacterial biogeography of British soils, Environ. Microbiol., 13(6), 1642–1654, doi:10.1111/j.1462-2920.2011.02480.x, 2011.

Haritos, V. S. and Dojchinov, G.: Carbonic anhydrase metabolism is a key factor in the toxicity of CO_2 and COS but not CS_2 toward the flour beetle Tribolium castaneum [Coleoptera: Tenebrionidae], Comp. Biochem. Physiol. Part C Toxicol. Pharmacol., 140(1), 139–147, doi:10.1016/j.cca.2005.01.012, 2005.

Hart, K. M., Kulakova, A. N., Allen, C. C. R., Simpson, A. J., Oppenheimer, S. F., Masoom, H., Courtier-Murias, D., Soong, R., Kulakov, L. A., Flanagan, P. V., Murphy, B. T. and Kelleher, B. P.: Tracking the Fate of Microbially Sequestered Carbon Dioxide in Soil Organic Matter, Environ. Sci. Technol., 47(10), 5128–5137, doi:10.1021/es3050696, 2013.

Heimann, M. and Reichstein, M.: Terrestrial ecosystem carbon dynamics and climate feedbacks, Nature, 451(7176), 289–292, doi:10.1038/nature06591, 2008.

Hesse, S. J. A., Ruijter, G. J. G., Dijkema, C. and Visser, J.: Intracellular pH homeostasis in the filamentous fungus Aspergillus niger, Eur. J. Biochem., 269(14), 3485–3494, doi:10.1046/j.1432-1033.2002.03042.x, 2002.

Hopkinson, B. M., Meile, C. and Shen, C.: Quantification of Extracellular Carbonic Anhydrase Activity in Two Marine Diatoms and Investigation of Its Role, Plant Physiol., 162(2), 1142–1152, doi:10.1104/pp.113.217737, 2013.

Jasoni, R. L., Smith, S. D. and Arnone, J. A.: Net ecosystem CO_2 exchange in Mojave Desert shrublands during the eighth year of exposure to elevated CO_2, Glob. Chang. Biol., 11(5), 749–756, doi:10.1111/j.1365-2486.2005.00948.x, 2005.

John, R. P.: An Ecological and Taxonomic Study of the Algae of British Soils, Ann. od Bot., 6(33), 323–349, 1942.

Kamezaki, K., Hattori, S., Ogawa, T., Toyoda, S., Kato, H., Katayama, Y. and Yoshida, N.: Sulfur Isotopic Fractionation of Carbonyl Sulfide during Degradation by Soil Bacteria, Environ. Sci. Technol., 50(7), 3537–3544, doi:10.1021/acs.est.5b05325, 2016.

Kesselmeier, J., Teusch, N. and Kuhn, U.: Controlling variables for the uptake of atmospheric carbonyl sulfide by soil, J. Geophys. Res. Atmos., 104(D9), 11577–11584, doi:10.1029/1999JD900090, 1999.

Konopka, A., Lindemann, S. and Fredrickson, J.: Dynamics in microbial communities: unraveling mechanisms to identify principles, ISME J., 9(7), 1488–1495, doi:10.1038/ismej.2014.251, 2015.

Krulwich, T. A., Sachs, G. and Padan, E.: Molecular aspects of bacterial pH sensing and homeostasis, Nat. Rev. Microbiol., 9(5), 330–343, doi:10.1038/nrmicro2549, 2011.

Kupriyanova, E., Villarejo, A., Markelova, A., Gerasimenko, L., Zavarzin, G., Samuelsson, G., Los, D. A. and Pronina, N.: Extracellular carbonic anhydrases of the stromatolite-forming cyanobacterium Microcoleus chthonoplastes, Microbiology, 153(4), 1149–1156, doi:10.1099/mic.0.2006/003905-0, 2007.

Larsson, U. and Hagström, A.: Fractionated phytoplankton primary production, exudate release and bacterial production in a Baltic eutrophication gradient, Mar. Biol., 67(1), 57–70, doi:10.1007/BF00397095, 1982.

Lauber, C. L., Hamady, M., Knight, R. and Fierer, N.: Pyrosequencing-Based Assessment of Soil pH as a Predictor of Soil Bacterial Community Structure at the Continental Scale, Appl. Environ. Microbiol., 75(15), 5111–5120, doi:10.1128/AEM.00335-09, 2009.

Lauber, C. L., Strickland, M. S., Bradford, M. A. and Fierer, N.: The influence of soil properties on the structure of bacterial and fungal communities across land-use types, Soil Biol. Biochem., 40(9), 2407–2415, doi:10.1016/j.soilbio.2008.05.021, 2008.

Leff, J. W., Jones, S. E., Prober, S. M., Barberán, A., Borer, E. T., Firn, J. L., Harpole, W. S., Hobbie, S. E., Hofmockel, K. S., Knops, J. M. H., McCulley, R. L., La Pierre, K., Risch, A. C., Seabloom, E. W., Schütz, M., Steenbock, C., Stevens, C. J. and Fierer, N.: Consistent responses of soil microbial communities to elevated nutrient inputs in grasslands across the globe, Proc. Natl. Acad. Sci., 112(35), 10967–10972, doi:10.1073/pnas.1508382112, 2015.

Lund, J. W. G.: Observations on Soil Algae II . Notes on Groups Other than Diatoms, New Phytol., 46(1), 35–60, 1947.

Mahecha, M. D., Reichstein, M., Carvalhais, N., Lasslop, G., Lange, H., Seneviratne, S. I., Vargas, R., Ammann, C., Arain, M. A., Cescatti, A., Janssens, I. A., Migliavacca, M., Montagnani, L. and Richardson, A. D.: Global Convergence in the Temperature Sensitivity of Respiration at Ecosystem Level, Science (80-.)., 329(5993), 838–840, doi:10.1126/science.1189587, 2010.

Masaki, Y., Ozawa, R., Kageyama, K. and Katayama, Y.: Degradation and emission of carbonyl sulfide, an atmospheric trace gas, by fungi isolated from forest soil, FEMS Microbiol. Lett., 363(18), 1–7, doi:10.1093/femsle/fnw197, 2016.

Metting, B.: The systematics and ecology of soil algae, Bot. Rev., 47(2), 195–312, doi:10.1007/BF02868854, 1981.

Moldrup, P., Olesen, T., Komatsu, T., Yoshikawa, S., Schjønning, P. and Rolston, D. E.: Modeling Diffusion and reaction in soils: X. A unifying model for solute and gas diffusivity in unsaturated soil, Soil Sci., 168(5), 321–337, doi:10.1097/01.ss.0000070907.55992.3c, 2003.

Montgomery, D. R., & Biklé, A. (2015). The Hidden Half of Nature: The Microbial Roots of Life and Health. WW Norton & Company.

Montzka, S. a., Aydin, M., Battle, M., Butler, J. H., Saltzman, E. S., Hall, B. D., Clarke, a. D., Mondeel, D. and Elkins, J. W.: A 350-year atmospheric history for carbonyl sulfide inferred from Antarctic firn air and air trapped in ice, J. Geophys. Res. Atmos., 109(D22), n/a-n/a, doi:10.1029/2004JD004686, 2004.

Moroney, J. V., Bartlett, S. G. and Samuelsson, G.: Carbonic anhydrases in plants and algae, Plant, Cell Environ., 24(2), 141–153, doi:10.1046/j.1365-3040.2001.00669.x, 2001.

Mortensen, H. D., Jacobsen, T., Koch, A. G. and Arneborg, N.: Intracellular pH Homeostasis Plays a Role in the Tolerance of Debaryomyces hansenii and Candida zeylanoides to Acidified Nitrite, Appl. Environ. Microbiol., 74(15), 4835–4840, doi:10.1128/AEM.00571-08, 2008.

Nowak, M. E., Beulig, F., von Fischer, J., Muhr, J., Küsel, K. and Trumbore, S. E.: Autotrophic fixation of geogenic CO_2 by microorganisms contributes to soil organic matter formation and alters isotope signatures in a wetland mofette, Biogeosciences, 12(23), 7169–7183, doi:10.5194/bg-12-7169-2015, 2015.

Ogawa, T., Kato, H., Higashide, M., Nishimiya, M. and Katayama, Y.: Degradation of carbonyl sulfide by Actinomycetes and detection of clade D of β-class carbonic anhydrase, FEMS Microbiol. Lett., 363(19), fnw223, doi:10.1093/femsle/fnw223, 2016.

Ogawa, T., Noguchi, K., Saito, M., Nagahata, Y., Kato, H., Ohtaki, A., Nakayama, H., Dohmae, N., Matsushita, Y., Odaka, M., Yohda, M., Nyunoya, H. and Katayama, Y.: Carbonyl Sulfide Hydrolase from Thiobacillus thioparus Strain THI115 Is One of the β-Carbonic Anhydrase Family Enzymes, J. Am. Chem. Soc., 135(10), 3818–3825, doi:10.1021/ja307735e, 2013.

Ogée, J., Sauze, J., Kesselmeier, J., Genty, B., Van Diest, H., Launois, T. and Wingate, L.: A new mechanistic framework to predict OCS fluxes from soils, Biogeosciences, 13(8), 2221–2240, doi:10.5194/bg-13-2221-2016, 2016.

Palmqvist, K. and Badger, M. R.: Carbonic anhydrase(s) associated with lichens: in vivo activities, possible locations and putative roles, New Phytol., 132(4), 627–639, doi:10.1111/j.1469-8137.1996.tb01881.x, 1996.

Pinheiro J, Bates D, Debroy S, Sarkar D and R Core Team.: nlme: Linear and Nonlinear Mixed Effects Models, R package version 3.1-120, 2015.

Plassart, P., Terrat, S., Thomson, B., Griffiths, R., Dequiedt, S., Lelievre, M., Regnier, T., Nowak, V., Bailey, M., Lemanceau, P., Bispo, A., Chabbi, A., Maron, P.-A., Mougel, C. and Ranjard, L.: Evaluation of the ISO Standard 11063 DNA Extraction Procedure for Assessing Soil Microbial Abundance and Community Structure, PLoS One, 7(9), e44279, doi:10.1371/journal.pone.0044279, 2012.

Protoschill-Krebs, G. and Kesselmeier, J.: Enzymatic Pathways for the Consumption of Carbonyl Sulphide (COS) by Higher Plants, Bot. Acta, 105(3), 206–212, doi:10.1111/j.1438-8677.1992.tb00288.x, 1992.

Protoschill-Krebs, G., Wilhelm, C. and Kesselmeier, J.: Consumption of carbonyl sulphide (COS) by higher plant carbonic anhydrase (CA), Atmos. Environ., 30(18), 3151–3156, doi:10.1016/1352-2310(96)00026-X, 1996.

Raich, J. W. and Schlesinger, W. H.: The global carbon dioxide flux in soil respiration and its relationship to vegetation and climate, Tellus B, 44(2), 81–99, doi:10.1034/j.1600-0889.1992.t01-1-00001.x, 1992.

Ramanan, R., Kim, B.-H., Cho, D.-H., Oh, H.-M. and Kim, H.-S.: Algae–bacteria interactions: Evolution, ecology and emerging applications, Biotechnol. Adv., 34(1),

14–29, doi:10.1016/j.biotechadv.2015.12.003, 2016.

Reay, D. (2015). Marine Nitrogen and Climate Change. In *Nitrogen and Climate Change* (pp. 125-143). Palgrave Macmillan UK.

Rowlett, R. S., Tu, C., McKay, M. M., Preiss, J. R., Loomis, R. J., Hicks, K. a., Marchione, R. J., Strong, J. a., Donovan, G. S. and Chamberlin, J. E.: Kinetic characterization of wild-type and proton transfer-impaired variants of β-carbonic anhydrase from Arabidopsis thaliana, Arch. Biochem. Biophys., 404(2), 197–209, doi:10.1016/S0003-9861(02)00243-6, 2002.

Sandoval-Soto, L., Stanimirov, M., von Hobe, M., Schmitt, V., Valdes, J., Wild, A. and Kesselmeier, J.: Global uptake of carbonyl sulfide (COS) by terrestrial vegetation: Estimates corrected by deposition velocities normalized to the uptake of carbon dioxide (CO_2), Biogeosciences, 2(2), 125–132, doi:10.5194/bg-2-125-2005, 2005.

Šantrůčková, H., Bird, M. I., Elhottová, D., Novák, J., Picek, T., Šimek, M. and Tykva, R.: Heterotrophic Fixation of CO_2 in Soil, Microb. Ecol., 49(2), 218–225, doi:10.1007/s00248-004-0164-x, 2005.

Sauze, J., Jones, S., Wingate, L., Wohl, S. and Ogée, J.: The role of soil pH on soil carbonic anhydrase activity, in prep.

Schipper, L. A., Hobbs, J. K., Rutledge, S. and Arcus, V. L.: Thermodynamic theory explains the temperature optima of soil microbial processes and high Q_{10} values at low temperatures, Glob. Chang. Biol., 20(11), 3578–3586, doi:10.1111/gcb.12596, 2014.

Schlesinger, W. H.: An evaluation of abiotic carbon sinks in deserts, Glob. Chang. Biol., 23(1), 25–27, doi:10.1111/gcb.13336, 2017.

Schlesinger, W. H., Belnap, J. and Marion, G.: On carbon sequestration in desert ecosystems, Glob. Chang. Biol., 15(6), 1488–1490, doi:10.1029/2007GB003077.Law, 2009.

Sherwood, A. R. and Presting, G. G.: Universal primers amplify a 23S rDNA plastid marker in eukaryotic algae and cyanobacteria, J. Phycol., 43(3), 605–608, doi:10.1111/j.1529-8817.2007.00341.x, 2007.

Shields, L. and Durrell, L.: Algae in relation to soil fertility, Bot. Rev., 30(165), 92–128 [online] Available from: http://link.springer.com/article/10.1007/BF02858614, 1964.

Smith, K. . and Ferry, J. G.: Prokaryotic carbonic anhydrases, FEMS Microbiol. Rev., 24(4), 335–366, doi:10.1016/S0168-6445(00)00030-9, 2000.

Smith, K. S., Jakubzick, C., Whittam, T. S. and Ferry, J. G.: Carbonic anhydrase is an ancient

enzyme widespread in prokaryotes, Proc. Natl. Acad. Sci., 96(26), 15184–15189, doi:10.1073/pnas.96.26.15184, 1999.

Starks, T. L. and Shubert, E.: Colonisation and succession of algae and soil-algal interactions associated with disturbed areas, 99–107, 1982.

Stokes, J. L.: The influence of environmental factors upon the development of algae and other microoganisms in soil., Soil Sci., 49(3), 171–184, 1940.

Sültemeyer, D.: Carbonic anhydrase in eukaryotic algae: characterization, regulation, and possible function during photosynthesis, Can. J. Bot., 76(6), 962–972, doi:10.1139/cjb-76-6-962, 1998.

Tans, P.: Oxygen isotopic equilibrium between carbon dioxide and water in soils, Tellus B, 50(2), 163–178, doi:10.1034/j.1600-0889.1998.t01-1-00004.x, 1998.

Tedersoo, L., Bahram, M., Polme, S., Koljalg, U., Yorou, N. S., Wijesundera, R., Ruiz, L. V., Vasco-Palacios, A. M., Thu, P. Q., Suija, A., Smith, M. E., Sharp, C., Saluveer, E., Saitta, A., Rosas, M., Riit, T., Ratkowsky, D., Pritsch, K., Poldmaa, K., Piepenbring, M., Phosri, C., Peterson, M., Parts, K., Partel, K., Otsing, E., Nouhra, E., Njouonkou, A. L., Nilsson, R. H., Morgado, L. N., Mayor, J., May, T. W., Majuakim, L., Lodge, D. J., Lee, S. S., Larsson, K.-H., Kohout, P., Hosaka, K., Hiiesalu, I., Henkel, T. W., Harend, H., Guo, L. -d., Greslebin, A., Grelet, G., Geml, J., Gates, G., Dunstan, W., Dunk, C., Drenkhan, R., Dearnaley, J., De Kesel, A., Dang, T., Chen, X., Buegger, F., Brearley, F. Q., Bonito, G., Anslan, S., Abell, S. and Abarenkov, K.: Global diversity and geography of soil fungi, Science, 346(6213), 1256688–1256688, doi:10.1126/science.1256688, 2014.

Terrat, S., Christen, R., Dequiedt, S., Lelièvre, M., Nowak, V., Regnier, T., Bachar, D., Plassart, P., Wincker, P., Jolivet, C., Bispo, A., Lemanceau, P., Maron, P.-A., Mougel, C. and Ranjard, L.: Molecular biomass and MetaTaxogenomic assessment of soil microbial communities as influenced by soil DNA extraction procedure, Microb. Biotechnol., 5(1), 135–141, doi:10.1111/j.1751-7915.2011.00307.x, 2012.

Thaler, C., Millo, C., Ader, M., Chaduteau, C., Guyot, F. and Ménez, B.: Disequilibrium $\delta^{18}O$ values in microbial carbonates as a tracer of metabolic production of dissolved inorganic carbon, Geochim. Cosmochim. Acta, 199, 112–129, doi:10.1016/j.gca.2016.10.051, 2017.

Thompson, J. R., Rivera, H. E., Closek, C. J. and Medina, M.: Microbes in the coral

holobiont: partners through evolution, development, and ecological interactions, Front. Cell. Infect. Microbiol., 4(January), 176, doi:10.3389/fcimb.2014.00176, 2015.

Welp, L. R., Keeling, R. F., Meijer, H. a J., Bollenbacher, A. F., Piper, S. C., Yoshimura, K., Francey, R. J., Allison, C. E. and Wahlen, M.: Interannual variability in the oxygen isotopes of atmospheric CO_2 driven by El Niño, Nature, 477(7366), 579–582, doi:10.1038/nature10421, 2011.

Wingate, L., Ogée, J., Burlett, R. and Bosc, A.: Strong seasonal disequilibrium measured between the oxygen isotope signals of leaf and soil CO_2 exchange, Glob. Chang. Biol., 16(11), 3048–3064, doi:10.1111/j.1365-2486.2010.02186.x, 2010.

Wingate, L., Ogee, J., Cuntz, M., Genty, B., Reiter, I., Seibt, U., Yakir, D., Maseyk, K., Pendall, E. G., Barbour, M. M., Mortazavi, B., Burlett, R., Peylin, P., Miller, J., Mencuccini, M., Shim, J. H., Hunt, J. and Grace, J.: The impact of soil microorganisms on the global budget of $\delta^{18}O$ in atmospheric CO_2, Proc. Natl. Acad. Sci., 106(52), 22411–22415, doi:10.1073/pnas.0905210106, 2009.

Wingate, L., Seibt, U., Maseyk, K., Ogée, J., Almeida, P., Yakir, D., Pereira, J. S. and Mencuccini, M.: Evaporation and carbonic anhydrase activity recorded in oxygen isotope signatures of net CO_2 fluxes from a Mediterranean soil, Glob. Chang. Biol., 14(9), 2178–2193, doi:10.1111/j.1365-2486.2008.01635.x, 2008.

Wohlfahrt, G., Fenstermaker, L. F. and Arnone, J. A.: Large annual net ecosystem CO_2 uptake of a Mojave Desert ecosystem, Glob. Chang. Biol., 14(7), 1475–1487, doi:10.1111/j.1365-2486.2008.01593.x, 2008.

Yuan, H., Ge, T., Wu, X., Liu, S., Tong, C., Qin, H., Wu, M., Wei, W. and Wu, J.: Long-term field fertilization alters the diversity of autotrophic bacteria based on the ribulose-1,5-biphosphate carboxylase/oxygenase (RubisCO) large-subunit genes in paddy soil, Appl. Microbiol. Biotechnol., 95(4), 1061–1071, doi:10.1007/s00253-011-3760-y, 2012.

Zancan, S., Trevisan, R. and Paoletti, M. G.: Soil algae composition under different agro-ecosystems in North-Eastern Italy, Agric. Ecosyst. Environ., 112(1), 1–12, doi:10.1016/j.agee.2005.06.018, 2006.

Supplementary information

Figure S1. Experimental setup used to measure continuously the CO_2, $CO^{18}O$ and OCS concentrations of gas exchange between the soil and the atmosphere sequentially on 6 microcosms and a control. Dry air comes from a compressor; the CO_2 and OCS concentrations are respectively expressed in ppm (parts per million or µmol/mol) and ppb (parts per billion or nmol/mol). All the mass flow controllers were set to 0.25 L min^{-1}.

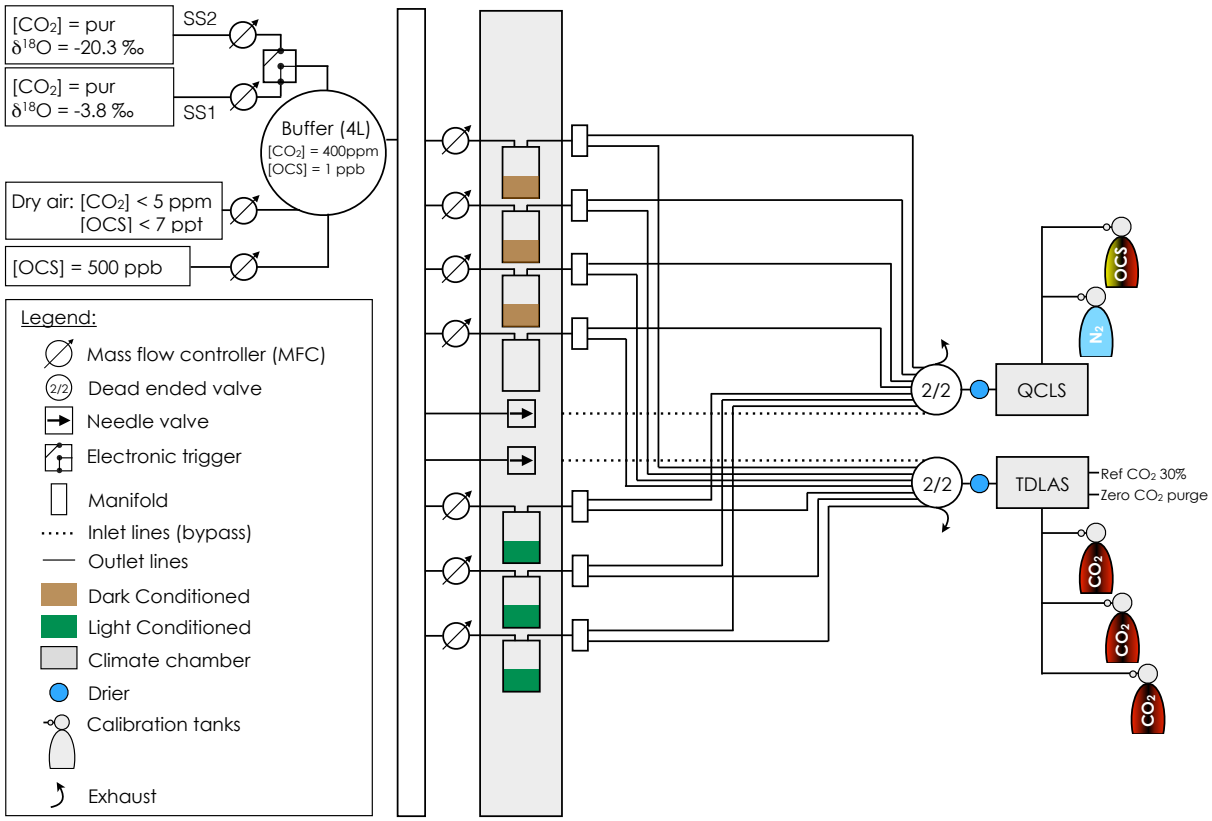

Figure S2. Time series of the mean variations (± SD, n=3) in the net OCS fluxes from the blank chamber (control) during the 24h of run of each different soil. For each soil, the four first squares represent the first 12h of measurement (*i.e.* in the light (LP)) and the next four squares represent the last 12h of measurement (*i.e.* in the dark (DP)).

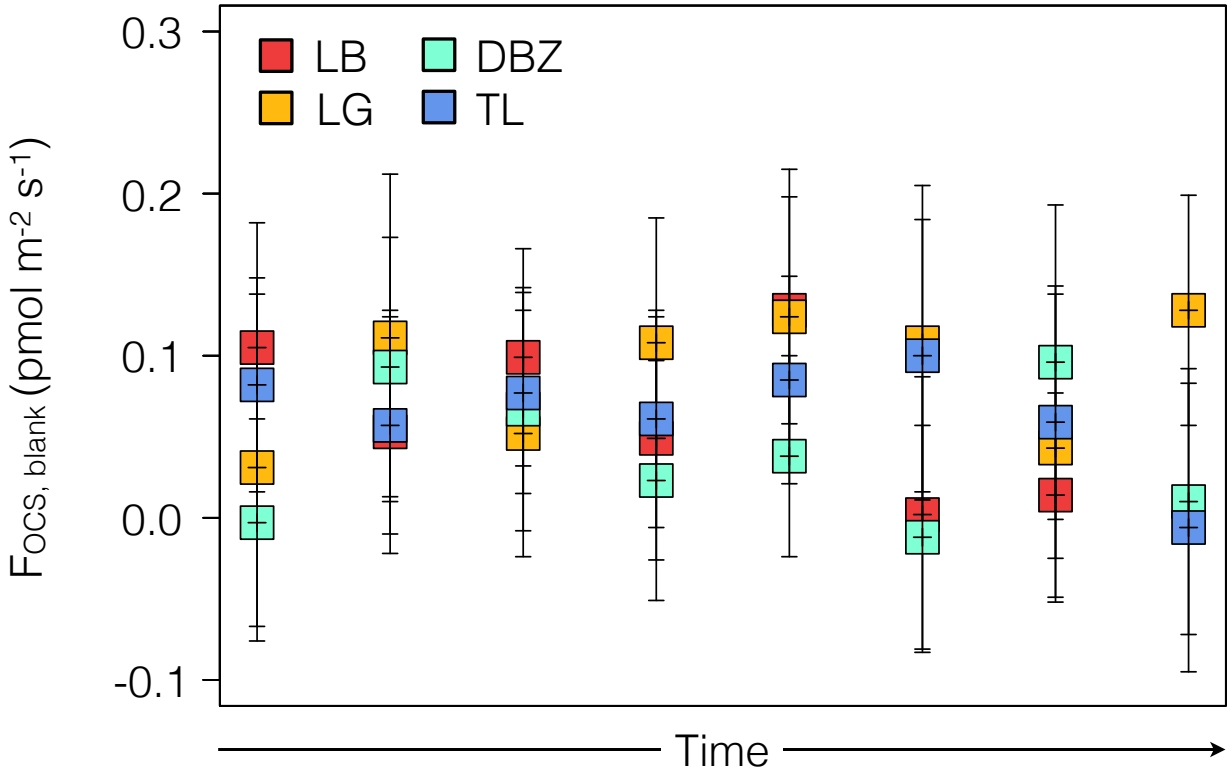

Figure S3. (a) Relative number of chlorophyll pigment a and b for the four soils (LB, LG, DBZ & TL) incubated in the dark (DC) and light (LC) after 40 days. (b) Photos of the top surface of the four soils incubated in the dark (DC) and light (LC) after 40 days and colonised or no by the photosynthetic communities.

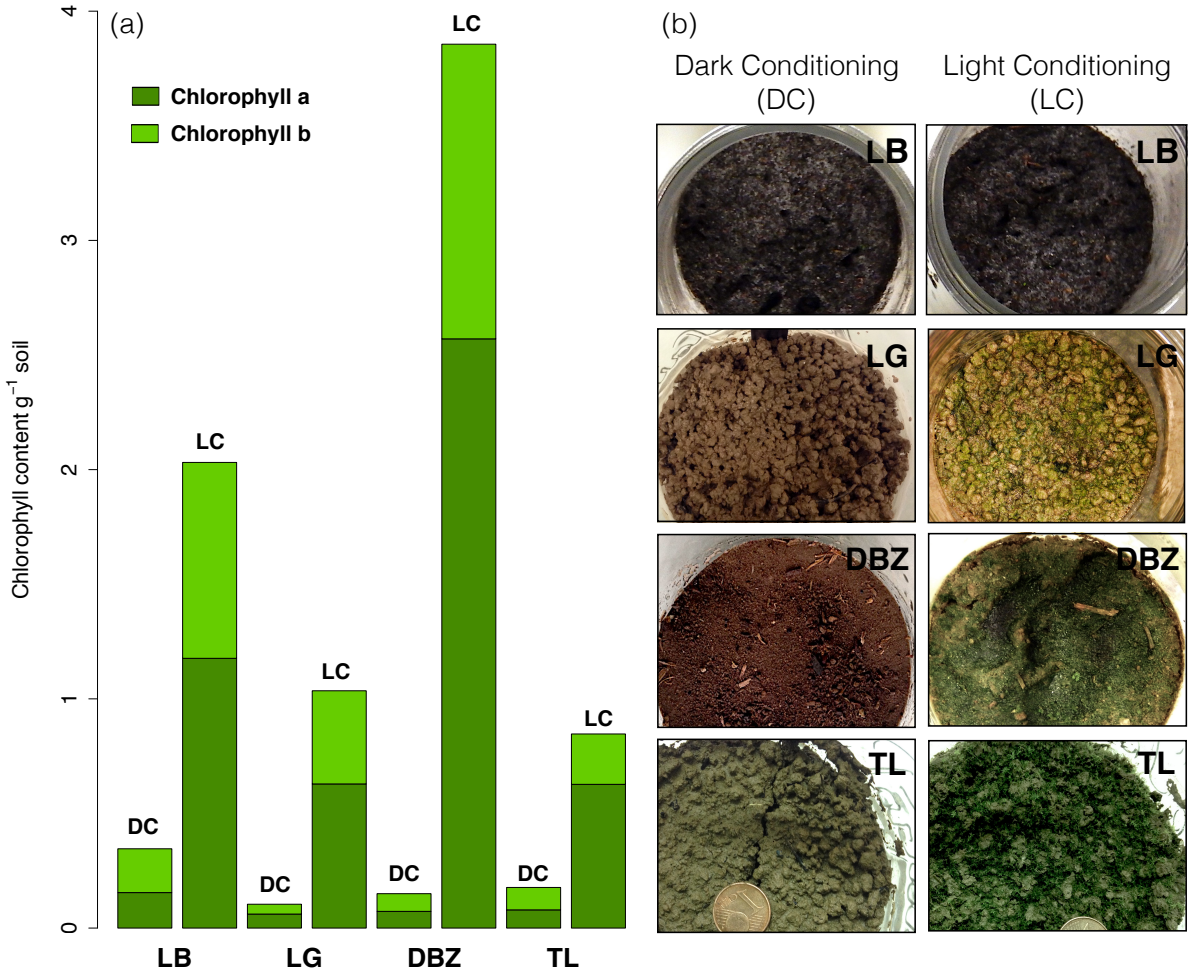

Figure S4. Relationship between the relative number of algal (23S) gene copies and the chlorophyll content pigment measured (Chl a + Chl b) for the four soils (LB, LG, DBZ & TL) incubated in the dark (DC) and light (LC) after 40 days.

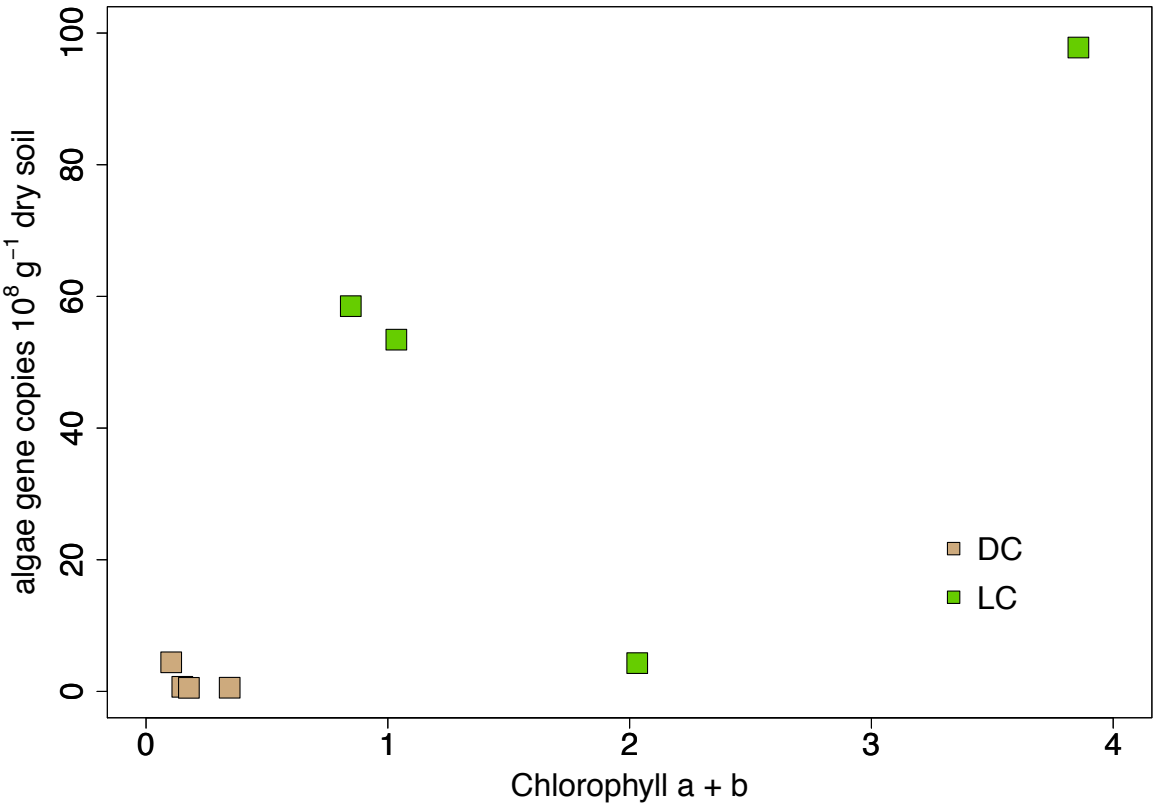

Chapitre 5 : Variabilité pan-européenne des échanges d'OCS entre les sols et l'atmosphère

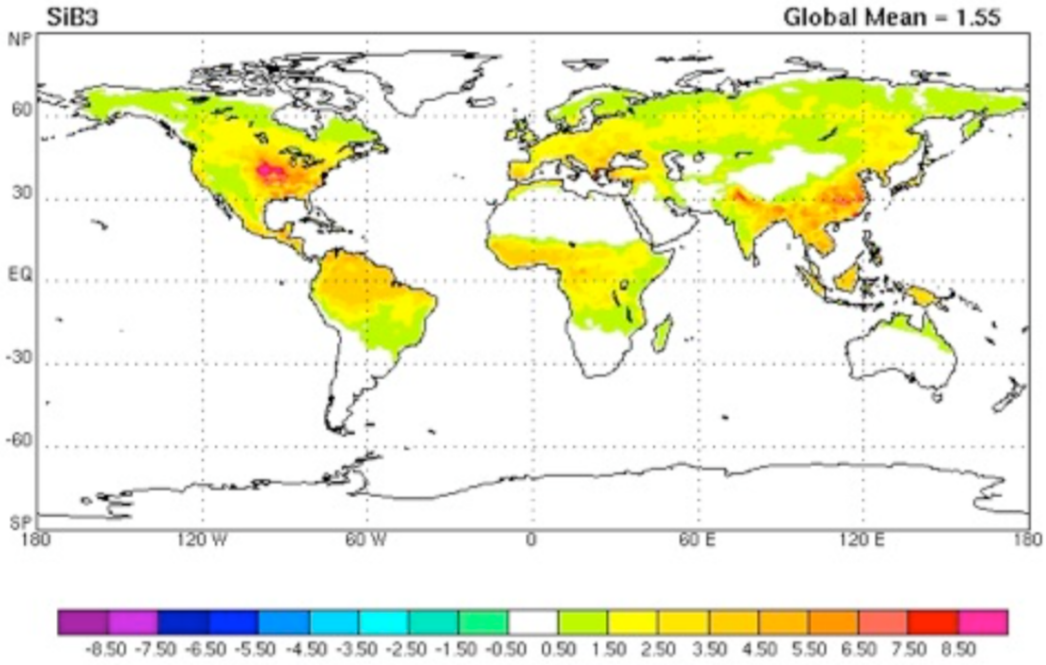

*Figure 5.1 : Carte mondiale des flux d'OCS absorbés par le sol et modélisés via SIB3 (**Si**mple **B**iosphere model version **3**, d'après Berry et al., 2013).*

Introduction au chapitre 5

Dans le chapitre 2, nous avons présenté une nouvelle approche permettant de modéliser les échanges d'OCS entre un sol et l'atmosphère (F_{OCS}), et nous avons évalué à partir de données de la littérature les capacités du modèle à reproduire la réponse de cet échange à des changements de température et de contenu en eau du sol (Ogée et al., 2016). Dans le chapitre 3, nous avons ensuite mis en évidence l'influence du pH sur l'activité de l'AC des sols vis-à-vis du CO_2 dans le cas d'un ajout d'une α-AC exogène (Sauze et al. en préparation-a). Nous avons aussi montré qu'un tel ajout en revanche ne modifiait pas le flux d'OCS, et ce quelque soit le pH du sol. Dans le chapitre 4, nous avons ensuite démontré que l'activité AC des sols répondait différemment vis-à-vis du CO_2 et de l'OCS. Pour le CO_2, cette activité répondait à l'abondance des microorganismes photosynthétiques alors que pour l'OCS, elle répondait à l'abondance des communautés de champignons (Sauze et al. en préparation-b). Parce que le pH et l'abondance des communautés microbiennes du sol sont intimement liés, nos résultats nous ont naturellement amenés à nous demander si les modèles actuels d'échanges d'OCS entre les sols et l'atmosphère permettaient, de manière empirique ou mécaniste, d'expliquer les variations de F_{OCS} observées sur des sols dévoilant une plus large gamme de pH, de texture et/ou d'abondance des communautés microbiennes. Ce dernier chapitre a donc pour objectif de répondre à cette question. Pour cela nous avons mesuré les flux d'OCS de 39 sols provenant de diverses régions d'Europe, puis nous avons testé notre capacité à reproduire la variabilité des flux observés à l'aide de trois approches de modélisation, deux approches empiriques issues de la littérature et l'approche mécaniste présentée au chapitre 2. Ce dernier chapitre est rédigé comme les chapitres précédents sous la forme d'un d'article, mais encore à l'état d'ébauche car les analyses qPCR sur la structure des communautés microbiennes des sols étudiés sont encore en cours. La liste des auteurs actuelle traduit seulement la contribution aux travaux présentés dans ce chapitre de thèse mais elle devrait évoluer une fois les résultats qPCR connus. Les conclusions générales de ce dernier chapitre pourraient elles aussi changer.

Spatial variability of summertime soil-atmosphere OCS exchange across Europe

Joana Sauze[1,*], Jérôme Ogée[1], Steven Wohl[1], Aurore Kaisermann[1], Thomas Launois[1], Lisa Wingate[1]

[1]ISPA, Bordeaux Science Agro, INRA UMR 1391, 33140 Villenave d'Ornon, France

Abstract

Rationale: A number of empirical and mechanistic models have now been developed to describe the exchange of OCS between soils and the atmosphere. It is now becoming increasingly important to challenge these models with data and explore how each additional level of mechanistic complexity helps describe the pattern of OCS exchange observed across soils varying widely in biogeochemical properties. This step is especially necessary if we are to evolve models that can be parameterised robustly for different biomes or soil types whilst retaining a structure that can still be simply implemented in large-scale land surface models.
Method: We collected a range of soils from different biomes within Europe to test and compare the ability of three different models to predict OCS fluxes from re-packed soils varying in a range of biogeochemical properties, including texture, soil pH, microbial biomass and land use. The variability of OCS emissions from dry soils was also measured as well as possible interactions with light.
Results: The majority of the soils from across Europe were net sinks for OCS when "moist", with the exception of three Mediterranean soils with extremely low volumetric water content (VWC). Net OCS fluxes varied between +0.35 to -5.79 pmol m^{-2} s^{-1} and soils with the strongest OCS uptake were the peatland and forest soils from boreal and temperate regions. Net OCS fluxes from dried soils varied from +4.49 to -2.36 pmol m^{-2} s^{-1} with no clear trend with land use or biome. Differences in the net OCS fluxes for the same soils measured in the light and the dark were observed with light generally decreasing the uptake rate of OCS on 'moist' soils and increasing the emission on 'air-dried' soils. However, no clear trend in this difference was found with land use or soil type. A weak linear relationship ($r = 0.40$, $P < 0.05$) between the net OCS uptake and heterotrophic respiration was found across all land uses, as would have been predicted by one of the empirical model tested. However our study found

that the empirical model relating OCS uptake to VWC seemed to describe better the variability in our data but only after modifying 3 of the 5 original parameters. Applying a more mechanistic model to our dataset indicated that current assumptions regarding the pH response of CA activity for OCS exchange in soils remain uncertain.

Conclusions: Our findings demonstrate that soil-atmosphere OCS exchange across a range of soil types is strongly controlled by moisture and microbial activity. However, reconciling these relationships in a mechanistic framework is currently difficult as the pH response of CA for OCS is poorly constrained for the various isozymes of CA in soils. Furthermore, it is currently unclear how the ratio of different CA isozymes in natural soils vary across biomes and land use types. Future studies addressing these two important factors should provide key breakthroughs in our theoretical understanding of soil OCS exchange with the atmosphere and help predict the spatial and temporal variability of OCS mixing ratios in the atmosphere, providing a novel theoretical framework for large-scale multi-tracer models of the global carbon cycle.

5.1. Introduction

Carbonyl sulphide (OCS) plays an important role in the production of stratospheric sulphate aerosols and the ozone chemistry of the stratosphere (Andreae and Crutzen, 1997; Crutzen, 1976). In the troposphere OCS concentrations measured at a network of NOAA background stations display a strong seasonal cycle that closely tracks the seasonal cycle of atmospheric CO_2 concentrations but with an amplitude about 6 times larger than CO_2 (Montzka et al., 2007). The amount of OCS removed from the atmosphere during the Northern Hemisphere summer is substantial and constitutes approximately 25% of the total atmospheric background concentration above terrestrial stations, demonstrating that the terrestrial biosphere is an extremely strong sink for OCS (Montzka et al., 2007; Sandoval-Soto et al., 2005). A number of studies have shown that this drawdown of OCS is probably dominated by the activity of the enzyme carbonic anhydrase (CA) in leaf mesophyll cells where OCS hydrolysis occurs (Protoschill-Krebs and Kesselmeier, 1992). The OCS uptake is thus closely linked to the photosynthetic activity of the biosphere and could constrain certain key parameters required to estimate CO_2 and water fluxes in land surface models, in particular stomatal conductance to CO_2 and consequently gross primary productivity (Berry et al., 2013; Sandoval-Soto et al., 2005; Seibt et al., 2009; Wehr et al., 2016; Wohlfahrt et al., 2012).

The uptake of OCS from the atmosphere is not only regulated by the CA activity of leaves. Soils have also been shown to take up OCS across a wide range of soil types and land use (Castro and Galloway, 1991; Chin and Davis, 1993; Van Diest and Kesselmeier, 2008; Kesselmeier et al., 1999; Kuhn et al., 1999; Lamb et al., 1987; Liu et al., 2010; Maseyk et al., 2014; Steinbacher et al., 2004; Whelan et al., 2013, 2016; Whelan and Rhew, 2015; Yang et al., 1996; Yi et al., 2007). This capacity for soils to take up OCS was initially thought to be caused by variations in the soil redox potential as anoxic soils, such as paddy fields, are a source of OCS to the atmosphere (Devai and DeLaune, 1995; Minami and Fukushi, 1981; Whelan et al., 2013). However, a number of key studies demonstrated that soil temperature and water content were also strong drivers of the OCS fluxes between soils and the atmosphere (Kesselmeier et al., 1999) and that they may have a non-negligible impact on the global atmospheric OCS budget and the seasonal drawdown of OCS from the atmosphere (Berry et al., 2013; Kettle et al., 2002; Launois et al., 2015). Thus if OCS is to be used in the future to estimate the magnitude of GPP at large scales it will be necessary to also quantify the contribution of soil fluxes to the OCS mass budget.

First attempts to assess the large-scale contribution of soil OCS exchange were made by Kettle et al., (2002) using empirical relationships between soil OCS uptake, soil water content and temperature derived by Kesselmeier et al. (1999):

$$F_{OCS} = F_0 \Phi_w(W) \Phi_T(T) \Phi_C(C_a), \quad (1)$$

where F_{OCS} is the modelled net OCS exchange rate (pmol m^{-2} s^{-1}), F_0 is a reference exchange rate, and $\Phi_w(W)$, $\Phi_T(T)$ and $\Phi_C(C_a)$ are parametric functions describing how soil water content (W, in % volume), temperature (T, in K) and ambient OCS mixing ratio above the soil surface (C_a, in pmol mol^{-1}), respectively modify the net OCS exchange rate. Kettle et al. (2002) parameterised their model based on observations from only one soil type, a temperate arable soil, and used a unique value of F_0 across the globe of F_0 = -10 pmol m^{-2} s^{-1}. They also considered W to be volumetric, not gravimetric, water content as was originally presented in Kesselmeier et al. (1999). Using this empirical approach, Kettle et al. (2002) estimated a global OCS sink from oxic soils of -130 ± 56 GgS yr^{-1}.

More recently, Berry et al. (2013) drew on empirical relationships by Yi et al. (2007) who observed that soil OCS uptake seemed to be proportional to the rate of heterotrophic soil respiration:

$$F_{OCS} = k_{soil} F_{CO_2}, \quad (2)$$

where k_{soil} is a proportionality constant that relates the OCS flux to heterotrophic respiration (F_{CO2}, in µmol m^{-2} s^{-1}). This formulation was subsequently implemented in a version of the Simple Biosphere Model (Sellers et al., 1996) called SIB3 (Berry et al., 2013) that estimates how F_{CO2} varies across the land surface in response to soil water content and temperature. Simulations with this model, using a value of k_{soil} of about -6 pmol(OCS) µmol$(CO_2)^{-1}$, estimated a much stronger sink strength for soils globally than Kettle et al. (2002) at -355 GgS yr^{-1}, highlighting a need for constraints on the contribution of soils to the global OCS budget. [Note that the value for k_{soil} given by Berry et al. (2013) in their paper is actually much larger (-120 pmol(OCS) µmol$(CO_2)^{-1}$) and inconsistent with the results of Yi et al. (2007) and the value that was actually used in the numerical code that was used to produce the results shown in this study. The value of -6 pmol(OCS) µmol$(CO_2)^{-1}$ has been re-estimated here to be consistent with the value used in their global simulations and their total sink strength of -355 GgS yr^{-1}.]

The rationale behind Eq. 1 is mostly based on physical considerations: OCS uptake by soils should depend on soil moisture and temperature because these variables act directly on the

transport of OCS to the CA reaction sites as well as on the reaction rates themselves. The rationale behind Eq. 2 is mostly based on ecological considerations: the uptake of OCS should be proportional to the size and activity of the soil heterotrophic community, which could co-vary with heterotrophic respiration. Bringing together these physical and ecological drivers into a single and more mechanistic model of the exchange of OCS between soils and the atmosphere has been attempted only recently (Ogée et al., 2016; Sun et al., 2015). Following the description proposed by Ogée et al. (2016) for homogeneous soil columns, the soil OCS flux should be related to soil moisture, temperature and microbial biomass according to:

$$F_{OCS} = -\sqrt{B(T)\theta D(\theta,T)k_h}\left(C_a - \frac{z_1^2 P}{D}\right)\frac{1-\xi^2}{1+\xi^2}, \quad (3a)$$

where θ is the volumetric water content ($m^3\ m^{-3}$, *i.e.* $W/100$), $B(T)$ is the solubility of OCS in water (m^3 air m^{-3} water) at temperature T, $D(\theta,T)$ is the effective diffusivity of OCS through the soil column, k_h (s^{-1}) is the effective OCS hydrolysis rate in soil water, $z_1^2 = D/kB\theta$ and $\xi = e^{-z_{max}/z_1}$, where z_{max} is soil depth. Different formulations relating the effective diffusivity and the soil moisture (and porosity) exist depending on whether the soil is repacked or not (Moldrup et al., 2003). Using only volumetric considerations, Ogée et al. (2016) argued that the OCS hydrolysis rate should be related to microbial biomass as:

$$k_h = \frac{k_{cat}}{K_m}[CA]_{in}\frac{B_v}{\theta}, \quad (3b)$$

where k_{cat} (s^{-1}) and K_m (mol m^{-3}) are the (community-average) turnover rate and the Michaelis-Menten constant of the enzymatic reaction, $[CA]_{in}$ (mol m^{-3}) is the mean CA concentration inside soil microbes and B_v (m^3 microbes m^{-3} soil) is the volumetric microbial biomass. The ratio k_{cat}/K_m was further assumed to respond to cytoplasmic pH according to:

$$\frac{k_{cat}}{K_m} = \frac{1}{1+10^{-pH_{in}+pK_{CA}}}, \quad (3c)$$

where pH_{in} is the microbial cytoplasmic pH (Krulwich et al., 2011; Slonczewski et al., 2009) and $pK_{CA} = 7.1$ corresponds to the CA response to pH of *Arabidopsis thaliana* β–CA for CO_2 hydration (Rowlett et al., 2002). This function was assumed appropriate for two reasons. The first is that most soils tend to be dominated by microbial β–CA (Elleuche, 2011; Smith et al., 1999) and the second is that Protoschill-Krebs et al. (1996) reported no pH optimum for β–CA extracted from *Pisum sativum* plants under a range of different pH values, but rather

reported a steadily increasing OCS consumption between pH 6 to 10. This reported pattern for OCS hydrolysis is also consistent with the CO_2 hydration response to pH described in Eq. 4. However, this function still remains an uncertainty whilst an absence of experiments evaluating the pK_a value for OCS persists.

A number of recent soil OCS flux studies have also reported that oxic soils are not only sinks for OCS, but can also be a source of OCS to the atmosphere (Berkelhammer et al., 2014; Kitz et al., 2017; Maseyk et al., 2014; Sun et al., 2016; Whelan et al., 2016; Whelan and Rhew, 2015). Often these studies indicate that the rate of OCS emission from soils varies closely with temperature and follows a simple Q_{10} relationship with soil temperature (Maseyk et al., 2014; Whelan et al., 2016). Some studies also indicate a potential abiotic component to this emission linked to changes in light intensity at the soil surface (Kitz et al., 2017; Whelan and Rhew, 2015). However, mechanisms to explain these emissions of OCS from oxic soils are currently putative and difficult to incorporate into a model. For this reason, Ogée et al. (2016) incorporated an OCS production term P (mol m^{-3} s^{-1}) that was assumed to respond to temperature only and whose basal rate had to be estimated empirically. Initial results testing this novel mechanistic approach against soil flux datasets have shown that the activity of the enzyme carbonic anhydrase (CA) known to catalyse the hydrolysis of OCS (Kesselmeier et al., 1999; Protoschill-Krebs and Kesselmeier, 1992) is consistent with the range of soil CA activities obtained from independent $CO^{18}O$ studies on soils (Ogée et al., 2016). However estimating the magnitude of OCS emissions across a range of soil types is required to develop a better understanding of how this basal rate varies and the potential mechanism(s) for explaining this variation.

As the mechanistic framework describing soil-atmosphere OCS exchange develops, it is becoming increasingly important to challenge these models with data and explore how each additional level of mechanistic complexity added to these models describes the pattern of OCS exchange observed across a range of soils varying widely in biogeochemical properties. This step is especially necessary if we are to evolve models that can be parameterised robustly for different biomes or soil types whilst retaining a structure that can still be simply implemented in large-scale land surface models. With this in mind we conducted a large-scale study by collecting a range of soils from different biomes within Europe (**Fig. 5.1**) to test and compare the ability of the three aforementioned models (Eqs. 1-3) to predict OCS fluxes from re-packed soils varying in a range of biogeochemical properties, including texture, soil pH, microbial biomass and land use. In addition our study also systematically uses this unique soil

experiment to investigate the extent of OCS emissions from dry soils and explore possible interactions with light.

5.2. Material and methods

5.2.1. Soil sampling, microcosms preparation and pre-incubation time

A total of 39 European soils were selected for this study (**Fig. 5.2**). These soils encompassed a wide range of abiotic and biotic characteristics (pH, texture, nitrogen and carbon content), climates (Mediterranean to boreal) and land use types (cropland, grassland, forest and peatland) (**Table 5.1**). At each location the litter layer was removed and a 0-10 cm layer of soil was sampled from the surface horizon and placed in a sealed plastic bag. At each site, three to five samples of soil were collected in this manner and sent to us. Upon arrival, soils were temporarily placed in a cold room at 5^{o}C. Thereafter composite soil samples from the same location were sieved using a 5 mm mesh and mixed together to reconstitute one homogenised soil mixture. For each soil, the maximum water holding capacity (WHC) and pH was then estimated on three replicates and six microcosms were prepared, consisting of 350-400 g of fresh soil re-packed in a 0.825 dm^3 glass jar. Each soil was then weighed and the soil height of between 5 and 7 cm recorded. All soil microcosms were then acclimated to 17°C in a climate-controlled chamber (MD1400, Snijders, Tillburg, NL), with a 12h dark/12h light photoperiod for 2-3 days.

5.2.2. Gas exchange experimental setup

After the acclimation period each microcosm was sealed with a customised glass lid fitted with three stainless steel Swagelok® bulkhead fittings connected to 0.25 inch (3.175 mm) Teflon™ inlet and outlet lines to form a flow-through gas exchange chamber and a stainless temperature probe (3-wire PT100) that measured the temperature of the soil surface at 2-4 cm depth. Three of the six microcosms were coated with aluminium to occlude light and all six soil microcosms were placed in a customised climate-control chamber (MD1400, Snijders, Tillburg, NL) to acclimate for 45 minutes minimum at 17°C with the lights on. An additional soil-free glass jar fitted with a temperature probe was also sealed and connected to a set of lines in the climate-control chamber in order to check that our setup was free of any OCS contamination.

Despite using a temperature controlled-climate chamber, we observed from all our measurements that soil temperature was not constant between all the soils studied and could vary between 17 and 23°C. This increase in soil temperature was different for each soil type, probably depending on their volumetric water content and light status. Soil OCS gas exchange was then measured on two separate occasions. The first measurements were made whilst the soil was still moist (field conditions) and again after allowing the soil to dry out naturally in the laboratory. When soils were re-measured care was taken to ensure the same soils measured in the dark (or light) when they were fresh were measured again in the dark (or light) when dry.

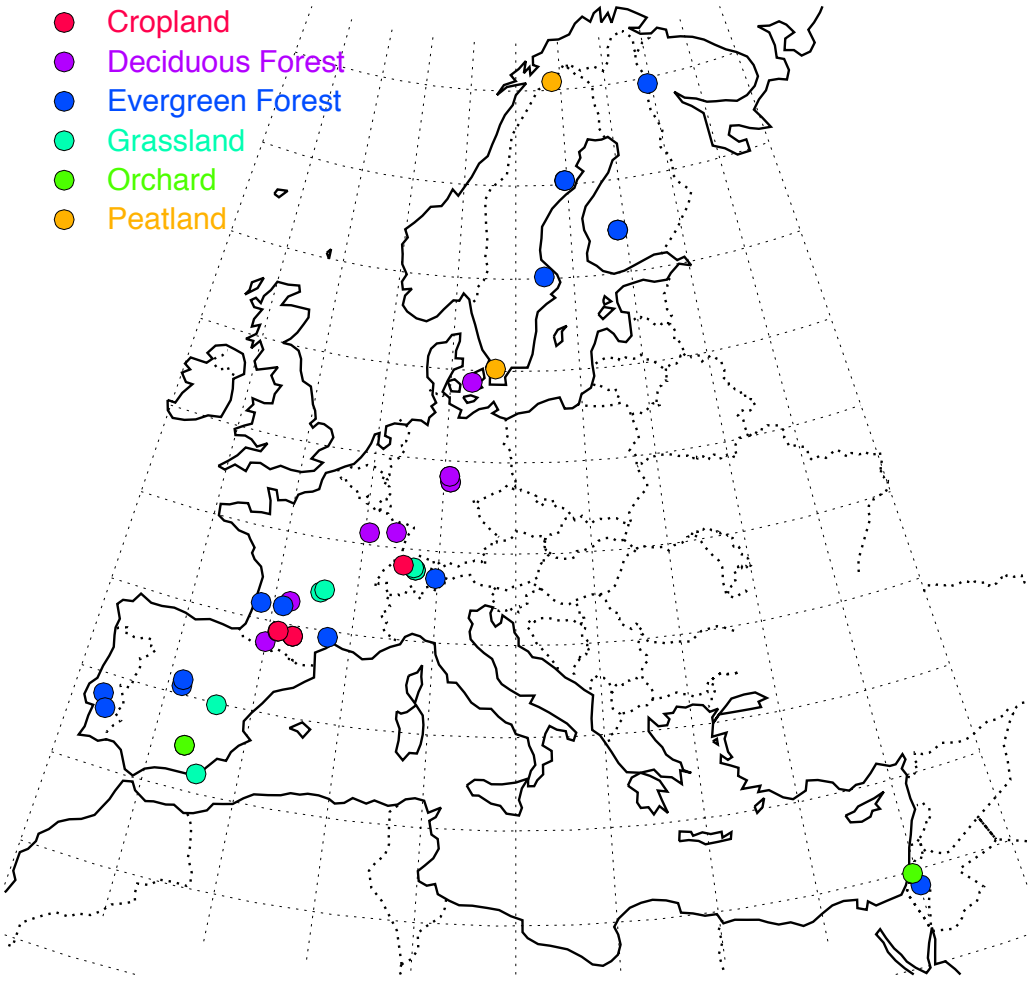

Figure 5.2: Map showing the location and land use of the sites where soils were sampled in this study.

Table 5.1. Main characteristics and locations of the different soils used for the study.

Site Name	Country	Latitude	Longitude	Soil pH	Biome	PFT
Abisko	Sweden	68.357	19.051	4.4	Boreal	Peatland
Varrio	Finland	67.757	29.616	5.3	Boreal	Evergreen Forest
Rosinedal	Sweden	64.17	19.748	5.2	Boreal	Evergreen Forest
Rosinedal	Sweden	64.17	19.748	4.5	Boreal	Evergreen Forest
Svartberget	Sweden	64.167	19.783	4.7	Boreal	Evergreen Forest
Hyytiala	Finland	61.848	24.295	4.6	Boreal	Evergreen Forest
Norunda	Sweden	60.088	17.467	4.4	Boreal	Evergreen Forest
Hyltemossa	Sweden	56.1	13.417	3.8	Boreal	Peatland
Soro	Denmark	55.486	11.645	4.2	Temperate	Deciduous Forest
Leinefelde	Germany	51.328	10.368	5.2	Temperate	Deciduous Forest
Hainich	Germany	51.079	10.453	6.0	Temperate	Deciduous Forest
Hesse	France	48.674	7.066	5.4	Temperate	Deciduous Forest
Oensingen	Switzerland	47.286	7.743	7.3	Temperate	Agriculture
Chamau	Switzerland	47.21	8.41	6.3	Temperate	Agriculture
Fruebuel	Switzerland	47.116	8.537	4.9	Temperate	Grassland
Lageren	Switzerland	47.115	8.537	6.3	Temperate	Deciduous Forest
Davos	Switzerland	46.814	9.856	4.3	Temperate	Evergreen Forest
Laquielle	France	45.772	2.964	4.6	Temperate	Grassland
Laquielle	France	45.643	2.736	5.7	Temperate	Grassland
Rouffignac	France	45.01	0.973	6.5	Temperate	Deciduous Forest
Gradignan	France	44.763	0.597	4.6	Temperate	Evergreen Forest
Le Bray	France	44.717	-0.769	4.8	Temperate	Evergreen Forest
Puechabon	France	43.742	3.596	6.9	Mediterranean	Evergreen Forest
Auch	France	43.638	0.603	8.5	Temperate	Agriculture
Auch	France	43.623	0.571	7.8	Temperate	Agriculture
Toulouse	France	43.536	1.507	5.7	Temperate	Agriculture
Toulouse	France	43.534	1.497	8.5	Temperate	Agriculture
Toulouse	France	43.531	1.508	8.6	Temperate	Agriculture
Lourdes	France	43.08	-0.04	7.9	Temperate	Deciduous Forest
Peguerinos	Spain	40.651	-4.209	6.2	Mediterranean	Evergreen Forest
Chapineroa	Spain	40.383	-4.194	5.5	Mediterranean	Evergreen Forest
Balsablanca	Spain	39.942	-2.033	8.4	Arid	Grassland
Coruche	Portugal	39.138	-8.333	5.7	Mediterranean	Evergreen Forest
Mitra	Portugal	38.541	-8	5.9	Mediterranean	Evergreen Forest
Ubeda	Spain	37.915	-3.227	8.6	Mediterranean	Agriculture
Ubeda	Spain	37.911	-3.228	8.4	Mediterranean	Agriculture
Amoladeras	Spain	36.834	-2.25	8.6	Arid	Grassland
Rehovot	Israel	31.909	34.812	7.8	Mediterranean	Agriculture
Yatir	Israel	31.347	35.051	8.1	Arid	Evergreen Forest

During the gas exchange measurements, air was supplied to each of the microcosms using a compressor (FM2 Atlas Copto, Nacka, Sweden), coupled to a chemical scrub column (Ecodry K-MT6, Parker Hannifin, Cleveland, OH, US) that first removed water vapour, CO_2 and OCS from ambient air in the lab. Concentrations in the scrubbed airstream were typically less than 5 μmol(CO_2) mol^{-1}, 7 pmol(OCS) mol^{-1} and -40°C dew point. A set of individual mass flow controllers (MFC, EL-Flow® Select, Bronkhorst, Ruurlo, NL) and stainless steel cylinders containing either pure CO_2 or CO_2-free dry air with 500 nmol(OCS) mol^{-1} (Linde, France) were then used to supply CO_2 and OCS to the air stream in a 4L aluminium buffer and reach concentrations around 420 μmol(CO_2) mol^{-1} (420 ppm) and 1000 pmol(OCS) mol^{-1} (1000 ppt). The (dry) air supplied to the inlet of each microcosm was taken from this buffer volume at a flow rate of 0.25 dm^3 min^{-1} (**Fig. S1**). The flow from the buffer volume to the microcosms was driven by a slight overpressure in the buffer of 20-30 mbar above atmosphere. Within a single flux measurement, the standard deviation on the inlet was less than 0.03 ppm(CO_2) and 1.5 ppt(OCS).

5.2.3. CO_2 and OCS mixing ratio measurements (QCLS)

The inlet or outlet airstream of a given microcosm was selected for OCS measurements by means of a 12-way rotary valve (EUTA-SD16WE VICI® 16-positions 2-way valve, Valco Instruments Co. Inc, Texas, USA). The selected airstream was pre-dried with a Nafion™ drier (MD-070-24-S-2, Perma Pure LLC, NJ, USA) before being measured with a mid-infrared quantum cascade laser spectrometer (QCLS, Aerodyne Research Inc. Billerica, MA, USA). Flow through the instrument was maintained with a TriScroll 600 pump (Agilent Technolgies, Santa Clara, CA, USA) connected to the QCLS *via* a vacuum line, and excess air was exhausted to the atmosphere. Instrument drift was corrected with frequent (every 16 minutes) background calibrations (with dry N_2) in all runs. After 12 minutes of measurements, a 4-min, two-point standard calibration was also implemented using the same dry N_2 bottle and compressed dry air from an Aculife®-treated cylinder with a known OCS concentration (524.8 ± 2.2 ppt) that had been prepared and calibrated for OCS by the NOAA Global Monitoring Division. The CO_2 concentration of the NOAA tank was calibrated in-house against a set of 3 aluminium calibration tanks containing CO_2-in-air mixtures (Deuste-Steininger, Germany) spanning the CO_2 concentration range of our measurements (374.9 ± 1.9, 474.6 ± 2.4 and 687.1 ± 4.0 ppm). CO_2 concentrations of these calibration gases were precisely characterised at the MPI for Biogeochemistry (Jena, Germany). The 2-point

calibration performed as part of the sequence allowed us to estimate instrument drift over the last 16 minutes and also account for possible span corrections. An Allan variance calculated from a 24h continuous measurement on tank air indicated a standard deviation of 2.1 ppt(OCS) and 0.1 ppm(CO_2) after 10 s averaging time, a deviation from pure white noise after more than 400 s and a standard deviation still below 1 ppt(OCS) after 900 s integration time. Although the instrument stability was very good, the implemented 2-point calibration scheme was also used to interpolate in time the calibration measurements and compute a calibration regression for each chamber inlet or outlet measurement

5.2.4. Soil sampling sequence

Each component of the system (inlet and outlet of each microcosm and the calibration tanks) was scanned at 1 Hz over 2 minutes and only the last 20 s were used to compute the mean gas concentrations, accounting for the flushing time of the tubes and analysers' cells (less than 30 s). In a given sequence, seven chambers (the six microcosms from a given soil and a blank chamber) were scanned sequentially by the OCS analyser and, when not measured, were continuously flushed through at the same constant flow rate. The full sequence of gas exchange measurements lasted 136 min. A example of such a sequence is shown in **Fig. S2**.

5.2.5. Soil characteristics

After the gas exchange measurements, each microcosm was characterised for soil water content, bulk density and water-filled pore space. Soil pH and redox-potential were also measured by diluting 20 g of soil in five times its volume of permuted water, stirred for five minutes at 250 rotations per minute and after a period of two hours to allow the decantation. Soil microbial biomass was also determined using the fumigation-potassium sulphate extraction method (Brookes et al., 1985; Vance et al., 1987). Extracts were kept frozen at -20^{o}C and shipped frozen to the INRA Arras platform where microbial C biomass was measured on the extracts. Air-dried soil samples from each location were also analysed by the same platform for soil texture (fractions of sand, silt and clay), $CaCO_3$ concentration and total carbon and nitrogen content.

5.3. Results

5.3.1. Spatial variability in OCS and CO_2 net fluxes

The majority of the soils measured from a range of land uses across Europe were net sinks for OCS when measured in their "moist" field state, with the exception of three Mediterranean soils that arrived in the lab with extremely low water contents (**Fig. 5.3a**). Net OCS fluxes varied between +0.35 to -5.79 pmol m^{-2} s^{-1}. In general the soils with the strongest OCS uptake were the peatland and forest soils from boreal and temperate regions. Within the forest types evergreen needle-leaf forests tended to have higher net OCS fluxes than evergreen broadleaf or deciduous forests. There was no clear trend for grasslands but managed croplands generally had lower uptake rates than boreal forests and had similar rates to deciduous forests. Most of the Mediterranean and arid soils from Spain (SP), Portugal (PT) and Israel (IS) had the lowest net OCS fluxes and were also occasionally emitting OCS to the atmosphere. Differences in the net OCS fluxes for the same "moist" soils measured in the light and the dark were observed for some sites, however these differences were not systematically different across all soils nor was there any clear trend apparent with the measured soil characteristics (**Fig. S3**). After air-drying, the majority of the soils surveyed became a net source of OCS to the atmosphere. Net OCS fluxes from dried soils varied from +4.49 to -2.36 pmol m^{-2} s^{-1} (**Fig. 5.4a**). There was no clear trend in OCS emissions with land use or biome. However grasslands had the highest OCS emission rates, especially the fertilised grassland in France. There was also no relationship between the magnitude of the net OCS flux when it was moist with the magnitude of the net OCS flux measured when it was dry. After air-drying, the majority of the soils surveyed exhibited systematic differences in their net OCS flux to the atmosphere depending on whether they had been measured in the light or in the dark (**Fig. S4**).

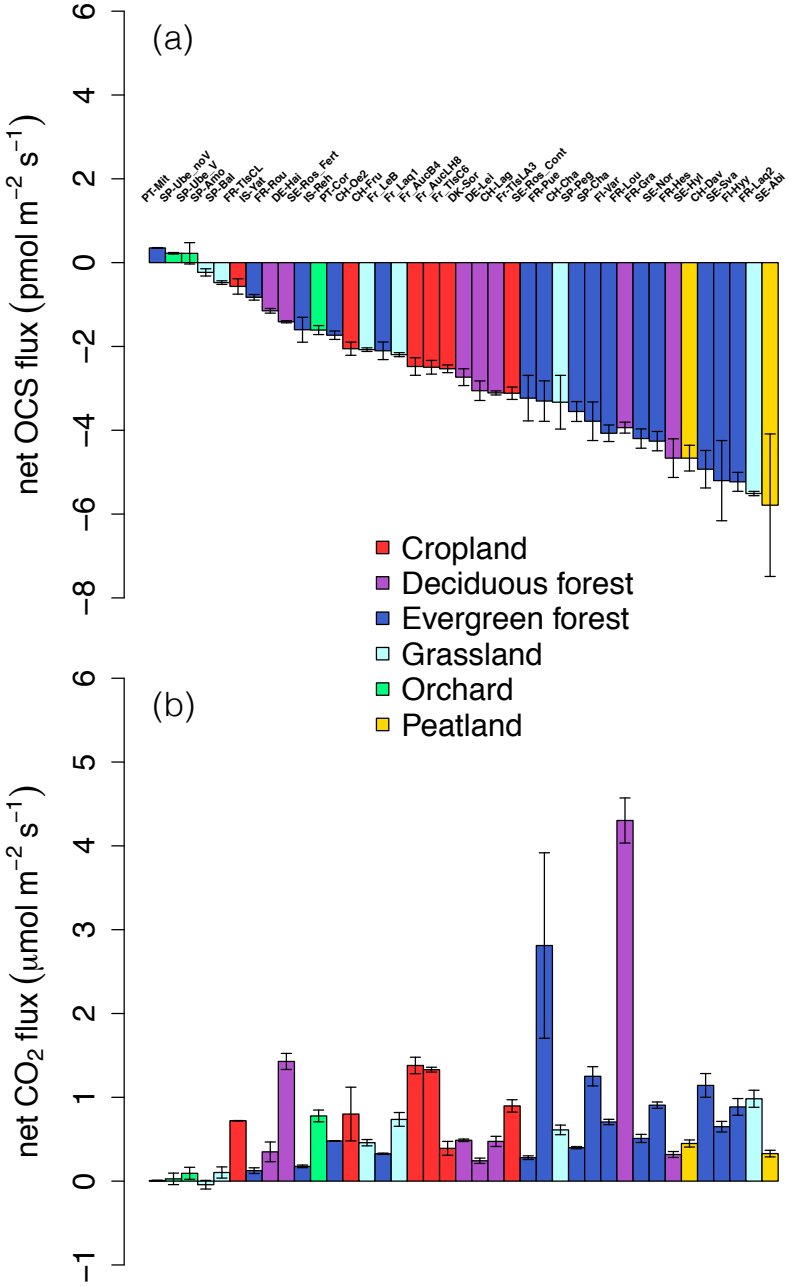

Figure 5.3: Variability in soil (a) OCS and (b) CO_2 fluxes for moist soils incubated in the dark.

The net CO_2 flux (assumed equivalent to heterotrophic respiration) measured on the "moist" soils varied from nearly zero to 4.3 µmol m^{-2} s^{-1} (**Fig. 5.3b**). No clear trend in respiration rates was observed for biome type or land use. The net CO_2 fluxes measured on dry soils were extremely small compared to those measured on moist soils and varied from between +0.3

to -0.43 µmol m^{-2} s^{-1} (**Fig. 5.4b**). The majority of the dry soil CO_2 fluxes were around zero but we clearly measured, on a few alkaline soils, a net uptake of CO_2 (**Fig. S5**). No significant difference was observed between CO_2 fluxes from soil microcosms measured in the light and in the dark (**Fig. S6**).

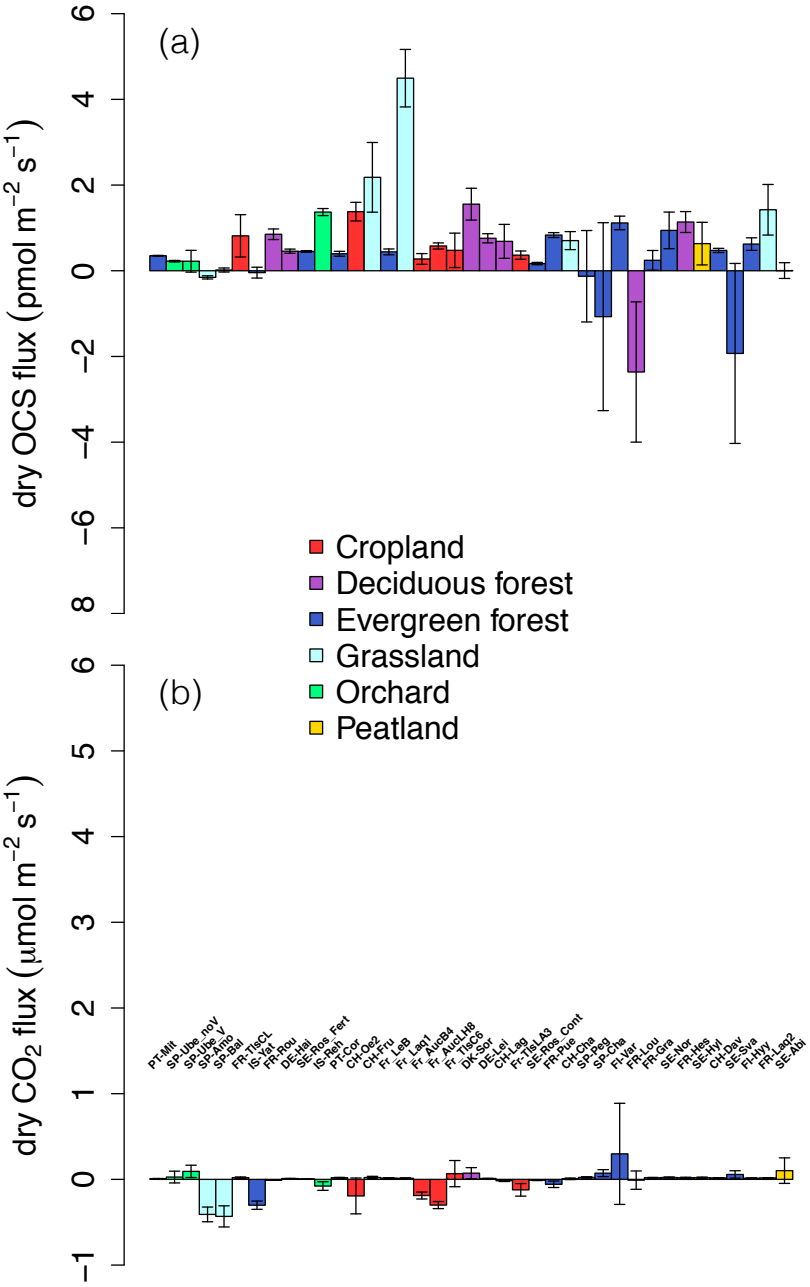

Figure 5.4: Variability in soil (a) OCS and (b) CO_2 fluxes for air-dried soils incubated in the dark.

5.3.2. Data comparison against the Yi-Berry empirical model (Eq. 2)

We tested the validity of Eq. 2 using our new dataset. From initial inspection it was not obvious that a relationship between OCS uptake and CO_2 emissions existed (**Fig. 5.3**). This may have arisen because the majority of our heterotrophic respiration rates were less than 2 µmol m^{-2} s^{-1} and somewhat smaller than the range of values observed by Yi et al. (2007) in sub-tropical forest soils (**Fig. 5.5**). Nonetheless, for these soils where CO_2 emissions were below this value, we found a weak linear relationship ($r = 0.40$, $P < 0.05$) between the net OCS uptake and heterotrophic respiration across all land uses (**Table 5.2**), and a mean value for k_{soil} of -1.74 pmol(OCS) µmol^{-1}(CO_2) when estimated over the entire dataset (**Fig. 5.5b** and **Table 5.2**). Overall our relationship with heterotrophic respiration was somewhat steeper than that observed by Yi et al. (2007) and was even steeper if we calculated k_{soil} for evergreen forest only (**Fig. 5.5b** and **Table 5.2**), becoming somewhat closer to the value used by Berry et al. (2013) in their global scale study (around -6 pmol(OCS) µmol^{-1}(CO_2), see Introduction).

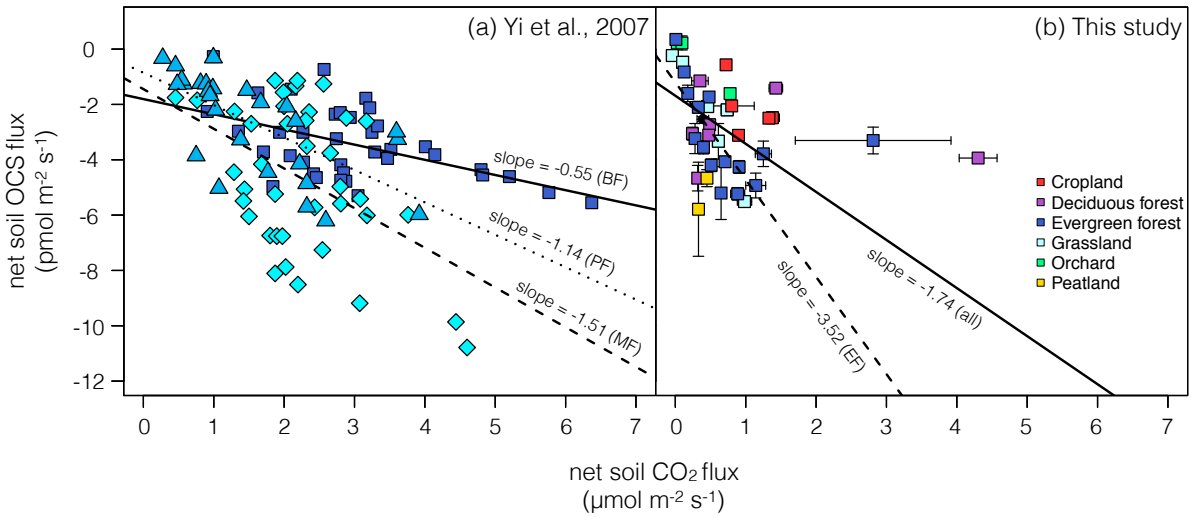

Figure 5.5: Relationship between net soil OCS and CO_2 fluxes from (a) Yi et al. (2007) on soils from evergreen broadleaf (BF), evergreen needlleaf (PF) and mixed evergreen forests (MF) and (b) this study, on a range of sieved and re-packed soils sampled across Europe and incubated in the dark at field water content.

Table 5.2. Linear model results for the relationship between net soil CO_2 and OCS fluxes.

Site description	Intercept (±SD)	Slope (±SD)	P-value	r^2	Reference study
Mixed Forest	-1.21 (± 1.08)	-1.51 (± 0.45)	<0.01	0.48	Yi et al. (2007)
Pine Forest	-0.92 (± 0.48)	-1.14 (± 0.26)	<0.01	0.69	Yi et al. (2007)
Broadleaf Forest	-1.79 (±0.48)	-0.55 (± 0.15)	<0.01	0.52	Yi et al. (2007)
Evergreen forest*	-1.20 (± 0.55)	-3.52 (± 0.83)	<0.01	0.60	This study
All land uses*	-1.69 (± 0.46)	-1.74 (± 0.67)	<0.05	0.16	This study

*Excluding two soils with net soil CO_2 fluxes > 2 µmol m-2 s^{-1} (see text).

5.3.3. Data comparison against the Kesselmeier-Kettle empirical model (Eq. 1)

Kesselmeier et al. (1999) demonstrated that the net flux of OCS was tightly controlled by soil temperature, OCS mixing ratios and the soil water content. In this study we controlled carefully the OCS mixing ratio of the air sent to the chamber and measured soils within a climatically-controlled chamber set to 17°C. However, we did not control soil water content but rather tried to capture the variability of soil moisture experienced by a range of European soils during a Northern Hemisphere summer. Inspection of the net OCS flux data suggested that soil water status might explain a large amount of the variability in net OCS fluxes from across Europe (**Fig. 5.6**).

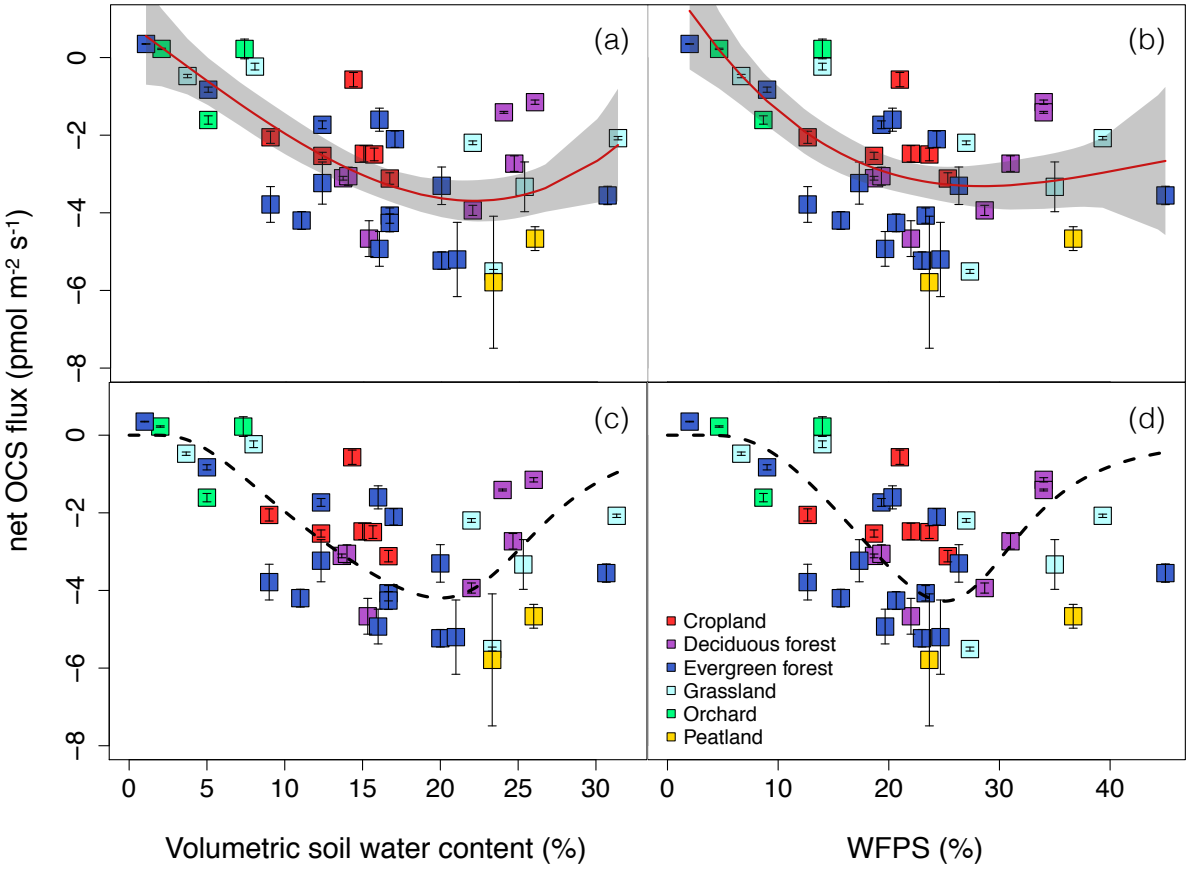

Figure 5.6: Relationship between the net soil OCS flux in the dark and either volumetric water content (a and c) or water-filled pore space observed across a range of European soils (squares) and modelled using either (a and b) a 3rd order polynomial or (c and d) the Kesselmeier et al. (1999) model (Eq. 1) with adjusted parameters (see text).

Using a 3rd order polynomial to fit the relationship between the net OCS flux and either soil volumetric water content or water filled pore space (WFPS) we found that volumetric water content explained more of the variability in soil OCS fluxes than WFPS (**Figs. 5.6a** and **5.6b**) and that the polynomial fits were significant (**Table 5.3**). We also tested the empirical model of Kesselmeier et al. (1999) (Eq. 1) against our data. We found that Eq. 1 could explain a large fraction of the site-to-site variability from our OCS flux dataset (**Figs. 5.6c** and **5.6d**). To do so however, we had to change 3 out of the 5 model parameters in the F_W function from their original values: the optimum water content was shifted from 12% originally to 20% (for VWC) or 25% (for WFPS), F_0 was adjusted from -10 pmol m^{-2} s^{-1} originally to -17 pmol m^{-2} s^{-1} (for VWC) or -8 pmol m^{-2} s^{-1} (for WFPS) and a third parameter was also adjusted to improve the curvature of the fit at high soil water contents.

Table 5.3 Polynomial model results for the relationship between net soil OCS fluxes and either volumetric water content (VWC) or WFPS.

Explanatory variable	Parameter *a*	Parameter *b*	Parameter *c*	r^2	P-value
VWC (%)	-0.29 (± 0.20)	-0.001 (± 0.014)	0.0002 (± 0.0002)	0.44	< 0.01
WFPS (%)	-0.46 (± 0.17)	0.012 (±0.008)	-0.000095 (±0.00012)	0.34	< 0.01

5.3.4. Data comparison against the Ogée model (Eq. 3)

The amount of microbial C biomass is often considered to be strongly coupled to the rate of microbial respiration (Serna-Chavez et al., 2013; Xu et al., 2013) and could provide a mechanistic basis for explaining the observations of Yi et al. (2007). We tested the link between microbial biomass and heterotrophic respiration rates on a subset of the European soils that had been measured for gas exchange. For a range of biomes and land use types we found that a very strong relationship existed between the net CO_2 flux (heterotrophic respiration rate) and microbial C biomass (**Fig. 5.7**).

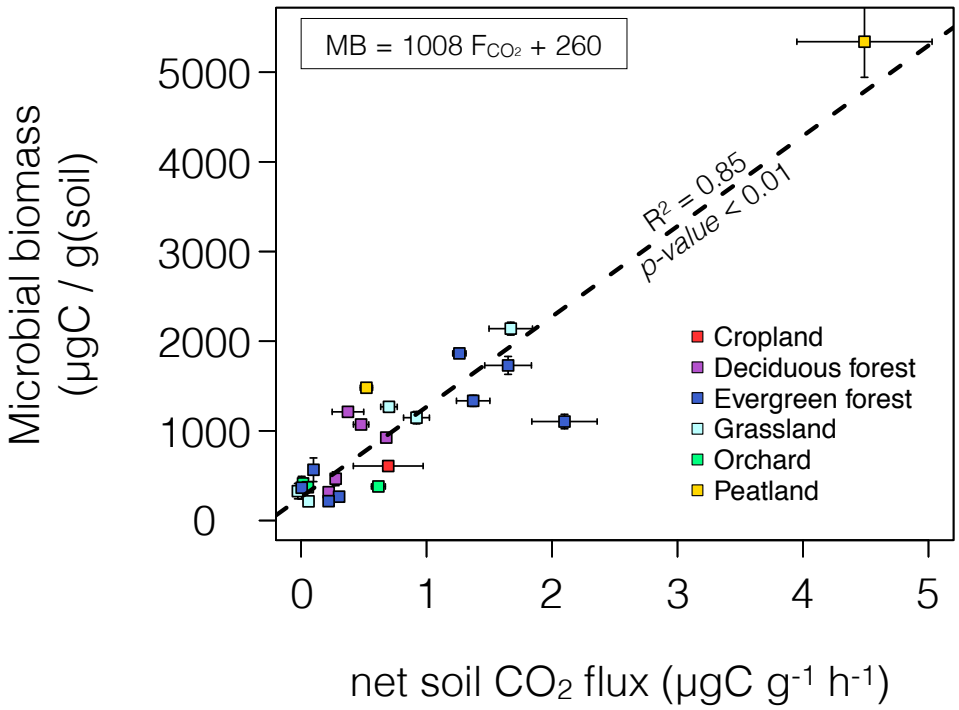

Figure 5.7. Relationship between the net soil CO_2 flux measured in the dark and microbial biomass across a range of land use types within Europe.

Assuming this relationship to be valid across our entire dataset we estimated microbial biomass for all the soils in order to test the Ogée model (Eq. 3) in its ability to predict the measured net OCS fluxes. As an initial step we simplified Eq. 3 assuming $z_{max} >> z_1$ (a fair assumption in our conditions). With these conditions Eq. 3 simplifies to:

$$F_{OCS} = -V_d C_a + P z_{max}, \quad (4a)$$

where $V_d = \sqrt{B(T)\theta D(\theta,T) k_h}$ is the so-called deposition velocity (m s^{-1}). We also assumed a constant temperature and pH_{in} across all our soils (according to Krulwich et al. (2011), pH_{in} should vary between 6.2 and 7.7), so that V_d should only depend on soil moisture, porosity and microbial biomass. Using the effective diffusivity model of Moldrup et al. (2003) for repacked soils, V_d should then satisfy:

$$V_d \propto \sqrt{\theta \cdot (\phi - \theta)^{2.5} / \phi \cdot B_v / \theta}, \quad (4b)$$

The relationship between our observed soil OCS fluxes and this proportionality factor was explored for both net (**Fig. 5.8a**) and gross (**Fig. 5.8c**) exchange rates. The latter was assumed equal to the difference between the measured OCS flux on moist and air-dried soils. Only very weak relationships were found ($R^2 < 0.16$ in both cases) between these variables. However a much stronger correlation (R^2 up to 0.60) was obtained if the proportionality factor was slightly modified whereby the factor B_v/θ in the square root was replaced by B_v alone (**Fig. 5.8b** and **Fig. 5.8d**).

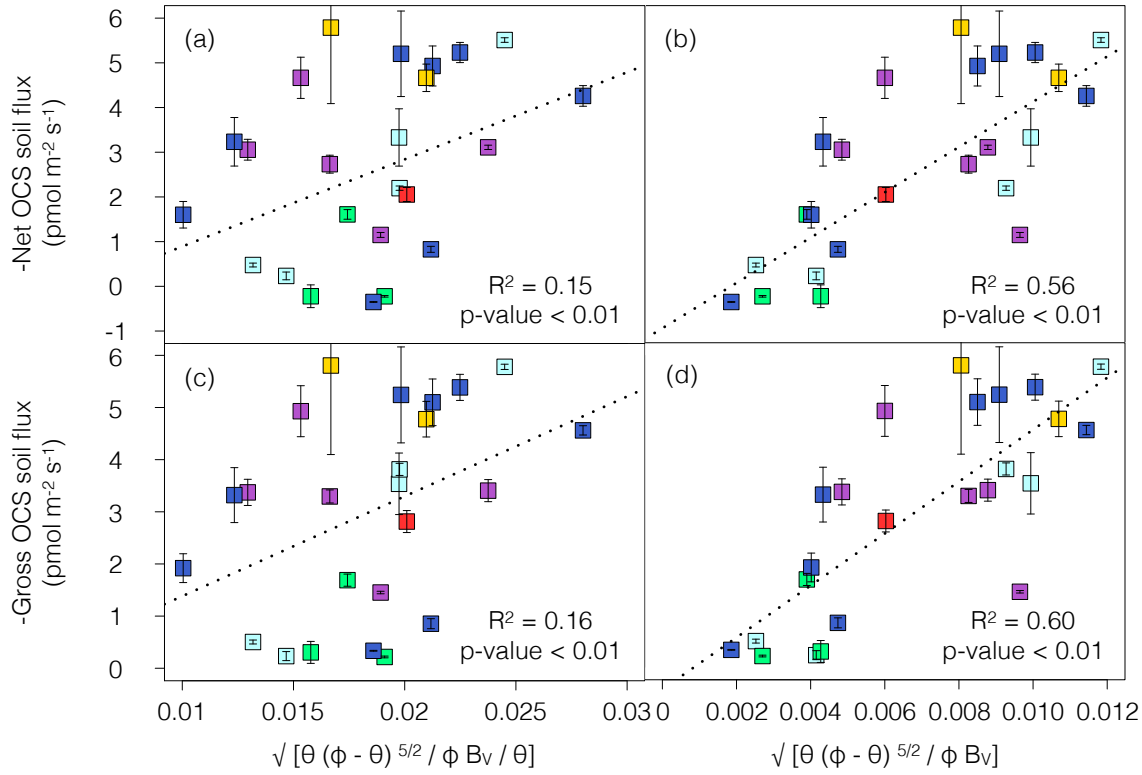

Figure 5.8. *Relationship between the measured net soil OCS flux (a and b) or gross soil OCS flux (c and d) with the simplified OCS deposition velocity from Ogée model (Eq. 4b, panels a and c) or a modification of it whereby the factor B_v/θ in the square root is replaced by B_v alone (panels b and d).*

The reason for modifying the proportionality factor defined by Eq. 4b is hard to explain unless some of the assumptions made to derive this equation were not verified. To explore this a bit further we also used the full model (Eq. 3a) and the measured net and gross OCS fluxes (representing respecitively F_{OCS} and Pz_{max} in Eq. 3a) to estimate the bulk soil OCS hydrolysis rate k_h. This was done using an iterative procedure as the model is a non-linear function of k_h. We then used Eq. 3b to estimate a community-average k_{cat}/K_m ratio and tested whether its dependency towards soil or internal pH followed Eq. 3c. Internal (cytoplasmic) pH was derived from soil pH according to the dataset collected by Krulwich et al. (2011). Inspection of the data indicated that the community-averaged k_{cat}/K_m was usually higher, and also more variable, at low soil pH (**Fig. 5.9a**). A similar trend persisted even when k_{cat}/K_m were plotted against internal pH (**Fig. 5.9b**). In contrast to the data, Eq. 3c predicts that k_{cat}/K_m should increase monotonically as soil and internal pH values increase (**Fig. 5.9c** and **Fig. 5.9d**). These results may indicate different microbial communities with different classes

of CA leading to large variations in the maximum community-average k_{cat}/K_m across all the studied sites. The original Ogée model assumed that $(k_{cat}/K_m)_{max}$ was 2.39 s^{-1} μM^{-1} at 20°C based on β–CA data from *P. sativum* (Protoschill-Krebs et al., 1996). However, for similar temperatures (17-23°C) the $(k_{cat}/K_m)_{max}$ values that fit the data appear somewhat lower, around 1.9 s^{-1} μM^{-1} in acidic soils and down to about 0.1 s^{-1} μM^{-1} in more alkaline soils (**Fig. 5.9d**).

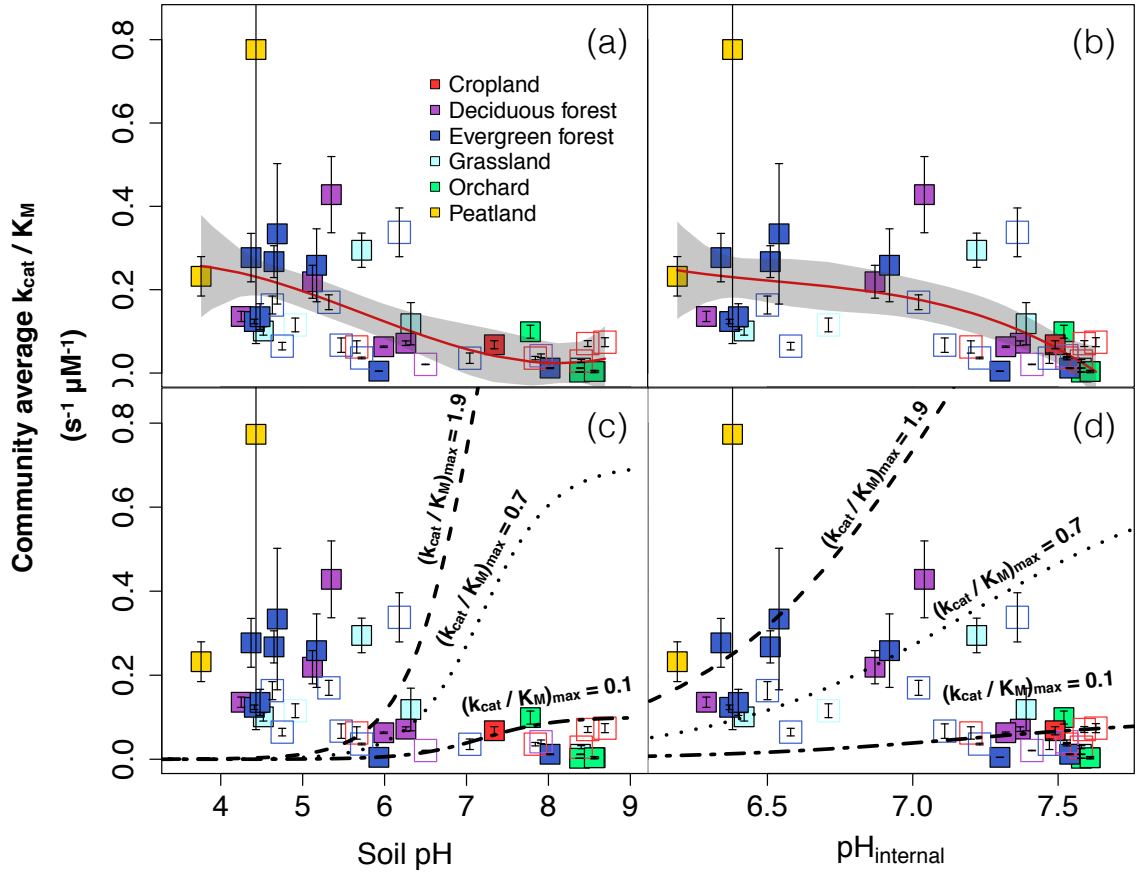

Figure 5.9. *Relationship between the measured soil community-averaged k_{cat}/K_m and either (a and c) soil pH or (b and d) microbial internal pH described by either (a and b) a 2nd order polynomial fit to the data or (c and d) the Ogée et al. (2016) model varying the parameter k_{cat}/K_m maximum.*

5.4. Discussion

5.4.1. Spatial patterns in soil-atmosphere OCS exchange rates

Variability in the net OCS flux measured at the 39 different sites across Europe are within the large range of OCS fluxes measured in both the laboratory and field using a range of chamber techniques and over a wider range of temperatures (Berkelhammer et al., 2014; Castro and Galloway, 1991; Chin and Davis, 1993; Van Diest and Kesselmeier, 2008; Kesselmeier et al., 1999; Kuhn et al., 1999; Lamb et al., 1987; Liu et al., 2010; Maseyk et al., 2014; Steinbacher et al., 2004; Whelan et al., 2013, 2016; Yang et al., 1996; Yi et al., 2007). However, compared to many of these studies the net OCS fluxes in our study were much less variable despite being sampled from a large range of biomes and land use types (**Table 5.1**). Previous studies clearly demonstrated that variations in soil temperature exert a strong control on the net OCS flux (Van Diest and Kesselmeier, 2008; Kesselmeier et al., 1999; Whelan et al., 2016) and this was minimised to some extent in our study by measuring our samples in relatively cool, climatically-controlled conditions. This may explain the narrower range of OCS fluxes across all our sites.

In general we found that oxic boreal and temperate forest and peatland sites tended to have relatively higher OCS uptake rates than grasslands, croplands and Mediterranean sites at the same temperature. These higher OCS uptake rates at northern European sites were also strongly related to soil pH, with higher OCS uptake rates observed at the more acidic soils (pH values between 3.8 and 6). Previous findings by Sauze et al. (in prep, Chapter 4) indicate that variations in the OCS sink strength of soils may be linked to soil community structure in interactions with soil pH. In particular, Sauze et al. (in prep, Chapter 4) measured a significant influence of the size of the fungal community on the soil OCS uptake rate that was linked to pH-driven changes in the 'size' of the algal community. In a similar manner, variations in the community structure driven by climatic and edaphic conditions such as soil pH could also have a role in regulating how OCS uptake varies spatially across our soils. Further analyses are currently underway to investigate whether the net OCS flux from the range of sites presented in this study varies with the community structure using a qPCR approach similar to those described in Chapter 4. Based on our previous findings we will test the hypothesis that variations in the fungal community drive the magnitude of the net OCS flux. Consequently, this analysis will also test the hypothesis that the abundance of fungi in soils is greater in the cooler, wetter northern boreal and temperate ecoystems than the warmer, drier Mediterranean

and arid ecosystems of the south. However, we also bear in mind that interactions with the abundance of algae can influence the fungal community size and thus interesting interactions may emerge in more alkaline soils that foster biocrust community members in warmer, drier ecosystems.

We also found that, at many of the sites, there were significantly different net OCS uptake rates depending on whether the soils were measured in the light or in the dark (**Fig. S3** and **Fig. S4**). Currently it is unclear what drives this result but it is a phenomenon that has been observed on other soils (Kitz et al., 2017; Sauze et al. in prep; Whelan and Rhew, 2015) and bryophytes (Gimeno et al., submitted). Whelan and Rhew (2015) concluded that abiotic photo-degradation promoted the release of OCS even when soils were sterile. We found no correlation in the differences between light and dark OCS fluxes and soil pH or soil water content (data not shown). On the other hand, our results indicate that when significant differences in OCS uptake occurred they always caused the net OCS flux to become smaller in the light treatment and, on occasion, convert the soil from being a sink to a source of OCS (**Fig. S3** and **Fig. S4**). This trend is consistent with the results of Whelan and Rhew (2015). In addition, a recent laboratory study using the same setup as here reported OCS emissions from well-watered bryophytes that responded positively to light-induced changes in temperature (Gimeno et al., submitted). Our soil temperatures across different replicates and sites were between 17-23^{o}C despite the climate chamber being set consistently to 17^{o}C. Currently we cannot tease apart the role of light and temperature on the OCS emission from these soils but more studies are underway to address this point.

5.4.2. Which soil-air OCS model describes best our spatial dataset?

Yi et al. (2007) proposed that heterotrophic respiration might be a good proxy for OCS fluxes (Eq. 2), at least in oxic soils. This would provide a simple algorithm to estimate OCS fluxes in global carbon cycle models that already estimate spatial and seasonal changes in heterotrophic respiration rates (Berry et al., 2013). However our results show that the relationship between net OCS uptake and heterotrophic respiration is quite weak when measured at the same soil temperature but over a range of soil pH, water content and texture (**Fig. 5.5** and **Table 5.2**). In addition, as respiration and OCS emission rates increase with temperature, and with different temperature sensitivities (Q_{10}), the relationship between the net OCS uptake with respiration is likely to vary strongly with any increase in soil temperature (Whelan et al., 2016). Testing

this hypothesis was beyond the scope of the present study but experiments on this topic are currently underway and should provide novel results in the near future.

The empirical model of Kesselmeier et al. (1999) that relates the net OCS exchange rate to soil moisture and temperature (Eq. 1) can also be easily implemented in global carbon cycle models as these variables are classic outputs of such models. In our study a relationship between F_{OCS} and *VWC* was found across all the soils measured in the dark when measured at similar temperatures and OCS mixing ratios. This relationship was mostly driven by the northern European sites that tended to have higher *VWC* during the summer period and to exhibit larger rates of OCS uptake (**Fig. 5.6**). However, this empirical model contains many parameters that will change in an unpredictable manner as OCS mixing ratios and temperature vary spatially or temporally (Van Diest and Kesselmeier, 2008). In addition, if we were to use the original parameterisation of the model proposed by Kesselmeier et al. (1999) and used at the global scale by Kettle et al. (2002), we would have predicted OCS flux rates 3 to 4 times smaller than what we observed for the same temperature and OCS mixing ratios. Clearly, the parameters used in this empirical model provide no mechanistic meaning or insight on the other processes that might be driving the spread of flux values around this fit. Thus although this empirical model partially captures the variability in our OCS fluxes, which demonstrates a strong control of soil water content, it is not simple to apply this type of empirical model at the global scale.

In contrast to the empirical model of Kesselmeier et al. (1999) the model of Ogée et al. (2016) incorporates theory that describes how OCS molecules diffuse within the soil matrix depending on the temperature and texture of the soil in addition to the amount of air and water-filled pore space. Thus the Ogée model provides a mechanistic framework to predict the behaviour observed in **Fig. 5.9** with knowledge of a few soil properties such as texture that can be obtained at the large scale (Serna-Chavez et al., 2013; Xu et al., 2013). Thus the physical components of the model can become dynamically simulated by changes in environmental drivers (temperature, soil moisture, OCS mixing ratios) either provided from large-scale databases (NOAA CMDL) or obtained from global carbon cycle models. In addition Ogée et al. (2016) hypothesised that the OCS hydrolysis rate k_h should scale with the amount of total microbial biomass B_v (assuming all microbes contain equal amounts of CA, Eq. 3b) and that the scaling factor would also vary with pH (assuming a similar pH response for all CA isozymes, Eq. 3c). However, applying this mechanistic model to our dataset challenged these two assumptions. First of all our results suggest that the dilution factor B_v/θ

of soil CA used in Eq. 3b could not explain alone our data and that k_h may rather be proportional to B_v alone (**Fig. 5.8**). This could indicate that the community-average k_{cat}/K_m ratio would also depend on soil moisture, at least at soil water contents when water discontinuity may impair microbial activity (Manzoni et al., 2014). Our results also suggest that our assumptions regarding the pH response of the community-average k_{cat}/K_m are incorrect. This could be because different CA isozymes with different catalytic efficiencies are present in the different soils, with relatively higher efficiencies at low pH (**Fig. 5.9**). However what is not considered in any of the models is the interaction of OCS with other enzymes that could be present in soils. For example, COSase (Ogawa et al., 2013), CS_2 hydrolase (Smeulders et al., 2011) or nitrogenase (Seefeldt et al., 1995), CO dehydrogenase (Ensign, 1995) and RuBISCO (Lorimer and Pierce, 1989) have also been shown to take up OCS with sometimes higher efficiencies than CA. In addition, some soil organisms expressing thiocyanate hydrolase have also been shown to release OCS (Masaki et al., 2016) (Katayama et al., 1992; Masaki et al., 2016). Currently, it is unclear how the ratio of different CA isozymes or other enzymes in natural soils vary across biomes and land use types, in response to changes in microbial community structure. Future studies addressing these important factors should provide key breakthroughs in our theoretical understanding of soil OCS exchange with the atmosphere and help predict the spatial and temporal variability of OCS mixing ratios in the atmosphere, providing a novel theoretical framework for large-scale multi-tracer models of the global carbon cycle.

References

Andreae, M. O. and Crutzen, P. J.: Atmospheric Aerosols: Biogeochemical Sources and Role in Atmospheric Chemistry, Science, 276(5315), 1052–1058, doi:10.1126/science.276.5315.1052, 1997.

Berkelhammer, M., Asaf, D., Still, C., Montzka, S., Noone, D., Gupta, M., Provencal, R., Chen, H. and Yakir, D.: Constraining surface carbon fluxes using in situ measurements of carbonyl sulfide and carbon dioxide, Global Biogeochem. Cycles, 28(2), 161–179, doi:10.1002/2013GB004644, 2014.

Berry, J., Wolf, A., Campbell, J. E., Baker, I., Blake, N., Blake, D., Denning, a. S., Kawa, S. R., Montzka, S. a., Seibt, U., Stimler, K., Yakir, D. and Zhu, Z.: A coupled model of the global cycles of carbonyl sulfide and CO_2 : A possible new window on the carbon cycle, J. Geophys. Res. Biogeosciences, 118(2), 842–852, doi:10.1002/jgrg.20068, 2013.

Brookes, P. C., Landman, A., Pruden, G. and Jenkinson, D. S.: Chloroform fumigation and the release of soil nitrogen: A rapid direct extraction method to measure microbial biomass nitrogen in soil, Soil Biol. Biochem., 17(6), 837–842, doi:10.1016/0038-0717(85)90144-0, 1985.

Castro, M. S. and Galloway, J. N.: A comparison of sulfur-free and ambient air enclosure techniques for measuring the exchange of reduced sulfur gases between soils and the atmosphere, J. Geophys. Res., 96(D8), 15427–15437, doi:10.1029/91JD01399, 1991.

Chin, M. and Davis, D. D.: Global sources and sinks of OCS and CS_2 and their distributions, Global Biogeochem. Cycles, 7(2), 321–337, doi:10.1029/93GB00568, 1993.

Crutzen, P. J.: The possible importance of CSO for the sulfate layer of the stratosphere, Geophys. Res. Lett., 3(2), 73–76, 1976.

Devai, I. and DeLaune, R. D.: Formation of volatile sulfur compounds in salt marsh sediment as influenced by soil redox condition, Org. Geochem., 23(4), 283–287, doi:10.1016/0146-6380(95)00024-9, 1995.

Elleuche, S.: Carbonic Anhydrase in Fungi and Fungal-Like Organisms - Functional Distribution and Evolution of a Gene Family, Mycota, 14, 257–274, doi:10.1007/978-3-540-87407-2, 2011.

Ensign, S. A. Biochemistry, 34, 5372-5381, 1995.

Gimeno, T.E., Ogée, J., Royles, J., Gibon, Y., West, J., Burlett, R., Jones, S.P., Sauze, J.,

Wohl, S., Griffiths, H., Benard, C. and Wingate, L.: Bryophyte gas-exchange dynamics along varying hydration status reveal a significant COS sink in the dark and COS source in the light, New Phytol (submitted).

Katayama, Y., Narahara, Y., Inoue, Y., Amano, F., Kanagawa, T., and Kuraishi, H.: A thiocyanate hydrolase of Thiobacillus thioparus, A novel enzyme catalyzing the formation of carbonyl sulfide from thiocyanate, J. Biol. Chem., 267, 9170-9175, 1992.

Kesselmeier, J., Teusch, N. and Kuhn, U.: Controlling variables for the uptake of atmospheric carbonyl sulfide by soil, J. Geophys. Res. Atmos., 104(D9), 11577–11584, doi:10.1029/1999JD900090, 1999.

Kettle, A., Kuhn, U., von Hope, M., Kesselmeier, J. and Andreae, O. J.: Global budget of atmospheric carbonyl sulfide: Temporal and spatial variations of the dominant sources and sinks, J. Geophys. Res., 107(D22), 4658, doi:10.1029/2002JD002187, 2002.

Kitz, F., Gerdel, K., Hammerle, A., Laterza, T., Spielmann, F. M. and Wohlfahrt, G.: In situ soil COS exchange of a temperate mountain grassland under simulated drought, Oecologia, doi:10.1007/s00442-016-3805-0, 2016.

Krulwich, T. A., Sachs, G. and Padan, E.: Molecular aspects of bacterial pH sensing and homeostasis, Nat. Rev. Microbiol., 9(5), 330–343, doi:10.1038/nrmicro2549, 2011.

Kuhn, U., Ammann, C., Wolf, A., Meixner, F. ., Andreae, M. . and Kesselmeier, J.: Carbonyl sulfide exchange on an ecosystem scale: soil represents a dominant sink for atmospheric COS, Atmos. Environ., 33(6), 995–1008, doi:10.1016/S1352-2310(98)00211-8, 1999.

Lamb, B., Westberg, H., Allwine, G., Bamesberger, L. and Guenther, A.: Measurement of biogenic sulfur emissions from soils and vegetation: Application of dynamic enclosure methods with Natusch filter and GC/FPD analysis, J. Atmos. Chem., 5(4), 469–491, doi:10.1007/BF00113906, 1987.

Launois, T., Peylin, P., Belviso, S. and Poulter, B.: A new model of the global biogeochemical cycle of carbonyl sulfide – Part 2: Use of ocs to constrain gross primary productivity of current vegetation models, Atmos. Chem. Phys. Discuss., 14(20), 27663–27729, doi:10.5194/acpd-14-27663-2014, 2014.

Liu, J., Geng, C., Mu, Y., Zhang, Y., Xu, Z. and Wu, H.: Exchange of carbonyl sulfide (COS) between the atmosphere and various soils in China, Biogeosciences, 7(2), 753–762, 2010.

Lorimer, G.H. and Pierce, J.: Carbonyl sulfide: an alternate substrate for but not an activator

of ribulose-1,5-bisphosphate carboxylase, Journal of Biological Chemistry, 264, 2764–2772, 1989.

Manzoni, S. and Katul, G. G.: Invariant soil water potential at zero microbial respiration explained by hydrological discontinuity in dry soils, Geophys. Res. Lett., 41, 7151–7158, doi:10.1002/2014GL061467, 2014.

Masaki, Y., Ozawa, R., Kageyama, K. and Katayama, Y.: Degradation and emission of carbonyl sulfide, an atmospheric trace gas, by fungi isolated from forest soil, edited by R. Boden, FEMS Microbiol. Lett., 363(18), 1–7, doi:10.1093/femsle/fnw197, 2016.

Maseyk, K., Berry, J. a, Billesbach, D., Campbell, J. E., Torn, M. S., Zahniser, M. and Seibt, U.: Sources and sinks of carbonyl sulfide in an agricultural field in the Southern Great Plains., Proc. Natl. Acad. Sci. U. S. A., 111(25), 9064–9, doi:10.1073/pnas.1319132111, 2014.

Minami, K. and Fukushi, S.: Volatilization of carbonyl sulfide from paddy soils treated with sulfur-containing substances, Soil Sci. Plant Nutr., 27(3), 339–345, doi:10.1080/00380768.1981.10431288, 1981.

Moldrup, P., Olesen, T., Komatsu, T., Yoshikawa, S., Schjønning, P. and Rolston, D. E.: Modeling Diffusion and reaction in soils: X. A unifying model for solute and gas diffusivity in unsaturated soil, Soil Sci., 168(5), 321–337, doi:10.1097/01.ss.0000070907.55992.3c, 2003.

Montzka, S. A., Calvert, P., Hall, B. D., Elkins, J. W., Conway, T. J., Tans, P. P. and Sweeney, C.: On the global distribution, seasonality, and budget of atmospheric carbonyl sulfide (COS) and some similarities to CO_2, J. Geophys. Res., 112(D9), D09302, doi:10.1029/2006JD007665, 2007.

Ogawa, T., Noguchi, K., Saito, M., Nagahata, Y., Kato, H., Ohtaki, A., Nakayama, H., Dohmae, N., Matsushita, Y., Odaka, M., Yohda, M., Nyunoya, H. and Katayama, Y.: Carbonyl Sulfide Hydrolase from Thiobacillus thioparus Strain THI115 Is One of the β-Carbonic Anhydrase Family Enzymes, J. Am. Chem. Soc., 135(10), 3818–3825, doi:10.1021/ja307735e, 2013.

Ogée, J., Sauze, J., Kesselmeier, J., Genty, B., Van Diest, H., Launois, T. and Wingate, L.: A new mechanistic framework to predict OCS fluxes from soils, Biogeosciences, 13(8), 2221–2240, doi:10.5194/bg-13-2221-2016, 2016.

Protoschill-Krebs, G. and Kesselmeier, J.: Enzymatic Pathways for the Consumption of Carbonyl Sulphide (COS) by Higher Plants, Bot. Acta, 105(3), 206–212,

doi:10.1111/j.1438-8677.1992.tb00288.x, 1992.

Protoschill-Krebs, G., Wilhelm, C. and Kesselmeier, J.: Consumption of carbonyl sulphide (COS) by higher plant carbonic anhydrase (CA), Atmos. Environ., 30(18), 3151–3156, doi:10.1016/1352-2310(96)00026-X, 1996.

Rowlett, R. S., Tu, C., McKay, M. M., Preiss, J. R., Loomis, R. J., Hicks, K. a., Marchione, R. J., Strong, J. a., Donovan, G. S. and Chamberlin, J. E.: Kinetic characterization of wild-type and proton transfer-impaired variants of β-carbonic anhydrase from Arabidopsis thaliana, Arch. Biochem. Biophys., 404(2), 197–209, doi:10.1016/S0003-9861(02)00243-6, 2002.

Sandoval-Soto, L., Stanimirov, M., von Hobe, M., Schmitt, V., Valdes, J., Wild, A. and Kesselmeier, J.: Global uptake of carbonyl sulfide (COS) by terrestrial vegetation: Estimates corrected by deposition velocities normalized to the uptake of carbon dioxide (CO2), Biogeosciences, 2(2), 125–132, doi:10.5194/bg-2-125-2005, 2005.

Sauze, J., Ogée, J., Maron, P.A., Nowak, V., Wohl, S., Kaiserman, A., Jones, S.P., Crouzet, O. and Wingate, L. : The contribution of soil phototrophs and fungi to soil CO_2 and OCS exchange and the associated carbonic anhydrase activity, in prep-b

Sauze, J., Jones, S.P., Wingate, L. and Ogée, J.: The role of pH on soil carbonic anhydrase activity, in prep-a

Seefeldt, L.C., Rasche, M.E., and Ensign, S.A.: Carbonyl sulfide and carbon dioxide as new substrates, and carbon disulfide as a new inhibitor, of nitrogenase, Biochemistry, 34, 5382–5389, 1995.

Seibt, U., Kesselmeier, J., Sandoval-Soto, L., Kuhn, U. and Berry, J. A.: A kinetic analysis of leaf uptake of COS and its relation to transpiration, photosynthesis and carbon isotope fractionation, Biogeosciences Discuss., 6(5), 9279–9300, doi:10.5194/bgd-6-9279-2009, 2009.

Sellers, P. J., Tucker, C. J., Collatz, G. J., Los, S. O., Justice, C. O., Dazlich, D. A. and Randall, D. A.: A Revised Land Surface Parameterization (SiB2) for Atmospheric GCMS. Part II: The Generation of Global Fields of Terrestrial Biophysical Parameters from Satellite Data, J. Clim., 9(4), 706–737, doi:10.1175/1520-0442(1996)009<0706:ARLSPF>2.0.CO;2, 1996.

Serna-Chavez, H. M., Fierer, N. and van Bodegom, P. M.: Global drivers and patterns of microbial abundance in soil, Glob. Ecol. Biogeogr., 22(10), 1162–1172, doi:10.1111/geb.12070, 2013.

Slonczewski, J. L., Fujisawa, M., Dopson, M. and Krulwich, T. A.: Cytoplasmic pH Measurement and Homeostasis in Bacteria and Archaea, in Advances in Microbial Physiology, vol. 55, pp. 1–79, Elsevier., 2009.

Smeulders, M. J., Barends, T. R. M., Pol, A., Scherer, A., Zandvoort, M. H., Udvarhelyi, A., Khadem, A. F., Menzel, A., Hermans, J., Shoeman, R. L., Wessels, H. J. C. T., van den Heuvel, L. P., Russ, L., Schlichting, I., Jetten, M. S. M. and Op den Camp, H. J. M.: Evolution of a new enzyme for carbon disulphide conversion by an acidothermophilic archaeon., Nature, 478(7369), 412–6, doi:10.1038/nature10464, 2011.

Smith, K. S., Jakubzick, C., Whittam, T. S. and Ferry, J. G.: Carbonic anhydrase is an ancient enzyme widespread in prokaryotes, Proc. Natl. Acad. Sci., 96(26), 15184–15189, doi:10.1073/pnas.96.26.15184, 1999.

Steinbacher, M., Bingemer, H. and Schmidt, U.: Measurements of the exchange of carbonyl sulfide (OCS) and carbon disulfide (CS_2) between soil and atmosphere in a spruce forest in central Germany, Atmos. Environ., 38(35), 6043–6052, doi:10.1016/j.atmosenv.2004.06.022, 2004.

Sun, W., Maseyk, K., Lett, C. and Seibt, U.: A soil diffusion–reaction model for surface COS flux: COSSM v1, Geosci. Model Dev., 8(10), 3055–3070, doi:10.5194/gmd-8-3055-2015, 2015.

Sun, W., Maseyk, K., Lett, C. and Seibt, U.: Litter dominates surface fluxes of carbonyl sulfide in a Californian oak woodland, J. Geophys. Res. Biogeosciences, 121(2), 438–450, doi:10.1002/2015JG003149, 2016.

Van Diest, H. and Kesselmeier, J.: Soil atmosphere exchange of carbonyl sulfide (COS) regulated by diffusivity depending on water-filled pore space, Biogeosciences, 5(2), 475–483, doi:10.5194/bg-5-475-2008, 2008.

Vance, E. D., Brookes, P. C. and Jenkinson, D. S.: An extraction method for measuring soil microbial biomass C, Soil Biol. Biochem., 19(6), 703–707, doi:10.1016/0038-0717(87)90052-6, 1987.

Wehr, R., Commane, R., Munger, J. W., McManus, J. B., Nelson, D. D., Zahniser, M. S., Saleska, S. R. and Wofsy, S. C.: Dynamics of canopy stomatal conductance, transpiration, and evaporation in a temperate deciduous forest, validated by carbonyl sulfide uptake, Biogeosciences Discuss., (September), 1–17, doi:10.5194/bg-2016-365, 2016.

Whelan, M. E., Hilton, T. W., Berry, J. A., Berkelhammer, M., Desai, A. R. and Campbell, J. E.: Carbonyl sulfide exchange in soils for better estimates of ecosystem carbon uptake, Atmos. Chem. Phys., 16(6), 3711–3726, doi:10.5194/acp-16-3711-2016, 2016.

Whelan, M. E., Min, D.-H. and Rhew, R. C.: Salt marsh vegetation as a carbonyl sulfide (COS) source to the atmosphere, Atmos. Environ., 73, 131–137, doi:10.1016/j.atmosenv.2013.02.048, 2013.

Whelan, M. and Rhew, R.: Carbonyl sulfide produced by abiotic thermal and photo-degradation of soil organic matter from wheat field substrate, J. Geophys. Res. Biogeosciences, 95343, n/a-n/a, doi:10.1002/2014JG002661, 2015.

Wohlfahrt, G., Brilli, F., Hörtnagl, L., Xu, X., Bingemer, H., Hansel, A. and Loreto, F.: Carbonyl sulfide (COS) as a tracer for canopy photosynthesis, transpiration and stomatal conductance: potential and limitations†, Plant. Cell Environ., 35(4), 657–667, doi:10.1111/j.1365-3040.2011.02451.x, 2012.

Xu, X., Thornton, P. E. and Post, W. M.: A global analysis of soil microbial biomass carbon, nitrogen and phosphorus in terrestrial ecosystems, Glob. Ecol. Biogeogr., 22(6), 737–749, doi:10.1111/geb.12029, 2013.

Yang, Z., Kanda, K., Tsuruta, H. and Minami, K.: Measurement of biogenic sulfur gases emission from some Chinese and Japanese soils, Atmos. Environ., 30(13), 2399–2405, doi:10.1016/1352-2310(95)00247-2, 1996.

Yi, Z., Wang, X., Sheng, G., Zhang, D., Zhou, G. and Fu, J.: Soil uptake of carbonyl sulfide in subtropical forests with different successional stages in south China, J. Geophys. Res., 112(D8), D08302, doi:10.1029/2006JD008048, 2007.

Supplementary Information

Figure S1. Experimental setup used to measure the soil-air CO_2 and OCS exchange rates sequentially on 6 soil microcosms and a control. Dry air comes from a compressor as described in the text.. Mass flow controllers through the chambers were set to 0.25 L min^{-1}.

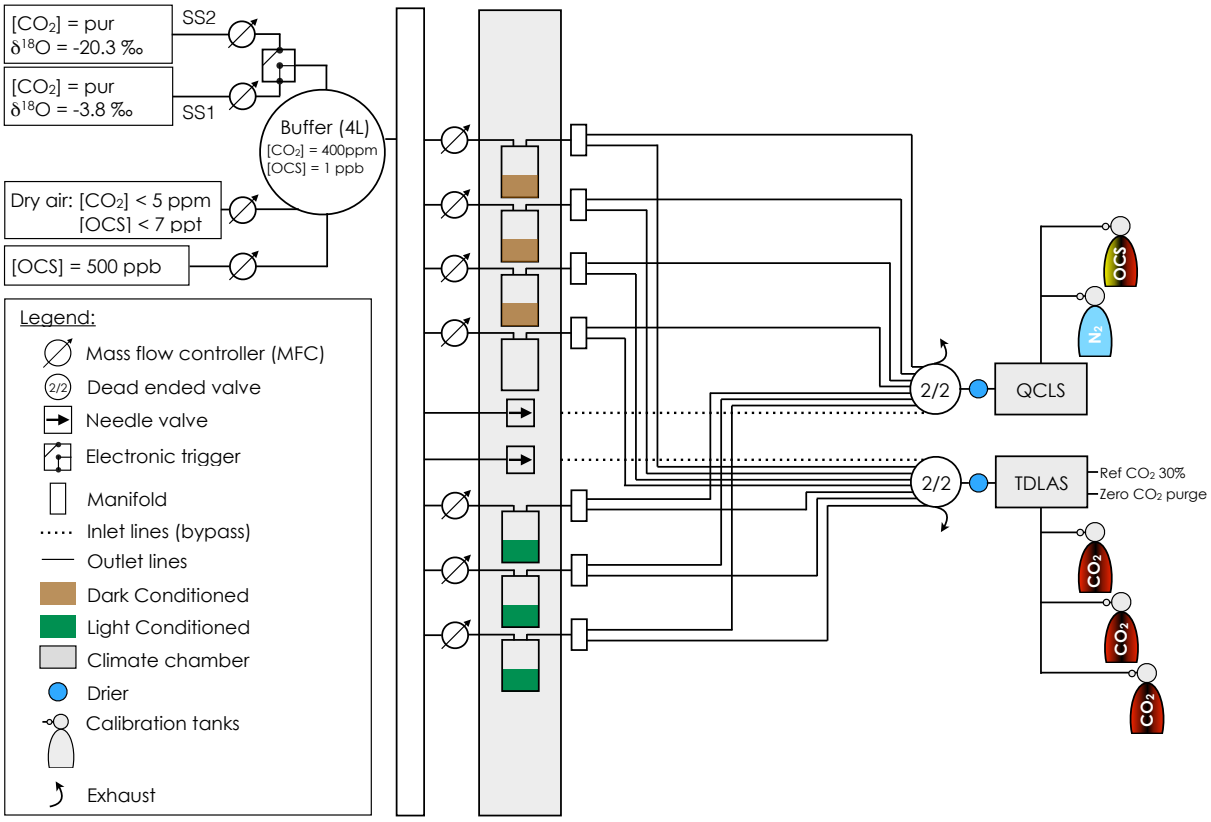

Figure S2. Example of the sequence used for the measurement of OCS and CO_2 fluxes from a soil microcosm and the control (blank) microcosm. CAL1: calibration tank #1. CAL2: calibration tank #2. ABG: auto-background. Mixing ratios are not recorded during the instrument auto-background. Measurements between ABG and CAL1 are for the inlet and outlet lines of the microcosm, measured sequentially 3 times.

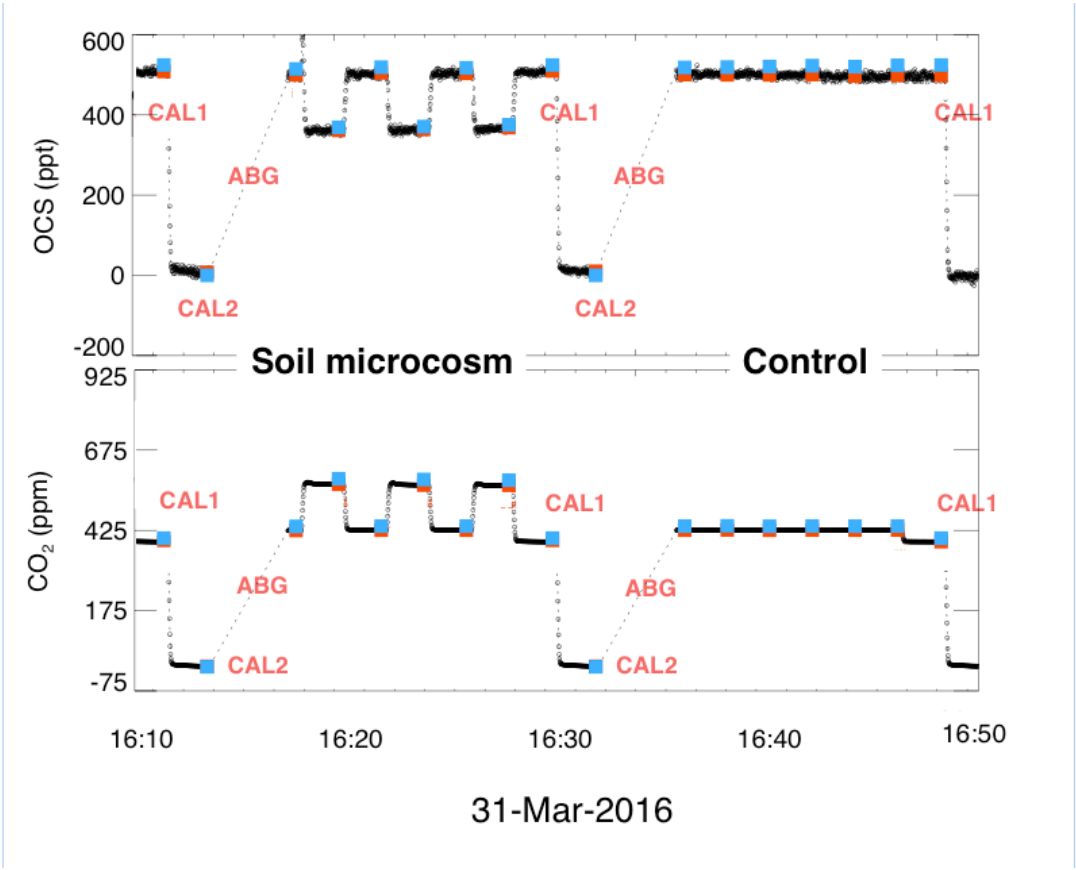

Figure S3. Variability in soil OCS fluxes for moist soils measured in the dark (full coloured bars) and in the light (stripes coloured bars). Statistically significant differences at the 5% level between light treatments are indicated by an asterisk (*).

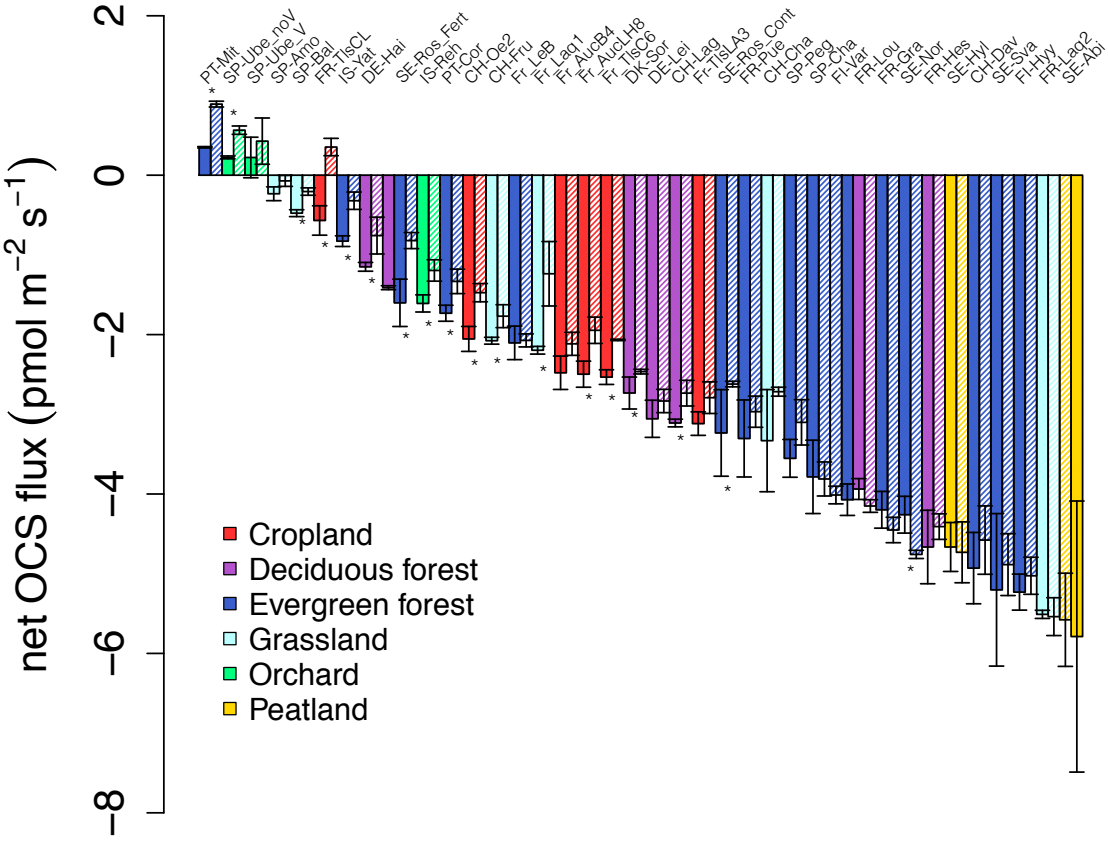

Figure S4. Variability in soil OCS fluxes for air-dried soils measured in the dark (full coloured bars) and in the light (stripes coloured bars). Statistically significant differences at the 5% level between light treatments are indicated by an asterisk (*).

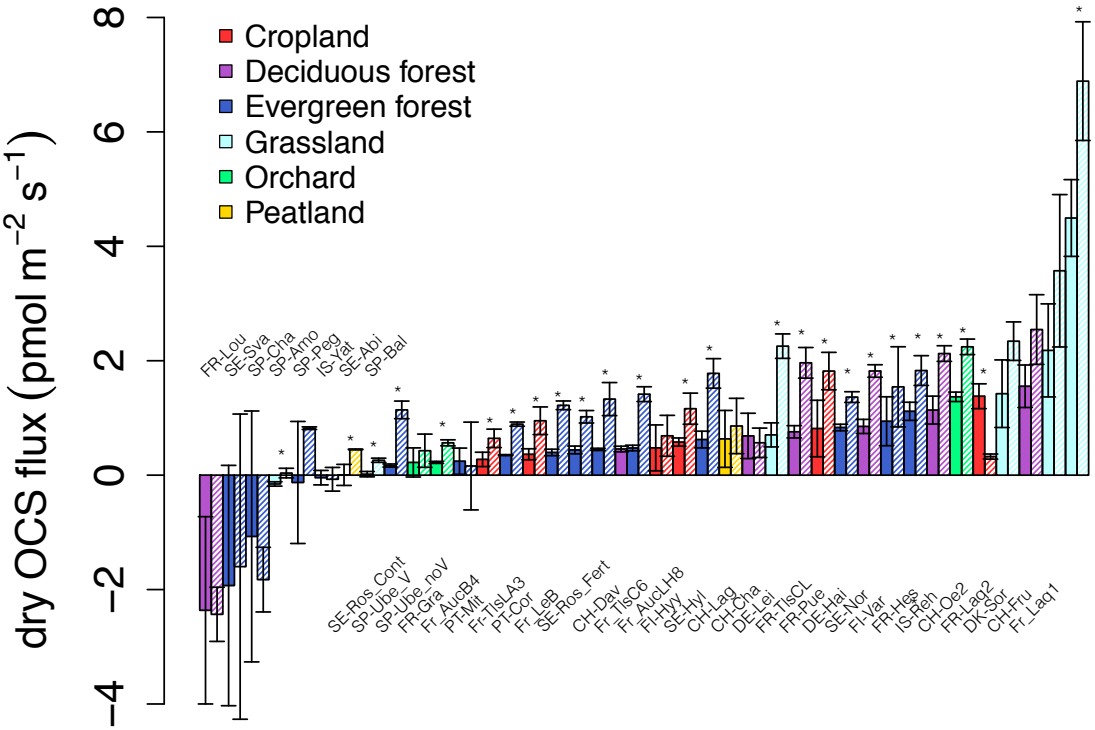

Figure S5. Variability in soil CO_2 fluxes for air-dried soils measured in the dark (close squares) and the light (open squares) with soil pH.

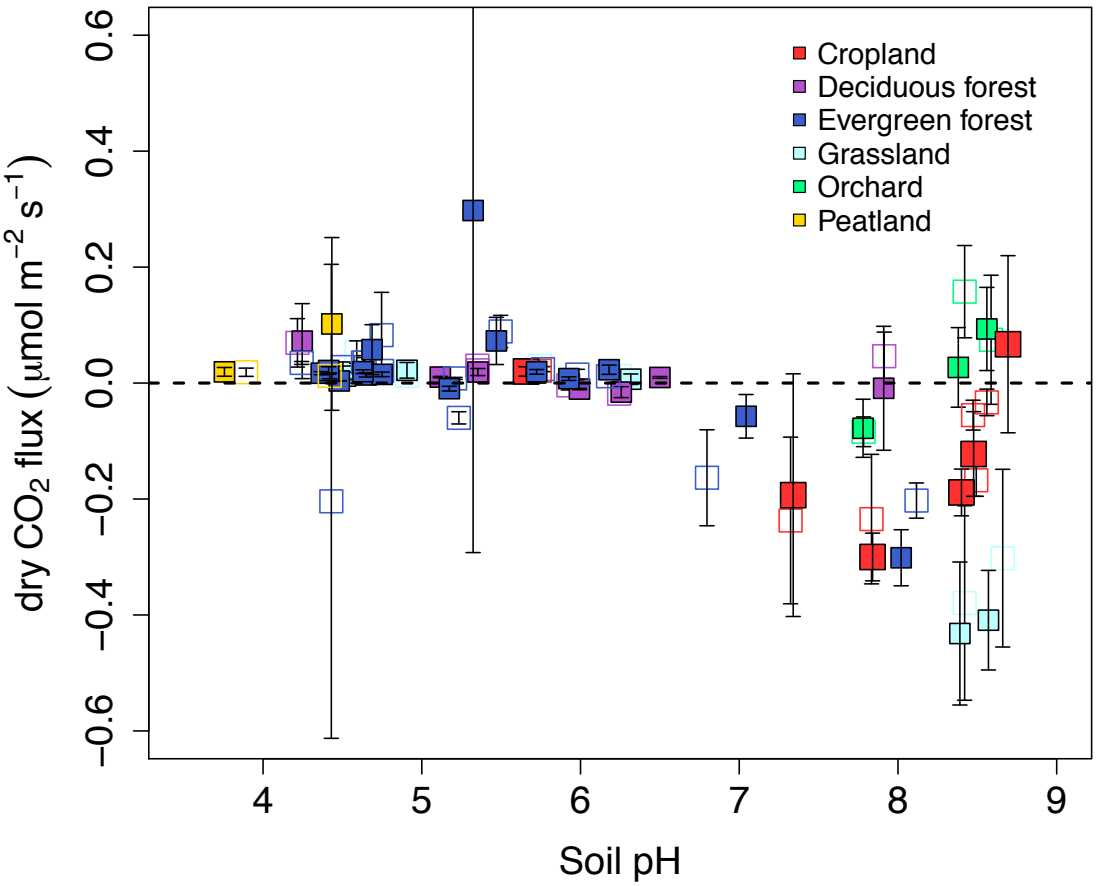

Figure S6. Variability in soil CO_2 fluxes for moist soils measured in the dark (full coloured bars) and in the light (stripes coloured bars).

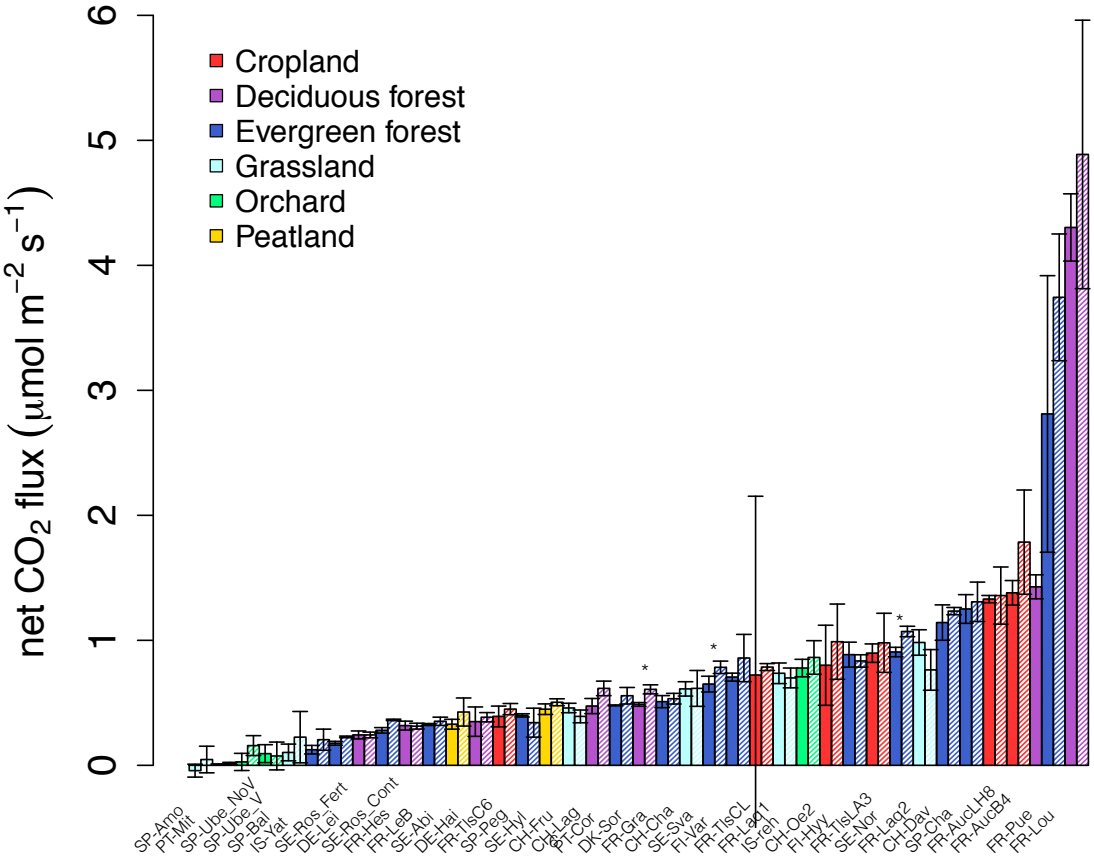

Conclusions générales et perspectives

L'objectif de cette thèse était de caractériser les variables biotiques et abiotiques responsables de la régulation de l'activité de l'anhydrase carbonique dans les sols. Pour cela nous avons couplé deux approches expérimentales basées sur deux traceurs du cycle du carbone, les isotopes stables de l'oxygène ($CO^{18}O$) et l'oxysulfure de carbone (OCS). Plus précisément, les travaux réalisés ont eu pour but de corréler l'activité de l'AC à un paramètre abiotique d'une part (le pH du sol) et à un paramètre biotique d'autre part (l'abondance des communautés de bactéries, de champignons et de microorganismes phototrophes du sol).

En accord avec la littérature, nous avons opté pour une sélection des sols en fonction de leur variabilité en terme de pH et nous avons fait l'hypothèse, ces deux paramètres étant intimement liés, que cela engendrerait une fluctuation naturelle au sein des communautés microbiennes du sol (Griffiths et al., 2011; Lauber et al., 2008; Tedersoo et al., 2014).

Pour évaluer l'importance de ces deux paramètres et identifier les mécanismes impliqués, nous avons réalisé une série d'expériences au laboratoire, sur des sols présentant une grande variabilité en terme de pH. Les travaux réalisés dans cette thèse ont représenté des avancées importantes en termes de méthodologie permettant d'estimer l'activité de l'AC du sol ainsi que de compréhension des mécanismes de régulation de cette enzyme, que son activité soit estimée à partir du $CO^{18}O$ ou de l'OCS.

Avancées « technologiques » :

Pour estimer l'activité de l'AC *via* deux traceurs du cycle de carbone (*i.e.* le CO_2 associé aux isotopes stables de l'oxygène et l'OCS), une première partie des travaux de cette thèse à porté sur le perfectionnement, le développement, voire la création de routines spécifiques pour chacun des traceurs utilisés (*i.e.* mesures des isotopes stables de l'oxygène (k_{iso}) ou des concentrations d'OCS (k_h). A partir des échanges isotopiques ayant lieu entre le sol et l'atmosphère nous avons ainsi proposé une nouvelle approche, non destructive, pour estimer dans un même temps la signature isotopique de l'eau du sol en équilibre avec le CO_2 atmosphérique et l'activité de l'AC du sol (Jones et al., in prep; Sauze et al., in prep). Nous avons par ailleurs décrit de manière mécaniste les échanges sol-atmosphère d'OCS, ce qui

nous a permis ensuite d'en dériver l'activité de l'AC du sol (Ogée et al., 2016). Ces deux nouvelles approches ont systématiquement été utilisées, parfois couplées, pour extraire de nos expériences les activités d'AC des différents sols.

Avancées scientifiques :

Bien que dans la littérature l'OCS soit utilisé comme un analogue du CO_2, au point que notre description mécaniste des flux sols-atmosphère d'OCS soit calquée sur celle du CO_2, nous avons mis en évidence que le comportement de l'anhydrase était finalement assez différents vis à vis de chacun de ces deux substrats. *In fine*, pour estimer l'activité de l'AC en utilisant correctement ces deux traceurs il est nécessaire, *a minima*, de décrire leurs réponses respectives au pH et leurs liens avec les communautés microbiennes du sol (bactérienne, fongique et algale). Plus précisément, dans le cas du CO_2 et des isotopes stables de l'oxygène, la réponse au pH du sol semble aujourd'hui ubiquiste. Principalement du fait de la spéciation du CO_2 dans l'eau, nous avons pu mettre en évidence qu'un sol au pH trop alcalin, où le CO_2 en solution est sous la forme HCO_3^- voir CO_3^{2-}, inhibait l'activité de l'α-AC, et probablement des autres formes d'AC, en raison du manque de substrat pour l'enzyme. Dans un sol au pH trop acide, c'est directement la fonctionnalité de l'α-AC qui est dégradée, engendrant à nouveau une inhibition de l'activité enzymatique. En estimant l'activité de la même α-AC, à partir des flux d'OCS, nous avons *a contrario* montré l'absence de réponse de l'α-AC au pH. Aujourd'hui nous ne sommes pas capables de dire si la réponse au pH du sol, dans le cas de l'utilisation de l'OCS est négligeable, incomprise ou bien si c'est le type d'AC utilisée qui n'est pas favorable à une catalyse de l'hydrolyse de l'OCS et qui engendre cette absence de réponse.

Pour décrire les flux d'OCS échangés entre le sol et l'atmosphère Sun et al. (2015), puis Ogée et al. (2016), ont montré qu'une approche mécaniste, intégrant différents niveaux de complexité dans la description des mécanismes impliqués, était nécessaire. Au vu de nos mesures effectuées sur une large gamme de sols collectés au travers de l'Europe, nous avons confirmé que l'approche proposée par Ogée et al. (2016) intégrant à la fois des mécanismes physico-chimiques (diffusion et hydrolyse de l'OCS dans la matrice de sol, réponse au pH…) et biologiques (dépendance à la biomasse microbienne) était l'approche la plus adaptée pour reproduire ces flux d'OCS et estimer l'activité d'AC associée. Mais notre compréhension des mécanismes régulant ces flux évolue toujours aujourd'hui et cette approche peut donc être affinée. En effet pour faire coller le modèle d'Ogée et al. à notre étude nous avons jouer sur les valeurs de $(k_{cat}/k_M)_{max}$ montrant dans un premier temps l'importance des différentes

familles d'AC qui peuvent être impliquées et la connaissance des propriétés structurales, cataboliques, *etc*… de ces enzymes. Nous avons également souligné que bien que l'hypothèse faite sur la dépendance des flux d'OCS à la biomasse microbienne soit cohérente avec une vue générale de nos résultats, la manière dont nous faisons intervenir aujourd'hui ce paramètre pourrait être améliorée.

Ces travaux nous ont également permis de mettre en lumière le rôle significatif des communautés microbiennes pour représenter à la fois les flux sol-atmosphère de CO_2 et d'OCS. Toutefois, une fois encore ces deux gaz ont répondu différemment aux divers paramètres biotiques mesurés. D'un coté les flux de CO_2 et de $CO^{18}O$, ainsi que l'activité d'AC associée, ont répondu positivement et exclusivement à l'abondance des communautés photosynthétiques du sol. Pour mémoire, le terme de microorganismes photosynthétiques, ou phototrophes, correspond dans le cas de notre étude aux algues eucaryotes et aux cyanobactéries procaryotes et n'inclut pas les bactéries phototrophes anoxygéniques qui pourraient également utiliser le CO_2 comme source de carbone. De l'autre, les flux d'OCS et l'activité d'AC associée, ont été strictement corrélés à l'abondance des champignons. Si nous souhaitons améliorer notre représentation des flux de carbone échangés entre le sol et l'atmosphère, nous devons donc nous appuyer sur une connaissance plus poussée de l'abondance des microorganismes photosynthétiques dans le cas des flux de CO_2, et intégrer l'abondance des champignons dans le cas de l'OCS.

Perspectives :

Suite aux résultats obtenus, deux grandes perspectives se dessinent pour continuer d'explorer plus en profondeur les différents paramètres contrôlant les mécanismes de régulation de l'activité de l'AC.

Approfondir nos connaissances sur les paramètres abiotiques de régulation de l'AC

Tout d'abord nous avons évoqué une inhibition de l'activité de l'AC en lien avec le pH du sol. Mais le pH n'est potentiellement pas le seul facteur inhibant/exaltant l'activité de l'AC. Il est également possible d'approfondir cette question en tenant compte la chimie du sol. En effet, la présence d'anions / cations spécifiques pourrait également expliquer, en partie, une plus ou moins grande activité de l'AC. A partir de mesures des isotopes stables de l'oxygène, les ions phosphates ont par exemple été proposés comme activateurs et inhibiteur de l'AC (Rowlett et al., 1991; Rusconi et al., 2004). Rowlett et al. (1991) ont également proposé que les ions

sulfates soient des inhibiteurs de l'activité de l'AC car en se liant à l'enzyme, ces ions en réduisent la réactivité.

Dans le cadre de cette thèse, nous avons nous-même mesuré la quantité totale de phosphore inorganique (P_i) de nos sols, lors de l'expérience testant la réponse de l'activité de l'α-AC au pH (Chapitre 3). Nos résultats ont suggéré que pour deux des sols étudiés, l'absence de réponse de l'α-AC, déterminée à partir de la mesure des isotopes stables de l'oxygène, soit corrélée à une valeur de P_i particulièrement élevée.

Des résultats annexes, obtenus récemment par notre équipe, semblent par ailleurs montrer que les ions nitrates pourraient, comme les ions sulfates, inhiber l'activité de l'AC, estimée à cette fois à partir des flux d'OCS. Ce résultat semble en accord avec la littérature (De Simone and Supuran, 2012) et pourrait ouvrir une nouvelle voie quant au rôle de la chimie du sol sur l'activité de l'AC estimée à partir des flux d'OCS. Surveiller le comportement des nitrates dans le sol semble d'autant plus intéressant qu'ils jouent par ailleurs un rôle important sur les microorganismes. La présence d'azote sous la forme de nitrate peut notamment favoriser certaines communautés plus que d'autres (comme les algues) et ainsi influencer le type d'AC présente dans le sol. A l'avenir, il serait donc intéressant de tester l'effet de certains ions tels que les sulfates, nitrates et phosphates sur l'activité de l'AC estimée toujours à partir de nos deux traceurs du cycle du C.

<u>Déterminer le rôle des communautés microbiennes (abondance et diversité) pour la régulation de l'activité de l'AC</u>

Une seconde perspectives serait d'aller plus loin dans le lien entre les communautés microbiennes présentes dans le sol et l'activité de l'AC du sol. Comme cela a été évoqué dans les Chapitres 4 et 5 de ce manuscrit, connaître l'abondance et la diversité des communautés microbiennes du sol (bactéries, champignons et microorganismes photosynthétiques) pourrait nous apporter des informations complémentaires sur les familles d'AC mises en jeu. En schématisant à l'extrême les informations trouvées dans la littérature, nous avons associé l'α-AC aux communautés photosynthétiques et plus précisément aux algues, la β-AC aux champignons et la γ-AC aux bactéries. Mais bien-sûr dans les faits ces trois types d'AC se retrouvent un peu dans chacune des familles de microorganismes cités. Connaître plus précisément la diversité des champignons du sol pourrait alors nous permettre de savoir si les changements observés dans les flux d'OCS, et probablement dans l'activité de l'AC, sont liés uniquement à des changements d'abondance de champignons ou si des modifications de diversité sont également importantes. Les résultats préliminaires de pyroséquençage que nous

avons à ce jour, et qui sont associés à l'expérience présentée dans le Chapitre 4, indiquent dans certains sols la présence de champignons du type *Mortierella* qui sont par ailleurs connus pour émettre de l'OCS (Masaki et al., 2016). Une analyse approfondie de ces résultats au regard des activités mesurées permettra de mieux appréhender le rôle de la diversité microbienne et d'identifier des groupes microbiens associés à la régulation de ces activités.
A terme, de nouvelles études couplant la détermination de l'activité de l'AC avec des mesures de la diversité microbienne sur des échantillonnages de grande ampleur (en termes de nombre de sols) représentatifs de sols contrastés (en termes pédoclimatiques) permettra d'affiner encore notre connaissance des paramètres microbiens de régulation de l'activité de cette enzyme dans le sol.

Modélisation à grande échelle des flux de carbone

Comme cela a été évoqué en introduction, améliorer notre compréhension et mieux décrire les mécanismes régulant l'activité de l'AC du sol a pour objectif ultime d'apporter de nouvelles contraintes à nos représentations à grandes échelles des flux de carbone. Nous nous sommes focalisés sur le compartiment sol, dont le rôle est relativement méconnu, mais dont la réponse au changement climatique est impérativement à dissocier de celle des plantes pour améliorer nos projections futures des flux globaux de carbone. Nous avons choisi d'orienter nos recherches exclusivement sur le sol mais bien-sûr une dernière perspective serait d'extrapoler les questions que nous nous sommes ici posées à d'autres compartiments de la biosphère, voire un système plus complexe comprenant les interactions sol-plantes-atmosphère. Dans cette perspective, des expériences ont déjà été réalisées au sein de mon groupe de recherche pour étudier les flux d'OCS dans le cas, très spécifique, des environnements dominés par les bryophytes (Gimeno et al., submitted New Phytologist). Les résultats obtenus sur deux types de bryophytes suggèrent que les flux bruts d'OCS mesurés seraient en fait le résultat de deux flux nets et de sens opposés : une émission et une adsorption d'OCS. Les émissions d'OCS par les bryophytes seraient d'autant plus grandes avec des températures et une luminosité élevées. Ces résultats n'ont pas encore pu être extrapolés à d'autres plantes. Toutefois si les échanges d'OCS ne sont *in fine* pas unidirectionnels, cela soulève des questions essentielles quant à l'utilisation de l'OCS comme traceur de la GPP. Avec cette expérience, et en toute cohérence avec les travaux détaillés dans ce manuscrit, nous avons également proposé que les émissions d'OCS par les bryophytes soient dépendantes des microorganismes qu'elles hébergent. Les deux espèces utilisées étaient en effet connues pour former des associations symbiotiques avec des champignons et des bactéries qui pour certains produisent de l'OCS.

L'hypothèse peut donc être émise que les symbiotes naturels contribuent aux flux nets d'OCS. Enfin, ces travaux nous ont permis d'ouvrir la porte à de nouveaux facteurs contrôlant l'activité de l'AC, et souligner une fois de plus la complexité des mécanismes impliquant l'AC. En effet, nous avons proposé que la dégradation des protéines formant les chaines d'acides aminés aurait aussi un impact sur l'activité de l'AC, qui en retour affecte les mécanismes de photosynthèses. En conclusion, nous avons à ce jour apporté de nombreux éléments de réponse quant aux facteurs contrôlant les mécanismes derrière l'activité de l'AC (biotiques et abiotiques), que ce soit pour son rôle dans la catalyse de l'hydratation du CO_2 ou de l'hydrolyse de l'OCS. Cependant il apparaît également clairement que nous avons ouvert la porte à de nombreuses questions, particulièrement autour de l'utilisation de l'OCS et de son potentiel comme traceur de GPP.

Références

Gimeno, T.E., Ogée, J., Royles, J., Gibon, Y., West, J., Burlett, R., Jones, S.P., Sauze, J., Wohl, S., Griffiths, H., Benard, C. and Wingate, L.: Bryophyte gas-exchange dynamics along varying hydration status reveal a significant COS sink in the dark and COS source in the light, New Phytol (submitted).

Griffiths, R. I., Thomson, B. C., James, P., Bell, T., Bailey, M. and Whiteley, A. S.: The bacterial biogeography of British soils, Environ. Microbiol., 13(6), 1642–1654, doi:10.1111/j.1462-2920.2011.02480.x, 2011.

Jones, S. P., Sauze, J., Ogée, J., , Wohl, S., Fernandez-Prado, N., Saavedra-Belanga, N., Sajus, T., Bosc, A., and Wingate, L.: Non-destructive estimates of soil carbonic anhydrase activity and soil water oxygen isotope composition, in prep

Lauber, C. L., Strickland, M. S., Bradford, M. A. and Fierer, N.: The influence of soil properties on the structure of bacterial and fungal communities across land-use types, Soil Biol. Biochem., 40(9), 2407–2415, doi:10.1016/j.soilbio.2008.05.021, 2008.

Masaki, Y., Ozawa, R., Kageyama, K. and Katayama, Y.: Degradation and emission of carbonyl sulfide, an atmospheric trace gas, by fungi isolated from forest soil, edited by R. Boden, FEMS Microbiol. Lett., 363(18), 1–7, doi:10.1093/femsle/fnw197, 2016.

Ogée, J., Sauze, J., Kesselmeier, J., Genty, B., Van Diest, H., Launois, T. and Wingate, L.: A new mechanistic framework to predict OCS fluxes from soils, Biogeosciences, 13(8), 2221–2240, doi:10.5194/bg-13-2221-2016, 2016.

Rowlett, R. S., Gargiulo, N. J., Santoli, F. A., Jackson, J. M. and Corbett, A. H.: Activation and Inhibition of Bovine Carbonic Anhydrase III by Dianions, J. Biol. Chem., 266(2), 933–941, 1991.

Rusconi, S., Innocenti, A., Vullo, D., Mastrolorenzo, A., Scozzafava, A. and Supuran, C. T.: Carbonic anhydrase inhibitors. Interaction of isozymes I, II, IV, V, and IX with phosphates, carbamoyl phosphate, and the phosphonate antiviral drug foscarnet, Bioorg. Med. Chem. Lett., 14(23), 5763–5767, doi:10.1016/j.bmcl.2004.09.064, 2004.

Sauze, J., Jones, S., Wingate, L., Wohl, S. and Ogée, J.: The role of soil pH on soil carbonic anhydrase activity, Biogeosciences, in prep

De Simone, G. and Supuran, C. T.: (In)organic anions as carbonic anhydrase inhibitors, J. Inorg. Biochem., 111, 117–129, doi:10.1016/j.jinorgbio.2011.11.017, 2012.

Tedersoo, L., Bahram, M., Polme, S., Koljalg, U., Yorou, N. S., Wijesundera, R., Ruiz, L. V., Vasco-Palacios, A. M., Thu, P. Q., Suija, A., Smith, M. E., Sharp, C., Saluveer, E.,

Saitta, A., Rosas, M., Riit, T., Ratkowsky, D., Pritsch, K., Poldmaa, K., Piepenbring, M., Phosri, C., Peterson, M., Parts, K., Partel, K., Otsing, E., Nouhra, E., Njouonkou, A. L., Nilsson, R. H., Morgado, L. N., Mayor, J., May, T. W., Majuakim, L., Lodge, D. J., Lee, S. S., Larsson, K.-H., Kohout, P., Hosaka, K., Hiiesalu, I., Henkel, T. W., Harend, H., Guo, L. -d., Greslebin, A., Grelet, G., Geml, J., Gates, G., Dunstan, W., Dunk, C., Drenkhan, R., Dearnaley, J., De Kesel, A., Dang, T., Chen, X., Buegger, F., Brearley, F. Q., Bonito, G., Anslan, S., Abell, S. and Abarenkov, K.: Global diversity and geography of soil fungi, Science (80-.)., 346(6213), 1256688–1256688, doi:10.1126/science.1256688, 2014.

Liste des figures

Liste des tables

Annexe 1

Bryophyte gas-exchange dynamics along varying hydration status reveal a significant COS sink in the dark and COS source in the light

Teresa E. Gimeno[1,*], Jérôme Ogée[1], Jessica Royles[2], Yves Gibon[3], Jason B. West[4], Régis Burlett[5], Sam P. Jones[1], **Joana Sauze**[1], Steven Wohl[1], Camille Benard[3], Bernard Genty[6], Lisa Wingate[1]

[1]ISPA, Bordeaux Science Agro, INRA, 33140 Villenave d'Ornon, France
[2]Department Plant Sciences, University of Cambridge, Cambridge CB2 3EA, UK
[3]Plateforme Métabolome du Centre de Génomique Fonctionnelle Bordeaux, PHENOME INRA, University of Bordeaux, UMR BFP 1332, 33140 Villenave d'Ornon, France.
[4]Department of Ecosystem Science & Management, Texas A&M University, College Station, TX, USA
[5]INRA, University of Bordeaux, UMR BIOGECO, 33450 Talence, France
[6]CNRS/CEA/Aix-Marseille University, UMR 6191 BVME, Saint-Paul-lez-Durance, France

[*]Corresponding author:
Teresa E. Gimeno
E-mail: teresa.gimeno@inra.fr
Phone: +33 (0) 5 57 12 25 96

Accepted in *New Phytologist* in March 2017

Bryophyte gas-exchange dynamics along varying hydration status reveal a significant COS sink in the dark and COS source in the light

Teresa E. Gimeno[1,*], Jérôme Ogée[1], Jessica Royles[2], Yves Gibon[3], Jason B. West[4], Régis Burlett[5], Sam P. Jones[1], Joana Sauze[1], Steven Wohl[1], Camille Benard[3], Bernard Genty[6], Lisa Wingate[1]

[1]ISPA, Bordeaux Science Agro, INRA, 33140 Villenave d'Ornon, France
[2]Department Plant Sciences, University of Cambridge, Cambridge CB2 3EA, UK
[3]Plateforme Métabolome du Centre de Génomique Fonctionnelle Bordeaux, PHENOME INRA, University of Bordeaux, UMR BFP 1332, 33140 Villenave d'Ornon, France.
[4]Department of Ecosystem Science & Management, Texas A&M University, College Station, TX, USA
[5]INRA, University of Bordeaux, UMR BIOGECO, 33450 Talence, France
[6]CNRS/CEA/Aix-Marseille University, UMR 6191 BVME, Saint-Paul-lez-Durance, France

[*]Corresponding author:
Teresa E. Gimeno
E-mail: teresa.gimeno@inra.fr
Phone: +33 (0) 5 57 12 25 96

Total word count: 6747

- Introduction: 1150
- Material and methods: 2638
- Results: 876
- Discussion: 1976
- Acknowledgements: 107

References: 56
Tables: 2
Figures: 5 (Fig. 1, 2 & 5 in colour, Fig. 3 in black and white and Fig. 4 in grey scales)
Supporting Information: 1 Table & 5 Figures

Submitted to *New Phytologist* in December 2016

SUMMARY

- *Rationale:* Carbonyl sulphide (COS) is a potential tracer of gross primary productivity (GPP), assuming a unidirectional COS flux into the vegetation that scales with GPP. However, carbonic anhydrase (CA), the enzyme that hydrolyses COS, is expected to be light independent, thus plants without stomata should continue to take up COS in the dark.
- *Method:* We measured net CO_2 (A^C) and COS (A^S) uptake rates from two astomatous bryophytes at different relative water contents (RWC), COS concentrations, temperatures and light intensities.
- *Results:* We found large A^S in the dark, indicating that CA activity continues without photosynthesis. More surprisingly, we found a non-zero COS compensation point in light and dark conditions, indicating a temperature-driven COS source with a Q_{10} (fractional change for a 10 °C temperature increase) of 3.7. This resulted in greater A^S in the dark than in the light at similar RWC. The processes underlying such COS emissions are still unknown.
- *Conclusion:* Our results suggest that ecosystems dominated by bryophytes might be strong atmospheric sinks of COS at night and weaker sinks or even sources of COS during daytime. Biotic COS production in bryophytes could result from symbiotic fungal and bacterial partners that could also be found on vascular plants

Keywords: carbohydrates, desiccation, liverwort, *Marchantia polymorpha*, moss, protein, *Scleropodium purum*, respiration.

INTRODUCTION

Carbonyl sulphide (COS) is the most abundant sulphur-containing gas in the troposphere and has the potential to serve as a proxy for estimating gross primary productivity (GPP, Sandoval-Soto *et al.*, 2005; Montzka *et al.*, 2007; Campbell *et al.*, 2008). The foundation for using COS as a GPP tracer is built on the assumption that terrestrial uptake is dominated by, and proportional to, plant photosynthetic activity. This is because COS is taken up by plants following a similar pathway to that of CO_2. COS diffuses into the vegetation through the stomatal pores and is hydrolysed by the enzyme carbonic anhydrase (CA) in the mesophyll cells (Protoschill-Krebs *et al.*, 1996). However, in contrast to CO_2 hydration by CA, COS hydrolysis by CA is irreversible (Notni *et al.*, 2007) and no other leaf-level processes have been identified in the production of COS (Bloem *et al.*, 2015). Thus, COS uptake (A^S) is assumed to be unidirectional and not the net result of two opposed fluxes (photosynthesis and respiration in the case of CO_2). This assumption is key for the calculation of GPP from COS fluxes, together with an estimate of the ratio between CO_2 and COS uptake, the so-called 'leaf relative uptake' (LRU, Campbell *et al.*, 2008). Relying on LRU for estimating GPP requires some important assumptions. Principally, the LRU approach assumes that the consumption of CO_2 and COS diffusing into the leaf is linked to downstream light-dependent reactions. However, CA activity is expected to be light independent (Protoschill-Krebs *et al.*, 1996). Thus, as long as stomata remain open, a sink for COS should be maintained in the dark when CO_2 uptake ceases and A^C becomes dominated by leaf respiration. Indeed an uncoupling of A^C and A^S (i.e. more variable and usually larger LRU values) has been reported at low light intensities in the lab (Stimler *et al.*, 2011) and in the field at night (Berkelhammer *et al.*, 2014; Commane *et al.*, 2015). Furthermore, the utility of COS as a tracer of GPP depends heavily on the assumption that the flux of COS between the atmosphere and the leaf is one-way and driven by CA activity alone. This assumption has been validated at the leaf level for certain species and environmental conditions (Stimler *et al.*, 2010; Sandoval-Soto *et al.*, 2012). However, recent field studies have shown that COS emissions from wheat leaves may occur during senescence and from deciduous forests during periods of high temperature and drought (Maseyk *et al.*, 2014; Commane *et al.*, 2015). Thus it is not entirely clear whether the unidirectional hypothesis holds in plants exposed to stress and whether COS emissions are masked to some extent by the stomata of vascular plants. Currently, the mechanisms underlying these COS emissions also remain unclear.

Plants without stomata such as bryophytes are a potentially useful model that could provide important insights on the dynamics of A^S under varying environmental conditions. These dynamics would otherwise be difficult to detect in the presence of stomata that actively impose diffusional limitations. In astomatous plants, the dynamics of leaf COS fluxes should be more closely related to changes in the enzymatic activity and substrate availability. Disentangling diffusional and enzymatic processes for plant COS fluxes may be especially critical since stomata have been shown to open in response to an increase in the atmospheric COS mixing ratio (Stimler *et al.*, 2010; Stimler *et al.*, 2012), creating a potential feedback on leaf COS and CO_2 uptake. Although some bryophytes have tiny pores that facilitate gas exchange, they lack stomatal regulation (Proctor *et al.*, 2007) and seem therefore better suited for assessment of changes in leaf COS fluxes in response to changing environmental conditions.

Bryophytes lack active control of transpiration so they rapidly equilibrate with prevailing environmental conditions (Proctor *et al.*, 2007). Desiccation tolerance in these organisms involves a number of biochemical mechanisms such as the accumulation of non-structural carbohydrates and other compatible solutes or the up- or down-regulation of gene expression and protein synthesis (Oliver *et al.*, 2005). To reduce the rate of water loss, bryophytes also deploy morphological adaptations and preserve a thin layer of capillary water on their leafy shoots (Marschall & Proctor, 2004). Capillary water slows tissue desiccation, but it is a barrier to CO_2 diffusion. As a consequence, bryophyte A^C commonly displays a three-phase response to tissue dehydration. Initially, as diffusion-resistance through capillary water decreases with evaporation, A^C increases until a plateau in A^C is reached indicating the optimal hydration status for photosynthetic activity. As evaporation continues, A^C decreases as cells dehydrate and photosynthesis becomes metabolically impaired (Dilks & Proctor, 1979; Royles *et al.*, 2013). This layer of capillary water should pose a resistance not only to CO_2, but also to COS, and thus we suggest that a similar optimum-like response of A^S to desiccation should be observed in the light. Alternatively, in bryophytes with carbon concentration mechanisms similar to those of algae and cyanobacteria (Smith & Griffiths, 2000), external CA activity could potentially counterbalance the initial expected increase in A^S with desiccation (Rech *et al.*, 2008). In the dark, A^C flux is negative as respiration dominates and the magnitude of the respiratory flux decreases progressively with desiccation. However, in the absence of stomata and because CA is expected to be light-independent (Gries *et al.*, 1994; Protoschill-Krebs *et al.*, 1996), we hypothesise that A^S should continue at similar rates to those observed in the light.

Bryophytes should also be a good model to test the assumption that COS emission does not occur, during the day/night cycle or in plants exposed to water or heat stress. Testing this hypothesis on vascular plants would be challenging, as A^S would be strongly limited by stomatal closure. The only previous study estimating the COS compensation point (Γ^S, the COS concentration at which A^S is zero) on non-vascular photoautotrophic organisms (lichens, Kuhn & Kesselmeier, 2000) suggested that Γ^S could be greater than zero. A positive Γ^S would imply that A^S is the net result of simultaneous COS uptake and emission. As far as we are aware no studies looking into the relationship between A^S-C^S have been conducted on astomatous plants to date.

Here, we challenge our current understanding of COS uptake by terrestrial plants using astomatous bryophytes as model organisms. Our aims were to provide a first estimate of the COS sink strength in bryophytes and to test some of the assumptions that underlie the proposed relationship between GPP and COS uptake. Specifically we hypothesised that (*1*) in astomatous bryophytes, COS uptake varies with tissue hydration analogously to CO_2 uptake in the light, (*2*) COS uptake dynamics during desiccation would be similar in the light and in the dark and (*3*) the COS compensation point would be zero. To test these hypotheses we ran a series of experiments under controlled conditions to characterise the response of A^S and A^C to desiccation, COS concentration and increasing light intensity and temperature, in two bryophyte species with contrasting life forms and evolutionary origin.

MATERIAL AND METHODS

Study species and sampling protocol

We chose two bryophytes with contrasting evolutionary origins and life forms, representative of temperate regions. The mat-forming liverwort *Marchantia polymorpha* L. has gametophytes with a complex thallus structure and occasional static pores to improve ventilation (Meyer *et al.*, 2008). The loosely packed weft-moss *Scleropodium purum* (Hedw.) Limpr. is a desiccation-tolerant slow-growing moss with feather-like shoots and poorly-developed rhizoids (Arroniz-Crespo *et al.*, 2008). Given their abundance and wide-spread distribution, both species have been the subjects of an ample body of literature. *Marchantia polymorpha* has served as a model bryophyte for characterizing plant physiology, metabolism and genetics (Bowman, 2016) while *S. purum* physiology and distribution have been widely studied in response to nutrient availability and heavy metal contamination (Arroniz-Crespo *et al.*, 2008).

Mats of moss and liverwort were collected locally from naturally growing populations at the INRA campuses of 'La Ferrade' (Villenave d'Ornon, France) and 'Pierroton' (Cestas, France). Mats of *M. polymorpha* were occasionally intermingled with *Lunularia cruciata* L., a liverwort with similar gametophytes to those of *M. polymorpha* in the absence of spore-bearing cups. The mats were collected 1-5 days before the experiments and maintained in ambient external light with regular watering. On the day before each experiment, green tissue was separated and rinsed with deionized (DI) water. Individual samples of 2.5-4 g (fresh mass) of green tissue were placed onto pierced aluminium circular trays (6.5 cm diameter). To fully rehydrate the tissue, sample trays were sprayed with DI water, placed onto moist paper and kept refrigerated in closed glass jars for 12-24 h. Before the start of the experiment, the jars were acclimated to room temperature for one hour. After blotting excess water from the trays, all trays were weighed to the nearest 0.1 mg and placed into gas-exchange chambers, a few minutes before the experiment. All trays were re-weighed at the end of each experiment.

Gas-exchange measurements

Experiments were carried out at the facility for online trace gas and stable isotope analyses at INRA-Bordeaux (France). The system comprised a set of gas analysers that measured CO_2, COS and H_2O mixing ratios of the inlet and outlet airstreams from seven multiplexed gas-exchange chambers. Each chamber consisted of a 0.5 L glass jar and a glass top fitted with two stainless steel Swagelok® connectors attached to 0.25 inch (3.175 mm) Teflon™ inlet and outlet lines. The gas-exchange chambers were housed in a climatically-controlled chamber that regulated air temperature, relative humidity and light intensity, outside the chambers (MD1400, Snijders, Tillburg, NL). Inside each chamber, temperature was monitored continuously with self-contained thermocouple data-loggers (Hygrochron Temperature & Humidity iButton, DS1923, Embedded Data Systems, Lawrenceburg, KY, US), placed on the aluminium trays in direct contact with the samples but not completely covered by them. Air pressure inside the chambers was established with a pressure-transducer (BMP180, Bosch GmbH, Gerlingen, Germany), during preliminary experiments with the exact same flow of air and measuring sequence.

The airflow into each chamber was set to 250 mL min^{-1} on a dry air basis using individual mass-flow controllers (MFC, EL-Flow® Select, Bronkhorst, Ruurlo, NL). CO_2 and COS mixing ratios (C^C and C^S, respectively) of the inlet air were adjusted by mixing synthetic CO_2- and COS-free dry air from a compressor (FM2 Atlas Copto, Nacka, Sweden),

coupled to a chemical scrub column (Ecodry K-MT6, Parker Hannifin, Cleveland, OH, US), with two cylinders of commercial gas mixtures (pure CO_2 and 500 nmol mol^{-1} COS). Inlet and outlet C^C and C^S were pre-dried with a Nafion™ dryer (MD-070-24-S-2, Perma Pure LLC, NJ, USA) before being measured with a mid-infrared quantum cascade laser spectrometer (QCLS, Aerodyne Research Inc. Billerica, MA, USA). Flow through the instrument was maintained with a TriScroll 600 pump (Agilent Technolgies, Santa Clara, CA, USA) connected to the QCLS *via* a vacuum line. Instrument drift was corrected with frequent (every 14 minutes) background calibrations (with dry N_2) in all runs. In most runs (75%) a two-point standard calibration was also implemented using dry N_2 (zero) and compressed dry air with a COS concentration of 524.8 ± 2.2 pmol mol^{-1} from an Aculife®-treated cylinder that was prepared and calibrated for COS by the NOAA Global Monitoring Division. The 14-min frequency was based on instrument stability estimated from an Allan variance calculated from a 24h continuous measurement on tank air that indicated a standard deviation at 10 s averaging of 2.1 pmol mol^{-1} for COS, a deviation from pure white noise after more than 400 s and a standard deviation <1 pmol mol^{-1} after 900 s integration time (Supplementary information, Fig. S1).

The QCLS alternately measured inlet and outlet C^C and C^S over 120 s and only the mean of the last 10 s was used in further calculations. For each chamber, three consecutive inlet/outlet pairs were measured and the seven chambers were measured sequentially. We calculated CO_2 (A^C) and COS (A^S) net assimilation rates from the inlet and outlet concentration difference as follows:

$$A = \frac{f(C_e - C_o)}{M_d} \qquad \text{Eq. 1}$$

where f (mol s^{-1}) is the inlet flow rate (dry air basis), C_e and C_o are the CO_2 or COS mixing ratios (mol mol^{-1}) entering and leaving the chamber in dry air and M_d is the sample dry mass (kg). Because mixing ratios were determined on a dry air basis (because of the Nafion dryer upstream of the QCLS) only the flow of dry air on the inlet of the chamber was necessary to perform the mass balance. Net assimilations (A^C and A^S) were calculated from inlet/outlet pairs and then averaged (n = 3) for consecutive pairs of the same chamber. The leaflet relative uptake (LRU) rates of A^C and A^S normalised to their ambient concentrations were then computed as (Stimler *et al.*, 2010):

$$\mathrm{LRU} = \frac{A^S}{A^C}\frac{C_o^S}{C_o^C} \qquad \text{Eq. 2}$$

Outlet water vapour concentration was measured with an infrared gas analyser (IRGA, LI-6262, LI-COR, Lincoln, NE, USA). Analyser calibration was made prior to the

experiment with a dew-point generator (LI-610, LI-COR). Outlet water vapour concentration (W) of each chamber was measured for 240 s, after having flushed the instrument for 600 s and the mean of the last 10 s (W_o, mol mol^{-1}) was used for further calculations. The instantaneous transpiration rate of each chamber was calculated as in Eq. 1, substituting W for C, with $W_e = 0$. We fitted a spline to transpiration over time to derive continuous values of instantaneous transpiration for each sample (E_t in mm s^{-1} kg^{-1}). The estimated cumulative transpiration of each sample (E_{cum} in mm kg^{-1}) was then calculated as:

$$E_{\text{cum}} = \sum_{i=0}^{i=n} E_{t,i}\,(t_i - t_{i-1}) \qquad \text{Eq. 3}$$

where t is time in seconds since the start of the experiment and n is the experiment duration. We then calculated the fresh mass (M_f) of each sample at any given point in time ($M_{f,t}$) as:

$$M_{\text{f,t}} = M_{\text{f,end}} + E_{\text{total}} - E_{\text{cum,t}} \qquad \text{Eq. 4}$$

where $M_{f,end}$ is the sample mass at the end of the experiment and E_{total} is total transpiration (i.e. maximum E_{cum}). Then, we calculated sample relative water content over time (RWC_t):

$$\text{RWC}_\text{t} = \frac{M_{\text{f,t}} - M_\text{d}}{M_\text{d}} 100 \qquad \text{Eq.5}$$

Experimental design

We performed four experiments to (*1*) characterize A^C and A^S during desiccation in the light and in the dark, (*2*) determine whether a COS compensation point and a COS source term could be detected, (*3*) evaluate the temperature sensitivity of any COS source term and (*4*) test for the effect of light intensity and temperature on COS uptake. Metabolite concentrations and gas-exchange dynamics during desiccation in the light and in the dark were characterised for both the moss, *S. purum*, and the liverwort, *M. polymorpha*, (Experiment 1), whilst COS, temperature and light curves were performed only for the liverwort (Experiments 2-4), with larger uptake rates per unit of dry mass.

1. Desiccation curves

We measured A^C and A^S during desiccation for 10-13 h, in moss and liverwort samples, in the light and in the dark (Supplementary information, Fig. S2). We ran desiccation curves separately for each bryophyte (moss and liverwort) and light/temperature regime (light on/21°C and light off/16°C). During each desiccation experiment, six trays with fully hydrated samples were placed into gas-exchange chambers whilst one empty tray (also containing a temperature data-logger) was placed into a seventh (blank) chamber to check for any COS contamination during the experiment. During the desiccation experiment the chambers were placed in a light regime with a photosynthetic photon flux density (PPFD) of

580 µmol m^{-2} s^{-1} supplied by fluorescent lamps (BriteGro 2084, Sylvania, BioSystems, Wageningen, NL). According to the manufacturer, the spectral power distribution of these lamps was 400-700 nm, with only two minor peaks detected below 400 nm (UV), of a magnitude ten times smaller than the peaks at all other wavelengths. The temperature of the climatically-controlled chamber was 16°C in the dark and 21°C in the light. Temperature inside the blank chamber was 1-2°C higher than that of the climatically-controlled chamber (Supplementary information, Fig. S3). Sample chamber temperature varied with hydration status and transpiration rate (Fig. S2). CO_2 and COS mixing ratios (C^C and C^S) of the inlet air were set to: 410 µmol mol^{-1} CO_2 and 540 pmol mol^{-1} COS.

2. COS curves for determination of the COS-compensation point (Γ^S)

To test for the existence of a COS-compensation point (Γ^S) in the liverwort, we measured A^C and A^S at varying COS concentrations, in the light at 21°C and in the dark at 16°C. To minimise the effect of drying, COS curves were limited to the plateau of the A-RWC curve. We sequentially measured A^C and A^S at five C^S (510, 285, 385, 105 and 5-10 pmol mol^{-1}) on four liverwort samples, C^C was kept constant (410 µmol mol^{-1}). The same four samples were measured in the light and in the dark. We then estimated Γ^S as the C^S at which $A^S = 0$.

3. Temperature response curves

To assess the effect of temperature on the COS source term (P^S), we performed additional COS curves at three chamber temperatures (16, 21 and 25°C), in the light and in the dark. We measured four liverwort samples for each combination of temperature set point and light regime (for 25 and 16°C in the light and 16°C in the dark, only three). We measured A^C and A^S at four C^S (120, 200, 400 and 520 pmol mol^{-1}) while C^C was kept constant (410 µmol mol^{-1}). For each sample, including those from Experiment 3, we estimated P^S as the intercept of the linear regression between A^S and C^S, i.e. A^S at $C^S = 0$.

4. Light and temperature curves

To assess the effect of light intensity and temperature on COS uptake and emission, we measured A^C and A^S whilst gradually increasing light intensity and temperature. Similar to the COS curves, to minimise the effect of RWC, we successively measured A^C and A^S at five PPFD levels (0, 90, 255, 420 and 580 µmol m^{-2} s^{-1}), within the plateau of the A^S-RWC curve. Light curves were performed under ambient C^C and C^S (410 µmol mol^{-1} and 510 pmol mol^{-1}, respectively) on four liverwort samples and under ambient C^C and near-zero C^S (5-10 pmol mol^{-1}) on four different samples. The temperature inside the gas-exchange chamber increased with light intensity (Fig. S3).

Biochemical assays

To assess the change in total protein and non-structural carbohydrate (NSC) content during desiccation we performed additional desiccation curves, under similar conditions as described above, in the light and in the dark, with successive sampling. We collected three replicate samples (per species and light level) consisting of 1-3 g of tissue at five points in time. For the liverworts, tissue RWC at different points in time was estimated from three independent samples (for each light level) that were conserved intact along the whole desiccation curve. For the mosses, tissue RWC was measured individually on a separate sub-sample at the time of collection.

Quantification of total protein content and NSC was performed following enzymatic digestion as in Biais *et al.* (2014) at the HitMe platform of the INRA-Bordeaux Metabolome Facility (France). Briefly, ~20 mg aliquots of frozen sample were powder-homogenised and fractionated three times at 95°C for 15 minutes with 250 and 150 µL (80 % v/v) and 250 µL (50% v/v) ethanol, 10 mM Hepes/KOH (pH 6). Glucose, fructose and sucrose concentrations were quantified from the ethanolic supernatant following an adapted procedure from Jelitto *et al.* (1992). Aliquots of 50 µL of ethanolic extract were added to 160 µL of a mix of 100 mM HEPES–KOH buffer (pH 7), 3 mM $MgCl_2$, 3 mM ATP, 1.3 mM NADP and 5 units of glucose-6-phosphate dehydrogenase. Then, 1 unit of hexokinase, 1 unit of phosphoglucose isomerase, and 30 units of invertase were added successively. Glucose, fructose and sucrose content were quantified from the difference in absorbance between successive steps. Total protein content and starch were determined from the pellet resuspended in 100 mM NaOH and heated at 95°C for 30 minutes (Hendriks *et al.*, 2003). Total protein content was quantified using Bradford reagent (Bradford, 1976). Analyses were run in duplicate. Extractions and assays were performed using a robotised Starlet platform (Hamilton, Villebon sur Yvette, France) and absorbencies were read at 340 nm for NSC and 600 nm for protein in MP96 readers (SAFAS, Monaco). All chemicals were purchased from Sigma-Aldrich Ltd. (Gillingham, UK) and enzymes from Roche Applied Science (Meylan, France)

Statistical analyses

To test that A^S would show an optimum-like response to desiccation similar to that of A^C in the light, and that A^S during desiccation would not differ between the light and the dark, we fitted general additive mixed models (GAMMs). GAMMs were fitted to A^C and A^S with RWC as a predictor and taking into account the random sample-to-sample variability (Wood, 2006). Significant differences (α = 0.05) between the light and the dark were assessed

graphically based on non-overlapping 95% CI's. We used package *mgcv*, in R version 3.3.1 (R Development Core Team, 2014). To quantify the effect of C^S on liverwort A^C and A^S, we fitted linear mixed models (LMMs) with C^S and light and temperature regime (dark/cool vs. light/warm) as fixed predictors and sample as random factor, using packages *lme4* and *lmerTest* and *investr*, to calculate Γ^S (Greenwell & Schubert Kabban, 2014). We obtained the COS source term (P^S) as the intercept of the A^S-C^S relationships measured at varying temperatures, in the light and in the dark. Since P^S increased exponentially with temperature, we fitted a linear relationship between ln-transformed P^S and temperature and then calculated the relative increase per 10°C increase (Q_{10}) as in Eq. 3 in Zaragoza-Castells *et al.* (2007). To analyse the effect of PPFD and COS availability on A^S we fitted a LMM with PPFD and source air (ambient vs. near-zero COS) as fixed predictors and the sample as a random factor. In our experimental setup, the increase in light intensity was coupled to a 5°C increase (Fig. S3), potentially affecting both COS uptake and emission, irrespective of light intensity. To partially disentangle the effects temperature on COS uptake and emission, we first estimated the P^S for each measurement from temperature and the Q_{10} and then calculated the gross COS uptake (U^S) as the sum of the net uptake and the source. Finally, we performed a similar LMM on estimated U^S with PPFD and source air as fixed predictors. For photosynthesis, the A^C shows a response to PPFD of the form:

$$A^C = R_d + A^C_{max}(1 - e^{-k\mathrm{PPFD}}) \qquad \text{Eq. 6}$$

where R_d is the net CO_2 emission in the dark, A_{max} is the asymptote of the curve and k is a constant, such that $A_{max}k$ is the slope of the initial part of the curve (Marschall & Proctor, 2004). We fitted Eq. 6 to A^C-PPFD measurements and tested for differences between ambient and near-zero C^S by comparing the 95% confidence interval of the fitted parameters. Finally, to assess the effect of light on total protein and NSC during desiccation, we performed linear model analyses with RWC, light and their interaction on metabolite concentrations. Prior to analyses, we checked for normality and ln-transformed metabolite concentrations and RWC (the latter for mosses only).

RESULTS

COS uptake dynamic along desiccation in the light and in the dark and LRU

The typical optimum-like response of the net CO_2 uptake (A^C) during dehydration in the light, characteristic of bryophytes, was clearly observed in liverwort*, M. polymorpha* (Fig. 1c),

while in moss, *S. purum*, the increase in A^C upon initial desiccation from maximum RWC was less evident (Fig. 1a). Maximum A^C in the light was similar between the moss and the liverwort (15.9 and 22.7 μmol kg^{-1} s^{-1}, respectively), in contrast maximum A^S was four times higher in *M. polymorpha*, the liverwort, compared to *S. purum*, the moss (20.7 ± 3.6 and 5.2 ± 2.3 pmol kg^{-1} s^{-1}, estimated maximum from fitted GAMM ± 95% CI). In the dark, at a cooler temperature (16°C), respiration ($A^C < 0$) decreased progressively during tissue desiccation until it reached zero (Fig. 1 a,c), whilst A^S followed an optimum-like response to desiccation similar to that observed for A^C in the light, in both bryophytes (Fig. 1 b,d). These data support our assumption that COS uptake by astomatous plants continues in the dark. Contrary to our expectations, however, A^S in the dark was higher under the dark and cooler conditions along the whole desiccation curve, in both the liverwort, *M. polymorpha*, and the moss, *S. purum* (Fig. 1b,d). Furthermore, towards the end of the desiccation curves in the light (and at 21°C), A^S shifted from net uptake to net emission in both species, while in the dark (and at 16°C) A^S remained positive, or not significantly different from zero, during the entire desiccation curve (Fig. 1 b,d). It is worth noting that during the desiccation experiments our blank chambers showed no signs of COS or CO_2 uptake or release throughout. Collectively, the above results led to negative values of leaflet relative uptake (LRU) not only in the dark, but also in the light when RWC fell below its optimum value for gas exchange (Table 1). At optimum RWC in the light, the calculated LRU was 0.22 for the moss and 0.89 for the liverwort.

COS compensation point (Γ^S) and temperature sensitivity of source term (P^S) in the liverwort

Both CO_2 photosynthetic uptake in the light and CO_2 respiratory release in the dark were unaffected by C^S (Fig. 2a, Supplementary information Table S1). In contrast, and as expected, A^S increased linearly with C^S ($P < 0.001$, Fig. 2b) regardless of the light and temperature regimen. LMM revealed that the rate of increase of A^S with C^S did not differ between the two light and temperature regimes ($P = 0.526$, Fig. 2b), but predicted P^S (A^S extrapolated at zero C^S) was significantly ($P = 0.005$) greater in the light at 21°C (21 ± 2.7 pmol mol^{-1}) than in the dark at 16°C (12 ± 1.9 pmol mol^{-1}). For *M. polymorpha*, we estimated a COS compensation point (Γ^S) of 345 ± 68 pmol mol^{-1} in the light at the warmer temperature and 199 ± 74 pmol mol^{-1} in the dark at the cooler temperature. During all experiments manipulating COS concentrations, light intensity and temperature in our blank chamber remained constant indicating that chamber artefacts such as COS emission or uptake

were minimised in our experimental set-up despite large changes in environmental conditions.

Our estimates of P^S (A^S at zero C^S) represent a COS emission rate coming from the liverwort. We found that P^S increased exponentially with temperature ($t = 6.5$, $P < 0.001$), regardless of the light/dark regime with a Q_{10} of 3.7 (Fig. 3).

Effect of light and temperature on net (A^S) and gross (U^S) COS uptake

In *M. polymorpha*, A^C increased with increasing light intensity and temperature, until it reached a plateau (Fig. 4) according to Eq. 4. We found that the A^C-PPFD relationship did not change between ambient and near-zero COS supply (Fig. 4 a); demonstrated by the overlap of the 95% confidence interval of the parameter estimates (Table S1). In contrast, A^S decreased with increasing light intensity and temperature, both under ambient and near-zero COS supply, but the rate of change with light intensity was lower under near-zero than ambient C^S (Fig. 4 b, Table S1). This decrease in A^S with light and temperature is partly explained by an increase in P^S with temperature (see above). However, even after accounting for the temperature effect on P^S, we found that the gross COS uptake ($U^S = A^S + P^S$) still decreased with light intensity under ambient COS (Fig. 3 c, Table S1). This could suggest an inhibitory effect of light intensity on COS uptake. However, we cannot completely discard the influence of an experimental artefact potentially biasing our observations. For example, given our experimental sequence, uptake rates at the highest light intensities were measured towards the end of the experiment, when decreasing RWC could have negatively affected uptake.

Total protein and NSC accumulation in the light and in the dark along desiccation

Total protein content decreased with desiccation in both the liverwort (*M. polymorpha*) and the moss (*S. purum* Table 2). In the moss, non-structural carbohydrates (NSC) and all its components (glucose, fructose, sucrose and starch) also decreased with desiccation (Fig. 5, Table 2). The decrease rate with RWC of protein and NSCs (in the moss) with desiccation did not differ between the light and the dark (Table 2).

DISCUSSION

Challenging the unidirectional flux assumption for the vegetation COS flux

Here, we aimed to critically assess some of the key assumptions underlying the relationship between COS and CO_2 uptake, in bryophytes. We hypothesised that COS uptake rates in bryophytes would be light independent. Our results on two astomatous bryophytes (one moss and one liverwort) partially agreed with this prediction as we found that net COS uptake (A^S) in the dark remained positive, and this supports the current idea that COS hydrolysis is dominated by the enzyme carbonic anhydrase (CA), which is assumed to be light-independent (Protoschill-Krebs *et al.*, 1996). However, our results also showed that A^S may be affected by light in an unexpected way. We found that for an equivalent hydration status, A^S was significantly greater in the dark than in the light. A plausible explanation for this observation is that bryophyte A^S is the net result of two opposing fluxes, uptake and emission, with COS emission being of greater magnitude at warmer temperatures in the light than in cooler dark conditions. All our other results are compatible with this explanation. Firstly, we observed that below an optimal hydration status, A^s shifted from net uptake to net emission in the light, but not in the dark. Also A^S decreased with increasing light intensity and warmer temperatures. Finally, we found a non-zero compensation point (Γ^S) that was greater in the light than in the dark. Previously, Kuhn & Kesselmeier (2000) had suggested the existence of a non-zero Γ^S in lichens. Non-zero Γ^S have also been observed in some higher plants (Kesselmeier & Merk, 1993) but its influence on the overall COS uptake rate seemed small (Seibt *et al.*, 2010; Stimler *et al.*, 2010). These observations, together with other studies conducted on plants senescing, under fungal attack or under heat and drought stress (Bloem *et al.*, 2012; Maseyk *et al.*, 2014; Commane *et al.*, 2015), suggest that plant COS emissions may be more ubiquitous than previously assumed. Our results encourage further studies revisiting COS fluxes from vascular plants, for example performing A^S-C^S curves at different temperatures, to determine whether COS emissions can be detected with the new generation of commercially available COS analysers offering much higher precision (~5ppt). In particular, experiments using mutants (Costa *et al.*, 2015) that maintain stomata open in the dark could provide a novel approach to detect COS emissions from vascular plants and how the gross COS fluxes respond to different environmental drivers.

The existence of a bi-directional COS flux contradicts our initial expectation for COS uptake by astomatous bryophytes, since there are currently no described leaf-level processes

that result in COS as a by-product (Protoschill-Krebs *et al.*, 1996; Bloem *et al.*, 2015). Previously, Fried *et al.* (1993) measured COS emissions in the light from a peat soil and moss microcosm, but they ascribed the emissions to the soil component. Indeed, Whelan & Rhew (2015) demonstrated that soils can emit COS and that the rate of COS emission increases in the light and with warmer temperatures. Whelan & Rhew (2015) suggested that COS originated from abiotic photo-degradation of dead organic matter by UV light, similar to COS emissions measured from sea, lake and precipitation water (Zepp & Andreae, 1994; Mu *et al.*, 2004; Du *et al.* 2016). However, based on the manufacturers specifications for our light source (see Methods) and because our chambers were not made of UV-transparent quartz glass, we assume that our bryophyte samples were not exposed to high intensity UV radiation. Thus it is unlikely that our COS emissions in the light would have been strongly affected by UV-driven organic matter degradation. Our results suggest that an additional light-independent process of biological origin underlies observed COS emission from bryophytes. We argue that this process is likely to be of biological origin because in the dark, COS emission at minimum hydration status (below 70% RWC) was not detectable, while our A^S-C^S curve demonstrated that COS emission still occurred in the dark at optimal hydration status. Despite uncertainties in the mechanistic driver of the emissions, in our study, we observed protein degradation during desiccation in the moss and below optimal hydration in the liverwort that could have led to the liberation and eventual catabolism of sulphur-containing amino acids (cysteine and methionine), potential precursors for COS production (Bloem et al. 2004; Du *et al.* 2016; Zepp & Andreae, 1994; Mu *et al.*, 2004). This protein degradation would have occurred while the leaflet tissues were metabolically active and was accompanied by a significant decrease in NSC content. This result alongside the gas exchange data suggest that as the leaflets became progressively water-stressed, protein degradation affected the photosynthetic machinery, including CA, and probably caused the increased apparent COS emission by reducing gross COS uptake. This is consistent with results in the literature on vascular plants that have shown that during water stress the total protein content decreases rapidly and is accompanied by a strong reduction in the activity of key enzymes involved in carbon assimilation (Majumdar *et al.*, 1991; Khanna-Chopra, 2012). The metabolic activity of accompanying microorganisms, sensitive to water stress too (Vacher *et al.*, 2016), could also be contributing to the observed COS emission in bryophytes. Bryophytes, like any other plants, host rich microbial communities and both liverworts and feather-like mosses are known to form symbiotic associations with fungi and bacteria (DeLuca *et al.*, 2002; Humphreys *et al.*, 2010; Davey *et al.*, 2012). It has recently been shown

494 that some fungal and bacterial enzymatic reactions produce COS (Masaki *et al.*, 2016; Ogawa
495 *et al.*, 2016); hence it is plausible that natural symbionts could also be contributing to the net
496 COS fluxes in bryophytes.
497
498 *Assessing the climatic sensitivity of COS uptake and emission*
499 In bryophytes, tissue water content is the main driver of net CO_2 exchange (A^C, Wagner *et al.*,
500 2013) and we expected the same for net COS uptake (A^S). We indeed observed that A^S was
501 strongly driven by tissue water content, but our results also showed that A^S was sensitive to
502 temperature. Our observations on liverworts in the dark showed that A^S at optimal water
503 content was lower at 21°C than at 16 °C, while CO_2 respiratory release was greater at the
504 warmer temperature (Supplementary information, Fig. S5). This seems to contradict the
505 increase of A^S observed in lichens by Kuhn & Kesselmeier (2000) for the same temperature
506 range. Since a thermal optimum below 21°C for enzymatic COS hydrolysis is not within the
507 range of published data (Burnell & Hatch, 1988), we argue that lower net A^S at a warmer
508 temperature (within our measurement range) is caused by higher COS emissions rather than
509 by reduced COS uptake. In fact, here we demonstrated that the COS source term (P^S,
510 estimated from A^S-C^S curves) is very sensitive to temperature, with a Q_{10} of 3.7. Our Q_{10}
511 estimate for COS emissions is higher than those reported for net COS fluxes in soils (Maseyk
512 *et al.*, 2014) but within the range of respiratory Q_{10} for several moss species (Wagner *et al.*,
513 2013).
514 Our results also seem to indicate a small, but statistically significant, decrease of the
515 gross COS uptake (U^S) with increasing light intensity. Given our current knowledge of the
516 temperature sensitivity of CA activity (Burnell & Hatch, 1988), it is unlikely that COS
517 hydrolysis was inhibited by the warming experienced inside the gas-exchange chamber
518 during our light curves. It could be argued that this decrease in U^S with light intensity was
519 simply driven by a reduction in tissue RWC along the experiment. In our experiment, for
520 light intensities above 400 μmol m^{-2} s^{-1} the mean RWC was 535 ± 25%, *i.e.*, close to the
521 point beyond which A^S starts to decrease. Yet, such reduction in RWC should have also
522 negatively affected A^C and we did not detect a major drop in A^C towards the end of the light
523 curve. Alternatively, other biological reasons may explain this decrease of U^S with light
524 intensity in bryophytes. For example, carbon concentration mechanisms (CCM) that
525 incorporate CA as a key constituent have evolved in some bryophyte lineages (specifically in
526 the Anthocerophyta, the hornworts), but there is no conclusive evidence from previous gas
527 exchange measurements for an active CCM in either mosses or liverworts (Smith & Griffiths,

2000; Badger, 2003; Meyer *et al.*, 2008). However, the presence of CAs of different types associated to a basal CCM has been hypothesised in all C_3 plants (Zabaleta *et al.*, 2012), thus one hypothesis that might deserve future study would be to test whether the observed decrease in A^S with light could be explained by activity of a light-sensitive CA (Rech *et al.*, 2008). However, in one of our study species (*M. polymorpha*, the liverwort), the photosynthetic CO_2 compensation point and carbon isotope discrimination did not respond to the addition of a CA-inhibitor, indicating that most likely it lacks any external CA or CCM activity (Smith & Griffiths, 2000).

The unexpected contribution of bryophytes to the COS budget

The quantification of COS fluxes in bryophytes is not only relevant to better understand the drivers of the net leaf COS flux in other species, but also to help constrain the global COS budget, as bryophytes are key constituents of many ecosystems (DeLuca *et al.*, 2002). The estimated leaflet relative uptake rates (LRU of 0.2 for the moss, *S. purum* and 0.9 for the liverwort, *M. polymorpha*, in the light and at optimal hydration status) found in our study, were lower than current LRU estimates for vascular plants, which range between 1.4 and 2 (Seibt *et al.*, 2010; Stimler *et al.*, 2010). If we were to estimate the contribution of cryptogamic covers to the global COS budget from their current estimates of CO_2 uptake (3.9 Pg C y^{-1} according to Elbert *et al.*, 2012) following the same LRU approach as proposed for vascular plants (Campbell *et al.*, 2008; Sandoval-Soto *et al.*, 2005), with atmospheric mixing ratios of 400 µmol CO_2 mol^{-1} and 540 pmol COS mol^{-1}, we would arrive at an estimate between 0.005 and 0.024 Tg COS y^{-1} (for LRU of 0.2 and 0.9, respectively). This flux is within the same order of magnitude as the estimate of COS uptake for swamps and marshes and is larger than current estimates for tundra, alpine and desert scrublands (see Table 3 of Sandoval-Soto *et al.*, 2005). These values could serve as first approximations for high latitudes in the summer, where extensive regions are dominated by uniform bryophyte carpets, daylight is continuous and the evaporative demand is low (Lindo *et al.*, 2013). However, bryophytes are also commonly found in areas where day-night cycles alternate and physiological activity is strongly constrained by tissue hydration (Elbert *et al.*, 2012). In these areas, during the day, when temperatures are high and air moisture is low, bryophytes would tend to dehydrate and CO_2 and COS uptake would be metabolically limited, whilst warmer temperatures and incident radiation would enhance unexpected COS emission. In contrast, at night, when the temperature is cooler and the evaporative demand is low, bryophytes would rehydrate towards full turgor and act as strong COS sinks, but CO_2 sources. Our estimated

Q_{10} constitutes a first step towards quantifying the contribution of the COS emissions. However, further work is required to understand the sensitivity of this parameter (P^S) to additional environmental constraints, particularly changes in tissue hydration and light regimes with seasons or ontogeny (Porada *et al*., 2013).

Conclusions

Here, using bryophytes as model organisms, we have demonstrated that net COS uptake continues in the dark, but is also progressively decreased as irradiance and temperature increase, mostly because of an unexpected, temperature-driven COS emission. Together, our results challenge a key underlying assumption for quantifying GPP from COS fluxes that vegetation COS uptake is unidirectional. Obviously, we cannot immediately extrapolate our findings to other terrestrial vascular plants; however our results should encourage further studies to revisit the unidirectional flux assumption in vascular plants making use of the improved laser spectrometers now available.

ACKNOWLEDGEMENTS

Many thanks to Prof. Ana M. De Miguel (Universidad de Navarra, Spain) for identifying bryophyte species, to Patricia Ballias and the rest of the INRA-BFP team for assistance during metabolic assays and to Prof. Howard Griffiths (University of Cambridge, UK) for his intellectual input and support. Funding was provided by the European Research Council (ERC) early career starting grant SOLCA (Grant Agreement No. 338264) and the French Agence National de la Recherche (ANR) project ORCA. TEG was funded by the IdEx post-doctoral programme of the Université de Bordeaux and by a Marie Skłodowska-Curie Intra-European fellowship (Grant Agreement No. 653223). JR was funded by the NERC grant NE/M00113X/1

AUTHOR CONTRIBUTIONS

TEG, LW, JO and JR conceived and designed the experiment. TEG, SJ, RB, SW, JS and JBW designed and took the gas-exchange measurements. TEG, CB and YG performed and interpreted the biochemical analyses. TEG, JO, JBW and LW analysed the data. TEG wrote the first manuscript draft. All authors commented and contributed to the final version.

596 **REFERENCES**

597

598 **Arroniz-Crespo M, Leake JR, Horton P, Phoenix GK. 2008.** Bryophyte physiological
599 responses to, and recovery from, long-term nitrogen deposition and phosphorus fertilisation
600 in acidic grassland. *New Phytologist* **180**(4): 864-874.
601 **Badger M. 2003.** The roles of carbonic anhydrases in photosynthetic CO2 concentrating
602 mechanisms. *Photosynthesis Research* **77**(2-3): 83-94.
603 **Berkelhammer M, Asaf D, Still C, Montzka S, Noone D, Gupta M, Provencal R, Chen**
604 **H, Yakir D. 2014.** Constraining surface carbon fluxes using in situ measurements of
605 carbonyl sulfide and carbon dioxide. *Global Biogeochemical Cycles* **28**(2): 161-179.
606 **Biais B, Benard C, Beauvoit B, Colombie S, Prodhomme D, Menard G, Bernillon S,**
607 **Gehl B, Gautier H, Ballias P, et al. 2014.** Remarkable Reproducibility of Enzyme Activity
608 Profiles in Tomato Fruits Grown under Contrasting Environments Provides a Roadmap for
609 Studies of Fruit Metabolism. *Plant Physiology* **164**(3): 1204-1221.
610 **Bloem E., Riemenschneider A., Volker J., Papenbrock J., Schmidt A., Salac I.,**
611 **Haneklaus S., Schnug, E. 2004.** Sulphur supply and infection with Pyrenopeziza brassicae
612 influence L-cysteine desulphydrase activity in *Brassica napus* L. *Journal of Experimental*
613 *Botany* **55**(406): 2305-2312.
614 **Bloem E, Haneklaus S, Kesselmeier J, Schnug E. 2012.** Sulfur Fertilization and Fungal
615 Infections Affect the Exchange of H_2S and COS from Agricultural Crops. *Journal of*
616 *Agricultural and Food Chemistry* **60**(31): 7588-7596.
617 **Bloem E, Haneklaus S, Schnug E. 2015.** Milestones in plant sulfur research on sulfur-
618 induced-resistance (SIR) in Europe. *Frontiers in Plant Science* **5**(779).
619 **Bowman JL. 2016.** A Brief History of *Marchantia* from Greece to Genomics. *Plant and Cell*
620 *Physiology* **57**(2): 210-229.
621 **Bradford MM. 1976.** Rapid and sensitive method for quantitation of microgram quantitites
622 of protein utilizing principle of protein-dye binding. *Analytical Biochemistry* **72**(1-2): 248-
623 254.
624 **Burnell JN, Hatch MD. 1988.** Low Bundle Sheath Carbonic-Anhydrase is Apparently
625 Essential for Effective C-4 Pathway Operation. *Plant Physiology* **86**(4): 1252-1256.
626 **Campbell JE, Carmichael GR, Chai T, Mena-Carrasco M, Tang Y, Blake DR, Blake**
627 **NJ, Vay SA, Collatz GJ, Baker I, et al. 2008.** Photosynthetic Control of Atmospheric
628 Carbonyl Sulfide During the Growing Season. *Science* **322**(5904): 1085-1088.

Commane R, Meredith LK, Baker IT, Berry JA, Munger JW, Montzka SA, Templer PH, Juice SM, Zahniser MS, Wofsy SC. 2015. Seasonal fluxes of carbonyl sulfide in a midlatitude forest. *Proceedings of the National Academy of Sciences of the United States of America* **112**(46): 14162-14167.

Costa JM, Monnet F, Jannaud D, Leonhardt N, Ksas B, Reiter IM, Pantin F, Genty B. 2015. OPEN ALL NIGHT LONG: The Dark Side of Stomatal Control. *Plant Physiology* **167**(2): 289-294.

Davey ML, Heegaard E, Halvorsen R, Ohlson M, Kauserud H. 2012. Seasonal trends in the biomass and structure of bryophyte-associated fungal communities explored by 454 pyrosequencing. *New Phytologist* **195**(4): 844-856.

DeLuca TH, Zackrisson O, Nilsson MC, Sellstedt A. 2002. Quantifying nitrogen-fixation in feather moss carpets of boreal forests. *Nature* **419**(6910): 917-920.

Dilks TJK, Proctor MCF. 1979. Photosynthesis, Respiration and Water-Content in Bryophytes. *New Phytologist* **82**(1): 97-&.

Du Q, Mu Y, Zhang C, Liu J, Zhang Y, Liu C. Photochemical production of carbonyl sulfide, carbon disulfide and dimethyl sulfide in a lake water. *Journal of Environmental Sciences*.

Elbert W, Weber B, Burrows S, Steinkamp J, Budel B, Andreae MO, Poschl U. 2012. Contribution of cryptogamic covers to the global cycles of carbon and nitrogen. *Nature Geoscience* **5**(7): 459-462.

Fried A, Klinger LF, Erickson DJ. 1993. Atmospheric carbonyl sulfide exchange in bog microcosms. *Geophysical Research Letters* **20**(2): 129-132.

Greenwell BM, Schubert Kabban CM. 2014. investr: An R Package for Inverse Estimation. *The R Journal* **6**(1): 90-100.

Gries C, Nash TH, Kesselmeier J. 1994. Exchange of reduced sulfur gases between lichens and the atmosphere. *Biogeochemistry* **26**(1): 25-39.

Hendriks JHM, Kolbe A, Gibon Y, Stitt M, Geigenberger P. 2003. ADP-glucose pyrophosphorylase is activated by posttranslational redox-modification in response to light and to sugars in leaves of Arabidopsis and other plant species. *Plant Physiology* **133**(2): 838-849.

Humphreys CP, Franks PJ, Rees M, Bidartondo MI, Leake JR, Beerling DJ. 2010. Mutualistic mycorrhiza-like symbiosis in the most ancient group of land plants. *Nature Communications* **1**: 7.

Jelitto T, Sonnewald U, Willmitzer L, Hajirezeai M, Stitt M. 1992. Inorganic pyrophosphate content and metabolites in potato and tobacco plants expressing Escherichia-coli pyrophosphatase in their cytosol. *Planta* **188**(2): 238-244.

Kesselmeier J, Merk L. 1993. Exchange of carbonyl sulphide (COS) between agricultural plants and the atmosphere – studies on the deposition of COS to peas, corn and rapeseed. *Biogeochemistry* **23**(1): 47-59.

Khanna-Chopra R. 2012. Leaf senescence and abiotic stresses share reactive oxygen species-mediated chloroplast degradation. *Protoplasma* **249**(3): 469-481.

Kuhn U, Kesselmeier J. 2000. Environmental variables controlling the uptake of carbonyl sulfide by lichens. *Journal of Geophysical Research-Atmospheres* **105**(D22): 26783-26792.

Lindo Z, Nilsson MC, Gundale MJ. 2013. Bryophyte-cyanobacteria associations as regulators of the northern latitude carbon balance in response to global change. *Global Change Biology* **19**(7): 2022-2035.

Majumdar S, Ghosh S, Glick BR, Dumbroff EB. 1991. Activities of Chlorophyllase, Phosphoenolpyruvate Carboxylase and Ribulose-1,5-Bisphosphate Carboxylase in the Primary Leaves of Soybean during Senescence and Drought. *Physiologia Plantarum* **81**(4): 473-480.

Marschall M, Proctor MCF. 2004. Are bryophytes shade plants? Photosynthetic light responses and proportions of chlorophyll a, chlorophyll b and total carotenoids. *Annals of Botany* **94**(4): 593-603.

Masaki Y, Ozawa R, Kageyama K, Katayama Y. 2016. Degradation and emission of carbonyl sulfide, an atmospheric trace gas, by fungi isolated from forest soil. *FEMS Microbiology Letters*. doi: 10.1093/femsle/fnw197

Maseyk K, Berry JA, Billesbach D, Campbell JE, Torn MS, Zahniser M, Seibt U. 2014. Sources and sinks of carbonyl sulfide in an agricultural field in the Southern Great Plains. *Proceedings of the National Academy of Sciences of the United States of America* **111**(25): 9064-9069.

Meyer M, Seibt U, Griffiths H. 2008. To concentrate or ventilate? Carbon acquisition, isotope discrimination and physiological ecology of early land plant life. *Philosophical Transactions of the Royal Society B-Biological Sciences* **363**(1504): 2767-2778.

Montzka SA, Calvert P, Hall BD, Elkins JW, Conway TJ, Tans PP, Sweeney C. 2007. On the global distribution, seasonality, and budget of atmospheric carbonyl sulfide (COS) and some similarities to CO2. *Journal of Geophysical Research-Atmospheres* **112**(D9).

Mu Y, Geng C, Wang M, Wu H, Zhang X, Jiang G. 2004. Photochemical production of carbonyl sulfide in precipitation. *Journal of Geophysical Research: Atmospheres* **109**(D13)

Notni J, Schenk S, Protoschill-Krebs G, Kesselmeier J, Anders E. 2007. The missing link in COS metabolism: A model study on the reactivation of carbonic anhydrase from its hydrosulfide analogue. *Chembiochem* **8**(5): 530-536.

Ogawa T, Kato H, Higashide M, Nishimiya M, Katayama Y. 2016. Degradation of carbonyl sulfide by Actinomycetes and detection of clade D of β-class carbonic anhydrase. *FEMS Microbiology Letters* **363**(19) doi: 10.1093/femsle/fnw223

Oliver MJ, Velten J, Mishler BD. 2005. Desiccation tolerance in bryophytes: A reflection of the primitive strategy for plant survival in dehydrating habitats? *Integrative and Comparative Biology* **45**(5): 788-799.

Porada P, Weber B, Elbert W, Poschl U, Kleidon A. 2013. Estimating global carbon uptake by lichens and bryophytes with a process-based model. *Biogeosciences* **10**(11): 6989-7033.

Proctor MCF, Oliver MJ, Wood AJ, Alpert P, Stark LR, Cleavitt NL, Mishler BD. 2007. Desiccation-tolerance in bryophytes: a review. *Bryologist* **110**(4): 595-621.

Protoschill-Krebs G, Wilhelm C, Kesselmeier J. 1996. Consumption of carbonyl sulphide (COS) by higher plant carbonic anhydrase (CA). *Atmospheric Environment* **30**(18): 3151-3156.

R Development Core Team R. 2014. R: A Language and Environment for Statistical Computing.

Rech M, Morant-Manceau A, Tremblin G. 2008. Carbon fixation and carbonic anhydrase activity in *Haslea ostrearia* (Bacillariophyceae) in relation to growth irradiance. *Photosynthetica* **46**(1): 56-62.

Royles J, Ogee J, Wingate L, Hodgson DA, Convey P, Griffiths H. 2013. Temporal separation between CO_2 assimilation and growth? Experimental and theoretical evidence from the desiccation-tolerant moss Syntrichia ruralis. *New Phytologist* **197**(4): 1152-1160.

Sandoval-Soto L, Kesselmeier M, Schmitt V, Wild A, Kesselmeier J. 2012. Observations of the uptake of carbonyl sulfide (COS) by trees under elevated atmospheric carbon dioxide concentrations. *Biogeosciences* **9**(8): 2935-2945.

Sandoval-Soto L, Stanimirov M, van Hobe M, Schmitt V, Valdes J, Wild A, Kesselmeier J. 2005. Global uptake of carbonyl sulfide (COS) by terrestrial vegetation: estimates corrected by deposition velocities normalized to the uptake of carbon dioxide (CO_2). *Biogeosciences* **2**: 125-132.

Seibt U, Kesselmeier J, Sandoval-Soto L, Kuhn U, Berry JA. 2010. A kinetic analysis of leaf uptake of COS and its relation to transpiration, photosynthesis and carbon isotope fractionation. *Biogeosciences* **7**(1): 333-341.

Smith EC, Griffiths H. 2000. The role of carbonic anhydrase in photosynthesis and the activity of the carbon-concentrating-mechanism in bryophytes of the class Anthocerotae. *New Phytologist* **145**(1): 29-37.

Stimler K, Berry JA, Montzka SA, Yakir D. 2011. Association between Carbonyl Sulfide Uptake and $^{18}\Delta$ during Gas Exchange in C-3 and C-4 Leaves. *Plant Physiology* **157**(1): 509-517.

Stimler K, Berry JA, Yakir D. 2012. Effects of Carbonyl Sulfide and Carbonic Anhydrase on Stomatal Conductance. *Plant Physiology* **158**(1): 524-530.

Stimler K, Montzka SA, Berry JA, Rudich Y, Yakir D. 2010. Relationships between carbonyl sulfide (COS) and CO_2 during leaf gas exchange. *New Phytologist* **186**(4): 869-878.

Vacher C, Hampe A, Porté AJ, Sauer U, Compant S, Morris CE. 2016. The Phyllosphere: Microbial Jungle at the Plant–Climate Interface. *Annual Review of Ecology, Evolution, and Systematics* **47**(1): 1-24.

Wagner S, Zotz G, Allen NS, Bader MY. 2013. Altitudinal changes in temperature responses of net photosynthesis and dark respiration in tropical bryophytes. *Annals of Botany* **111**(3): 455-465.

Whelan ME, Rhew RC. 2015. Carbonyl sulfide produced by abiotic thermal and photodegradation of soil organic matter from wheat field substrate. *Journal of Geophysical Research: Biogeosciences* **120**(1): 54-62.

Wood S. 2006. *Generalized Additive Models: An Introduction with R*: Chapman & Hall/CRC.

Zabaleta E, Martín MV, Braun HP. 2012. A basal carbon concentratin mechanism in plants? *Plant Science* **187**: 97-104.

Zaragoza-Castells J, Sanchez-Gomez D, Valladares F, Hurry V, Atkin OK. 2007. Does growth irradiance affect temperature dependence and thermal acclimation of leaf respiration? Insights from a Mediterranean tree with long-lived leaves. *Plant Cell and Environment* **30**(7): 820-833.

Zepp RG, Andreae MO. 1994. Factors affecting the photochemical production of carbonyl sulfide in seawater. *Geophysical Research Letters* **21**(25): 2813-2816.

762 **SUPPORTING INFORMATION**

763

764 **Figure S1.** Allan variance plot showing the standard deviation for the QCLS.

765

766 **Figure S2.** Tissue relative water content and sample temperature along desiccation.

767

768 **Figure S3.** Sample temperature inside the gas-exchange chamber during light curves.

769

770 **Figure S4.** Individual metabolite (protein and non-structural carbohydrate) concentrations.

771

772 **Figure S5.** CO_2 and COS net uptake rates in the dark along desiccation at two temperatures.

773

774 **Table S1.** Estimated regression coefficients and summary statistics of the linear mixed
775 models performed to assess the effects of COS concentration in the light and in the dark, and
776 light intensity under ambient and near-zero COS mixing rations on CO_2 and COS uptake rate.

FIGURE LEGENDS

Figure 1. CO_2 (A^C, a and c) and COS (A^S, b and d) net assimilation in the light at 21 °C (red) and in the dark at 16 °C (blue) along decreasing tissue relative water content (RWC) in the moss (a and b) and in the liverwort (c and d). Each symbol is an individual sample, the lines are smooth curves (fitted with a generalized additive model) and the blue and red areas denote the 95% confidence interval for A^C and A^S in the light (red) or in the dark (blue). Areas where the confidence interval do not overlap denote a significant effect at $\alpha = 0.05$. The non-RWC dependent black regions (at approximately 0) denote the mean (± sd) fluxes of the blank chamber.

Figure 2. Mean (± se, $n = 4$) CO_2 (A^C, a) and COS (A^S, b) net assimilation along a COS mixing ratio (C^S) gradient in the light at 21 °C (open symbols and red areas) and in the dark at 16 °C (closed symbols and blue areas), in the liverwort. Lines and areas represent linear fits ($P < 0.001$, $R^2 = 0.9$ in b), and their 95% confidence intervals. Black regions denote the mean (± sd) fluxes of the blank chamber.

Figure 3. Relationship between mean measurement temperature (T, $n = 4$ measurements) and estimated (± se) COS source (P^S) from the intercept of A^S-C^S curves (A^S is net COS assimilation and C^S is the COS mixing ratio). Open and closed symbols represent estimated P^S from A^S-C^S curves performed in the light or in the dark, respectively, in the liverwort. The lines represent the modelled common temperature response (continuous line) and its uncertainty (dashed lines) over the entire experimental temperature range: $P^S_{\text{modelled}} = e^{\frac{\log(Q_{10})}{10}}$ with $Q_{10} = 3.7$

Figure 4 Relationship between light intensity (PPFD) and mean (± se, $n = 4$) net measured CO_2 (A^C, a) and COS assimilation (A^S, b, closed symbols and solid lines) and gross estimated assimilation (U^S, c, open symbols and dashed lines) under ambient COS mixing ratio (Amb COS, squares) and near-zero COS mixing ratio (Zero COS, circles), in the liverwort. Lines and grey areas correspond to the exponential (in a) and linear (in b and c) fits and their 95% confidence interval. Black regions denote the mean (± sd) fluxes of the blank chamber.

809 **Figure 5.** Protein and total non-structural carbohydrates (NSC) content, per unit of dry
810 weight (DW), in the moss (upper panels) and the liverwort (lower panels) measured along
811 decreasing relative water content (RWC) in the dark (filled bars) and in the light (open bars).
812 Bars are the means (+se, n = 1-5) for grouped data according to four categorical levels of
813 RWC (very high, high, intermediate and low), RWC values on the x-axis are the overall
814 means for the light and dark treatments for each RWC level. In the liverwort, (glucose),
815 fructose, sucrose, (total NSC) and protein content were (marginally) higher in the light than
816 in the dark (F = 2.98, 4.41, 4.97, 3.93 and 4.94; P = 0.098, 0.047, 0.036, 0.06 and 0.037,
817 respectively; according to the results of a two-way ANOVA of light and RWC, the latter
818 included as a categorical variable with four levels).

Tables

Table 1. Estimated net uptake (se) of CO_2 (A^C in μmol kg^{-1} s^{-1}), COS (A^S in pmol kg^{-1} s^{-1}) and leaflet relative uptake (LRU), in the light at 21 °C and in the dark at 16 °C, at the optimal (when A^S was maximal) and minimal tissue relative water content (RWC in %) in the moss (*Scleropodium purum*) and the liverwort (*Marchantia polymorpha*).

			RWC	A^C	A^S	A^C	LRU
Moss	Optimum	Light	887	15.3 (0.6)	4.3 (1.0)	15.3 (0.6)	0.22
		Dark	661	-4.9 (0.2)	18.0 (1.1)	-4.9 (0.2)	-3.08
	Minimum	Light	1	-0.3 (0.3)	-6.9 (0.5)	-0.3 (0.3)	15.12
		Dark	1	-0.3 (0.1)	-1.3 (0.6)	-0.3 (0.1)	3.43
Liverwort	Optimum	Light	762	18.8 (1.7)	20.2 (1.8)	18.8 (1.7)	0.89
		Dark	598	-10.7 (0.3)	42.9 (1.9)	-10.7 (0.3)	-3.04
	Minimum	Light	42	-1.5 (1.8)	-7.5 (1.8)	-1.5 (1.8)	4.14
		Dark	1	-0.4 (0.1)	-2.1 (0.7)	-0.4 (0.1)	4.24

826 **Table 2.** Results of the linear model (*t* and *P*) to assess the effect of relative water content
827 (RWC), light and temperature regime (light/21 °C and dark/16 °C) and their interaction on
828 different metabolite concentrations (proteins and non-structural carbohydrates, NSC) in the
829 liverwort and the moss.

		RWC		Light		RWC x Light	
	Metabolite	**t**	***P***	**t**	***P***	**t**	***P***
Liverwort	Glucose	-0.597	0.556	0.319	0.752	0.529	0.601
	Fructose	-0.591	0.56	0.084	0.934	0.932	0.36
	Sucrose	-0.416	0.681	0.008	0.994	1.047	0.305
	Starch	-0.626	0.536	-0.095	0.925	0.661	0.514
	Total NSC	-0.533	0.599	0.161	0.873	0.798	0.432
	Protein	2.267	**0.032**	1.036	0.31	-0.241	0.812
Moss	Glucose	2.485	**0.022**	0.28	0.782	-0.336	0.74
	Fructose	2.752	**0.013**	0.282	0.781	-0.081	0.936
	Sucrose	3.953	**<0.001**	0.381	0.708	0.241	0.812
	Starch	10.077	**<0.001**	0.842	0.41	-0.3	0.767
	Total NSC	5.458	**<0.001**	0.512	0.615	-0.115	0.91
	Protein	5.262	**<0.001**	0.18	0.859	-0.383	0.706

830

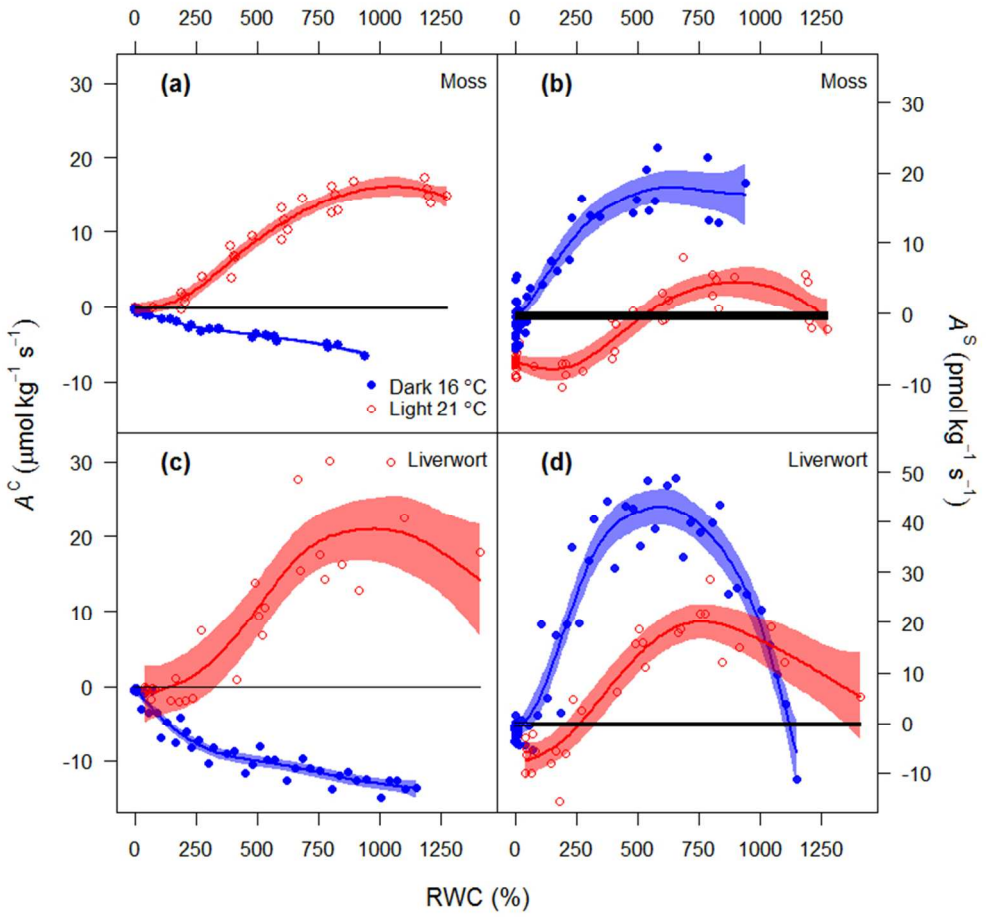

CO_2 (A^C, a and c) and COS (A^S, b and d) net assimilation in the light at 21 °C (red) and in the dark at 16 °C (blue) along decreasing tissue relative water content (RWC) in the moss (a and b) and in the liverwort (c and d). Each symbol is an individual sample, the lines are smooth curves (fitted with a generalised additive model) and the blue and red areas denote the 95% confidence interval for A^C and A^S in the light (red) or in the dark (blue). Areas where the confidence interval do not overlap denote a significant effect at α = 0.05. The non-RWC dependent black regions (at approximately 0) denote the mean (± sd) fluxes of the blank chamber.

Fig. 1

173x163mm (120 x 120 DPI)

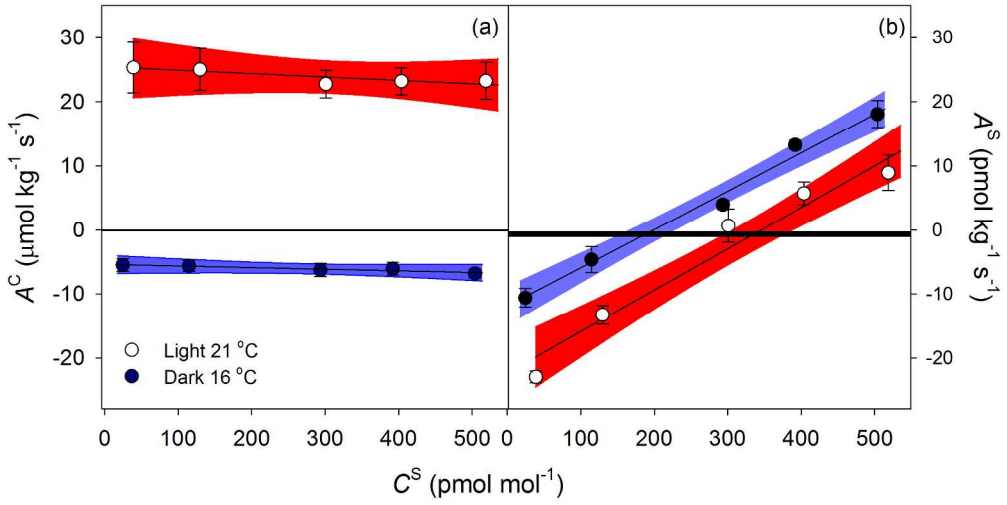

Mean (± se, n = 4) CO_2 (A^C, a) and COS (A^S, b) net assimilation along a COS mixing ratio (C^S) gradient in the light at 21 °C (open symbols and red areas) and in the dark at 16 °C (closed symbols and blue areas), in the liverwort. Lines and areas represent linear fits ($P < 0.001$, $R^2 = 0.9$ in b), and their 95% confidence intervals. Black regions denote the mean (± sd) fluxes of the blank chamber.

Fig. 2

222x123mm (300 x 300 DPI)

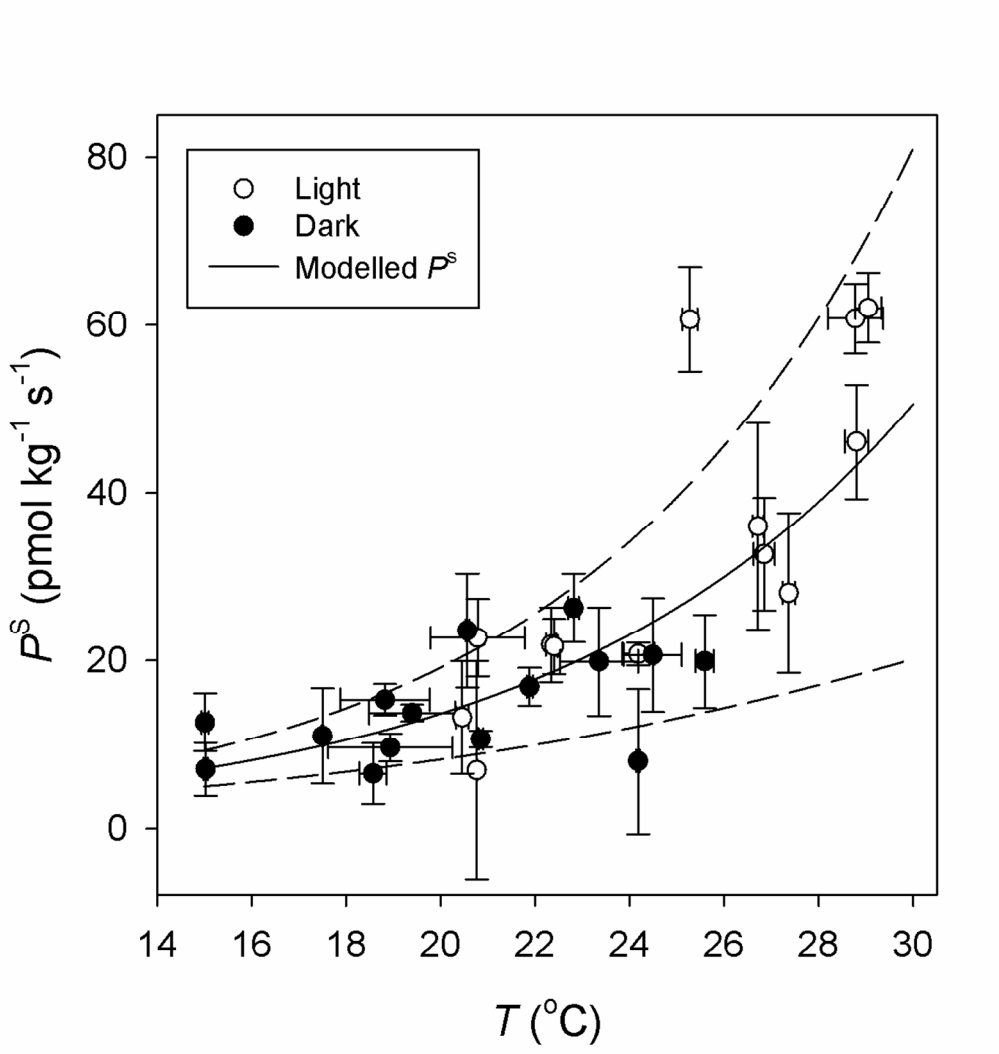

Relationship between mean measurement temperature (T, n = 4 measurements) and estimated (± se) COS source (P^S) from the intercept of A^S-C^S curves (A^S is net COS assimilation and C^S is the COS mixing ratio). Open and closed symbols represent estimated P^S from A^S-C^S curves performed in the light or in the dark, respectively, in the liverwort. The lines represent the modelled common temperature response (continuous line) and its uncertainty (dashed lines) over the entire experimental temperature range: $P_{modelled}{}^S = e^{(\log\ (Q_{10})/10)}$ with Q_{10} = 3.7

Fig. 3

115x122mm (300 x 300 DPI)

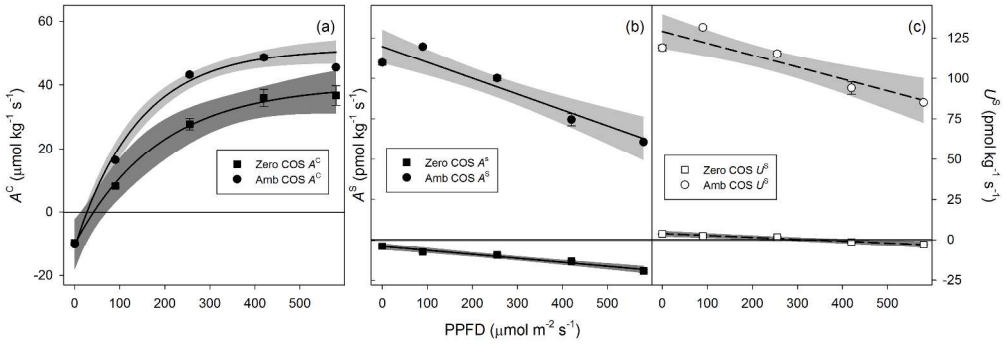

Relationship between light intensity (PPFD) and mean (± se, n = 4) net measured CO_2 (A^C, a) and COS assimilation (A^S, b, closed symbols and solid lines) and gross estimated assimilation (U^S, c, open symbols and dashed lines) under ambient COS mixing ratio (Amb COS, squares) and near-zero COS mixing ratio (Zero COS, circles), in the liverwort. Lines and grey areas correspond to the exponential (in a) and linear (in b and c) fits and their 95% confidence interval. Black regions denote the mean (± sd) fluxes of the blank chamber.

Fig. 4

321x121mm (300 x 300 DPI)

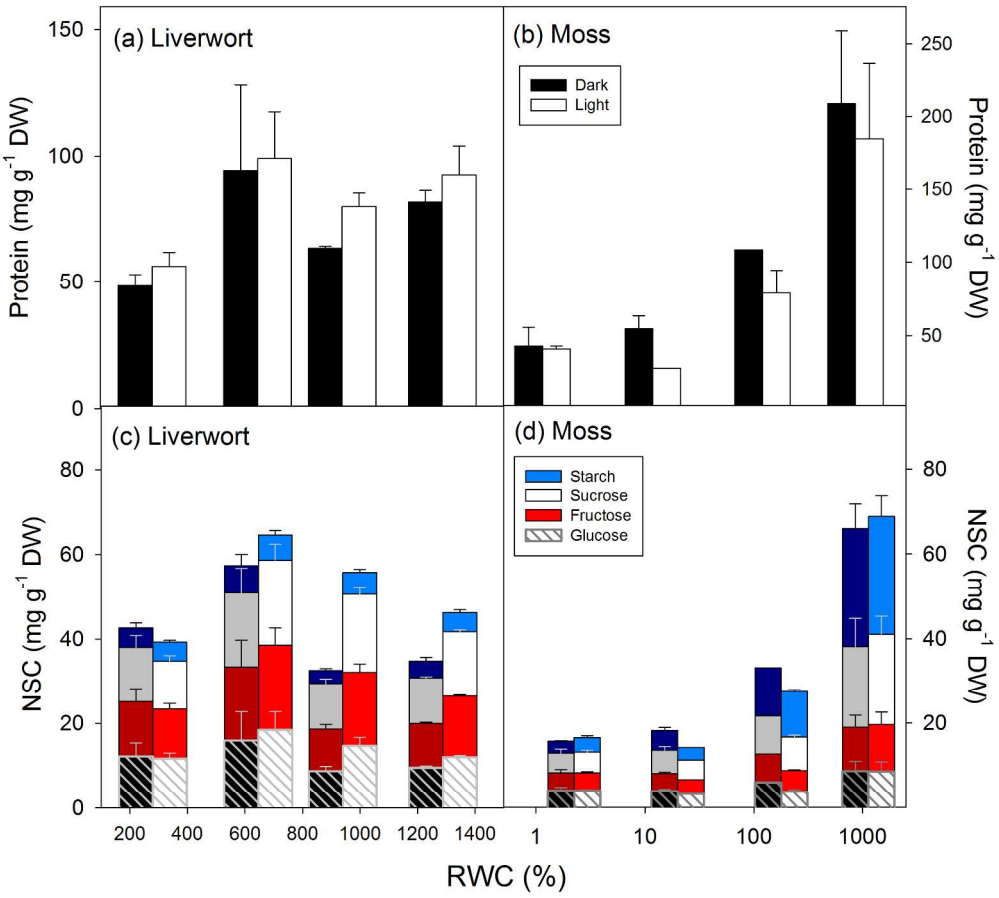

Protein and total non-structural carbohydrates (NSC) content, per unit of dry weight (DW), in the moss (upper panels) and the liverwort (lower panels) measured along decreasing relative water content (RWC) in the dark (filled bars) and in the light (open bars). Bars are the means (+se, *n* = 1-5) for grouped data according to four categorical levels of RWC (very high, high, intermediate and low), RWC values on the x-axis are the overall means for the light and dark treatments for each RWC level. In the liverwort, (glucose), fructose, sucrose, (total NSC) and protein content were (marginally) higher in the light than in the dark (*F* = 2.98, 4.41, 4.97, 3.93 and 4.94; *P* = 0.098, 0.047, 0.036, 0.06 and 0.037, respectively; according to the results of a two-way ANOVA of light and RWC, the latter included as a categorical variable with four levels).
Fig. 5
224x206mm (300 x 300 DPI)

Annexe 2

A new mechanistic framework to predict OCS fluxes from soils

Jérôme Ogée*[1], **Joana Sauze**[1], Jürgen Kesselmeier[2], Bernard Genty[3], Heidi Van Diest[2], Thomas Launois[1] and Lisa Wingate[1]

[1]INRA, UMR 1391 ISPA, 33140 Villenave d'Ornon, France
[2]Max Planck Institute for Chemistry, Biogeochemistry Department, Mainz, Germany
[3]CNRS/CEA/Aix-Marseille University, UMR 6191 BVME, Saint-Paul-lez-Durance, France

*Corresponding author:
Jérôme Ogée
E-mail: jerome.ogee@inra.fr
Phone: +33 (0) 5 57 12 24 22

Accepted in *Biogeosciences* in March 2016

Biogeosciences, 13, 2221–2240, 2016
www.biogeosciences.net/13/2221/2016/
doi:10.5194/bg-13-2221-2016

Biogeosciences Open Access EGU

A new mechanistic framework to predict OCS fluxes from soils

Jérôme Ogée[1], Joana Sauze[1], Jürgen Kesselmeier[2], Bernard Genty[3], Heidi Van Diest[2], Thomas Launois[1], and Lisa Wingate[1]

[1]INRA, UMR 1391 ISPA, 33140 Villenave d'Ornon, France
[2]Max Planck Institute for Chemistry, Biogeochemistry Department, Mainz, Germany
[3]CNRS/CEA/Aix-Marseille University, UMR 6191 BVME, Saint-Paul-lez-Durance, France

Correspondence to: Jérôme Ogée (jerome.ogee@bordeaux.inra.fr)

Received: 27 August 2015 – Published in Biogeosciences Discuss.: 22 September 2015
Revised: 15 March 2016 – Accepted: 21 March 2016 – Published: 18 April 2016

Abstract. Estimates of photosynthetic and respiratory fluxes at large scales are needed to improve our predictions of the current and future global CO_2 cycle. Carbonyl sulfide (OCS) is the most abundant sulfur gas in the atmosphere and has been proposed as a new tracer of photosynthetic gross primary productivity (GPP), as the uptake of OCS from the atmosphere is dominated by the activity of carbonic anhydrase (CA), an enzyme abundant in leaves that also catalyses CO_2 hydration during photosynthesis. However soils also exchange OCS with the atmosphere, which complicates the retrieval of GPP from atmospheric budgets. Indeed soils can take up large amounts of OCS from the atmosphere as soil microorganisms also contain CA, and OCS emissions from soils have been reported in agricultural fields or anoxic soils. To date no mechanistic framework exists to describe this exchange of OCS between soils and the atmosphere, but empirical results, once upscaled to the global scale, indicate that OCS consumption by soils dominates OCS emission and its contribution to the atmospheric budget is large, at about one third of the OCS uptake by vegetation, also with a large uncertainty. Here, we propose a new mechanistic model of the exchange of OCS between soils and the atmosphere that builds on our knowledge of soil CA activity from CO_2 oxygen isotopes. In this model the OCS soil budget is described by a first-order reaction–diffusion–production equation, assuming that the hydrolysis of OCS by CA is total and irreversible. Using this model we are able to explain the observed presence of an optimum temperature for soil OCS uptake and show how this optimum can shift to cooler temperatures in the presence of soil OCS emission. Our model can also explain the observed optimum with soil moisture content previously described in the literature as a result of diffusional constraints on OCS hydrolysis. These diffusional constraints are also responsible for the response of OCS uptake to soil weight and depth observed previously. In order to simulate the exact OCS uptake rates and patterns observed on several soils collected from a range of biomes, different CA activities had to be invoked in each soil type, coherent with expected physiological levels of CA in soil microbes and with CA activities derived from CO_2 isotope exchange measurements, given the differences in affinity of CA for both trace gases. Our model can be used to help upscale laboratory measurements to the plot or the region. Several suggestions are given for future experiments in order to test the model further and allow a better constraint on the large-scale OCS fluxes from both oxic and anoxic soils.

1 Introduction

The terrestrial biosphere is, along with the ocean, the largest sink in the global atmospheric CO_2 budget, with a very large year-to-year variability (e.g. Gurney and Eckels, 2011). Yet there is a scarcity of observations on how photosynthetic gross primary productivity (GPP) and respiration over land respond individually to warmer temperatures, increasing atmospheric CO_2 mixing ratios and changes in water availability (Beer et al., 2010; Frankenberg et al., 2011; Welp et al., 2011; Wingate et al., 2009). Obtaining new observational constraints of these two opposing land CO_2 gross fluxes at large scales is key to improving our models of the land C sink and providing robust projections of the atmospheric CO_2 budget and future climate (Friedlingstein et al., 2006; Piao et al., 2013).

In this context, additional tracers such as carbonyl sulfide (OCS), an analogue of CO_2 in many respects, could be very useful (Berry et al., 2013; Campbell et al., 2008; Kettle et al., 2002; Montzka et al., 2007). Indeed, the uptake rate of OCS by foliage is strongly related to GPP (Sandoval-Soto et al., 2005; Stimler et al., 2010) or more generally to the rate of CO_2 transfer into foliage (e.g. Seibt et al., 2010; Wohlfahrt et al., 2011). This is because both OCS and CO_2 molecules diffuse into foliage through the same stomatal pores and through mesophyll cells, where they are rapidly hydrated in an enzymatic reaction with carbonic anhydrase (CA) (Protoschill-Krebs and Kesselmeier, 1992). However, unlike CO_2, which is reversibly hydrated and converted into bicarbonate, OCS molecules are irreversibly hydrolysed (Elliott et al., 1989) and are not expected to diffuse back to the atmosphere, given the high affinity of CA towards OCS and the high activity of CA usually found in leaves (Protoschill-Krebs et al., 1996; Stimler et al., 2012).

Carbonic anhydrase is also widespread in diverse species from the Archaea, Bacteria, Fungi and Algae domains (Smith et al., 1999), so that OCS uptake can theoretically take place in soils. Several field studies provide support for this by showing that soils generally act as an OCS sink when measured at ambient concentrations (Castro and Galloway, 1991; Kuhn et al., 1999; J. Liu et al., 2010; Steinbacher et al., 2004; White et al., 2010; Yi et al., 2007) and that the uptake rate is reduced when the soil is autoclaved (Bremner and Banwart, 1976). Kesselmeier et al. (1999) also observed a significant ($> 50\,\%$) reduction of the OCS uptake rate in soil samples after adding ethoxyzolamide, one of the most efficient known CA inhibitors (e.g. Isik et al., 2009; Syrjänen et al., 2013). This finding strongly supports the idea that OCS uptake by soils is dominated by soil CA activity.

Soils can also emit OCS into the atmosphere as reported in some agricultural fields (Maseyk et al., 2014; Whelan and Rhew, 2015) or in anoxic soils (Devai and Delaune, 1995; Mello and Hines, 1994; Whelan et al., 2013; Yi et al., 2008) but the exact mechanisms for such emissions are still unclear (Mello and Hines, 1994; Whelan and Rhew, 2015). At the global scale, OCS consumption by soils seems to dominate OCS emission, and its contribution to the atmospheric budget is large, at about one third of the OCS uptake by vegetation, but with a large uncertainty (Berry et al., 2013; Kettle et al., 2002; Launois et al., 2015).

This large uncertainty in the OCS exchange rate from soils is partly caused by the variety of approaches used to obtain a global estimate of this flux. Kettle et al. (2002) assumed soil OCS fluxes responded to soil surface temperature and moisture only and used a parameterisation derived by Kesselmeier et al. (1999) from incubation measurements performed on a single agricultural soil in Germany. They recognised the limitation of such parameterisation and also noted the important role of some intrinsic properties of the soil and particularly its redox potential (Devai and Delaune, 1995), but did not account for it in their analysis. More recent approaches have assumed that the OCS flux from soils is proportional to other soil–air trace gas fluxes, such as heterotrophic (microbial) respiration (Berry et al., 2013) or the H_2 deposition rate (Launois et al., 2015). Experimental evidence that supports such scaling between different trace gas fluxes, however, is scarce and with mixed results. In summary, all the approaches to estimating soil OCS fluxes at large scales remain essentially empirical or based on hypotheses that are largely unvalidated. Given the supposedly important contribution of soils in the global OCS atmospheric budget, it becomes apparent that a deeper understanding of this flux and its underlying mechanisms is urgently needed. Until then estimating global GPP using OCS as an additional tracer of the carbon cycle remains elusive.

A plethora of process-based models exist that describe the transport and fate of trace gases in porous media (Falta et al., 1989; Olesen et al., 2001). Transport processes are fairly well understood and similar between different trace gases. On the other hand the processes responsible for the emission or destruction are usually quite unique, i.e. specific to each trace gas. The main difficulty then resides in understanding these emission and destruction processes. Very recently Sun et al. (2015) proposed parameterisations of OCS emission and destruction in soils. However their parameterisations remain largely empirical and lack important drivers such as soil pH or redox potential. In this paper we propose a mechanistic framework to describe OCS uptake and release from soil surfaces, based on our current understanding of OCS biogeochemistry in soils. Our model includes OCS diffusion and advection through the soil matrix, OCS dissolution and hydrolysis in soil water and OCS production. Soil microbial activity contributes to OCS hydrolysis, through a pseudo first-order CA-catalysed chemical reaction rate that varies with soil temperature and moisture, pH and CA concentration. OCS production, either abiotic or biotic, is also accounted for using a simple Q_{10}–type temperature response modulated by the soil redox potential. Using the model we explore the theoretical response of OCS fluxes to soil water content, soil temperature, soil depth and soil pH. We also evaluate our model against observed soil OCS uptake rates and patterns from the literature and discuss how the CA-catalysed reaction rates for each soil type can be reconciled with those typically observed for CO_2 hydration, given the differences in affinity of CA for OCS and CO_2.

2 Model description

2.1 Partitioning of OCS in the different soil phases

Carbonyl sulfide, like any other trace gas, can be present in the soil matrix in three forms: (1) vaporised in the air-filled pore space, (2) dissolved in the water-filled pore space or (3) adsorbed on the surface of the soil matrix (mineral and organic matter solid particles). The total OCS concentra-

tion C_{tot} (mol m^{-3} soil) is thus the sum of the OCS concentration in each phase weighted by their volumetric content: $C_{tot} = \varepsilon_a C + \theta C_l + \rho_b C_s$ where ε_a (m^3 air m^{-3} soil) is the volumetric air content, θ (m^3 water m^{-3} soil) is the volumetric water content, ρ_b (kg m^{-3}) is soil bulk density, C (mol m^{-3} air) and C_l (mol m^{-3} water) denote OCS concentration in soil air and liquid water respectively and C_s (mol kg^{-1} soil) denotes the OCS concentration adsorbed on the soil matrix.

In the following we will assume full equilibrium between the three phases. We will also assume linear sorption/desorption behaviour (a fair assumption at ambient OCS concentrations), so that C_l and C_s can be linearly related to C: $C_l = BC$ where B (m^3 water m^{-3} air) is the solubility of OCS in water and $C_s = (K_{sg} + BK_{sw})C$ where K_{sg} (m^3 air kg^{-1} soil) and K_{sw} (m^3 water kg^{-1} soil) are the solid/vapour and solid/liquid partitioning coefficients respectively (Olesen et al., 2001). The solubility B is related to Henry's law constant K_H (mol m^{-3} Pa^{-1}): $B = K_H RT$ where $R = 8.31446$ J mol^{-1} K^{-1} is the ideal gas constant and T (K) is soil water temperature. It has been shown that K_H is fairly independent of pH (at least for pH below 9, see De Bruyn et al. (1995); Elliott et al., 1989) but decreased with temperature and salinity (De Bruyn et al., 1995; Elliott et al., 1989). In the following we will use the parameterisation of Wilhelm et al. (1977) assuming low salinity levels in the soil:

$$K_H = 0.021 \exp[24900/R(1/T - 1/298.15)].$$

We preferred this expression rather than the more recent expression proposed by De Bruyn et al. (1995) that was based on one single data set rather than a compilation of multiple data sets. The difference between the two expressions is shown in Fig. 1a.

Expressions of K_{sg} and K_{sw} for OCS are currently not available. For organic vapours it has been shown that K_{sw} is highly correlated with soil characteristics such as C content (Petersen et al., 1995), specific surface area or clay content (Yamaguchi et al., 1999), and that K_{sg} is usually significant at soil water contents corresponding to less than five molecular layers of water coverage (Petersen et al., 1995). In this range of soil moisture, direct chemical adsorption onto dry mineral surfaces dominates and can increase the adsorption capacity of soils by several orders of magnitude. For these organic vapours the relationship of K_{sg} with soil moisture can be related to soil specific surface area (Petersen et al., 1995) or clay content (Yamaguchi et al., 1999). However these relationships obtained for organic vapours are unlikely to be applicable for OCS because the adsorption mechanisms may be completely different. Liu and colleagues have estimated OCS adsorption capacities of several mineral oxides and found that quartz (SiO_2) and anatase (TiO_2) did not adsorb OCS but other oxides with higher basicity adsorbed, reversibly or not, rather large quantities of OCS (Liu et al., 2008, 2009, 2010a). They also recognised that these estimates of the adsorption capacity of the minerals were an upper limit owing to the competitive adsorption of other gases such as CO_2, H_2O and

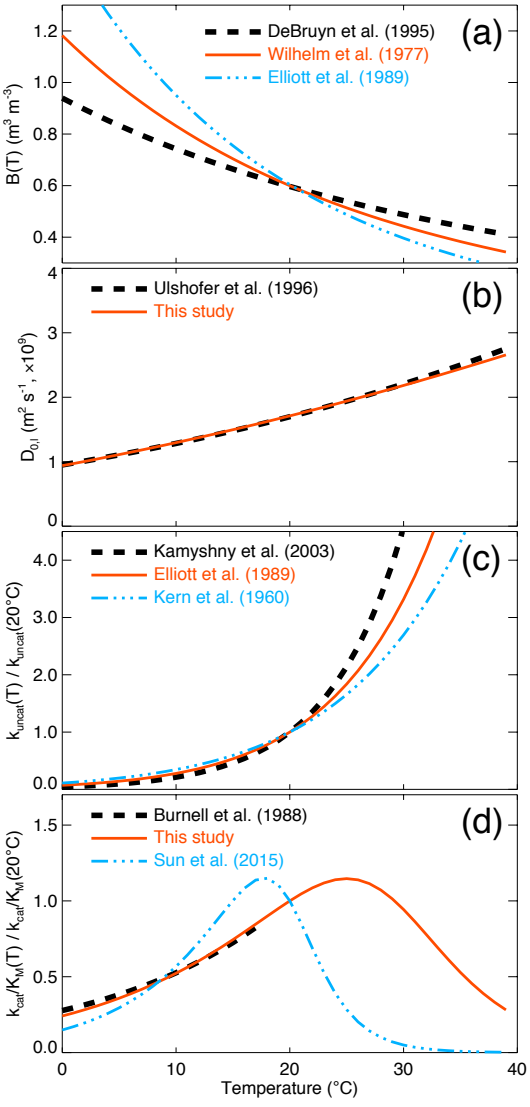

Figure 1. Temperature response of **(a)** the OCS solubility in water, **(b)** the OCS diffusivity in liquid water and **(c)** the uncatalysed and **(d)** CA-catalysed OCS hydrolysis rates. Red lines indicate the parameterisation used for this study.

NO_x that occur in the real Earth's atmosphere (Liu et al., 2009, 2010a) and the somewhat lower OCS partial pressure in ambient air compared to that used in their experimental setup. Also, at steady state, adsorption should have little influence on the soil–air OCS exchange rate, unless heterogeneous (surface) reactions occur and continuously remove OCS from the adsorbed phase (Liu et al., 2010a). In the following we will neglect adsorption of OCS on solid surfaces, but we recognise that this assumption might be an oversimplification.

2.2 Mass balance equation

The transport of OCS through the soil matrix occurs by either pressure-driven (advective-dispersive) or concentration-driven (diffusive) fluxes. Carbonyl sulfide can also be destroyed or emitted, owing to abiotic and/or biotic processes. The general mass balance equation for OCS in a small soil volume can then be written as follows:

$$\frac{\partial \varepsilon_{\mathrm{tot}} C}{\partial t} = -\nabla F_{\mathrm{diff}} - \nabla F_{\mathrm{adv}} + P - S, \quad (1)$$

where $\varepsilon_{\mathrm{tot}} = \varepsilon_{\mathrm{a}} + \theta B + \rho_{\mathrm{b}} \ (K_{\mathrm{sg}} + \ B K_{\mathrm{sw}}) \approx \ \varepsilon_{\mathrm{a}} + \theta B$ ($\mathrm{m^3\,air\,m^{-3}}$ soil) is total OCS soil porosity, F_{diff} ($\mathrm{mol\,m^{-2}\,s^{-1}}$) represents the diffusional flux of OCS through the soil matrix, F_{adv} ($\mathrm{mol\,m^{-2}\,s^{-1}}$) is the advective flux of OCS, P ($\mathrm{mol\,m^{-3}\,s^{-1}}$) the OCS production rate, S ($\mathrm{mol\,m^{-3}\,s^{-1}}$) the OCS consumption rate and $\nabla = \partial/\partial x + \partial/\partial y + \partial/\partial z$ denotes the differential operator, i.e. the spatial gradient in all three directions x, y and z.

If the soil is horizontally homogeneous (that is, the soil properties are independent of x and y) and the soil lateral dimensions are much larger than its total depth (minimal edge effects), the OCS concentration is only a function of soil depth z and time t. Eq. (1) may be simplified:

$$\frac{\partial \varepsilon_{\mathrm{tot}} C}{\partial t} = -\frac{\partial F_{\mathrm{diff}}}{\partial z} - \frac{\partial F_{\mathrm{adv}}}{\partial z} + P - S, \quad (2)$$

2.3 Diffusive fluxes

Diffusion in the gas phase is commonly described by Fick's first law (Bird et al., 2002; Scanlon et al., 2002):

$$F_{\mathrm{diff,a}} = -D_{\mathrm{eff,a}} \frac{\partial C}{\partial z}, \quad (3)$$

where $F_{\mathrm{diff,a}}$ ($\mathrm{mol\,m^{-2}\,s^{-1}}$) is the diffusive flux of gaseous OCS and $D_{\mathrm{eff,a}}$ ($\mathrm{m^3\,air\,m^{-1}\,soil\,s^{-1}}$) is the effective diffusivity of gaseous OCS through the soil matrix. The latter is commonly expressed relative to the binary diffusivity of OCS in free air $D_{0,\mathrm{a}}$ ($\mathrm{m^2\,air\,s^{-1}}$): $D_{\mathrm{eff,a}}/D_{0,\mathrm{a}} = \tau_{\mathrm{a}}\varepsilon_{\mathrm{a}}$ where τ_{a} is the so-called air tortuosity factor that accounts for the tortuosity of the air-filled pores, as well as their constrictivity and water-induced disconnectivity (e.g. Moldrup et al., 2003). The air-filled porosity (ε_{a}) appears in this equation to account for the reduced cross-sectional area in the soil matrix relative to free air, although the effective porosity for diffusion could be smaller if the soil contains small pores that do not contribute to the overall transport such as dead end or blind pores. Expressions for τ_{a} differ depending on whether the soil is repacked or undisturbed (Moldrup et al., 2003). For undisturbed soils the most commonly used equations are those of Penman (1940); $\tau_{\mathrm{a}} = 0.66$, hereafter referenced as Pen40, and Millington and Quirk (1961); $\tau_{\mathrm{a}} = \varepsilon_{\mathrm{a}}^{7/3}/\varphi^2$, where φ is total soil porosity, hereafter referred to as MQ61. For repacked soils, equations proposed by Moldrup et al. (2003); $\tau_{\mathrm{a}} = \varepsilon_{\mathrm{a}}^{3/2}/\varphi$, hereafter referred to as Mol03r are preferred. For undisturbed soils with high porosity such as volcanic ash, the expression proposed by Moldrup et al. (2003; $\tau_{\mathrm{a}} = \varepsilon_{\mathrm{a}}^{1+3/b}/\varphi^{3/b}$, where b is the pore-size distribution parameter) seems a better predictor (Moldrup et al., 2003). Recently a new density-corrected expression for undisturbed soils has also been proposed by Deepagoda et al. ((2011); $\tau_{\mathrm{a}} = [0.2(\varepsilon_{\mathrm{a}}/\varphi)^2 + 0.004]/\varphi$) that seems to be superior to previous formulations and has the advantage of not requiring knowledge of the pore-size distribution parameter b. A summary of these different formulations of the tortuosity factor and their range of application is given in Table 1.

Diffusion in the liquid phase is described in a similar fashion to the gas phase (Olesen et al., 2001):

$$F_{\mathrm{diff,l}} = -D_{\mathrm{eff,l}} \frac{\partial C_{\mathrm{l}}}{\partial z} = -D_{\mathrm{eff,l}} \left\{ B \frac{\partial C}{\partial z} + C \frac{\mathrm{d}B}{\mathrm{d}T} \frac{\partial T}{\partial z} \right\}, \quad (4)$$

where $F_{\mathrm{diff,l}}$ ($\mathrm{mol\,m^{-2}\,s^{-1}}$) is the diffusive flux of dissolved OCS in soil water and $D_{\mathrm{eff,l}}$ ($\mathrm{m^3\,water\,m^{-1}\,soil\,s^{-1}}$) is the effective diffusivity of dissolved OCS through the soil matrix. As for gaseous diffusion $D_{\mathrm{eff,l}}$ is commonly expressed relative to the binary diffusivity of OCS in free water $D_{0,\mathrm{l}}$ ($\mathrm{m^2\,water\,s^{-1}}$): $D_{\mathrm{eff,l}}/D_{0,\mathrm{l}} = \tau_{\mathrm{l}}\theta$ where τ_{l} is the tortuosity factor for solute diffusion. Different expressions for τ_{l} can also be found in the literature (Table 1).

Diffusion of OCS in the adsorbed phase can theoretically occur and can be described in a similar fashion to other trace gases (e.g. see Choi et al. (2001) for ozone). However we will neglect such a diffusion flux in the adsorbed phase because it is expected to be orders of magnitude smaller than in the two other phases. Also the binary diffusivity of any trace gas is several orders of magnitude higher in the air than it is for its dissolved counterpart in liquid water so that, in unsaturated (oxic) soils, $F_{\mathrm{diff}} = F_{\mathrm{diff,a}} + F_{\mathrm{diff,l}}$ is dominated by the gas-phase OCS diffusion flux $F_{\mathrm{diff,a}}$. The role of $F_{\mathrm{diff,l}}$ in the OCS transport equations becomes significant only when the soil is waterlogged.

The binary diffusivity $D_{0,\mathrm{a}}$ depends on pressure and temperature and is assumed here to follow the Chapman–Enskog theory for ideal gases (i.e. Bird et al., 2002): $D_{0,\mathrm{a}}(T, p) = D_{0,\mathrm{a}}(T_0, p_0) \ (T/T_0)^{1.5} \ (p_0/p)$. A value for $D_{0,\mathrm{a}}$ (25 °C, 1 atm) of $1.27 \times 10^{-5}\,\mathrm{m^2\,s^{-1}}$ is used and derived from the value for the diffusivity of water vapour in air at 25 °C ($2.54 \times 10^{-5}\,\mathrm{m^2\,s^{-1}}$, see Massman, 1998) and the CO_2 / OCS diffusivity ratio of 2.0 ± 0.2 derived from the Chapman–Enskog theory and the difference in molar masses of OCS and CO_2 (Seibt et al., 2010). The binary diffusivity $D_{0,\mathrm{l}}$ also depends on temperature (Ulshöfer et al., 1996). Because the Stokes–Einstein equation only applies to spherical suspended particles, we preferred to use an empirical equation that works well for both the self-diffusivity of water and the diffusivity of dissolved CO_2 in liquid water (Zeebe, 2011): $D_{0,\mathrm{l}}(T) = D_{0,\mathrm{l}}(T_0) \ (T/T_0 - 1)^2$, with $D_{0,\mathrm{l}}$ (25 °C) $= 1.94 \times 10^{-9}\,\mathrm{m^2\,s^{-1}}$ (Ulshöfer et al., 1996) and

Table 1. Summary of tortuosity factor formulations for gaseous (τ_a) and liquid (τ_l) diffusion from the literature. ε_a: air porosity; φ: total porosity; θ: soil water content; b: pore-size distribution parameter; NA: data not available.

Notation	τ_a	τ_l	Soil treatment	Reference
Pen40	0.66	0.66	NA	Penman (1940)
MQ61	$\varepsilon_a^{7/3}/\varphi^2$	$\theta^{7/3}/\varphi^2$	NA	Millington and Quirk (1961)
Mol03r	$\varepsilon_a^{3/2}/\varphi$	$\theta^{b/3}/\varphi^{b/3-1}$	repacked	Moldrup et al. (2003)
Mol03u	$\varepsilon_a^{1+3/b}/\varphi^{3/b}$	$\theta^{b/3}/\varphi^{b/3-1}$	undisturbed	Moldrup et al. (2003)
Deepa11	$[0.2(\varepsilon_a/\varphi)^2+0.004]/\varphi$	NA	undisturbed	Deepagoda et al. (2011)

$T_0 = 216$ K. This value of T_0 was chosen to be intermediate between the value used for water (215.05 K) and dissolved CO_2 (217.2 K) (Zeebe, 2011), and results in a temperature dependency of $D_{0,l}$ for OCS in water in very good agreement with relationships found in other studies (Fig. 1b).

2.4 Advective fluxes

Advection of OCS can occur in both the liquid and gas phases when the carrier fluid (water or air) moves relative to the soil matrix:

$$F_{adv,l} = q_l C_l = q_l B C, \tag{5a}$$

$$F_{adv,a} = q_a C, \tag{5b}$$

where q_l (m s^{-1}) and q_a (m s^{-1}) are the velocity fields for liquid water and air respectively. If the flow in the porous soil is laminar these velocity fields are given by Darcy's law (Massman et al., 1997; Scanlon et al., 2002):

$$q_l = -\frac{k_l}{\mu_l}\frac{\partial \Psi_l}{\partial z} = -K_l\left(\frac{\partial h_l}{\partial z}+1\right), \tag{6a}$$

$$q_a = -\frac{k_a}{\mu_a}\left(\frac{\partial p_a}{\partial z}+\rho_a g\right). \tag{6b}$$

In Eqs. (6a) and (6b) k_l and k_a (m^2) denote soil permeabilities for liquid water and air respectively, μ_l and μ_a (kg m^{-1} s^{-1}) are water and air dynamic viscosities, $\Psi_l = \rho_l g(h_l + z)$ is total soil water potential (Pa), ρ_l is water density (1000 kg m^{-3}), h_l (m) is matric potential height, g is gravitational acceleration (9.81 m s^{-2}), ρ_a is air density (ca. 1.2 kg m^{-3}) and p_a (Pa) is air pressure. We also defined the soil hydraulic conductivity K_l (m s^{-1}): $K_l = k_l \rho_l g/\mu_l$. In practice p_a can be expressed as the sum of the hydrostatic pressure ($p_{ah} = -\rho_a g z$) and a fluctuating (non-hydrostatic) part: $p_a = -\rho_a g z + p'_a$ so that Eq. (6b) can be replaced by:

$$q_a = -\frac{k_a}{\mu_a}\frac{\partial p'_a}{\partial z}. \tag{6c}$$

From Eq. (6c) we can see that advection in the gas phase can result from pressure fluctuations, caused by, e.g. venting the soil surface (according to Bernouilli's equation) or turbulence above the soil surface. Typical air pressure fluctuations are of the order of 10 Pa (Maier et al., 2012; Massman et al., 1997). Pressure fluctuations can also result from non-hydrostatic density fluctuations caused by a change in the air composition with gas species of different molar mass as air or by temperature gradients, but the resulting flux is significant only in highly permeable (i.e. fractured) soils.

When averaged over a long enough timescale (> 1 h) the advective flux starts to become negligible compared to the diffusive flux (e.g. Massman et al., 1997). Integration timescales of a few minutes were already assumed to allow liquid–vapour equilibration in Eq. (5a). In the following we will thus neglect advective fluxes in the OCS budget equation, keeping in mind that such an assumption is valid only for time scales of about 1h or longer.

Even when advective fluxes are negligible, advection through porous media generates a diffusive-like flux called mechanical dispersion that reflects the fact that not everything in the porous medium travels at the average water or gas flow speed. Some paths are faster, some slower, some longer and some shorter, leading to a net spreading of the gas or solute plume that looks very much like diffusive behaviour. Since mechanical dispersion depends on the flow, it is expected to increase with increasing flow speed:

$$F_{disp,l} = -D_{disp,l}\frac{\partial C_l}{\partial z} = -\alpha_l |q_l| \frac{\partial BC}{\partial z}, \tag{7a}$$

$$F_{disp,a} = -D_{disp,a}\frac{\partial C}{\partial z} = -\alpha_a |q_a| \frac{\partial C}{\partial z}, \tag{7b}$$

where α_l (m) and α_a (m) are the longitudinal dynamic dispersivity of liquid water and air flow respectively and $D_{disp,l}$ (m^2 s^{-1}) and $D_{disp,a}$ (m^2 s^{-1}) are the corresponding dispersive diffusivities. Transverse dispersion (i.e. in a plane perpendicular to the flow) can also occur but will be neglected here.

In practice, because of advective–dispersive fluxes, we must know the liquid water and air velocity fields q_l and q_a in order to solve the trace gas OCS mass budget Eq. (2). This requires solving the total mass balance equations for liquid water and air separately. However, except during rain infiltration and immediate redistribution, q_l rarely exceeds a few millimetres per day while the drift velocity, defined as the ratio $F_{diff,a}/C$, is typically of the order of a few millimetres per minute. For this reason, advection fluxes are generally neglected in soil gas transport models. Dispersive fluxes can

still be accounted for as a correction factor to true diffusion, provided we have parameterisations of the dispersion diffusivities that are independent of the advective flux (e.g. expressions for $D_{\mathrm{disp,a}}$ independent of q_{a}). For example Maier et al. (2012) proposed expressions of $D_{\mathrm{disp,a}}/D_{0,\mathrm{a}}$ that rely on the air-filled porosity (ε_{a}) and permeability (μ_{a}) of the soil and the degree of turbulence above the soil surface (characterised by the friction velocity u_*).

2.5 Consumption and production rates

The processes of consumption or production of OCS in a soil are not fully understood. Carbonyl sulfide can be consumed through hydrolysis in the bulk soil water at an uncatalysed rate k_{uncat} (s^{-1}) that depends mostly on temperature T and pH (Elliott et al., 1989). In the following we will use the expression proposed by Elliott et al. (1989) because it covers the widest range of temperature and pH:

$$k_{\mathrm{uncat}} = 2.15\cdot 10^{-5}\exp\left(-10450\left(\frac{1}{T}-\frac{1}{298}\right)\right) + 12.7\cdot 10^{-\mathrm{pK_w}+\mathrm{pH}}\exp\left(-6040\left(\frac{1}{T}-\frac{1}{298}\right)\right), \quad (8)$$

where $\mathrm{pK_w}$ is the dissociation constant of water. Other expressions are available in the literature and compared to Eq. (8) for both temperature (Fig. 1c) and pH (Fig. 2a) responses. Using Eq. (8) the uncatalysed OCS uptake rate is then computed as $S_{\mathrm{uncat}} = k_{\mathrm{uncat}} B\theta C$. The volumetric soil water content θ appears in this equation to convert the hydration rate from $\mathrm{mol\,m^{-3}}$ water $\mathrm{s^{-1}}$ to $\mathrm{mol\,m^{-3}}$ soil $\mathrm{s^{-1}}$.

This uncatalysed rate is rather small and cannot explain the large OCS uptake rates observed in oxic soils (Kesselmeier et al., 1999; J. Liu et al., 2010; Van Diest and Kesselmeier, 2008). The main consumption of OCS is thought to be enzymatic and governed by soil microorganism CA activity (Kesselmeier et al., 1999; J. Liu et al., 2010; Van Diest and Kesselmeier, 2008). We will assume that such a catalysed reaction by CA-containing organisms can be described by Michaelis–Menten kinetics, as was observed for OCS in several marine algae species (Blezinger et al., 2000; Protoschill-Krebs et al., 1995) and one flour beetle (Haritos and Dojchinov, 2005). Because of the low concentrations of OCS in ambient air (500 ppt) and the comparatively high values of the Michaelis–Menten coefficient for OCS (K_{m}, see Ogawa et al. (2013); Protoschill-Krebs et al., 1995, 1996) the catalysed uptake rate S_{cat} ($\mathrm{mol\,m^{-3}\,s^{-1}}$) can be approximated:

$$S_{\mathrm{cat}} = \theta k_{\mathrm{cat}}[\mathrm{CA}]\frac{BC}{K_{\mathrm{m}}+BC} \approx \frac{k_{\mathrm{cat}}}{K_{\mathrm{m}}}[\mathrm{CA}]B\theta C, \quad (9)$$

where k_{cat} ($\mathrm{s^{-1}}$) and K_{m} ($\mathrm{mol\,m^{-3}}$) are the turnover rate and the Michaelis–Menten constant of the enzymatic reaction respectively and [CA] ($\mathrm{mol\,m^{-3}}$) is the total CA concentration in soil water. We recognise that Eq. (9) is an oversimplification of the reality in the sense that k_{cat} and K_{m} are not true kinetic parameters but rather volume-averaged parameters for the entire soil microbial community. Also Eq. (9) neglects the competition for CA by CO_2 molecules and the co-limitation of the uptake by diffusional constraints. Given the Michaelis–Menten constant of CA for CO_2 ($K_{\mathrm{m,CO_2}}$, of the order of 3 mM at 25 °C and pH 8–9) and the range of CO_2 mixing ratios encountered in soil surfaces (300–5000 ppm or 0.01–0.15 mM at 25 °C and 1 atm), we can conclude that the competition with CO_2 is negligible (i.e. the denominator in Eq. (9) would need to be multiplied by a factor $1+[CO_2]/K_{\mathrm{m,CO_2}}$ which would deviate from unity by less than 5 %). We recognise that the CO_2 concentration inside microbial cells (i.e. at the CA sites) must be somewhat larger than in the surrounding soil water but certainly not to an extent to justify accounting for competition between the two substrates. Also, using typical values of transfer conductance across cell wall and plasma membrane (Evans et al., 2009), we can show that the limitation of OCS uptake by diffusion into the microbial cells is negligible for calculating the OCS uptake rate (see Appendix A for a derivation). In the following we will therefore assume Eq. (9) to be valid.

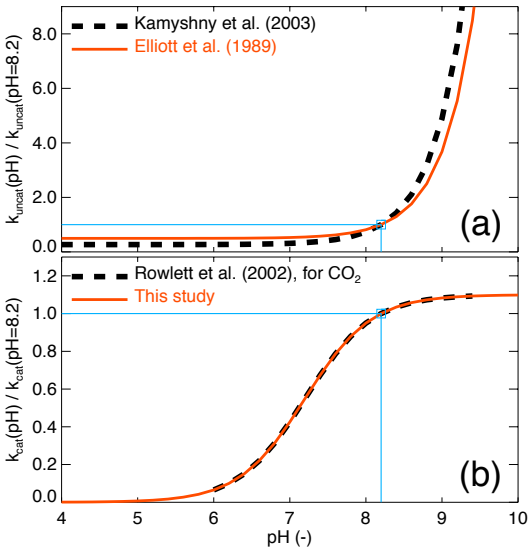

Figure 2. Response of the normalised **(a)** uncatalysed and **(b)** CA-catalysed OCS hydrolysis rates to changes in soil pH. Red lines indicate the parameterisation used for this study. The blue lines indicate the normalisation at pH = 8.2.

As found for any enzymatic reaction, k_{cat} and K_{m} depend on temperature and internal pH ($\mathrm{pH_{in}}$). In the following we will assume that the ratio $k_{\mathrm{cat}}/K_{\mathrm{m}}$ has a temperature dependency that can be approximated:

$$\frac{k_{\mathrm{cat}}}{K_{\mathrm{m}}} \propto x_{\mathrm{CA}}(T) = \frac{\exp(-\Delta H_{\mathrm{a}}/RT)}{1+\exp(-\Delta H_{\mathrm{d}}/RT+\Delta S_{\mathrm{d}}/R)}, \quad (10a)$$

where ΔH_{a}, ΔH_{d} and ΔS_{d} are thermodynamic parameters. In the following we will take $\Delta H_{\mathrm{a}} = 40\,\mathrm{kJ\,mol^{-1}}$, $\Delta H_{\mathrm{d}} = 200\,\mathrm{kJ\,mol^{-1}}$ and $\Delta S_{\mathrm{d}} = 660\,\mathrm{J\,mol^{-1}\,K^{-1}}$, that leads

to a temperature optima $T_{opt,CA} = 25\,°C$ and reproduces well the temperature response of β-CA found on maize leaf extracts observed in the range 0–17 °C by Burnell and Hatch (1988) (Fig. 1d). To our knowledge this is the only study that reports the temperature response of β-CA, the dominant CA class expected in soils (Smith et al., 1999). Interestingly our parameterisation of $x_{CA}(T)$, based on direct measurements on β-CA from Burnell and Hatch (1988), is very different from the one used by Sun et al. (2015), especially at temperatures above 20 °C (Fig. 1d).

The pH response of CA activity for OCS hydrolysis was described by a monotonically decreasing function towards more acidic pH_{in}, as observed in plant β-CA for both OCS (Protoschill-Krebs et al., 1996) and CO_2 (Rowlett et al., 2002). In the following we will use the expression proposed by Rowlett et al. (2002) for CO_2:

$$\frac{k_{cat}}{K_m} \propto y_{CA}(pH_{in}) = \frac{1}{1 + 10^{-pH_{in}+pK_{CA}}}. \quad (10b)$$

A value of $pK_{CA} = 7.2$ was used that corresponds to the CA response of the wild-type *Arabidopsis thaliana* (Rowlett et al., 2002). The shape of the function y_{CA} is shown in Fig. 2b.

A β-CA K_M value for OCS (39 μM at 20 °C and pH 8.2) was estimated on pea (*Pisum sativum*) by Protoschill-Krebs et al. (1996). From a reanalysis of the same data set we also estimated a k_{cat} of 93 s^{-1} at the same temperature and pH, leading to a k_{cat}/K_m value of 2.39 $s^{-1}\,\mu M^{-1}$. To our knowledge this is the only report of k_{cat} and K_m values for OCS in β-CA.

The breaking of water film continuity that occurs at low soil water content leads to a reduction in microbial activity owing to the spatial separation of the microbes and their respiratory substrates (Manzoni and Katul, 2014). In our case soil water discontinuity should not affect OCS supply as gaseous OCS should be equally available in all soil pores. On the other hand different organisms may have different k_{cat}/K_m values so that the spatially-averaged k_{cat}/K_m could vary with drought-induced changes in microbial diversity. However our knowledge of how k_{cat}/K_m for OCS varies amongst different life forms is too scarce to know if it should increase or decrease during drought stress. We will therefore assume that soil water discontinuity does not affect k_{cat}/K_m directly. CA concentration ([CA]) could also vary during drought stress, although it is not clear in which direction. During water stress, microbial activity such as respiration or growth is usually reduced, but slow growth rates and heat stress have been shown to cause an up-regulation of CA-gene expression in *Escherichia coli* (Merlin et al., 2003), probably because of a need of bicarbonate for lipid synthesis. For this study we thus make the simplifying assumption that CA concentration does not vary with soil water content. The catalysed OCS uptake rate S_{cat} is then simply proportional to soil water content (Eq. 9).

Destruction of OCS can also occur in the solid phase and was observed on pure mineral oxides with high basicity (Liu et al., 2008, 2009, 2010a). However, such catalytic reaction should be significant only in very dry soils (with only a few molecular layers of water) and in the absence of other competitive adsorbents such as CO_2 (Liu et al., 2008, 2010b) and is therefore neglected in our model. The total soil OCS uptake rate is thus computed as $S = kB\,\theta C$:

$$k = k_{uncat}(T, pH) + \frac{x_{CA}(T)}{x_{CA}(20\,°C)} \frac{y_{CA}(pH_{in})}{y_{CA}(8.2)} 2390\,[CA]. \quad (11a)$$

Following common practice in the CO_2 literature, we will also express k with respect to the uncatalysed rate at 25 °C and pH 4.5:

$$k = f_{CA} k_{uncat}(25\,°C, pH = 4.5) x_{CA}(T)/x_{CA}(25\,°C), \quad (11b)$$

where f_{CA} is the so-called soil CA enhancement factor. We can see from Eqs. (11a)–(b) that f_{CA} is not an intrinsic property of the soil and will vary with temperature and pH, even at constant CA concentration. In the case where the catalysed rate dominates k in Eq. (11a) and the internal pH is close to 8.2 we have: $f_{CA} \approx 111$ [CA], where [CA] is in nM.

In some situations the OCS uptake rates can be overridden by OCS production. This is the case when soil temperature rises above 25 °C (Maseyk et al., 2014; Whelan and Rhew, 2015) or soil redox potential falls below −100 mV (Devai and Delaune, 1995). Light has also been proposed as an important trigger of OCS production, assuming photoproduction processes similar to those observed in ocean waters can occur (Whelan and Rhew, 2015). However the literature and data on this possible mechanism is still too scarce and not quantitative enough to be accounted for in our model.

The soil redox potential (E_h) is a very dynamic variable that is not easily measured in the field, especially in unsaturated soils (e.g. van Bochove et al., 2002). Although E_h and pH are linked, their relationship is not unique and depends on the set of oxidants and reductants present in the soil solution (e.g. Delaune and Reddy, 2005). Furthermore the soil redox potential is probably a more direct trigger for OCS production, as it defines when sulfate ions start to become limiting for the plants or the soil microbes (Husson, 2012). For this study we thus consider that, for anoxic soils at least, E_h is the primary driver of OCS production, independently of pH:

$$P = P_{ref} y_P(E_h)\; Q_{10}^{(T-T_{ref})/10}, \quad (12a)$$

where P_{ref} (mol m^{-3} s^{-1}) is the production rate at temperature T_{ref} (K) and low E_h (typically −200 mV) and Q_{10} is the multiplicative factor of the production rate for a 10 °C temperature rise. Because soil OCS emission, when observed in oxic soils, usually occurs at temperature around 25 °C or higher, we will set T_{ref} as 25 °C and thus $P_{ref} = P_{25}$. According to results from Devai and DeLaune (1995), the function $y_P(E_h)$ may be expressed in the following manner:

$$y_P(E_h) = \frac{1}{1 + \exp(-(E_h - 100\,mV)/20\,mV)}, \quad (12b)$$

For oxic soils, Eq. (12a) would probably need to be modified to incorporate the effect of light on the OCS production rate (Whelan and Rhew, 2015) and the function $y_P(E_h)$ given by Eq. (12b) may not hold. In any case it would be difficult to evaluate. Whether we should use UV light only or total solar radiation could also be debated. For all these reasons we decided in this study to only look at the effect of temperature on the OCS production rate and its consequences on the total OCS deposition rate.

2.6 Steady-state solution

The one-dimensional mass balance equation (Eq. 2) can be rewritten:

$$\frac{\partial \varepsilon_t C}{\partial t} = \frac{\partial}{\partial z}\left\{\left(D_{\mathrm{eff,a}} + \alpha_a |q_a|\right)\frac{\partial C}{\partial z} + \left(D_{\mathrm{eff,l}} + \alpha_l |q_l|\right)\frac{\partial BC}{\partial z}\right\} + P - kB\theta C. \quad (13)$$

Assuming steady-state conditions, isothermal and uniform soil moisture and porosity through the soil column, this simplifies to the following:

$$D\frac{d^2C}{dz^2} - kB\theta C = -P, \quad (14)$$

with:

$$D = D_{\mathrm{eff,a}} + \alpha_a |q_a| + \left(D_{\mathrm{eff,l}} + \alpha_l |q_l|\right) B. \quad (15)$$

Boundary conditions are $C(z=0) = C_a$, the OCS concentration in the air above the soil column and $dC/dz\ (z = z_{max}) = 0$, i.e. zero flux at the bottom of the soil column, located at depth z_{max} (the case for laboratory measurements). With such boundary conditions, the solution of Eq. (14) is the following:

$$C(z) = z_1^2 P + (C_a - z_1^2 P)\frac{e^{-z/z_1} + \xi^2 e^{+z/z_1}}{1+\xi^2}, \quad (16a)$$

with $z_1^2 = D/kB\theta$ and $\xi = e^{-z_{max}/z_1}$. This leads to an OCS efflux at the soil surface:

$$F = \sqrt{kB\theta D}\left(C_a - \frac{z_1^2 P}{D}\right)\frac{1-\xi^2}{1+\xi^2}, \quad (16b)$$

from which we can deduce the deposition velocity $V_d = -F/C_a$.

For field data sets, the condition at the lower boundary should be modified to $dC/dz\ (z \to \infty) = 0$ and the production rate P should be positive and uniform only over a certain depth z_P below the surface. In this case the steady-state solution becomes the following:

$$F = \sqrt{kB\theta D}\cdot\left(C_a - \frac{z_1^2 P}{D}(1 - \exp(-z_P/z_1)\right). \quad (17)$$

We can verify that both equations give the same results if $z_{max} \to \infty$ and $z_P \to \infty$ and also that Eq. (17) leads to $F \to -P \times z_P$ when $k \to 0$.

2.7 Soil incubation data sets used for model validation

The steady-state OCS deposition model presented here (Eq. 16) was evaluated against measurements performed on different soils in the laboratory. For this purpose we revisited the data set presented in Van Diest and Kesselmeier (2008). Volumetric soil moisture content (θ, in m^3 (H_2O) m^{-3}(soil)) was converted from gravimetric soil water content data ($M_{w,soil}$, in g(H_2O) g(soil)$^{-1}$) by means of the bulk density of the soil inside the chamber (ρ_b, in g cm^{-3}): $\theta = M_{w,soil}\rho_b/\rho_w$, where $\rho_w = 1\ g\,cm^{-3}$ is the density of liquid water. The soil bulk density was itself estimated from the maximum soil moisture content after saturation ($\theta_{max} = M_{w,soil,max}\rho_b/\rho_w$), assuming the latter corresponded to soil porosity ($\varphi = 1 - \rho_b/2.66$), i.e. ($\rho_b = 1/(M_{w,soil,max}/\rho_w + 1/2.66)$. Soil thickness ($z_{max}$) was further estimated using ρ_b, soil dry weight (200 g for the German soil, 80 g for the other soils) and soil surface area (165.1 cm^2) assuming soil density was uniform. Air porosity was calculated as $\varepsilon_a = \varphi - \theta$. These estimates of θ, φ and ε_a were then used to compute D (Eq. (15), assuming $|q_a| = |q_l| = 0$) and F (Eq. (16b), with $P = 0$ and k estimated using Eq. (11b), with different f_{CA} values for each soil temperature incubation). Note that in these experiments, the air in the chamber headspace was stirred with fans above the soil surface so that dispersion fluxes may be large (i.e. $|q_a|$ may not be zero). Without any more information about turbulence intensity at the soil surface in these experiments, we had to neglect this possible complication. We will discuss below how this simplification may affect the results of our simulations of these experiments.

3 Results

3.1 Sensitivity to diffusivity model

Given the large diversity of expressions for the air tortuosity factor (τ_a) used to compute the effective diffusivity of OCS through the soil matrix, we felt it important to perform a sensitivity analysis of the model to different formulations available in the literature for τ_a. In Fig. 3 we show how the steady-state soil OCS deposition velocity model (Eq. 16b) responds to soil moisture or soil temperature for three different formulations of τ_a: Pen40 ($\tau_a = 0.66$), MQ61 ($\tau_a = \varepsilon_a^{7/3}/\varphi^2$) and Mol03r ($\tau_a = \varepsilon_a^{3/2}/\varphi$). We also indicate the optimal soil moisture (θ_{opt}) and temperature (T_{opt,V_d}) for each formulation.

We found that the optimal temperature and the general shape of the response to temperature were not affected by the choice of the diffusivity model (Fig. 3, right panel). On the other hand the optimal soil moisture and the general shape of the response to soil moisture strongly depended on the choice made for τ_a (Fig. 3, left panel). In particular the model of Penman (1940) gives a perfectly symmetric response to soil

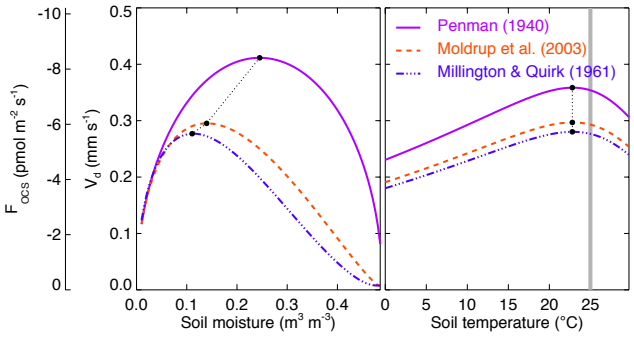

Figure 3. Sensitivity of the modelled OCS flux (F_{OCS}) and deposition velocity (V_d) to the formulation used to describe gaseous and solute diffusion. The soil moisture and temperature response curves shown here were obtained assuming no source term, a soil depth and pH of 1 m and 7.2 respectively and a CA enhancement factor for OCS hydrolysis of 30 000. Closed circles indicate the temperature or soil moisture optimum of each response curve and the grey thick line in the right panel indicates the set optimal temperature for CA activity (25 °C in this case).

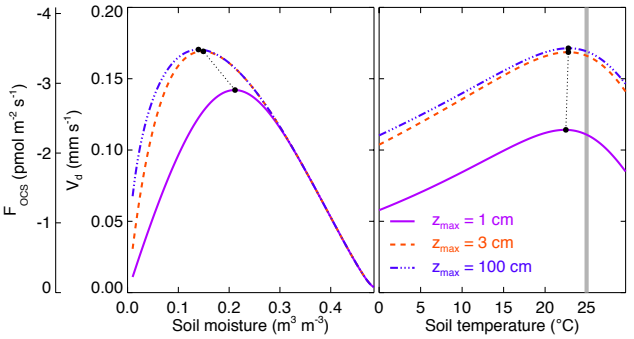

Figure 4. Sensitivity of the modelled OCS flux (F_{OCS}) and deposition velocity (V_d) to soil column depth. The soil moisture and temperature response curves shown here were obtained using the diffusivity model of Moldrup et al. (2003) and assuming no source term, a soil pH of 7.2 and a CA enhancement factor for OCS hydrolysis of 10 000. Closed circles indicate the temperature or soil moisture optimum of each response curve and the grey thick line in the right panel indicates the set optimal temperature for CA activity (25 °C in this case).

moisture with an optimal value at $\theta_{opt} = 0.50\varphi$, unlike other formulations: $\theta_{opt} \approx 0.23\varphi$ for Millington and Quirk (1961) and $\theta_{opt} \approx 0.29\varphi$ for Moldrup et al. (2003).

It is also noticeable on the right panel of Fig. 3 that the optimal temperature for V_d (T_{opt,V_d}) is actually lower than the prescribed optimal temperature for the catalysed OCS hydrolysis rate ($T_{opt,CA} = 25$ °C in this case), even in the absence of an OCS source term. This is because T_{opt,V_d} integrates other temperature responses from the total effective diffusivity (D) and the OCS solubility (B). Although these variables do not exhibit a temperature optimum, their temperature responses affect the overall value of T_{opt,V_d}. It can be shown analytically that this leads to $T_{opt,V_d} < T_{opt,CA}$.

3.2 Sensitivity to soil depth

Laboratory-based measurements of soil–air OCS fluxes are generally performed on small soil samples with a thickness of no more than a few centimetres. In contrast flux measurements performed in the field account for the entire soil column beneath the chamber enclosure. In order to see whether results from laboratory measurements could be directly applied to field conditions we performed a sensitivity analysis of the model to soil thickness (Fig. 4). We found that the responses to both soil moisture and soil temperature were affected by maximum soil depth (z_{max}), at least when z_{max} was below a few centimetres. Thin soils lead to lower maximum deposition rates but higher values of θ_{opt} and T_{opt,V_d}. In Fig. 4 this is true mostly for $z_{max} = 1$ cm, and as soon as z_{max} reaches values above or equal to 3 cm, the response curve becomes almost indistinguishable from that obtained with $z_{max} = 100$ cm.

However this threshold on z_{max} also depends on soil CA activity. Results shown in Fig. 4 were obtained with an enhancement factor for OCS hydrolysis f_{CA} of only 10 000. An even smaller enhancement factor would have led to a deeper transition zone (e.g. about 10 cm with f_{CA} of 1000). This is because in Eq. (16b), the steady-state model of OCS deposition is proportional to $\tanh(z_{max}/z_1)$. Given the shape of the hyperbolic tangent function, we expect our steady-state OCS deposition velocity model to become insensitive to z_{max} as soon as $z_{max}/z_1 \geq 2$. With $z_1 = \sqrt{D/kB\theta}$ and because k is proportional to f_{CA} we can see that this condition on z_{max}/z_1 will depend on f_{CA}. At $f_{CA} = 1000$, we have $z_1(\theta_{opt}) \sim 5$ cm while at $f_{CA} = 10\,000$ we have $z_1(\theta_{opt}) \sim 1.5$ cm.

This response to soil depth was already observed by Kesselmeier et al. (1999), who reported measurements of OCS deposition velocity that increased linearly with the quantity of soil in their soil chamber enclosure up to 200 g of soil and then reached a plateau at around 400 g. Because their soil samples were evenly spread inside the soil chamber, an increase in the quantity of soil directly translates into an increase in soil thickness. Using an enhancement factor f_{CA} of 27 000 we were able to reproduce their saturation curve with soil weight using our steady-state model (Fig. 5). A lower f_{CA} value would have reduced the curvature of the model but would have also lowered the maximum V_d (not shown, but see Fig. 6). A value for f_{CA} of 27 000 was the best compromise to match the observed saturation curve. Because different soil weights were measured at different times with new soil material each time, it is possible that they would correspond to slightly different f_{CA} values and this could explain the slight mismatch between the model and the fitted curve on the observations.

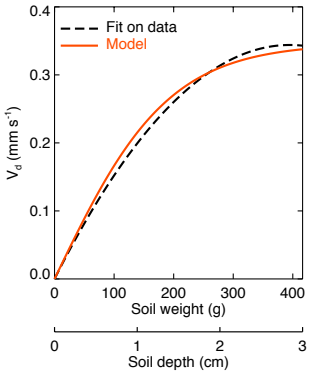

Figure 5. Modelled (solid line) and observed (dotted line) response of the modelled OCS deposition velocity (V_d) to soil column depth. Soil column depth is also converted into soil weight assuming a soil surface area of 165.1 cm^2 and a soil bulk density and pH of 0.85 kg m^3 and 7.2 respectively, to be comparable with the experimental setup used in Kesselmeier et al. (1999) to derive the observed response curve. Model results shown here were obtained using the diffusivity model of Moldrup et al. (2003) and assuming an enhancement factor and an optimum temperature for OCS hydrolysis of 26 000 and 25 °C respectively and no source term. Soil water content and temperature were also set to 11 % weight and 17 °C respectively, to be comparable with the experimental data, while the fit on observed uptake rates that was originally reported were converted into deposition velocities assuming a constant mixing ratio of 600 ppt (Kesselmeier et al., 1999).

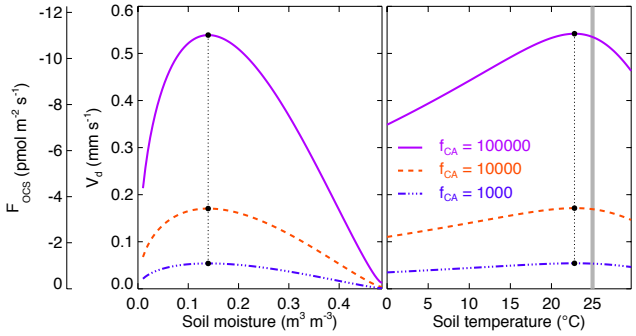

Figure 6. Sensitivity of the modelled OCS flux (F_{OCS}) and deposition velocity (V_d) to soil CA activity. The soil moisture and temperature response curves shown here were obtained using the diffusivity model of Moldrup et al. (2003) and assuming no source term, a soil pH of 7.2 and a soil depth of 1 m. Closed circles indicate the temperature or soil moisture optimum of each response curve and the grey thick line in the right panel indicates the set optimal temperature for CA activity (25 °C in this case).

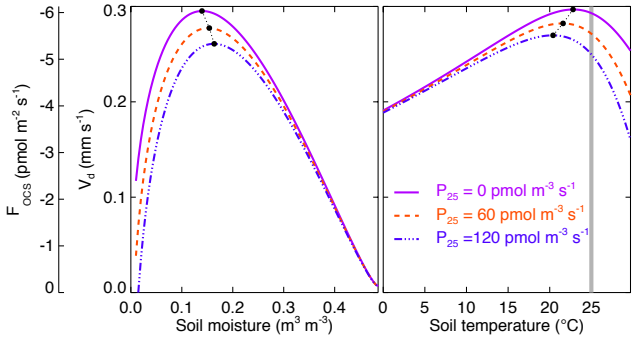

Figure 7. Sensitivity of the modelled OCS flux (F_{OCS}) and deposition velocity (V_d) to soil OCS emission rate. The soil moisture and temperature response curves shown here were obtained using the diffusivity model of Moldrup et al. (2003) and assuming a CA enhancement factor of 30 000, a soil pH of 7.2 and a soil depth of 1 m. OCS source is assumed to occur only in the top 5 cm. Closed circles indicate the temperature or soil moisture optimum of each response curve and the grey thick line in the right panel indicates the set optimal temperature for CA activity (25 °C in this case).

3.3 Sensitivity to soil CA activity and OCS emission rates

Our model has two main parameters that need to be constrained by observations: these are the CA concentration (or conversely the CA enhancement factor f_{CA}) and the OCS production rate at 25 °C (P_{25}). A sensitivity analysis of our steady-state OCS deposition model to these two parameters is shown in Figs. 6 and 7. Both parameters affect the maximum deposition rates but in opposite directions, with high f_{CA} values leading to higher V_d and high P_{25} values leading to lower V_d. This was expected from Eq. (16b) as V_d is proportional to $\sqrt{f_{CA}}$ and is linearly and negatively related to P_{25}.

Interestingly, the optimal soil moisture is not modified by changes in f_{CA} (Fig. 6, left panel) and only slightly by P_{25} (Fig. 7, left panel). This means that, provided that z_{max} is known precisely (or larger than $2z_1$, see Sect. 3.2), the overall shape of the response to soil moisture (as typically measured during a drying cycle) and the exact value of θ_{opt} are indicative solely of the diffusivity model to be used (Fig. 3). This result is important and should help us to at least decide whether the Pen40 formulation for τ_a must be used instead of a more asymmetrical one (the Mol03r and MQ61 formulations are harder to distinguish, see Fig. 3).

The value of T_{opt,V_d} is also insensitive to changes in f_{CA} (Fig. 6, right panel), but diminishes when P_{25} increases (Fig. 7, right panel). This means that very low optimal temperature values T_{opt,V_d} (i.e. unusually low compared to expected values for enzymatic activities and $T_{opt,CA}$) should be indicative of an OCS emission term, even if the values of V_d remain positive (i.e. the soil acts as a sink) in the temperature range explored. Of course at higher temperatures, and because in our model the OCS source term responds exponentially with temperature (Q_{10} response) while k exhibits an optimal temperature ($T_{opt,CA}$), the V_d should reach negative values if the value of P_{25} is large and f_{CA} is low. In some extreme cases where P_{25} fully dominates over f_{CA}, our model could even predict OCS fluxes close to zero at temperatures below ∼ 10 °C that would increase exponentially at warmer

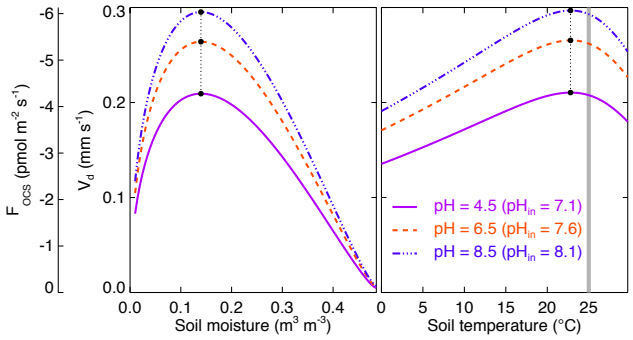

Figure 8. Sensitivity of the modelled OCS flux (F_{OCS}) and deposition velocity (V_d) to soil pH. The soil moisture and temperature response curves shown here were obtained using the diffusivity model of Moldrup et al. (2003) and assuming no source term, a CA concentration in the soil of 330 nM and a soil depth of 1 m. Closed circles indicate the temperature or soil moisture optimum of each response curve and the grey thick line in the right panel indicates the set optimal temperature for CA activity (25 °C in this case).

temperatures, as it has been observed in some agricultural soils (J. Liu et al., 2010; Maseyk et al., 2014; Whelan and Rhew, 2015).

3.4 Sensitivity to soil pH

The sensitivity of our model to different soil pH was also tested. Because the effect of soil pH is mostly to modify the hydration rate k, we could not set a constant value of f_{CA}. Instead we fixed the CA concentration in the soil (330 nM) and also adjusted the internal pH, assuming partial homeostasis with changes in soil pH, as observed in bacteria (Krulwich et al., 2011): $pH_{in} = 6 + 0.25$ pH (Fig. 8). By assuming pH_{in} to vary with changes in soil pH, we changed k_{cat} (Eq. 11a) and this was equivalent to changing f_{CA}. Indeed results shown in Fig. 8 are very similar to those shown in Fig. 6 where low pH (and pH_{in}) correspond to low f_{CA} values. If we had assumed that pH_{in} was not modified by soil pH (and fixed at 8.2) no change in k_{cat} would have been observed and the change in k would have only been caused by the effect of soil pH on k_{uncat} (Eq. 11a). Unless the soil contains very little CA or the soil pH moves to very alkaline values (Fig. 2), this change in k_{uncat} would have been too small to significantly affect V_d. Indeed at a CA concentration of 330 nM and with a pH_{in} maintained at 8.2, our model Eq. (16b) gives exactly the same values for soil pH ranging from 4 to 9. In summary, within the range of soil pH found in nature, the response of V_d to this environmental factor is only happening through its influence on pH_{in} and hence on k_{cat} (Eq. 10b and Fig. 2b).

3.5 Model evaluation against lab-based drying curves

Our steady-state OCS deposition model was further evaluated against experimental data from Van Diest and Kesselmeier (2008) and results are shown in Figs. 9–12 for different soils. Because OCS deposition values observed by Van Diest and Kesselmeier (2008) were all positive we set the source term to zero ($P_{25} = 0$), although we recognise that this may be an oversimplification. We also set the optimum temperature for the catalysed OCS hydration rate to 25 °C. A value for f_{CA} was then manually adjusted for each soil and each temperature, between 21 600 and 336 000, depending on the soil origin and temperature (Figs. 9–12). Once this adjustment on f_{CA} was done, our model, with the diffusivity formulation of Moldrup et al. (2003), was able to reproduce most observed response curves to soil drying (Figs. 9–12, left and middle panels). The model was also able to reproduce, within the measurement uncertainties, the temperature dependency of V_d at a soil moisture level of 0.12 m^3 m^{-3} (far right panels in Figs. 9–12).

4 Discussion

4.1 Can the proposed model explain observations realistically?

Many studies have clearly demonstrated that soil moisture strongly modulates OCS uptake by soils, with an optimal soil moisture content usually around 12 % of soil weight (Kesselmeier et al., 1999; J. Liu et al., 2010; Van Diest and Kesselmeier, 2008). As noted in some of these studies, such a bell-shape response is indicative of reactional and diffusional limitations at low and high soil moisture contents respectively. Using our steady-state formulation for shallow soils (Eq. 16b) we were able to reproduce the soil moisture response observed experimentally (Figs. 9–12). We also found that the observed asymmetric response to soil moisture was best captured by the soil diffusivity model of Moldrup et al. (2003) or Millington and Quirk (1961) and showed that the optimum soil moisture could be related to soil porosity: $\theta_{opt} = 0.3\varphi/1.3$ for MQ61 and $\theta_{opt} = 2\varphi/7$ for Mol03r. Using our model we were also able to explain the response of OCS uptake to soil weight (i.e. soil thickness) observed by Kesselmeier et al. (1999) (Fig. 5).

We also tested our model against observations of the temperature response of V_d. Empirical studies showed that, for a given soil, the maximum OCS uptake rate was modulated by incubation temperature, with an optimal temperature ranging from 15 to 35 °C (Kesselmeier et al., 1999; J. Liu et al., 2010; Van Diest and Kesselmeier, 2008). This temperature response was interpreted as an enzymatically catalysed process, governed by soil microorganism CA activity (Kesselmeier et al., 1999; J. Liu et al., 2010; Van Diest and Kesselmeier, 2008). To reproduce this response of V_d to incubation temperature using our steady-state model, we had to manually adjust f_{CA} for each incubation temperature. We will argue here that using different f_{CA} values on the same soil is justified given the way measurements were performed. Van Diest and Kesselmeier (2008) wanted to characterise

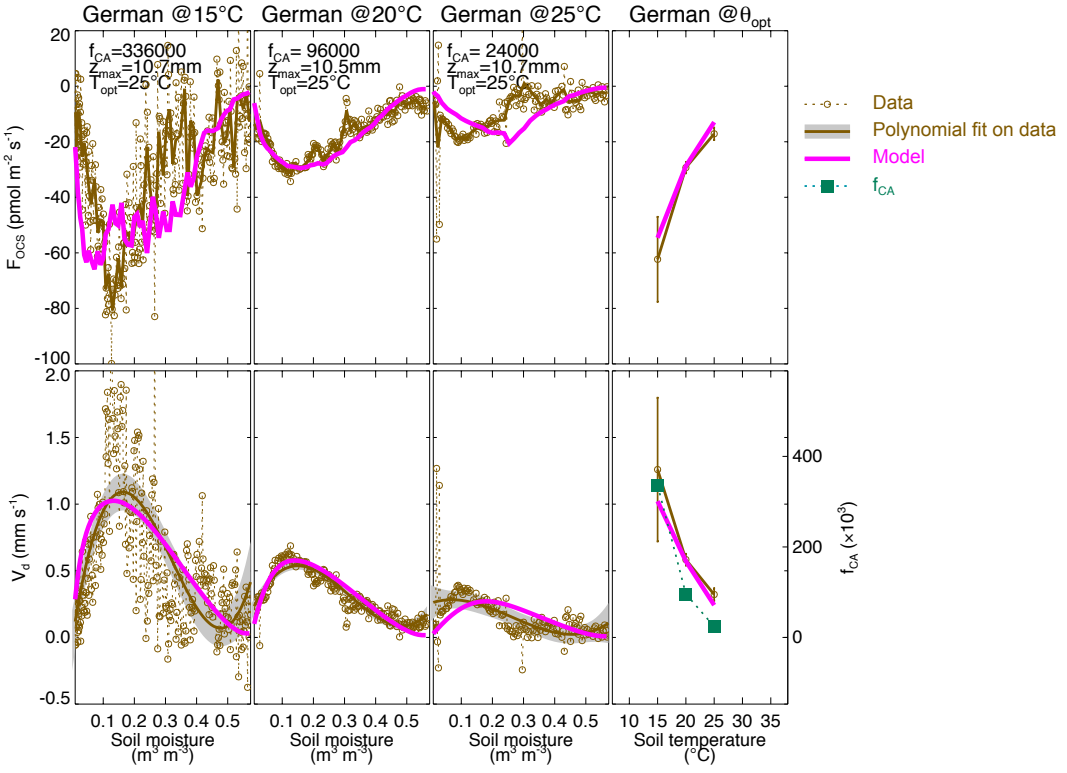

Figure 9. Observed and modelled soil–air OCS flux (F_{OCS}) and deposition velocity (V_d) during soil drying at different incubation temperatures (indicated above each panel) and their value at a soil moisture content $W_{opt} = 0.12\,m^3\,m^{-3}$ (far right panels). The soil moisture and temperature response curves shown here were recalculated from data by Van Diest and Kesselmeier (2008) (open circles and brown line) or computed with our model (thick pink line) using the diffusivity model of Moldrup et al. (2003). For each incubation temperature, a different set of model parameters (f_{CA}, z_{max}, T_{opt}) was used as indicated in each panel. The data shown here are representative of an agricultural soil near Mainz in Germany (soil weight is 200 g).

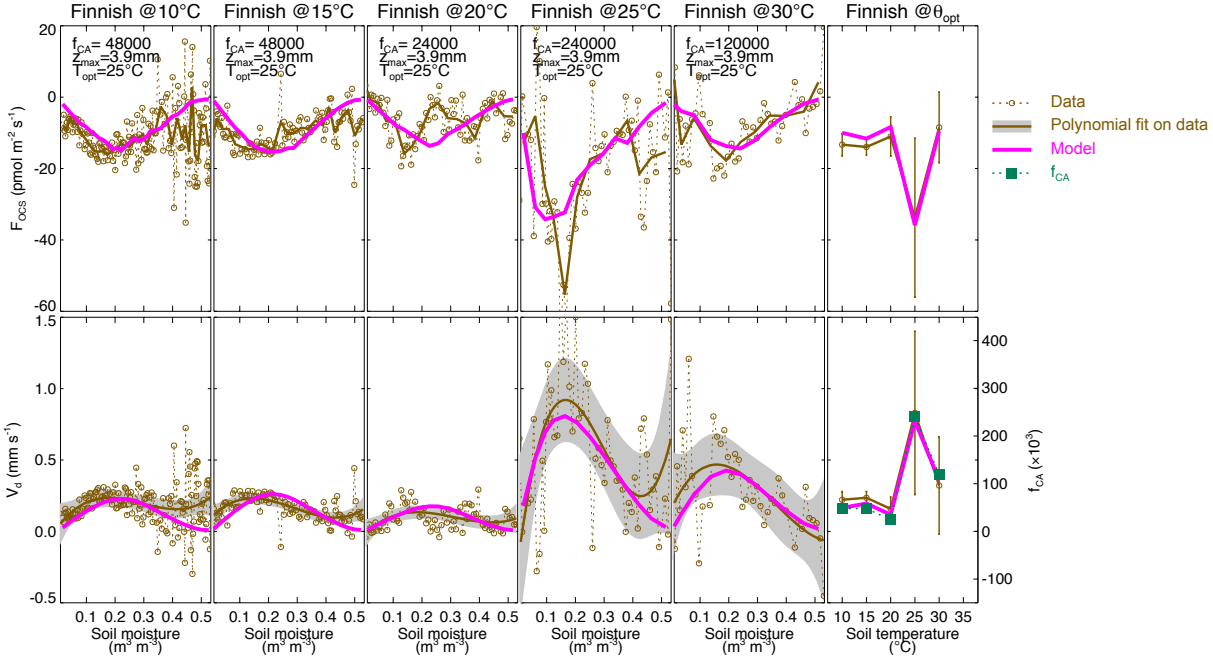

Figure 10. Same as Fig. 9 but for an agricultural soil near Hyytiala in Finland (soil weight is 80 g).

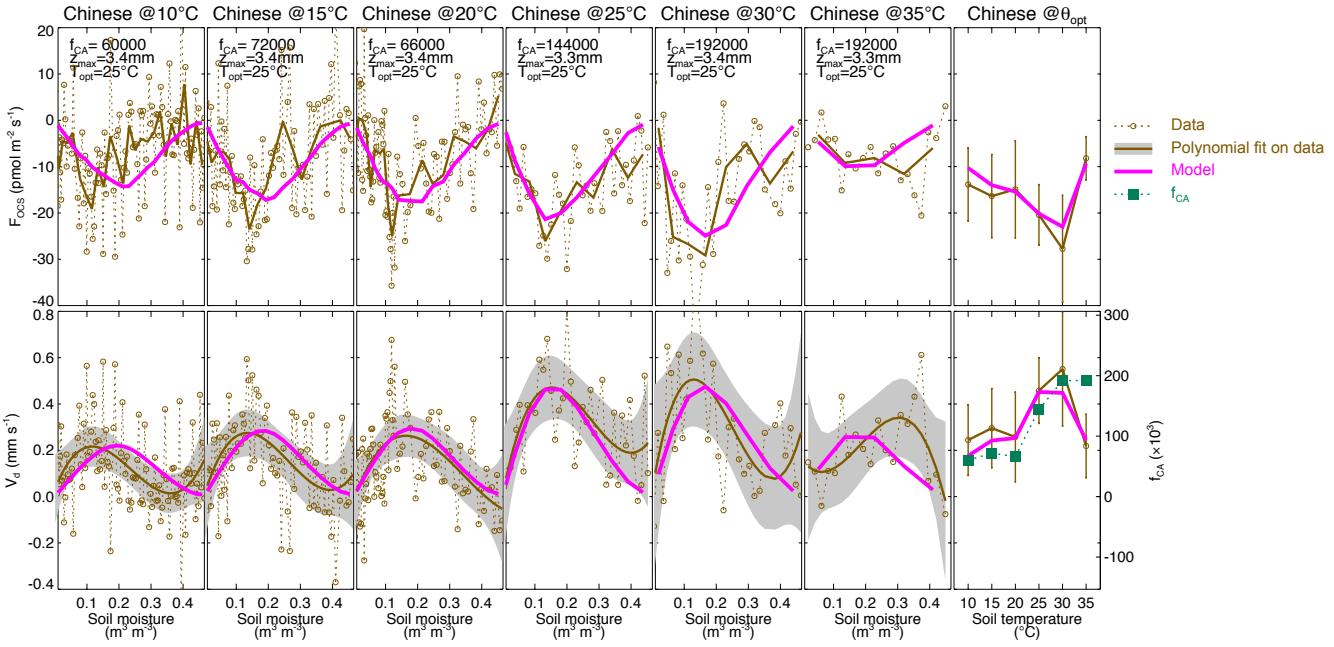

Figure 11. Same as Fig. 9 but for an agricultural soil from north-eastern China (soil weight is 80 g).

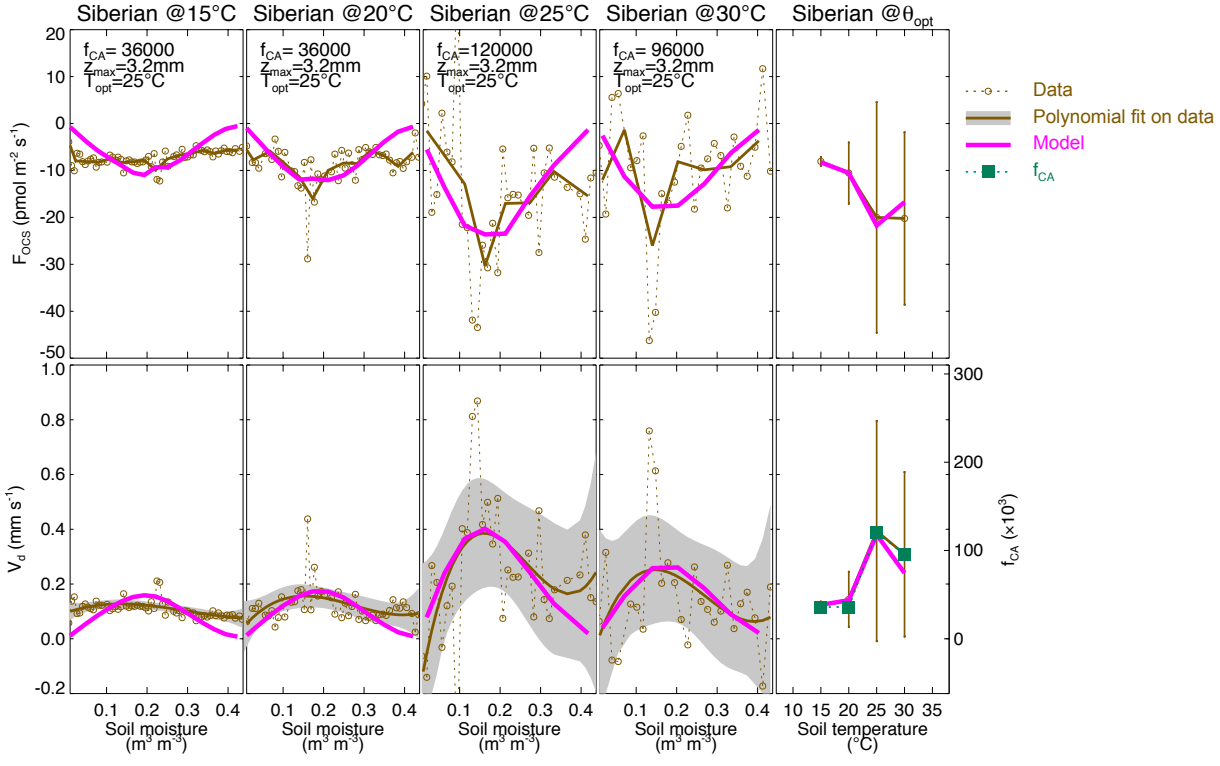

Figure 12. Same as Fig. 9 but for an agricultural soil from Siberia (soil weight is 80 g).

the V_d response to soil drying at a set temperature and for this, they saturated a soil sample with water and acclimated it to a given temperature (between 5 and 35 °C), they then recorded the OCS exchange immediately and continued to measure until the soil was completely dry, which usually lasted one to two days. The same soil sample, or a different one from the same geographical location, was then rewatered and reacclimated to a different temperature and another cycle of measurements started. Sometimes several months separated measurements at two different temperatures but storage time (at 5 °C) did not seem to affect the soil CA activity (measurements on the same soil and incubation temperature were reproducible). On the other hand incubation temperature clearly differ and, at least for the German soil, samples were not all collected in the same season. This means that, for a given soil origin, the microbial community was experiencing different environmental conditions and history between each drying curve. Thus, the size and diversity of the microbial population were likely different for each incubation temperature, thus justifying the use of different enhancement factors at each temperature. Interestingly f_{CA} tends to increase with incubation temperature, as we would expect for the microbial biomass. Only the German soil has a higher f_{CA} at low temperature (15 °C) and this corresponds to a soil sampled at a different period (March) than the other two incubation temperatures (June).

Following this argument it seems that the optimum temperatures observed by Van Diest and Kesselmeier (2008) for different soil types are not a good proxy for the optimal temperature of CA activity ($T_{opt,CA}$). Using our model we already showed that the optimum temperature for V_d (T_{opt,V_d}) was different from $T_{opt,CA}$, at least for deep soils (Fig. 4). A closer inspection of the results shown in Figs. 9–12 also show that the adjusted f_{CA} values closely follow the patterns of the maximum V_d at θ_{opt} (see right panels in Figs. 9–12). This means that the optimum temperature observed by Van Diest and Kesselmeier (2008) is a better indicator of maximum f_{CA} or equivalently maximum CA concentration (assuming all the CAs in the soil have similar k_{cat}/K_M as the pea extracts measured by Protoschill-Krebs et al. (1996)). This could explain why the optimum for the German soil was so low (around 15 °C), i.e. lower than expected for $T_{opt,CA}$. The presence of a competing enzymatic process, such as OCS emission, could have explained this low T_{opt,V_d} value (Fig. 7) but it is more likely that the soil sample studied at 15 °C contained more CA than those used for other incubation temperatures. Measurements on microbial biomass could have helped confirm this hypothesis but were unfortunately not made.

Because f_{CA} is a fitting parameter in our model, it is important to see if the values that we derived for the different soils are realistic. There are two ways to do so. First, we have a relatively good idea of how much CA is needed inside the cytosol of leaf mesophyll cells or in unicellular algae, which is of the order of 100 μM (Tholen and Zhu, 2011). Assuming this CA concentration value is also applicable to microbial cells and using estimates of the soil microbial population size, we can convert this physiological CA concentration ($[CA]_{in}$) into a CA concentration in the soil matrix ([CA]): $[CA]\theta = [CA]_{in}\rho_{mic}$, where ρ_{mic} (m^3 microbes m^{-3} soil) denotes the volumetric microbial content of the soil. Using a typical microbial population size of 3×10^9 cm^{-3} and an average cell size of 1 μm^3 (Wingate et al., 2009), we obtain a microbial content of $\rho_{mic} = 0.003\ m^3\ m^{-3}$ and a soil CA content of about 1000 nM (we used $\theta = 0.3$). Using this value of [CA] and the k_{cat}/K_M value for OCS (2.39 $s^{-1}\ \mu M^{-1}$ at 20 °C and pH_{in} 8.2) this leads to an f_{CA} value of about 127 000 for OCS, which is in the same order of magnitude as those found for the different soils in this study (between 21 600 and 336 000, with a median value at 66 000). From this crude calculation we can conclude that our f_{CA} estimates are physiologically meaningful.

Another way of checking if our f_{CA} estimates are meaningful is to convert them into f_{CA} equivalents for soil CO_2 isotope fluxes, for which we have a better idea of what the expected values should be (Seibt et al., 2006; Wingate et al., 2008, 2009, 2010). The k_{cat}/K_M value for CO_2 in pea extracts has been measured for a pH range of 6–9 and at 25 °C (Bjorkbacka et al., 1999). The pH response described a similar pattern as the one found for *Arabidopsis* by Rowlett et al. (2002) (Fig. 2) with a pK_a of 7.1. Using $x_{CA}(T)$ and y_{CA} (pH_{in}) to convert those values to pH_{in} 8.2 and 20 °C, we obtain a k_{cat}/K_M value for CO_2 of 50 $s^{-1}\ \mu M^{-1}$, i.e. about 20 times greater than the k_{cat}/K_M for OCS. Given the difference in uncatalysed hydration rates between the two gas species (12 000 μs^{-1} for CO_2 and 21.5 μs^{-1} for OCS at 25 °C and pH = 4.5) this means that at equal soil CA concentration, the f_{CA} for CO_2 should be about 30 times smaller than that derived for OCS. This corresponds to a median f_{CA} value of 2200 for CO_2, i.e. at the higher end of values observed in different soils (Wingate et al., 2009).

The calculation above considers only β-CA kinetic parameters to relate the soil CA enhancement factor for OCS to the f_{CA} for CO_2. However other enzymes can catalyse OCS hydrolysis and not have a strong affinity to CO_2. For example Smeulders et al. found a carbon disulfide hydrolase from an acido-thermophilic archaeon that was very efficient at catalysing OCS hydrolysis but did not have CO_2 as one of its substrates (Smeulders et al., 2012). More recently, Ogawa et al. (2013) found in *Thiobacillus thioparus*, a sulfur-oxidising bacterium widely distributed in soils and freshwaters, an enzyme that shared a high similarity with β-CAs and was able to catalyse OCS hydrolysis with a similar efficiency ($K_M = 60\ \mu M$, $k_{cat} = 58\ s^{-1}$ at pH 8.5 and 30 °C) but whose CO_2 hydration activity was 3–4 orders of magnitude smaller than that of β-CAs. For this reason they called this enzyme carbonyl sulfide hydrolase (COSase). The carbon disulfide hydrolase identified by Smeulders et al. (2012) may only be present in extremely acidic environments such as volcanic solfataras, but the COSase found in *T. thioparus*

may be more ubiquitous in soils. If this was the case this would imply that the f_{CA} ratio of OCS to CO_2 is not unique and could, in some soils, be higher than the same ratio derived from β-CA kinetic parameters only. This could partly explain the highest f_{CA} values obtained here for OCS.

Higher than expected values of f_{CA} could also be explained by the fact that we neglected dispersion fluxes when we compared the model against observations. Indeed dispersion fluxes would enhance OCS diffusion (Eq. 15) and result in larger deposition velocities (Eq. 16b) for the same level of CA concentration. Results from Maier et al. (2012) show that the diffusivity D could be easily doubled by the presence of turbulence above the soil surface, which would be equivalent to a doubling of k (D and k appear as a product in the sink term of Eq. 16b). This means that if dispersion occurred in the experiments (a possibility that we cannot rule out), the f_{CA} values that we derived from them may be overestimated by a factor of two, bringing them closer to values compatible with CO_2 studies.

To conclude, the f_{CA} values derived here for OCS seem compatible with physiological CA contents and also compatible with f_{CA} values reported in CO_2 isotope studies, given possible affinity differences of some CAs towards OCS and CO_2 and possible artefacts of mechanical dispersion caused by fans in some laboratory experiments.

4.2 Can we transpose laboratory data to field conditions?

Response curves of OCS deposition rates to soil moisture and temperature have been derived from laboratory experiments similar to those presented here (Kesselmeier et al., 1999) and the derived equations have been used to estimate the OCS uptake by soils at the global scale (Kettle et al., 2002). In addition Van Diest and Kesselmeier have proposed that the optimum (gravimetric) soil moisture content for OCS deposition was around $0.12\,g\,g^{-1}$, independently of soil type (Van Diest and Kesselmeier, 2008). Our model allows us to verify if such simplification or extrapolation is justified, on a theoretical point of view at least. For semi-infinite soil columns we showed that θ_{opt} varied with soil porosity from 0.23φ to 0.5φ, depending on the soil diffusivity model used. Assuming soil bulk density is $2.66(1-\varphi)$, this leads to gravimetric soil moisture contents of between $0.61\varphi(1-\varphi)$ and $1.33\varphi(1-\varphi)$, which is clearly dependent on soil type. Also from Fig. 4 we can see that the general shape of the soil moisture response and θ_{opt} strongly depend on the exact soil depth used during the experiment, at least for soil less than 3 cm thick (or more if the CA activity is lower). For thicker soils the deepest soil layers do not contribute to the exchange and we reach the saturation point with soil weight shown in Fig. 5. However in both aforementioned studies (Kesselmeier et al., 1999; Van Diest and Kesselmeier, 2008), care was taken not to reach the saturation point (using soil weights of about 80 g). From our model results we can see that this would lead to an overestimation of θ_{opt} and an overall underestimation of V_d (Fig. 4). Thus based on this observation we would recommend to use soil depths of at least 5–6 cm in future studies so that the results can be more readily extrapolated to field conditions.

Another difficulty when we want to extrapolate laboratory data to the natural environment is that soil disturbance prior to the experiment (sieving, repacking ...) strongly modifies the gas diffusivity properties of the soil. Our results show that OCS deposition rates can be extremely sensitive to the choice of the diffusivity model used (Fig. 3). In highly compacted, highly aggregated soils the gas diffusivity response to soil moisture content can even become bimodal (Deepagoda et al., 2011), which would certainly have a strong impact on the $V_d-\theta$ relationship. Even without such a complication, our results suggest that deposition rate measurements on repacked soils may not be representative of field conditions because the soil treatment would modify the diffusivity properties of the soil and alter the soil moisture response of the OCS deposition rate. On the other hand, our model (Eq. 17, for semi-infinite soil column) with a soil diffusivity formulation for undisturbed soils (i.e. Mol03u or Deepa11, see Table 1) could be used for interpreting field measurements.

5 Perspectives

Our model so far has been tested under steady-state conditions and with fairly uniform soil properties (temperature, moisture, pH ...). In the natural environment such conditions are the exception rather than the rule. The model has not been tested either on true temperature response curves as happens in nature with strong diurnal variations of temperature at nearly constant soil moisture content. Indeed data from Van Diest and Kesselmeier (2008) have been collected at constant incubation temperatures and are therefore more indicative of the range of f_{CA} and V_d values one would expect over a growing season for a given soil type. Surprisingly we could not find published laboratory measurements of V_d where soil temperature was varied diurnally.

Another point that should be addressed in future studies is the characterisation of the soil microbial community size and structure, which should be done systematically with the soil OCS deposition measurements. This would allow us to test whether our upscaling of CA activity to the soil level (Eq. 11a) is correct or not and compatible with physiologically realistic CA contents in soil microbes. Our results so far suggest that the CA contents that we derive seem physiologically meaningful and also compatible with CO_2 isotope studies, given the uncertainties in the k_{cat}/K_M values of different CAs for the two substrates and in the diffusivity model formulation for different experimental setup (see above). Concurrent microbial data on the soil samples could have greatly constrained our downscaling exercise and lead to a more precise picture of possible mismatch between our model and the observations. When combined with both OCS

and CO_2 isotope gas exchange measurements, it could also help identify the microbial communities that are more prone to express specific CAs which favour OCS uptake such as the COSase found in *T. thioparus*.

Finally our study mostly focused on the temperature response of the OCS production term, but there is a growing body of evidence that other environmental variables trigger OCS production from soils, independently of temperature. In oxic soils, light-induced OCS emissions have been observed (Whelan and Rhew, 2015) whereas in anoxic soils, redox potential seems to be the main trigger (Devai and Delaune, 1995). The mechanisms leading to these OCS emission rates should be better understood before we can incorporate them into a modelling framework and estimate OCS fluxes at large scales. For this reason we strongly suggest systematically reporting measurements of light and soil redox potential (and/or S speciation) in future soil OCS flux studies.

Appendix A

Here we derive an equation for the catalysed OCS sink term (S_{cat}) that accounts for the co-limitation between the enzymatic reaction that takes place inside microorganisms (at pH_{in} and with an OCS concentration C_{in}) and the OCS diffusion through the cell wall of the microbes. In this situation, Eq. (9) needs to be rewritten:

$$S_{cat} = \theta k_{cat} [CA] \frac{B C_{in}}{K_m + B C_{in}} \approx \frac{k_{cat}}{K_m} [CA] B \theta C_{in}. \quad (A1)$$

The OCS uptake can also be written in terms of transport across the cell wall and the plasma membrane of the microbial cell (see for example Tholen and Zhu (2011):

$$S_{cat} = G_{wall} V_{mol} (C - C_{in}) S_{wall}, \quad (A2)$$

where G_{wall} (mol(air) m^{-2} wall s^{-1}) is the cell wall and plasma membrane aggregated conductance to OCS, V_{mol} (m^3 air mol(air)$^{-1}$) is the molar volume of air and S_{wall} (m^2 wall m^{-3} soil) is the microbial cell wall surface density in the soil. Combining Eqs. (A1)–(A2) we can eliminate C_{in} and express S as a function of C only:

$$S_{cat} = \frac{B \theta k_{cat} [CA]}{K_m + B \theta k_{cat} [CA] r_{wall}} C, \quad (A3)$$

where we defined $1/r_{wall} = G_{wall} V_{mol} S_{wall}$. Equation (A3) simplifies to Eq. (9) under the following condition:

$$B \theta k_{cat} [CA] r_{wall} \ll K_m. \quad (A4)$$

Accounting for the dilution of CA in soils, i.e. $[CA]\theta = [CA]_{in} \rho_{mic}$, where ρ_{mic} (m^3 microbes m^{-3} soil) is the volumetric density of the soil microbes (that can be expressed as $n_{mic} V_0$ in which n_{mic} is the number of microbes per soil volume and V_0 the volume of a single microbial cell), Eq. (A4) can be written as follows:

$$\frac{B k_{cat} [CA]_{in}}{G_{wall} V_{mol}} \frac{V_0}{S_{wall0}} \ll K_m, \quad (A5)$$

where S_{wall0} is the single cell wall surface area. If the microbes are spherical with diameter D_0, we have $V_0/S_{wall0} = D_0/6$. With typical values of $D_0 = 1\,\mu m$, $B = 0.5\,m^3\,m^{-3}$, $V_{mol} = 0.025\,m^3\,mol^{-1}$, $k_{cat} = 93\,s^{-1}$ and $G_{wall} = 0.14\,mol\,m^{-2}\,s^{-1}$ (i.e. $0.35\,cm\,s^{-1}$, see the note under Table 2 in Evans et al., 2009), the left-hand side of Eq. (A5) equals $0.22\,\mu M$, which is much smaller than K_m ($39\,\mu M$ at 20 °C, (Protoschill-Krebs et al., 1996). In this situation the transport of OCS through the membrane is not a colimiting factor to the OCS uptake (for CO_2 it is less true because the left-hand side of Eq. (A5) is around 0.57 mM for a K_m around 3 mM). Note also that CA is not spread in the entire cell volume so that the cell volume appearing in Eq. (A5) should be somewhat smaller. Although there are large uncertainties on the value of cytoplasmic CA concentration or k_{cat}/K_M, our derivation indicates that these parameters would need to be much higher (by two orders of magnitude) to justify the need to account for the transport of OCS into the cell during microbial consumption. In this study we assumed Eq. (9) to be valid, bearing in mind that the CA concentration we derived from it remains sensitive to the k_{cat}/K_M value we use.

Acknowledgements. This work was funded by the European Research Council (ERC starting grant SOLCA), the French national research agency (ANR project ORCA) and the Institut National de la Recherche Agronomique (INRA PhD grant to Joana Sauze). We would like to thank three anonymous reviewers for their constructive comments on an earlier version of this manuscript.

Edited by: X. Wang

References

Beer, C., Reichstein, M., Tomelleri, E., Ciais, P., Jung, M., Carvalhais, N., Rödenbeck, C., Arain, M. A., Baldocchi, D., Bonan, G. B., Bondeau, A., Cescatti, A., Lasslop, G., Lindroth, A., Lomas, M., Luyssaert, S., Margolis, H., Oleson, K. W., Roupsard, O., Veenendaal, E., Viovy, N., Williams, C., Woodward, F. I., and Papale, D.: Terrestrial Gross Carbon Dioxide Uptake: Global Distribution and Covariation with Climate, Science, 329, 834–838, doi:10.1126/science.1184984, 2010.

Berry, J. A., Wolf, A., Campbell, J. E., Baker, I., Blake, N., Blake, D., Denning, A. S., Kawa, S. R., Montzka, S. A., Seibt, U., Stimler, K., Yakir, D., and Zhu, Z.: A coupled model of the global cycles of carbonyl sulfide and CO_2: A possible new window on the carbon cycle, J. Geophys. Res.-Biogeo., 118, 842–852, doi:10.1002/jgrg.20068, 2013.

Bird, R. B., Stewart, W. E., and Lightfoot, E. N.: Transport phenomena, John Wiley & Sons, New York, 2002.

Bjorkbacka, H., Johansson, I.-M., and Forsman, C.: Possible Roles for His 208 in the Active-Site Region of Chloroplast Carbonic Anhydrase from *Pisum sativum*, Arch. Biochem. Biophys., 361, 17–24, 1999.

Blezinger, S., Wilhelm, C., and Kesselmeier, J.: Enzymatic consumption of carbonyl sulfide (COS) by marine algae, Biogeochemistry, 48, 185–197, 2000.

Bremner, J. M. and Banwart, W. L.: Sorption of sulfur gases by soils, Soil Biol. Biochem., 8, 79–83, 1976.

Burnell, J. N. and Hatch, M. D.: Low bundle sheath carbonic anhydrase is apparently essential for effective C_4 pathway operation, Plant Physiol., 86, 1252–1256, 1988.

Campbell, J. E., Carmichael, G. R., Chai, T., Mena-Carrasco, M., Tang, Y., Blake, D. R., Blake, N. J., Vay, S. A., Collatz, G. J., Baker, I., Berry, J. A., Montzka, S. A., Sweeney, C., Schnoor, J. L., and Stanier, C. O.: Photosynthetic Control of Atmospheric Carbonyl Sulfide During the Growing Season, Science, 322, 1085–1088, doi:10.1126/science.1164015, 2008.

Castro, M. S. and Galloway, J. N.: A comparison of sulfur-free and ambient air enclosure techniques for measuring the exchange of reduced sulfur gases between soils and the atmosphere, J. Geophys. Res.-Atmos., 96, 15427–15437, 1991.

Choi, J.-G., Do, D. D., and Do, H. D.: Surface Diffusion of Adsorbed Molecules in Porous Media: Monolayer, Multilayer, and Capillary Condensation Regimes, Ind. Eng. Chem. Res., 40, 4005–4031, doi:10.1021/ie010195z, 2001.

De Bruyn, W. J., Swartz, E., Hu, J. H., Shorter, J. A., Davidovits, P., Worsnop, D. R., Zahniser, M. S., and Kolb, C. E.: Henry's law solubilities and Śetchenow coefficients for biogenic reduced sulfur species obtained from gas-liquid uptake measurements, J. Geophys. Res.-Atmos., 100, 7245–7251, 1995.

Deepagoda, T. K. K. C., Moldrup, P., Schjønning, P., Wollesen de Jonge, L., Kawamoto, K., and Komatsu, T.: Density-Corrected Models for Gas Diffusivity and Air Permeability in Unsaturated Soil, Vadose Zone J., 10, 226–238, doi:10.2136/vzj2009.0137, 2011.

Delaune, R. D. and Reddy, K. R.: Redox Potential, in: Encyclopedia of Soils in the Environment, edited by: Hillel, D., 366–371, 2005.

Devai, I. and Delaune, R. D.: Formation of volatile sulfur compounds in salt marsh sediment as influenced by soil redox condition, Org. Geochem., 23, 283–287, 1995.

Elliott, S., Lu, E., and Rowland, F. S.: Rates and mechanisms for the hydrolysis of carbonyl sulfide in natural waters, Environ. Sci. Technol., 23, 458–461, doi:10.1021/es00181a011, 1989.

Evans, J. R., Kaldenhoff, R., Genty, B., and Terashima, I.: Resistances along the CO_2 diffusion pathway inside leaves, J. Exp. Bot., 60, 2235–2248, doi:10.1093/jxb/erp117, 2009.

Falta, R. W., Javandel, I., Pruess, K., and Witherspoon, P. A.: Density-Driven Flow of Gas in the Unsaturated Zone Due to the Evaporation of Volatile Organic-Compounds, Water Resour. Res., 25, 2159–2169, 1989.

Frankenberg, C., Fisher, J. B., Worden, J., Badgley, G., Saatchi, S. S., Lee, J.-E., Toon, G. C., Butz, A., Jung, M., Kuze, A., and Yokota, T.: New global observations of the terrestrial carbon cycle from GOSAT: Patterns of plant fluorescence with gross primary productivity, Geophys. Res. Lett., 38, L17706, doi:10.1029/2011GL048738, 2011.

Friedlingstein, P., Bopp, L., Rayner, P., Cox, P. M., Betts, R., Jones, C., Bloh, Von, W., Brovkin, V., Cadule, P., and Doney, S. C.: Climate-carbon cycle feedback analysis: Results from the C4MIP model intercomparison, J. Climate, 19, 3337–3353, 2006.

Gurney, K. R. and Eckels, W. J.: Regional trends in terrestrial carbon exchange and their seasonal signatures, Tellus B, 63, 328–339, doi:10.1111/j.1600-0889.2011.00534.x, 2011.

Haritos, V. S. and Dojchinov, G.: Carbonic anhydrase metabolism is a key factor in the toxicity of CO_2 and COS but not CS_2 toward the flour beetle *Tribolium castaneum* [Coleoptera: Tenebrionidae], Comp. Biochem. Phys. C, 140, 139–147, doi:10.1016/j.cca.2005.01.012, 2005.

Husson, O.: Redox potential (Eh) and pH as drivers of soil/plant/microorganism systems: a transdisciplinary overview pointing to integrative opportunities for agronomy, Plant Soil, 362, 389–417, doi:10.1007/s11104-012-1429-7, 2012.

Isik, S., Kockar, F., Aydin, M., Arslan, O., Guler, O. O., Innocenti, A., Scozzafava, A., and Supuran, C. T.: Carbonic anhydrase inhibitors: inhibition of the beta-class enzyme from the yeast *Saccharomyces cervevisiae* with sulfonamides and sulfamates, Bioorgan. Med. Chem., 17, 1158–1163, doi:10.1016/j.bmc.2008.12.035, 2009.

Kesselmeier, J., Teusch, N., and Kuhn, U.: Controlling variables for the uptake of atmospheric carbonyl sulfide by soil, J. Geophys. Res, 104, 11577–11584, 1999.

Kettle, A. J., Kuhn, U., Hobe, von, M., Kesselmeier, J., and Andreae, M. O.: Global budget of atmospheric carbonyl sulfide: Temporal and spatial variations of the dominant sources and sinks, J. Geophys. Res, 107, 4658, doi:10.1029/2002JD002187, 2002.

Krulwich, T. A., Sachs, G., and Padan, E.: Molecular aspects of bacterial pH sensing and homeostasis, Nat. Rev. Microbiol., 9, 330–343, doi:10.1038/nrmicro2549, 2011.

Kuhn, U., Ammann, C., Wolf, A., Meixner, F., Andreae, M., and Kesselmeier, J.: Carbonyl sulfide exchange on an ecosystem scale: soil represents a dominant sink for atmospheric COS, Atmos. Environ., 33, 995–1008, 1999.

Launois, T., Peylin, P., Belviso, S., and Poulter, B.: A new model of the global biogeochemical cycle of carbonyl sulfide – Part 2: Use of carbonyl sulfide to constrain gross primary productivity in current vegetation models, Atmos. Chem. Phys., 15, 9285–9312, doi:10.5194/acp-15-9285-2015, 2015.

Liu, J., Geng, C., Mu, Y., Zhang, Y., Xu, Z., and Wu, H.: Exchange of carbonyl sulfide (COS) between the atmosphere and various soils in China, Biogeosciences, 7, 753–762, doi:10.5194/bg-7-753-2010, 2010.

Liu, Y., He, H., and Ma, Q.: Temperature Dependence of the Heterogeneous Reaction of Carbonyl Sulfide on Magnesium Oxide, J. Phys. Chem. A, 112, 2820–2826, doi:10.1021/jp711302r, 2008.

Liu, Y., Ma, Q., and He, H.: Comparative study of the effect of water on the heterogeneous reactions of carbonyl sulfide on the surface of α-Al_2O_3 and MgO, Atmos. Chem. Phys., 9, 6273–6286, doi:10.5194/acp-9-6273-2009, 2009.

Liu, Y., Ma, J., and He, H.: Heterogeneous reactions of carbonyl sulfide on mineral oxides: mechanism and kinetics study, Atmos. Chem. Phys., 10, http://www.atmos-chem-phys.net/10/10335/2010/acp-10-10335-2010-supplement.pdf, 2010a.

Liu, Y., Ma, J., Liu, C., and He, H.: Heterogeneous uptake of carbonyl sulfide onto kaolinite within a temperature range of 220–330 K, J. Geophys. Res, 115, D24311, doi:10.1029/2010JD014778, 2010b.

Maier, M., Schack-Kirchner, H., Aubinet, M., Goffin, S., Longdoz, B., and Parent, F.: Turbulence Effect on Gas Transport in Three Contrasting Forest Soils, Soil Sci. Soc. Am. J., 76, 1518, doi:10.2136/sssaj2011.0376, 2012.

Manzoni, S. and Katul, G. G.: Invariant soil water potential at zero microbial respiration explained by hydrological discontinuity in dry soils, Geophys. Res. Lett., 41, 7151–7158, doi:10.1002/2014GL061467, 2014.

Maseyk, K., Berry, J. A., Billesbach, D., Campbell, J. E., Torn, M. S., Zahniser, M., and Seibt, U.: Sources and sinks of carbonyl sulfide in an agricultural field in the Southern Great Plains, P. Natl. Acad. Sci. USA, 111, 9064–9069, doi:10.1073/pnas.1319132111, 2014.

Massman, W. J., Sommerfeld, R. A., Mosier, A. R., Zeller, K. F., Hehn, T. J., and Rochelle, S. G.: A model investigation of turbulence-driven pressure-pumping effects on the rate of diffusion of CO_2, N_2O, and CH_4 through layered snowpacks, J. Geophys. Res.-Atmos., 102, 18851–18863, 1997.

Massman, W. J.: A review of the molecular diffusivities of H_2O, CO_2, CH_4, CO, O_3, SO_2, NH_3, N_2O, NO, and NO_2 in air, O_2 and N_2 near STP, Atmos. Environ., 32, 1111–1127, 1998.

Mello, W. Z. and Hines, M. E.: Application of static and dynamic enclosures for determining dimethyl sulfide and carbonyl sulfide exchange in *Sphagnum* peatlands: Implications for the magnitude and direction of flux, J. Geophys. Res, 99, 14-601–14-607, 1994.

Merlin, C., Masters, M., McAteer, S., and Coulson, A.: Why Is Carbonic Anhydrase Essential to *Escherichia coli*?, J. Bacteriol., 185, 6415–6424, doi:10.1128/JB.185.21.6415-6424.2003, 2003.

Millington, R. J. and Quirk, J. P.: Permeability of porous solids, T. Faraday Soc., 57, 1200–1207, 1961.

Moldrup, P., Olesen, T., Komatsu, T., Yoshikawa, S., Schjønning, P., and Rolston, D. E.: Modeling diffusion and reaction in soils: X. A unifying model for solute and gas diffusivity in unsaturated soil, Soil Sci., 168, 321–337, doi:10.1097/00010694-200305000-00002, 2003.

Montzka, S. A., Calvert, P., Hall, B. D., Elkins, J. W., Conway, T. J., Tans, P. P., and Sweeney, C.: On the global distribution, seasonality, and budget of atmospheric carbonyl sulfide (COS) and some similarities to CO_2, J. Geophys. Res, 112, D09302, doi:10.1029/2006JD007665, 2007.

Ogawa, T., Noguchi, K., Saito, M., Nagahata, Y., Kato, H., Ohtaki, A., Nakayama, H., Dohmae, N., Matsushita, Y., Odaka, M., Yohda, M., Nyunoya, H., and Katayama, Y.: Carbonyl Sulfide Hydrolase from *Thiobacillus thioparus* Strain THI115 Is One of the β-Carbonic Anhydrase Family Enzymes, J. Am. Chem. Soc., 135, 3818–3825, doi:10.1021/ja307735e, 2013.

Olesen, T., Gamst, J., Moldrup, P., Komatsu, T., and Rolston, D.: Diffusion of sorbing organic chemicals in the liquid and gaseous phases of repacked soil, Soil Sci. Soc. Am. J., 65, 1585–1593, 2001.

Penman, H.: Gas and vapour movements in the soil: I. The diffusion of vapours through porous solids, J. Agr. Sci., 30, 437–462, 1940.

Petersen, L. W., Moldrup, P., Elpharan, Y. H., Jacobsen, O. H., Yamaguchi, T., and Rolston, D. E.: The Effect of Moisture and Soil Texture on the Adsorption of Organic Vapors, J. Environ. Qual., 24, 752–759, 1995.

Piao, S., Sitch, S., Ciais, P., Friedlingstein, P., Peylin, P., Wang, X., Ahlström, A., Anav, A., Canadell, J. G., Cong, N., Huntingford, C., Jung, M., Levis, S., Levy, P. E., Li, J., Lin, X., Lomas, M. R., Lu, M., Luo, Y., Ma, Y., Myneni, R. B., Poulter, B., Sun, Z., Wang, T., Viovy, N., Zaehle, S., and Zeng, N.: Evaluation of terrestrial carbon cycle models for their response to climate variability and to CO_2 trends, Glob. Change Biol., 19, 2117–2132, doi:10.1111/gcb.12187, 2013.

Protoschill-Krebs, G. and Kesselmeier, J.: Enzymatic pathways for the consumption of carbonyl sulphide (COS) by higher plants, Bot. Acta, 105, 206–212, 1992.

Protoschill-Krebs, G., Wilhelm, C., and Kesselmeier, J.: Consumption of Carbonyl Sulphide by *Chlamydomonas reinhardtii* with Different Activities of Carbonic Anhydrase (CA) Induced by Different CO_2 Growing Regimes, Bot. Acta, 108, 445–448, 1995.

Protoschill-Krebs, G., Wilhelm, C., and Kesselmeier, J.: Consumption of carbonyl sulphide (COS) by higher plant carbonic anhydrase (CA), Atmos. Environ., 30, 3151–3156, 1996.

Rowlett, R. S., Tu, C., McKay, M. M., Preiss, J. R., Loomis, R. J., Hicks, K. A., Marchione, R. J., Strong, J. A., Donovan Jr., G. S., and Chamberlin, J. E.: Kinetic characterization of wild-type and proton transfer-impaired variants of β-carbonic anhydrase from *Arabidopsis thaliana*, Arch. Biochem. Biophys., 404, 197–209, 2002.

Sandoval-Soto, L., Stanimirov, M., von Hobe, M., Schmitt, V., Valdes, J., Wild, A., and Kesselmeier, J.: Global uptake of carbonyl sulfide (COS) by terrestrial vegetation: Estimates corrected by deposition velocities normalized to the uptake of carbon dioxide (CO_2), Biogeosciences, 2, 125–132, doi:10.5194/bg-2-125-2005, 2005.

Scanlon, B. R., Nicot, J. P., and Massmann, J. W.: Soil gas movement in unsaturated systems, in: Soil Physics Companion, CRC Press, Boca Raton, FL, 297–341, 2002.

Seibt, U., Wingate, L., Lloyd, J., and Berry, J. A.: Diurnally variable $\delta^{18}O$ signatures of soil CO_2 fluxes indicate carbonic anhydrase activity in a forest soil, J. Geophys. Res, 111, G04005, doi:10.1029/2006JG000177, 2006.

Seibt, U., Kesselmeier, J., Sandoval-Soto, L., Kuhn, U., and Berry, J. A.: A kinetic analysis of leaf uptake of COS and its relation to transpiration, photosynthesis and carbon isotope fractionation, Biogeosciences, 7, 333–341, doi:10.5194/bg-7-333-2010, 2010.

Smeulders, M. J., Barends, T. R. M., Pol, A., Scherer, A., Zandvoort, M. H., Udvarhelyi, A., Khadem, A. F., Menzel, A., Hermans, J., Shoeman, R. L., Wessels, H. J. C. T., van den Heuvel, L. P., Russ, L., Schlichting, I., Jetten, M. S. M., and Op den Camp, H. J. M.: Evolution of a new enzyme for carbon disulphide conversion by an acidothermophilic archaeon, Nature, 478, 412–416, doi:10.1038/nature10464, 2012.

Smith, K., Jakubzick, C., Whittam, T., and Ferry, J.: Carbonic anhydrase is an ancient enzyme widespread in prokaryotes, P. Natl. Acad. Sci. USA, 96, 15184–15189, 1999.

Steinbacher, M., Bingemer, H., and Schmidt, U.: Measurements of the exchange of carbonyl sulfide (OCS) and carbon disulfide (CS_2) between soil and atmosphere in a spruce forest in central Germany, Atmos. Environ., 38, 6043–6052, doi:10.1016/j.atmosenv.2004.06.022, 2004.

Stimler, K., Montzka, S. A., Berry, J. A., Rudich, Y., and Yakir, D.: Relationships between carbonyl sulfide (COS) and CO_2 during leaf gas exchange, New Phytol., 186, 869–878, doi:10.1111/j.1469-8137.2010.03218.x, 2010.

Stimler, K., Berry, J. A., and Yakir, D.: Effects of Carbonyl Sulfide and Carbonic Anhydrase on Stomatal Conductance, Plant Physiol., 158, 524–530, doi:10.1104/pp.111.185926, 2012.

Sun, W., Maseyk, K., Lett, C., and Seibt, U.: A soil diffusion-reaction model for surface COS flux: COSSM v1, Geosci. Model Dev., 8, 3055–3070, doi:10.5194/gmd-8-3055-2015, 2015.

Syrjänen, L., Vermelho, A. B., de Almeida Rodrigues, I., Corte-Real, S., Salonen, T., Pan, P., Vullo, D., Parkkila, S., Capasso, C., and Supuran, C. T.: Cloning, Characterization, and Inhibition Studies of a β-Carbonic Anhydrase from Leishmania donovani chagasi, the Protozoan Parasite Responsible for Leishmaniasis, J. Med. Chem., 56, 7372–7381, doi:10.1021/jm400939k, 2013.

Tholen, D. and Zhu, X.-G.: The Mechanistic Basis of Internal Conductance: A Theoretical Analysis of Mesophyll Cell Photosynthesis and CO_2 Diffusion, Plant Physiol., 156, 90–105, doi:10.1104/pp.111.172346, 2011.

Ulshöfer, V. S., Flock, O. R., Uher, G., and Andreae, M. O.: Photochemical production and air-sea exchange of carbonyl sulfide in the eastern Mediterranean Sea, Mar. Chem., 53, 25–39, 1996.

van Bochove, E., Beauchemin, S., and Thériault, G.: Continuous multiple measurement of soil redox potential using platinum microelectrodes, Soil Sci. Soc. Am. J., 66, 1813–1820, 2002.

Van Diest, H. and Kesselmeier, J.: Soil atmosphere exchange of carbonyl sulfide (COS) regulated by diffusivity depending on water-filled pore space, Biogeosciences, 5, 475–483, doi:10.5194/bg-5-475-2008, 2008.

Welp, L. R., Keeling, R. F., Meijer, H. A. J., Bollenbacher, A. F., Piper, S. C., Yoshimura, K., Francey, R. J., Allison, C. E., and Wahlen, M.: Interannual variability in the oxygen isotopes of atmospheric CO_2 driven by El Niño, Nature, 477, 579–582, doi:10.1038/nature10421, 2011.

Whelan, M. E. and Rhew, R. C.: Carbonyl sulfide produced by abiotic thermal and photodegradation of soil organic matter from wheat field substrate, J. Geophys. Res.-Biogeo., 120, 54–62, doi:10.1002/2014JG002661, 2015.

Whelan, M. E., Min, D.-H., and Rhew, R. C.: Salt marsh vegetation as a carbonyl sulfide (COS) source to the atmosphere, Atmos. Environ., 73, 131–137, doi:10.1016/j.atmosenv.2013.02.048, 2013.

White, M. L., Zhou, Y., Russo, R. S., Mao, H., Talbot, R., Varner, R. K., and Sive, B. C.: Carbonyl sulfide exchange in a temperate loblolly pine forest grown under ambient and elevated CO_2, Atmos. Chem. Phys., 10, 547–561, doi:10.5194/acp-10-547-2010, 2010.

Wilhelm, E., Battino, R., and Wilcock, R. J.: Low-pressure solubility of gases in liquid water, Chem. Rev., 77, 219–262, 1977.

Wingate, L., Seibt, U., Maseyk, K., Ogée, J., Almeida, P., Yakir, D., Pereira, J. S., and Mencuccini, M.: Evaporation and carbonic anhydrase activity recorded in oxygen isotope signatures of net CO_2 fluxes from a Mediterranean soil, Glob. Change Biol., 14, 2178–2193, doi:10.1111/j.1365-2486.2008.01635.x, 2008.

Wingate, L., Ogée, J., Cuntz, M., Genty, B., Reiter, I., Seibt, U., Yakir, D., Maseyk, K., Pendall, E. G., Barbour, M. M., Mortazavi, B., Burlett, R., Peylin, P., Miller, J., Mencuccini, M., Shim, J. H., Hunt, J., and Grace, J.: The impact of soil microorganisms on the global budget of delta-^{18}O in atmospheric CO_2, P. Natl. Acad. Sci. USA, 106, 22411–22415, doi:10.1073/pnas.0905210106, 2009.

Wingate, L., Ogée, J., Burlett, R., and Bosc, A.: Strong seasonal disequilibrium measured between the oxygen isotope signals of leaf and soil CO_2 exchange, Glob. Change Biol., 16, 3048–3064, doi:10.1111/j.1365-2486.2010.02186.x, 2010.

Wohlfahrt, G., Brilli, F., Hörtnagl, L., Xu, X., Bingemer, H., Hansel, A., and Loreto, F.: Carbonyl sulfide (COS) as a tracer for canopy photosynthesis, transpiration and stomatal conductance: potential and limitations, Plant Cell Environ., 35, 657–667, doi:10.1111/j.1365-3040.2011.02451.x, 2011.

Yamaguchi, T., Poulsen, T., Moldrup, P., and Fukushima, T.: Predictive model for adsorption of volatile organic chemicals on soils, Environmental Engineering Research, 36, 477–482, 1999.

Yi, Z., Wang, X., Sheng, G., Zhang, D., Zhou, G., and Fu, J.: Soil uptake of carbonyl sulfide in subtropical forests with different successional stages in south China, J. Geophys. Res, 112, D08302, doi:10.1029/2006JD008048, 2007.

Yi, Z., Wang, X., Sheng, G., and Fu, J.: Exchange of carbonyl sulfide (OCS) and dimethyl sulfide (DMS) between rice paddy fields and the atmosphere in subtropical China, Agr. Ecosyst. Environ., 123, 116–124, doi:10.1016/j.agee.2007.05.011, 2008.

Zeebe, R. E.: On the molecular diffusion coefficients of dissolved CO_2, HCO_3^- and CO_3^{2-} and their dependence on isotopic mass, Geochim. Cosmochim. Ac., 75, 2483–2498, doi:10.1016/j.gca.2011.02.010, 2011.

Identification des moteurs de l'activité de l'anhydrase carbonique dans les sols et son impact sur les échanges sol-atmosphère de $CO^{18}O$ et OCS, deux traceurs complémentaires du cycle du carbone

Les anhydrases carboniques (AC) sont des enzymes qui catalysent les réactions d'hydratation du CO_2 et d'hydrolyse de l'OCS. L'AC présente dans les plantes et les microorganismes du sol influence le bilan atmosphérique d'OCS ainsi que celui du $CO^{18}O$ car les isotopes de l'oxygène sont échangés avec ceux des pools d'eau pendant l'hydratation du CO_2. L'utilisation de l'OCS et du $CO^{18}O$ comme traceurs du cycle du C global ouvre une nouvelle voie pour estimer les contributions de la photosynthèse et de la respiration à grande échelle. Ceci requiert néanmoins une meilleure compréhension des facteurs contrôlant l'activité de l'AC des sols. Nous avons étudié le rôle du pH du sol et des communautés microbiennes sur l'activité de l'AC. Nous avons testé l'hypothèse que l'activité de l'AC serait (H1) inhibée dans les sols acides, et que (H2) les échanges isotopiques CO_2-H_2O seraient réduits dans les sols alcalins. Nous avons également présumé que l'activité de l'AC serait (H3) positivement corrélée à l'abondance des microorganismes phototrophes, et que (H4) la structure des communautés affecterait différemment les flux de $CO^{18}O$ et d'OCS. Nos résultats valident H1 et H2. Ils montrent aussi que les flux de CO_2 dans le sol et l'activité d'AC associée sont positivement corrélés à l'abondance des microorganismes phototrophes (H3), tandis que le dépôt d'OCS dans les sols dépend de l'abondance des champignons (H4). Ces résultats sont en cours d'intégration dans un modèle de l'activité de l'AC des sols mondiaux, ce qui permettra une estimation robuste des flux globaux de photosynthèse et de respiration à partir de bilans atmosphériques de COS et $CO^{18}O$.

Mots clés : anhydrase carbonique, CO_2, $CO^{18}O$, OCS, microorganismes du sol, pH

Identifying the drivers of carbonic anhydrase activity in soils and its impact on soil-atmosphere exchanges of $CO^{18}O$ and OCS, two complementary tracers of the global carbon cycle

Carbonic anhydrases (CA) are a group of enzymes that catalyse CO_2 hydration and OCS hydrolysis. The presence of CA in plants and soil microorganisms is responsible for the largest atmosphere-biosphere exchange of OCS but also $CO^{18}O$, because oxygen isotopes are exchanged with soil and plant water pools during CO_2 hydration. Consequently, $CO^{18}O$ and OCS atmospheric mixing ratios have been proposed as complementary tracers of the global C cycle that could open avenues to estimate the contribution of photosynthesis and respiration at global scales. However, a mechanistic understanding of the drivers of CA activity is required. We investigated the role of soil pH and microbial community on soil CA activity. We hypothesised that CA activity should be (**H1**) inhibited in acidic soils but that (**H2**) the associated CO_2-H_2O exchange would also be reduced in alkaline soils. We further assumed that (**H3**) soil CA activity would be enhanced by an increase in soil phototrophs abundance, but that (**H4**) soil community structure would affect differently $CO^{18}O$ and OCS fluxes. Our results confirmed **H1** and **H2**. We also confirmed that soil CO_2 fluxes and the associated CA activity were positively correlated with phototrophic communities abundance (**H3**), while soil OCS uptake and the associated CA activity seemed driven by fungal abundance (**H4**). These findings are now being incorporated into a model of soil CA activity worldwide that will allow robust estimates of photosynthesis and respiration at large scales from the atmospheric budgets of OCS and $CO^{18}O$.

Keywords : carbonic anhydrase, CO_2, $CO^{18}O$, OCS, soil microorganisms, pH